

---

Doctoral

Science

---

2016-7

## Predictive Biomarkers of Cellular Radiosensitivity for Clinical Radiotherapy Treatment

Lisa White

Technological University Dublin, [lisa.white2@mydit.ie](mailto:lisa.white2@mydit.ie)

Follow this and additional works at: <https://arrow.tudublin.ie/sciendoc>



Part of the [Oncology Commons](#), and the [Radiology Commons](#)

---

### Recommended Citation

White, L. (2016) *Predictive biomarkers of cellular radiosensitivity for clinical radiotherapy treatment*. Doctoral Thesis. Technological University Dublin. doi:10.21427/D70W2X

This Theses, Ph.D is brought to you for free and open access by the Science at ARROW@TU Dublin. It has been accepted for inclusion in Doctoral by an authorized administrator of ARROW@TU Dublin. For more information, please contact [yvonne.desmond@tudublin.ie](mailto:yvonne.desmond@tudublin.ie), [arrow.admin@tudublin.ie](mailto:arrow.admin@tudublin.ie), [brian.widdis@tudublin.ie](mailto:brian.widdis@tudublin.ie).



This work is licensed under a [Creative Commons Attribution-Noncommercial-Share Alike 3.0 License](#)

# Predictive Biomarkers of Cellular Radiosensitivity for Clinical Radiotherapy Treatment

Lisa White BSc



A thesis submitted to the Dublin Institute of Technology for the  
award of PhD

Supervised by:

Dr. Orla Howe  
Prof. Fiona Lyng  
Dr. Aidan Meade

04.07.2016

## **ABSTRACT**

Radiotherapy is prescribed to more than 50% of cancer patients during their treatment schedule. Due to intrinsic factors, individual variation in response exists, which will result in side effects or toxicity in a number of patients. Therefore, development of an assay or biomarker for the prediction and assessment of radiosensitivity among cancer patients undergoing radiotherapy would be beneficial. Such an assay would limit toxicities and facilitate dose-escalation for those patients who require it.

Assays for predicting intrinsic cellular radiosensitivity remains as the established G2 chromosomal radiosensitivity and most promising,  $\gamma$ H2AX foci assay. They can be applied to blood samples from donors and are sensitive enough to detect individual radiosensitivity. Therefore, both assays were applied to normal control cohorts compared to 'radiosensitive' cells to assess their efficacy as potential predictive assays for the clinic. Different low doses and energies of Linac radiation was applied to cells to assess their impact on patient intrinsic radiosensitivity and the most radiosensitive dose was confirmed at 0.5Gy (6MV photon beam) Linac radiation in cells. In addition to this, intrinsic radiosensitivity which could be measured at initial diagnosis and treatment planning stages for patients was investigated. The assays were applied to patients sampled at various time-points throughout a course of their radiotherapy treatment. The time-points included pre-treatment, post hormone treatment, last day of radiotherapy and the 2 and 8 month follow ups. Both assays were capable of depicting a dose response and differences between treatment visits.

The DNA damage based assays indicated that cell cycle regulation through the DNA damage response (DDR) activated by radiation was central to the underlying mechanistic response. Therefore, the molecular mechanisms of radiosensitivity were studied with an

emphasis of genes related to the cell cycle and DDR. Furthermore, genetic targets that emerged from this work could potentially be biomarkers of radiosensitivity that could also be incorporated into the clinic.

Following from the emergence of cell cycle and DDR genes, potential biomarkers for predicting radiosensitivity was analysed in a collaboration with Public Health England. This was done using the most sensitive genes which were found from bio dosimetry microarray studies carried out by the group (P21, PCNA, SESN1 and FDXR). Again this work was done on blood from healthy controls, prostate cancer patients and radiosensitive cells from Ataxia Telangiectasia donors. The genes in combination were able to depict a clear difference in the cohorts analysed in which expression was collectively highest in the healthy controls, less expression was observed in the Prostate cancer cohort and the least expression was observed in the radiosensitive cells from Ataxia Telangiectasia donors.

Finally, investigation of the miRNA composition of exosomes in healthy cells and cells from Ataxia telangiectasia donors was done to identify novel biomarkers for radiosensitivity prediction, in a collaboration with Trinity College Dublin. A subgroup of the let-7 family of miRNA's was among the top 88 expressed miRNA's in this chapter. Additionally, most miRNA's were not as highly expressed in radiosensitive cells compared to normal healthy cells. This work forms the basis for future work on prostate cancer patient samples.

## **DECLARATION**

I certify that this thesis which I now submit for examination for the award of Doctor of Philosophy (PhD), is entirely my own work and has not been taken from the work of others, save and to the extent that such work has been cited and acknowledged within the text of my work. This thesis was prepared according to the regulations for postgraduate study by research of the Dublin Institute of Technology and has not been submitted in whole or in part for another award in any other third level Institution. The work reported on in this thesis conforms to the principles and requirements of the DIT's guidelines for ethics in research.

DIT has permission to keep, lend or copy this thesis in whole or in part, on condition that any such use of the material of the thesis be duly acknowledged.

Signature \_\_\_\_\_ Date \_\_\_\_\_

## **ACKNOWLEDGEMENTS**

I would like to express my deepest appreciation to my primary supervisor Dr. Orla Howe for all of the help, advice, time, patience and direction she gave me both academically and personally to complete this work which certainly wouldn't be done without her help. I have found in Orla a friend for life. I would also like to thank my Supervisors Prof. Fiona Lyng and Dr. Aidan Meade for their continued guidance and time dedicated to help me complete this work. A special thanks to Dr. Natasha Coen for all her help with the cytogenetics techniques and all her advice, guidance and giggles.

Sincere thanks to all of the RESC staff and FOCAS Research Staff who made the time during my PhD amazing fun, I will never forget the experience! To Dr. Hayley Furlong, who took me under her wing when I first moved to Dublin and gave me survival tips living away from home as well as lab protocols and taught me many molecular biology techniques - I miss you! To Dr. Jane Bryant who helped massively throughout my PhD and made early morning and late evening lab times less stressful and more fun. To Dr. Adrian Maguire who acted as another big brother throughout, helping me with maths/physics/computer problems and gave me a right laugh when I needed to de-stress – you gave me a better outlook on stress and life! Additional thanks to Garret Rochford, Gillian Conway and Daire O'Donnell for their amazing help and problem solving skills.

I would also like to express my deepest and sincere gratitude to my family. Especially to my mother Mary-Kate White who was my best friend through this work, the most hard-working, enthusiastic woman I know and who completely and whole heartedly supported me emotionally to get through the final stages. You are amazing Mum! To my dad Paddy White, who joked about and mocked me making me more determined to finish the thesis earlier – there is no other person in the world like you and I am thankful for all you have taught me in life, and I am glad that I have inherited my hard-working ethic and fantastic “woman” driving skills from you. Thanks to my brother Christopher and wife Colleen White. I have looked up to Christopher for the best part of my life so far and he encouraged me to do the best academically that I can do – thank you big bro! A special thank-you extends to my Grandmother Maureen McCabe, for all of her fun quotes

and her attitude toward experiencing new things and approach and outlook on life, and all of those cups of tea with biscuits!

Big hugs and treats for the furbabies in my life, Rusty, George, Cooper, Tilly and the late Choatsy and Scoobie (RIP) who without even knowing it helped me through the stress of this work. I look forward to getting my next graduation puppy! ☺

Special thanks to my best friend of 15 years Donna Kelly, who stuck by me through all the times of happiness, sadness, sickness and stress and helped with all those spins and coffee visits to Starbucks – you are the most amazing person, keep being awesome! Additional thanks to my great friends Amanda Creane and Mary-Elizabeth McCrohan who are the most fun and amazing friends a girl could ask for! Many thanks to M, Liz and Mr. T for their continued support, comfort and fun times through the writing of this thesis (and for the food and chocolatey coated pancakes every Sunday).

Sincere thanks and gratitude go to Prof. Brendan McClean, Laura Shields, Chris Walker and Pdraig Creane for their help and cooperation on this project.

Finally, thank you to Science Foundation Ireland for funding this work which would not be complete otherwise. Thank you to DoReMi for funding amazing training courses and conferences all over the world which broadened my knowledge, networking and experience.

## **GLOSSARY OF TERMS**

4D CT	4 dimensional computed tomography
3D CRT	3 Dimensional Computed Tomography
8-oxodG	8-oxo-7, 8-dihydro-2'-deoxyguanosine
ADT	Androgen Deprivation Therapy
AIF	Apoptosis inducing factor
ALC1	Amplified in liver cancer gene
ALIX	Apoptosis linked Gene 2 interacting Protein
ALL	Acute Lymphocytic Leukaemia
AP	Apurinic/Apyrimidinic
APAF	Apoptotic protease activating factor
APLF	Aprataxin and PNK like factor
Apo	Apolipoprotein
APS	Ammonium Persulphate
ARTEMIS	DNA cross link repair protein
AT	Ataxia Telangiectasia
ATF2	Activating transcription factor 2
ATLD	AT-Like Disorder
ATM	Mutated AT
ATP	Adenosine triphosphate
ATRIP	ATR interacting protein
BAK	BCL2 homologous antagonist/killer protein
BAX	BCL2 associated X protein
Bca	Breast Cancer
BCL2	B cell lymphoma 2



BER	Base excision repair
BIRC5	Baculoviral inhibitor of apoptosis repeat containing 5
BLAP75	BLM Associated protein of 75kDa
BLM	Blooms Syndrome Gene
BRCA1	Breast cancer associated gene 1
BS	Blooms Syndrome
Ca <sup>2+</sup>	Calcium
CAD	Caspase activated Dnase
CCNG1	Cyclin G1
CDC	Cell division cycle
CDK	Cyclin dependent kinase
CDKN1A	CDK1 p21
cDNA	Complementary DNA
CEPX	X Chromosome Enumeration Probe
CHK2/1	Checkpoint kinase 2 or 1
CHOP	C/EBP homologous protein
Cin	Chromosomal Instability
CMA	Centre for Microscopy and Analysis
60Co	Cobalt 60
CPD	Cyclobutane pyrimidine dimer
CRT	Conformal RT
CTCAE	Common Terminology Criteria for Adverse Events
Cte	Chromatid Exchange
Ctip	retinoblastoma binding protein 8
DDB1/2	Damage specific DNA binding repair protein 1/2
DDR	DNA damage response

dG	Deoxyguanine
DGCR8	DiGeorge syndrome chromosomal region 8
DIABLO	Direct IAP binding protein with low pI
DISC	Death inducing signalling complex
DNA	Deoxyribonucleic acid
DNA PK	DNA protein kinase
DPX	Distrene, Plasticiser, Xylene
DR	Death receptor
DRE	Digital Rectal Examination
DROSHA	Ribonuclease type iii
DSB	Double strand break
EBRT	External Beam RT
ECL	Enhanced Chemiluminescence
eLND	Extended Lymph Node Dissection
ER	Endoplasmic reticulum
ERO1	Endoplasmic reticulum oxidoreductin
ESCRT	Endosomal Sorting Complex Required For Transport
FA	Fanconi Anaemia
FADD	Fas-associated death domain
FANC	Fanconi Anaemia C
FAS	Tumour necrosis factor receptor superfamily
FBS	Foetal Bovine Serum
FDXR	Ferredoxin Reductase
FISH	Fluorescent in situ hybridisation
FVC	Forced Vital Capacity
GADD	Growth arrest and DNA damage

GENE-PARE	Genetic Predictors of Adverse Radiotherapy Affects
GGR	Global genomic repair
GI	Genomic Instability
GTP	Guanosine triphosphate
GWAS	Genome wide association studies
H2AX	Histone H2A
HAT	Histone acetyl transferases
HC	Healthy Control
HDAC	Histone deacetyl tranferase
HDR	High Dose Rate
HIV	Human Immunodeficiency virus
HMW	High Molecular Weight
HP1	Heterochromatin protein 1
HPRT1	Hypoxanthine Phosphoribosyltransferase 1
HR	Homologous recombination
HRP	Horse Raddish Peroxidase
IAP	Inhibitor of Apoptosis
ICORG	All Ireland Cooperative Clinical Research Group
ICRP	International commission on radiological protection
IGA	Immunoglobulin A
IGH	Immunoglobulin Heavy Chain
IMRT	Intensity Modulate RT
IR	Ionizing radiation
KCl	Potassium Chloride
KPS	Karnofsky Performance Status
Ku	X Ray Repair Cross Complementing 5 (XRCC5)

KV	Kilovoltage
LCL	Lymphoblastoid Cell Lines
LDR	Low Dose Rate
LET	Linear energy transfer
Linac	Linear Accelerator
LRP	Laprascopic Radical Prostatectomy
MDM2	Mouse double minute homolog
MeV	Mega electron volt
MFI	Mean Fluorescence Intensity
MGMT	DNA methyl transferase
MIN	Microsatellite Instability
MIn	Mitotic Inhibition
MiRBASE	MicroRNA Database
miRNA	Micro RNA
MK	MAPK activated protein kinase
MMR	Mismatch repair
MN	Micronucleus
MOF	K lysine acetyltransferase or Males Absent on the First
MQRT-PCR	Multiplex Quantative Real Time PCR
MRE11	Meoitic Recombination 11
MTOR	Mechanistic Target of Rapamycin
MTT	3-(4, 5-dimethylthiazolyl-2)-2, 5-diphenyltetrazolium bromide)
MutS/L	Mutator S/L
MV	Megavoltage
NBS	Nijmegen Breakage Syndrome
NBS1	Nibrin1

NCI	National Cancer Institute
NER	Nucleotide excision repair
NER	Nucleotide excision repair
NHEJ	non-homologous end joining
NHL	Non Hodgkins Lymphoma
NIH	National Intitute of Health
NIN	Nucleotide Instability
NM23-H1	Dnase nucleotide diphosphate kinase
NURD	Nucleosome remodelling deacetylase
OAR	Organs at Risk
OBI	On board imaging
P21	Cyclin dependent kinase inhibitor 1
p53	Tumour Protein 53
PARP	Poly ADP ribose polymerase
PCa	Prostate Cancer
PCA	Principal Component Analysis
PCNA	Proliferating cell nuclear antigen
PCR	Polymerase Chain Reaction
PHA	Phytohaemagglutinin
PHPT1	Phosphohistidine phosphatase
PI3/PI4	Phosphoinositide 3 and 4
PNK	Polynucleotide Kinase
PSA	Prostate Specific Antigen
PTV	Planning Target Volume
PUMA	P53 upregulator of apoptosis
RAB14	Member of RAS Oncogene Family

RAD17	cell cycle checkpoint protein
RAD51	DNA repair protein homolog 1
RAN	RAS related nuclear protein
RARP	Robot assisted radical prostatectomy
RB	Retinoblastoma
RBP	Retinoblastoma Protein
RIBE	Radiation induced bystander effect
RIG2	Radiation induced G2 Score
RIPA	Radioimmunoprecipitation assay buffer
RISC	RNA induced silencing complex
RMP	Recombination mediator proteins
RNA	Ribonucleic Acid
ROS	Reactive oxygen species
RPA	Replication protein A
RPMI	Roswell Park Memorial Institute medium
RT	Radiotherapy
SCID	Severe Combined immuno-deficiency
SDS PAGE	Sodium dodecyl sulfate polyacrylamide gel electrophoresis
SESN1/2/3	Sestrin 1, 2 and 3
SET	Nuclear Proto- Oncogene
SMAC	Second mitochondria-derived activator of caspases
SNP	Single nucleotide polymorphisms
SOD	Superoxide dismutase
SSB	Single strand break
SSBR	single strand break repair
TCR	Transcription coupled repair

TEM	Transmission Electron Microscopy
TEMED	Tetramethylethylenediamine
TGF $\beta$	Tumour growth factor $\beta$
TIP60	60kDa tat interacting protein
TNF	Tumour necrosis factor
TNM	Tumour Node Metastasis
TopIIIa	Topoisomerase iii alpha
TRBP	Tar RNA binding protein
TRIS	Trisaminomethane
TS	Translesion synthesis
TSG	Tumour suppressor gene
TSG101	Tumour Suppressor Gene 101
UV	Ultraviolet
WHO	World Health Organisation
WRN	Werner's syndrome
XLF	non-homologous end joining factor 1
XP	Xeroderma Pigmentosa
XPC	Xeroderma pigmentosum complementation group C
XPF	DNA Repair Endonuclease
XRCC1/2	X-ray repair cross complementing protein 1 and 2

# **TABLES AND FIGURES OF ILLUSTRATIONS**

## **Figures**

Figure 1.1 Genomic location of the ATM gene which is highlighted by the red dash

Figure 1.2 Examples of DNA damaging agents

Figure 1.3 Illustration depicting the direct effect of ionizing radiation and the indirect effect

Figure 1.4 Interplay of factors in the basal state before DSB occurrence

Figure 1.5 Sequence of signalling events after a DSB occurs

Figure 1.6 Overview of DSB signalling with a timescale of events which occur in the DDR cascade

Figure 1.7 Overview of cell cycle checkpoints in response to various cellular stresses

Figure 1.8 Non homologous end joining (NHEJ) and Homologous Recombination (HR) pathways

Figure 1.9 Simplified schematic of the intrinsic and extrinsic pathways of Apoptosis

Figure 1.10 Example of a) Nucleotide instability (NIN) and b) first contraction of a microsatellite sequence

Figure 1.11 Informative results from comet assay analysis

Figure 1.12 Biogenesis of miRNA and functions

Figure 2.1 Chromatid type aberrations according to criteria 2 of the Radiation Biology Centre, Kyoto Japan

Figure 2.2 Irradiation procedure set up

Figure 2.3 Distribution of mitotic index values from 42 healthy donors

Figure 2.4 Distribution of individual G2 radiosensitivity scores from 42 healthy donors

Figure 2.5 Range of radiosensitivity scores from 42 healthy donors at 0.05Gy (a) and 0.5Gy (b)

Figure 2.6 Differences in G2 chromosomal radiosensitivity between smoker and non-smoking donors

Figure 2.7 Pearson R correlation of age with mitotic inhibition (MIn) and Radiosensitivity score

Figure 2.8 Pearson R correlation of Mitotic inhibition (MIn) with Radiosensitivity score



Figure 2.9 Correlations between month of blood sampling from healthy donors

Figure 2.10 Comparison of radiation induced G2 scores from whole blood vs pre extracted lymphocytes

Figure 2.11 Checkpoint response as calculated from radiation induced mitotic inhibition at a) 0.05Gy and b) 0.5Gy

Figure 2.12 G2 Chromosomal radiosensitivity at low doses from clinical sources

Figure 3.1 Gleason histological staging drawn by D.F Gleason

Figure 3.2 Checkpoint response from the male subset of a healthy control donor cohort

Figure 3.3 Baseline (V1) checkpoint response in Prostate Cancer (PCa) donors

Figure 3.4 Checkpoint response from 3 PCa donors for all 5 hospital visits

Figure 3.5 Checkpoint response from 3 PCa donors for 4 hospital visits

Figure 3.6 Examples of chromosomal aberrations recorded by microscopy in this chapter

Figure 3.7 Range of Healthy controls (HC's) and Prostate Cancer (PCa) patients in each category

Figure 3.8 G2 Radiosensitivity in Healthy controls (HC) compared to Prostate Cancer patients

Figure 3.9 Radiosensitivity scores at 0.05Gy for Prostate Cancer (PCa) patients through their radiotherapy regimes

Figure 3.10. Radiosensitivity scores from Prostate Cancer (PCa) patient blood samples irradiated at 0.5Gy throughout radiotherapy visits

Figure 4.1 Survival after irradiation of LCL's measured by their relative growth at 72hrs

Figure 4.2 Cell viability as a percentage of the non-irradiated control.

Figure 4.3 Cytotoxicity at 1hr and 24hrs post irradiation.

Figure 4.4 Mean fluorescence intensity (MFI) of  $\gamma$ H2AX at 1hr after irradiation

Figure 4.5 Mean fluorescence intensity (MFI) of  $\gamma$ H2AX at 72hrs after irradiation

Figure 4.6 Average foci per cell of normal compared to AT cell lines

Figure 4.7 Average foci per cell observed in normal and AT cell lines

Figure 4.8 Mitotic inhibition from normal and AT cell lines

Figure 4.9 Radiation induced G2 score from normal and AT cell lines

Figure 4.10. Coefficient of variation (%) between healthy control cells and AT cells

Figure 4.11 G-Banding of the 2139 cell line showing an abnormal karyotype

Figure 4.12 G-Banding and karyotype of AT2Bi showing loss of X chromosome

Figure 4.13 G-Banding and karyotype of AT3Bi showing numerous additions and deletions

Figure 4.14 FISH analysis using the ATM probe set for AT3Bi cell line

Figure 4.15 Interphase FISH using dual ATM-TP53 probe

Figure 5.1 Overview of the 4 genes used in this chapter for radiosensitivity prediction

Figure 5.2. Combined relative gene expression in healthy controls (HC) compared to Prostate Cancer (PCa) patients

Figure 5.3 Gene expression in two AT cell lines

Figure 5.4. Differential gene expression between Healthy controls (HC), prostate cancer (PCa) and Ataxia Telangiectasia (AT) cell lines (1hr)

Figure 5.5. Gene expression in healthy controls (HC), prostate cancer (PCa) patients and cells from Ataxia Telangiectasia (AT) cell lines (24hrs)

Figure 5.6. Gene expression in Prostate Cancer (PCa) patients pre and post hormonal androgen deprivation therapy (ADT) treatment

Figure 6.1 Western Blot identification of exosomal marker TSG101 present at 43kDA

Figure 6.2 Identification of exosomes in samples by transmission electron microscopy

Figure 6.3 Average Cp values of common miRNA's in each sample

Figure 6.4 Graphical illustration of the microRNA content

Figure 6.5 Heat map and unsupervised hierarchical clustering

Figure 6.6 PCA plot of miRNA's from AT cell lines

Figure 7.1 Progression of work and summary over 4 years of the PhD

Figure 7.2 Summary of interplay between the molecular markers of radiosensitivity

## **Tables**

Table 1.1 Examples of rate of DNA damaging agents and rate of occurrences daily in human cells

Table 1.2 FISH probes used for chapter 4 of this thesis

Table 2.1 Summary of radiosensitivity cut off values, radiation type and doses used from previous reports in the literature

Table 2.2 Summary of inter-individual and intra-individual variation values by author

Table 2.3 Intra individual variation values for three healthy donors who consented for multiple samples over a period of 4 years

Table 2.4 Summary of statistics from G2 scoring of 42 healthy controls

Table 2.5 Summary of statistics for radiation induced G2 scores for all beam sources at 0.05Gy and 0.5Gy

Table 3.1 Tumour, node, metastasis (TNM) staging system

Table 4.1 Results of the G-band analysis of each of the cell lines

Table 4.2 Non-clonal aberrations that were detected by G-band analysis

Table 4.3 FISH analysis of each of the cell lines to include probes for CEPX, IGH, TP53 and ATM.

Table 5.1 Primer and probe sequences used in this work for genes analysed with MQRT-PCR

Table 5.2 Inter individual variation in Healthy controls

Table 5.3 Inter individual variation of gene expression in 6 Prostate cancer patients

Table 6.1 Components and concentrations used for SDS-PAGE

Table 6.2 Differentially expressed miRNAs in each cell line

Table 6.3 Summary of the roles of miRNAs of interest

Table 6.4 Potential radiosensitivity miRNA's

# **TABLE OF CONTENTS**

<b>ABSTRACT .....</b>	<b>.....</b>
<b>DECLARATION .....</b>	<b>.....</b>
<b>ACKNOWLEDGEMENTS .....</b>	<b>.....</b>
<b>GLOSSARY OF TERMS .....</b>	<b>.....</b>
<b>TABLES AND FIGURES OF ILLUSTRATIONS .....</b>	<b>.....</b>
<b>TABLE OF CONTENTS.....</b>	<b>.....</b>
<b>1. THESIS INTRODUCTION .....</b>	<b>1</b>
<b>1.1. Clinical radiotherapy.....</b>	<b>1</b>
<b>1.2. Clinical radiobiology – the 5 R’s.....</b>	<b>4</b>
1.2.1. Repair.....	4
1.2.2. Redistribution.....	5
1.2.3. Repopulation .....	5
1.2.4. Reoxygenation .....	5
1.2.5. Radiosensitivity.....	6
<b>1.3. Radiosensitive Phenotypes .....</b>	<b>7</b>
1.3.1. Cancer .....	11
<b>1.4. Cellular Sensitivity to radiation.....</b>	<b>12</b>
1.4.1. Types of DNA damaging agents .....	12
1.4.2. Types of DNA damage .....	16
1.4.3. Damage Recognition and signal propagation .....	18
1.4.3.1. ATM - MRN .....	20
1.4.3.2. DNA – PKcs - KU .....	21
1.4.3.3. ATR - ATRIP.....	22
1.4.4. Cell Cycle Checkpoints.....	24
1.4.5. Cell Fate after DNA damage.....	27
1.4.5.1. DNA Repair processes .....	28
1.4.5.2. Cell Death mechanisms.....	31
1.4.5.3. Genomic Instability and Carcinogenesis.....	36
<b>1.5. Predictive Biomarkers of radiosensitivity.....</b>	<b>38</b>
1.5.1. Cell based assays.....	38
1.5.2. Cytogenetics Based Assays.....	39
1.5.3. DNA Damage Markers .....	45
1.5.4. Genomic markers of radiation exposure .....	47
1.5.5. Single nucleotide polymorphisms (SNP’s).....	48

1.5.6.	Histone Modifications.....	48
1.5.7.	Micro RNA's Exosomes .....	49
<b>1.6.</b>	<b>Novel tools for predicting radiosensitivity .....</b>	<b>51</b>
1.6.1.	Raman Spectroscopy.....	51
<b>1.7</b>	<b>Aims and objectives of Thesis;.....</b>	<b>53</b>
<b>2.</b>	<b>OPTIMISATION AND VALIDATION OF THE G2 CHROMOSOMAL RADIOSENSITIVITY ASSAY ON HEALTHY DONOR BLOOD SAMPLES .....</b>	<b>54</b>
<b>2.1</b>	<b>Introduction.....</b>	<b>54</b>
<b>2.2</b>	<b>Materials &amp; Methods.....</b>	<b>66</b>
2.2.1.	Blood samples and Ethics .....	66
2.2.2	Whole blood cultures .....	66
2.2.3	Histopaque Lymphocyte Isolation .....	66
2.2.4	Irradiation procedure.....	67
2.2.5	Post irradiation Cytogenetics .....	69
2.2.6	Statistical Analysis.....	70
<b>2.3</b>	<b>Results .....</b>	<b>70</b>
2.3.1	Mitotic index.....	71
2.3.2	G2 chromosomal radiosensitivity scores .....	72
2.3.3	Validation of the assay – Variation and Radiosensitivity Cut off.....	73
2.3.4	Correlations.....	77
2.3.5	Culturing Effects .....	81
2.3.6	Beam energy effect .....	82
<b>2.4</b>	<b>Discussion.....</b>	<b>86</b>
2.4.1	Checkpoint Response.....	86
2.4.2	G2 Chromosomal Radiosensitivity .....	87
2.4.3	Correlation Analysis .....	89
2.4.4	Assay Validation .....	90
2.4.5	Beam Energy Effect.....	91
<b>2.5</b>	<b>Aims of chapter and conclusions .....</b>	<b>92</b>
<b>3.</b>	<b>CYTOGENETIC ANALYSIS OF RADIOSENSITIVITY OF PROSTATE CANCER PATIENTS THROUGHOUT THEIR RADIOTHERAPY REGIME AND FOLLOW UP .....</b>	<b>93</b>
<b>3.1</b>	<b>Introduction.....</b>	<b>93</b>
3.1.1	Prostate Cancer detection, diagnosis and staging .....	94
3.1.2	Types of therapy for PCa and outcomes .....	97
3.1.3	Patient toxicity and side effects .....	103
3.1.4	Assays for measuring PCa Patient Toxicity.....	104
<b>3.2</b>	<b>Methods.....</b>	<b>106</b>

3.2.1	Blood culture set up .....	106
3.2.2	Histopaque Lymphocyte Isolation .....	106
3.2.3	Irradiation Conditions .....	106
3.2.4	G2 chromosomal radiosensitivity assay .....	106
3.2.5	Statistical Analysis.....	107
<b>3.3</b>	<b>Results .....</b>	<b>107</b>
3.3.1	G2 Checkpoint response .....	107
3.3.2	G2 Chromosomal Radiosensitivity .....	111
3.3.3	Radiosensitivity and Toxicity .....	115
<b>3.4</b>	<b>Discussion.....</b>	<b>116</b>
<b>3.5</b>	<b>Chapter Conclusions and Summary .....</b>	<b>118</b>
<b>4.</b>	<b>FURTHER EXPLORATION OF BIOMARKERS OF RADIOSENSITIVITY DRIVEN BY CELLULAR MECHANISMS .....</b>	<b>119</b>
<b>4.1</b>	<b>Introduction.....</b>	<b>119</b>
<b>4.2</b>	<b>Methods.....</b>	<b>123</b>
4.2.1	Cell lines and Cell culture and Irradiation setup .....	123
4.2.2	Cell viability and Cytotoxicity .....	124
4.2.3	Cell Survival .....	124
4.2.4	DNA Damage.....	125
4.2.5	Cytogenetics and Microscopic analysis .....	125
4.2.6	G-Banding.....	125
4.2.7	Fluorescent <i>In Situ</i> Hybridisation (FISH) cytogenetics .....	126
4.2.8	Statistical Analysis.....	127
<b>4.3</b>	<b>Results .....</b>	<b>127</b>
4.3.1	Cell Growth and DNA Damage Post Irradiation .....	127
4.3.2	Cell viability and Cytotoxicity .....	128
4.3.3	DNA Damage.....	131
4.3.4	G2 Chromosomal Radiosensitivity .....	135
4.3.4.1	Radiation induced Mitotic Inhibition and G2 Radiosensitivity .....	135
4.3.4.2	LCL variation in radiosensitivity response .....	137
4.3.5	G-Banding.....	138
4.3.6	Fluorescent <i>in situ</i> Hybridisation (FISH).....	146
<b>4.4</b>	<b>Discussion.....</b>	<b>149</b>
<b>4.5</b>	<b>Chapter Conclusions and Summary .....</b>	<b>152</b>
<b>5.</b>	<b>POTENTIAL OF A FOUR-GENE SIGNATURE FOR THE PREDICTION OF RADIOSENSITIVITY IN HEALTHY DONOR AND PROSTATE CANCER PATIENTS COMPARED TO ATAXIA TELANGIECTASIA SAMPLES .....</b>	<b>153</b>

<b>5.1</b>	<b>Introduction.....</b>	<b>153</b>
<b>5.2</b>	<b>Methods.....</b>	<b>158</b>
5.2.1	Samples and Cell Culture.....	158
5.2.2	RNA extraction and Quantification .....	159
5.2.3	CDNA Synthesis .....	160
5.2.4	Multiplex Quantative Real Time PCR .....	160
<b>5.3</b>	<b>Results .....</b>	<b>162</b>
5.3.1	Healthy Controls .....	162
5.3.2	Prostate Cancer .....	165
5.3.3	Cells from Ataxia Telangiectasia Donors .....	165
5.3.4	Combined Cohort Analysis.....	166
5.3.5	Use of MQRT-PCR panel through PCa treatment visits.....	169
<b>5.4</b>	<b>Discussion.....</b>	<b>172</b>
<b>5.5</b>	<b>Chapter Conclusions.....</b>	<b>176</b>
<b>6.</b>	<b>A PANEL OF EXOSOMAL MIRNA’S CAN DISTINGUISH EXTREME RADIOSENSITIVITY FROM NORMAL CONTROLS.....</b>	<b>178</b>
<b>6.1</b>	<b>Introduction.....</b>	<b>178</b>
<b>6.2</b>	<b>Methods.....</b>	<b>180</b>
6.2.1	Cell Culture .....	180
6.2.2	Isolation of Exosomes .....	181
6.2.3	Characterisation by Transmission Electron Microscopy (TEM) .....	181
6.2.4	Protein extraction and analysis of Cell and Exosome Extracts.....	181
6.2.5	Sodium Dodecyl Sulphate-Polyacrylamide Gel Electrophoresis (SDS-PAGE) gel electrophoresis .....	182
6.2.6	Western Blotting .....	183
6.2.7	Antibody Probing.....	184
6.2.8	Chemiluminescent Detection and Imaging .....	184
6.2.9	Real Time PCR Panel Analysis (Exiqon) .....	184
6.2.9.1	Detection of 5 known miRNA’s in Cells and Exosomes .....	185
6.2.9.2	Full miRNA Panel analysis of Cell Extracts.....	185
6.2.10	Data Analysis .....	186
<b>6.3</b>	<b>Results .....</b>	<b>187</b>
6.3.1	Characterisation .....	187
6.3.2	Detection of miRNA in Cell and Exosome samples .....	188
6.3.3	Heat map and unsupervised clustering from Exiqon .....	191
6.3.4	Differential Expression of miRNA between Normal and Radiosensitive.....	192



6.3.5	Differentially expressed miRNA's.....	194
<b>6.4</b>	<b>Discussion.....</b>	<b>199</b>
<b>6.5</b>	<b>Chapter Summary and conclusions.....</b>	<b>201</b>
<b>7.</b>	<b>GENERAL THESIS DISCUSSION .....</b>	<b>203</b>
<b>8.</b>	<b>LIMITATIONS AND FUTURE WORK .....</b>	<b>209</b>
<b>9.</b>	<b>REFERENCES .....</b>	<b>211</b>
<b>10.</b>	<b>APPENDICES .....</b>	<b>236</b>
<b>10.1</b>	<b>Inclusion/Exclusion Criteria for Prostate Cancer Donor Recruitment .....</b>	<b>236</b>
<b>10.2</b>	<b>Reagents, Suppliers and Catalogue numbers .....</b>	<b>238</b>
<b>10.3</b>	<b>Protocols used in this thesis.....</b>	<b>240</b>
<b>10.4</b>	<b>Raw Data.....</b>	<b>261</b>

# **1. THESIS INTRODUCTION**

## **1.1. Clinical radiotherapy**

Radiotherapy (RT) is one of the three most prescribed treatment modalities for cancer including chemotherapy and/or surgery and RT remains the most cost effective cancer treatment modality globally<sup>1</sup>. More than 50% of cancer patients will experience RT as part of their treatment plan and it accounts for 40% of the curative treatment for cancer<sup>2</sup>. RT can be used to control the spread of malignant tumours after surgery, cure, and for palliative treatment to alleviate symptoms in elderly patients. According to the world health organisation (WHO), Prostate cancer (PCa) is the second most commonly diagnosed cancer in males and 4<sup>th</sup> most common cancer (gender combined) worldwide<sup>3</sup>. RT is used for a number of reasons but mainly to cure or control metastasis and it can be used in conjunction with surgery as a neo-adjuvant treatment (before) or adjuvant treatment (after). The most common type of radiation therapy is external beam RT (EBRT) (outside the body) and internal brachytherapy (small radioactive rods placed inside the body in close proximity of the tumour)<sup>4</sup>. Within EBRT, treatment can be either conformal RT (CRT) or intensity modulated RT (IMRT) which varies dose across the region of the tumour, proven to reduce long term side effects<sup>5</sup>. Radiation treatment allows for cure (considerable levels of local tumour control if treated in the early stages of disease) and palliative care (relief of symptoms by controlling the tumour size, and pain relief). Although in its curative and palliative effects, radiation treatment causes unwanted side effects, similar to many curative drug treatments.

Development of clinical radiation treatment and planning has progressed considerably during the past century. The discovery of X – rays by Rontgen<sup>6</sup> was followed by the finding of natural radioactivity by Becquerel<sup>7</sup> and isolation of radium by Curie<sup>8</sup> from 1895 – 1898 which all paved the way for development of two of the main RT techniques

still used today; EBRT and Brachytherapy. Gastric and basal cell carcinoma were the first tumours treated with RT in 1896<sup>9</sup> and harmful effects of radiation were discovered soon after.

Two factors became apparent in early clinical radiation treatment planning; (1) to aim for as close to 100% dose delivery per target volume and (2) to reduce the risk of harmful radiation damage in healthy surrounding tissue. Only successful treatment of superficial tumours or highly radiosensitive tumours was done with the use of kilovoltage (KV) energies between 1900 – 1940<sup>10</sup> as higher energy beams in the megavoltage range were developed. Around this time, 3 fundamental areas to advance RT were discovered; (1) the law of radiosensitivity by Bergonie and Tribondeau who were the first to describe the “susceptibility” of cells to ionizing radiation<sup>11</sup>, (2) The use of fractionated radiotherapy with 2Gy fractions by Coutard who showed greater normal tissue recovery by delivering small fractions of radiation dosage<sup>12</sup>, and (3) development of the International Commission on Radiological Protection (ICRP) agency in 1928 which would set out and monitor guidelines, usage and practises of radiation use throughout the world<sup>13</sup>.

Early in the megavoltage (MV) era, the first Cobalt 60 (<sup>60</sup>Co) teletherapy unit was installed in Hamilton in Canada, with a higher radiation photon beam of 1.2 MeV (Mega electron Volt) energy<sup>14</sup>. This allowed for treatment of deep seated tumours (such as prostate, bladder, bowel, brain) and cases of Hodgkin Lymphoma. As <sup>60</sup>Co teletherapy units required much maintenance especially for the disposal of radioactive <sup>60</sup>Co at the end of its half-life, a new clinical radiation source was introduced as the first linear accelerator (Linac) in 1948<sup>15</sup>.

The development of the Linac allowed for delivery of MV energies with much higher absorbed (total amount of radiation absorbed in the tissue of interest) doses of 60 – 70Gy without exceeding the tolerance dose (i.e. the dose at which the patient can receive before increase in normal tissue complications) and could also deliver electron beam RT for

superficial tumours within the one machine unit<sup>16</sup>. Computer assisted RT joined with <sup>60</sup>Co Teletherapy and Linac RT from 1996 to the present day and have 3 main modalities; (1) Intensity modulated RT (IMRT) which is a method of EBRT that uses shaping of the beam to achieve a high tumour dose while sparing healthy surrounding tissue<sup>17</sup>, (2) Stereotactic RT for medically inoperable tumours<sup>18</sup> and (3) 4 dimensional computed tomography (4D CT) RT which is a type of stereotactic RT used for example in lung cancer which provides CT images for better treatment dose planning, taking into account the motion of the lungs during respiration<sup>19</sup>. These developments have revolutionised modern RT practices which allow for better RT control and incorporate the shaping of photon beams, image guidance and patient movements<sup>20</sup>.

Current plans for future development of RT involve particle therapy such as proton therapy, carbon ion therapy and hyper-fractionation. Proton therapy is a promising type of RT as the proton beam allows for a spread out Bragg Peak (i.e. a dose-depth measurement which peaks at its highest dose in a depth of tissue). The spread out of the Bragg peak allows for a high dose in a larger volume with little to no dosage in normal healthy tissue and is very promising for its future use<sup>21</sup>. Carbon ion therapy is also a type of particle therapy, with the same spread out Bragg Peak properties as proton therapy, however some differences in beam penumbra, linear energy transfer (LET) and overall better relative biological effectiveness gives credibility to more investigation using carbon ion therapy<sup>22</sup>. In 2013 a report by Fujii *et al* compared patient outcome between proton and carbon ion therapy, and although there was no significant differences in 3 year survival rates, progression free survival and local tumour control were observed and a slightly higher percentage in each of the measures were found after carbon ion therapy<sup>22</sup>. Therefore, particle ion therapy looks promising for future routine clinical use. Hyper fractionation allows for more fractions of slightly reduced fraction dose, more often (usually twice a week instead of once) resulting in the same overall dose. Sapkota *et al*

conducted a randomized trial in 2013 which showed significantly better tumour response in the hyper fractionated treatment group<sup>23</sup>. It is also clear that advances in RT treatment devices along with experimental radiobiological data will help pave the way for improvement of future radio therapeutic approaches for individual patients suffering from different cancer types. The relationship between clinical radiobiology and radiotherapy is associated with the 5 R's. The 5 R's of RT are key to how experimental radiobiology leads to adjustment of treatment regimes.

## **1.2. Clinical radiobiology – the 5 R's**

One of the first most important milestones to influence RT with experimentation was the therapeutic treatment of a hairy mole by Leopold Freund in 1896<sup>24</sup>. In the early 1900's, Regaud *et al* found that sterilisation of a rams testes was not possible using only a single dose of radiation but rather multiple doses over a period of weeks was required for minimal skin reaction and successful sterilisation<sup>25</sup>. This is the theory of fractionation, which is still used today and relates to redistribution which is one of the 5 R's of radiobiology and explained below.

### **1.2.1. Repair**

Sub-lethal and lethal damage results from deoxyribonucleic acid (DNA) being traversed by radiation tracks. The effect of this collision can be direct – where the structure of DNA is physically damaged from the DNA-radiation collision. Or the effect can lead to indirect interaction of ionized particles with water molecules, leading to the formation of highly reactive oxygen radicals. RT utilises the cells molecular repair mechanisms for appropriate cell killing of cancerous tissue and repair of sub-lethal damage in healthy tissue as discussed in later sections. As normal cells are well oxygenated, healthy tissue should repair within a few hours of radiation treatment, whereas hypoxic tumours should ultimately die. Repair of healthy tissue after RT is dependent on the correct and efficient

functioning of DNA damage and repair response which is often not the case in many cancer patients.

#### 1.2.2. Redistribution

When irradiation occurs, cells are distributed in different parts of the cell cycle. Those cells which are in the most sensitive phases (G2 and M) are more likely to go through cell death pathways. Fractionation allows time for redistribution of more resistant cells within the cell cycle to move to a more sensitive phase on the next round of treatment. This revolutionary theory came from Claudius Regaud's work in 1911, who figured that a ram's testes could be sterilized if three separate irradiations were delivered 15 days apart<sup>25</sup>.

#### 1.2.3. Repopulation

Evidence suggests that after a course of radiation treatment, cell death and damage may induce an increased rate of cell proliferation. Originally described in the 1970s, Muneyasu *et al* reported that tumour cells exhibited a rapid proliferation after irradiation which was followed by a growth delay<sup>26</sup>. This gives promise to the theory of accelerated therapy, where less fractions but a higher dose is given during RT. Ciervide *et al* found this to be advantageous when breast cancer patients were recruited in two groups in 2012 for 2.8Gy delivered in 15 fractions and 2.7Gy in 15 fractions compared to 2Gy in 25 fractions for each group, and they reported no invasive recurrence within a 5 year follow up period<sup>27</sup>. This area is still under intense investigation, and is most certainly affected by patient radiosensitivity.

#### 1.2.4. Reoxygenation

In order for a tumour to grow and develop, an efficient vasculature network is needed to bring an adequate supply of nutrients and oxygen and this is first supplied by the host. The rapid rate of growth of abnormal cells soon requires the tumours own vasculature system which is developed through angiogenesis and is far from normal. Vessels are

primitive in nature with a loss of basement membranes, no pericytes and lack of smooth muscle which all contributes to the glucose and energy deprivation, high lactate and oxygen deficiency observed in these tumours<sup>28</sup>. Tumours are naturally hypoxic, but heterogeneity in cellular oxygenation can be a problem and is influenced by tumour size and site<sup>29</sup> as tumours are said to fluctuate between hypoxia (reduced oxygen levels) and normoxia (normal oxygen levels). A recent article by Bayer *et al* describes how oversimplified reoxygenation has been portrayed over these past decades and how it has affected radiosensitivity. For example, at oxygen concentrations of <0.1% and during fluctuation of hypoxia-normoxia, malignant cells can still undergo permanent genomic and epigenetic modifications which could lead to aggressive survival strategies for the abnormal cell<sup>30</sup>.

#### 1.2.5. Radiosensitivity

Defined by Bergonie and Tribondeau in 1959 as the “susceptibility of cells to the effects of ionizing radiation,” radiosensitivity has been the subject of intense investigation for decades<sup>11</sup>. Varying levels of sensitivity are found in different cell types. Rapidly dividing cells (such as benign and malignant tumours but not exclusive) have higher radiation sensitivity than those cell types which do not rapidly divide (e.g. nerve cells). The more rapidly dividing the cell, the more times the cell will move through the cell cycle and therefore the higher the probability of detection of damage. This is an example of how a radiobiological investigation was advantageous for RT. Giving multiple fractions over a period of time allows for the death of cancerous cells while repair in healthy cells takes place by the cells repair mechanisms. Mechanisms of radiosensitivity come from molecular functional studies on genes which control DNA Damage Response (DDR) mechanisms. Most genes which are affected in this response correspond to disorders which all possess a highly radiosensitive phenotype (Ataxia Telangiectasia, Fanconi’s

Anaemia, Blooms Syndrome, Xeroderma Pigmentosa, Severe Combined Immuno Deficiency and AT-Like Disorder).

### **1.3. Radiosensitive Phenotypes**

Radiosensitive cohorts of patients suffering from neurodegenerative disorders have factors in common; mutation and defects in DNA damage repair genes, an increased sensitivity to the effects of ionizing radiation, and predisposition to cancer. The following examples of radiosensitive cohorts have been a major focus in different radiosensitivity studies worldwide which describe defective DNA damage or repair mechanisms due to specific mutated genes. Important radiosensitive cohorts which have been under intense investigation include Ataxia telangiectasia (AT) and ATLD, Fanconi Anaemia (FA), Xeroderma pigmentosa (XP), Blooms Syndrome (BS) and Severe combined immunodeficiency disorder (SCID). They are described briefly below, but of most relevance to this work are Ataxia Telangiectasia (AT) described below and Prostate cancer cohorts described in Chapter 3, section 3.1.

**AT** was one of the first radiosensitive patient cohorts to be described clinically in the literature with first reports dating back to 1920's but not clinopathologically defined until 1967<sup>31</sup>. Boder *et al* described the clinical causes of death in 1975 from a series of 9 autopsies to be persistent Sino pulmonary infection and lymphoreticular malignancy as the first and second most common causes of death for AT<sup>31</sup>. AT is phenotypically characterised by a neurodegenerative immune disorder with uncontrolled cerebellar motor control<sup>32</sup>. ATM (Mutated AT gene) is considered the central transducer of damage from ionizing radiation induced double strand breaks (DSB's) in the DDR which controls phosphorylation and activation of downstream DDR events activating cell cycle arrest. Mutations of the ATM gene result in AT, with other mutations including decreased amounts of the ATM protein or reduced kinase activity which results in a milder form of



the disease<sup>32</sup>. The ATM gene was cloned in 1995<sup>33</sup> and was mapped to chromosome 11q22-23 (Figure 1.1) and represents 69 exons spread across approximately 150kilobases of DNA, from a 12 kilobase transcript<sup>34</sup>. ATM is part of the Phosphoinositide 13 and 14 (P13/P14) kinase family which is involved in phosphorylation and regulator of downstream that control cell cycle progression, such as tumour protein (p53), breast cancer associated gene (BRCA1), checkpoint kinase 2 (CHK2) and Nibrin 1 (NBS1)<sup>35</sup>. As mentioned later, PI kinases under regulation of phosphatase enzymes can autophosphorylate and/or phosphorylate other substrates such as effectors in the DDR. AT is an autosomal recessive disorder, in which both parents of the affected offspring would have carried one functional and one mutated copy of the ATM gene in heterozygous form and therefore the offspring inherited each of the mutated copies in homozygous form. The disorder was first described as a pleiotropic phenotype originally in 1926 by Syllaba and Henner<sup>36</sup>, but not clinically described until years later by Sedgwick and Boder<sup>37</sup>. It was not long after that the abnormally high sensitivity to radiation was observed and increased predisposition to cancer was reported using cultured skin fibroblasts as an *in vitro* model<sup>33,38,39</sup>.

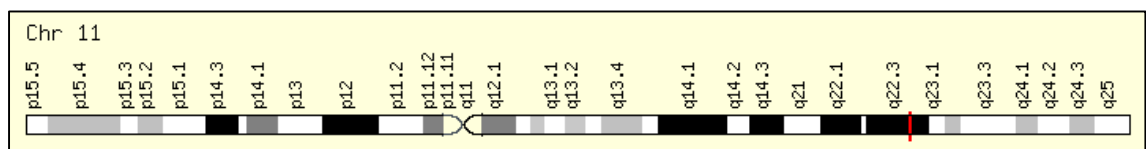


Figure 1.1 Genomic location of the ATM gene which is highlighted by the red dash. The ATM gene is located as a cytogenetic band at 11q22.3 and is comprised of 146,619 bases. Image and information taken from GeneCards<sup>35</sup>

Attempts have been made to use the ATM gene to predict individual radiosensitivity in patients with promising outcomes. Cesaretti *et al* showed that ATM sequence variants could correlate well and predict adverse reactions of prostate tumours to RT<sup>40</sup>. The group suggest that gene sequence variants (not only ATM) are involved in radiosensitivity and could potentially be used as a predictor of radiosensitivity. Such genes include transforming growth factor beta (TGFβ), X-Ray Cross Complementing protein 1 and 2, (XRCC1 and 2) and superoxide dismutase (SOD) <sup>40</sup>.

**AT-Like Disorder (ATLD)** is similar in clinical presentation to that of AT and is a result of a mutation in the meiotic recombination homolog 11 (hMRE11) gene. This gene is an important constituent of the MRN complex alongside DNA repair protein (RAD51) and NBS<sup>41</sup>. As the components responsible for AT and Nijmegen Breakage Syndrome (NBS) are within the same complex, it would be automatically presumed that patients with these syndromes would present with similar clinical symptoms, however this is not the case. One similar presentation is radiosensitivity and an increased predisposition to cancer. ATLD is similar to AT disorder, in that patients present with ocular apraxia, slurred speech and increased incidence of respiratory infections, but patients do not have immunodeficiency as in AT or NBS. In NBS, symptoms include microcephaly, growth retardation and immunodeficiency<sup>41</sup>. Cells from AT, ATLD and SCID are virtually indistinguishable in their response to ionizing radiation, as all show an increased in radiosensitivity involving different genes, but differences in their clinical presentation outline the need for further investigation to observe if other co – factors are involved<sup>42</sup>.

**FA** is a rare genetic condition which is characterised clinically by defects in normal development, bone marrow failure, hyper-radiosensitivity and increased cancer predisposition, with 15 genetic subtypes of the disorder reported<sup>43</sup>. A high frequency of mutations have been found in patients with FA (most recently FANC-A, -C, -G and -

D2)<sup>44</sup> which proves difficult to find a comprehensive diagnostic test for all FA patients and incredibly most often produces false positives while testing<sup>45</sup>. Cells from FA patients have been found to be hypersensitive to chromosomal breaks and a classical chromosomal breakage test was done in combination with multiplex ligation- dependant probe amplification (MLDP)<sup>46</sup> on patients directly for diagnosis of the condition. However, more recently whole exome sequencing of the FANCA gene is used<sup>45</sup>.

**XP** was first described in the 1800's by Hebra<sup>47</sup>, and is an inherited autosomal disorder classified clinically by pigment disorders, photosensitivity, increased susceptibility to tumour development as a result of defects in DNA repair processes<sup>48</sup>. Reviewed in a case series by Butt *et al* in 2010<sup>48</sup>, XP has 8 genetic sub variants, 7 of which result from defects in the nucleotide excision pathway of repair (NER) in response to ultraviolet (UV) induced DNA damage<sup>49</sup>.

**BS** also targets defects in repair pathways. This is a genetic autosomal recessive disorder which is characterised clinically by a photosensitive rash, short stature and a predisposition to cancer, which results from excessive homologous recombination (HR) repair and possesses one of the strongest correlations between chromosomal radiosensitivity and cancer predisposition<sup>50</sup>. The disorder, which is a result of a mutation in the Blooms Syndrome (BLM) gene, encodes DNA helicases that are important in DNA stability and helicase activities within the replication fork during homologous recombination<sup>51</sup>.

**SCID** syndrome is a result of defects in the non-homologous end joining (NHEJ) pathway. In cases of SCID associated with radiosensitivity, proteins with mutations that interact to re-join DSB's (including DNA cross link repair protein (ARTEMIS), non-homologous end joining factor 1 (XLF) and DNA ligase IV, as well as DNA – PKcs) are mutated, with ARTEMIS mutations the most common in SCID patients and the knockout

of all of these proteins resulted in lethality in mice<sup>52</sup>. Patients lack a fully functioning immune system and therefore lack of helper T cells in the immune response. This results in SCID patients being reported as highly radiosensitive and vulnerable to normal every day infectious agents<sup>53</sup>.

### 1.3.1. Cancer

Healthy cells can repair and adapt in response to a number of cellular stresses such as fluctuations in calcium levels, nutrient deprivation, and oxygen status. In response to DNA damage from ionizing radiation, the cell can cease dividing completely. Cellular stress causing DNA damage is accurately monitored by cell cycle control, repair and cell fate mechanisms to ensure correct repair or disposal of a faulty cell. Cancer cells in general tend to have mutations in genes associated within the control mechanism steps. One of the most extensively studied is p53 because of its multifunctional role in cellular mechanisms leading it to be considered as ‘the guardian of the genome’ if subjected to any type of damage. P53 is a tumour suppressor gene and is the most commonly mutated in most cancer types<sup>54</sup>. Recent evidence suggests that even though loss of function TP53 could result in carcinogenesis, mutated TP53 with gain of function results in more aggressive cancer types using mouse models<sup>55</sup>. This was shown to influence the correct homeostasis of tissues, and allows for tumour growth and spread.

Due to increased proliferation rate, tumour cells tend to be more radiosensitive than normal cells (if they remain normoxic)<sup>30</sup>. This is due to the high rate of passage through the cell cycle. Therefore, samples from cancer cohorts are generally more radiosensitive than those from healthy donors. For example, the majority of PCa cases show mutated P53 (a crucial tumour suppressor gene) which results in the accumulation of inactive P53<sup>56</sup>. P53 is therefore crucial in regulating radiosensitivity, and reinstatement of mutated P53 to wild type P53 in tumours could potentially increase radiosensitivity and sensitize

cells to radiation<sup>57</sup>. The crucial role of P53 in radiosensitive cohorts will be investigated later in this thesis.

Targeting cellular sensitivity or resistance are key radiobiological mechanisms which are manipulated for therapeutic gain.

#### **1.4. Cellular Sensitivity to radiation**

Cellular radiosensitivity is affected by many factors which can be subdivided into individual intrinsic genetic differences (radiosensitive phenotypes described previously) as well as experimental test model and conditions. In 1989, Sanford *et al* reported a number of experimental conditions that affected the *in vitro* radiosensitivity of human skin fibroblast cultures which included pH and temperature, cell culture medium batch, cell density of cultures used and bacterial contamination<sup>58</sup>. Although the molecular mechanisms of individual intrinsic radiosensitivity are currently still poorly understood, it is known that gender, environmental and lifestyle factors such as diet and exercise can play a huge role<sup>59</sup>.

##### 1.4.1. Types of DNA damaging agents

Up to 10,000 natural errors in DNA replication can happen in mammalian cells each day<sup>60</sup>. Cells are also continually exposed to different exogenous agents that can further compromise the genome. To cope with such a high rate of DNA damage, the cell has its own comprehensive DNA repair system which responds to various endogenous and exogenous DNA damage each day. The cell is able to cope with exogenous damage (which causes single strand break (SSB) and DSB) by using the highly specialised repair systems for SSB repair and DSB repair processes (discussed more later). The list of damaging agents is much larger than what is described in this section. The main types of DNA damage with relevance to disease and mutagenesis include chemical agents, UV and ionizing radiation (IR) insults. Figure 1.2 shows examples of DNA damaging agents

with lesion types, cell checkpoint control by checkpoints and the array of downstream cellular changes that can occur due to damage.

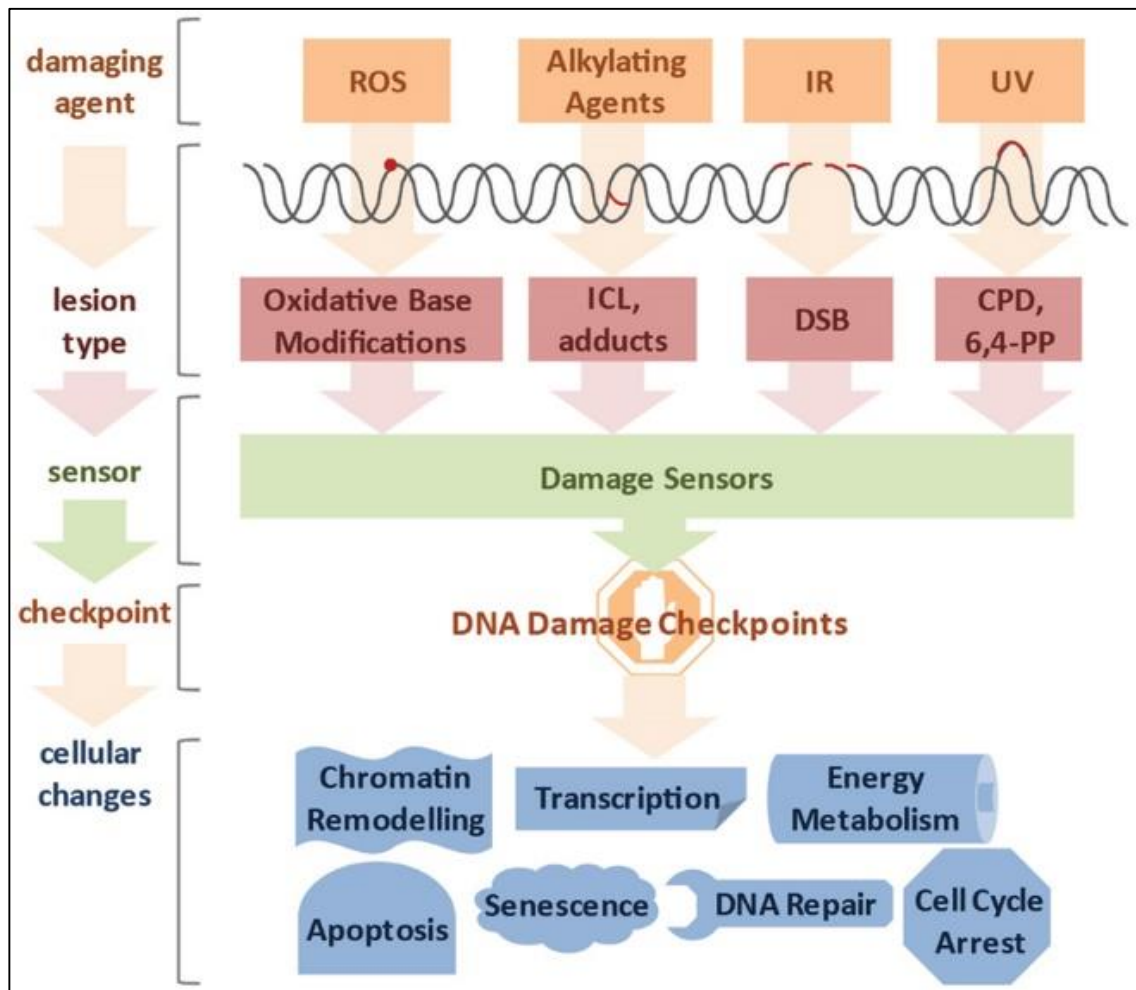


Figure 1.2 Examples of DNA damaging agents. Base modifications, adducts, Double strand breaks (DSB) and cyclobutane pyrimidine dimers (CPD) are defects caused by Reactive oxygen species (ROS), alkylating agents, ionizing radiation (IR) and ultraviolet (UV) irradiation. The cell has a DNA damage and repair system (DDR) capable of detecting and repairing the damages mentioned, or changes the cells fate.

DNA can be damaged through Reactive oxygen species (ROS) as a result of metabolism of oxygen within the cell. Normally, ROS is a natural part of oxygen metabolism within the cell, but when an accumulation of ROS results from e.g. IR, homeostasis of the cell is disrupted and ROS can affect the DNA structure, as well as react with amino acids and other enzymes within the cell. These type of highly reactive molecules can cause DNA damage by modifying DNA bases, producing inter-and intra-strand crosslinks, protein-DNA crosslinks and SSB's and DSB's respectively<sup>61</sup>. ROS can be produced through the indirect interaction of radiation particle tracks with water molecules. Reduction of oxygen can produce superoxide, which serves as a precursor for other reactive species. A three step pathway converting hydroxyl radical to hydrogen peroxide, superoxide and ultimately back to oxygen takes place<sup>62</sup>.

The most notable alkylating agents which cause DNA damage are well established anti-cancer drugs, which are mostly methylating agents forming adducts at the N and O atoms in DNA bases<sup>63</sup>. More commonly used anti-cancer drugs like chlorambucil are bifunctional alkylating agents which produce more complicated DNA lesions and require a more robust DNA repair mechanism. The primary adducts are repaired through methyl-guanine DNA methyl transferase (MGMT) but secondary adducts like inter-strand crosslinks require nuclear excision repair (NER) factors, DNA repair endonuclease (XPF), FA and HR<sup>64</sup>.

The effects of DNA damage through UV and its influence in skin cancer are well studied. Direct or indirect irradiation of DNA through UVB range (230nm – 320nm) or artificial UVC (254nm) range causes dimerization of pyrimidines which leads to the formation of *cis-syn* cyclobutane pyrimidine dimers (CPD's) and pyrimidine pyrimidone photoproducts<sup>65</sup>. UVA and UVB can also cause the formation of oxidised bases such as 8-oxo-7, 8-dihydro-2'-deoxyguanosine (8-oxodG)<sup>66</sup>. The formation of 8-oxodG is rapidly

repaired by the cells repair systems, but CPD's are more persistent DNA lesions and can potentially lead to mutagenesis<sup>67</sup>. These lesions are commonly attributed to the mutagenic causes of melanoma.

The most relevant DNA damage causing agent in this thesis is IR at both the clinical radiobiological and radio therapeutic level. Damaging effects of IR come from its ability to ionise or eject electrons from molecules within the cell<sup>68</sup>. The ejected electrons can then set of a chain of ionizing events causing further damage within the traversal track of irradiation and causing clusters of DNA damage<sup>69</sup>. Therefore, DNA damage from IR can be either direct or indirect (Figure 1.3). Direct damage to DNA is caused when photons interact directly with the DNA structure, causing damage to the sugar-phosphate backbone and strand breaks. Although the cell has specialised repair processes to repair DNA damage, clustered strand breaks which are induced by IR are more difficult to repair. Evidence from early work by Warters and Hofer in 1977 show that DNA is the critical target of IR induced cell killing as they used alpha particles produced by small polonium needles to irradiate only the plasma membranes and cytoplasm of the cell but not the nucleus where DNA is housed, and the cell was able to recover and survive<sup>70</sup>.



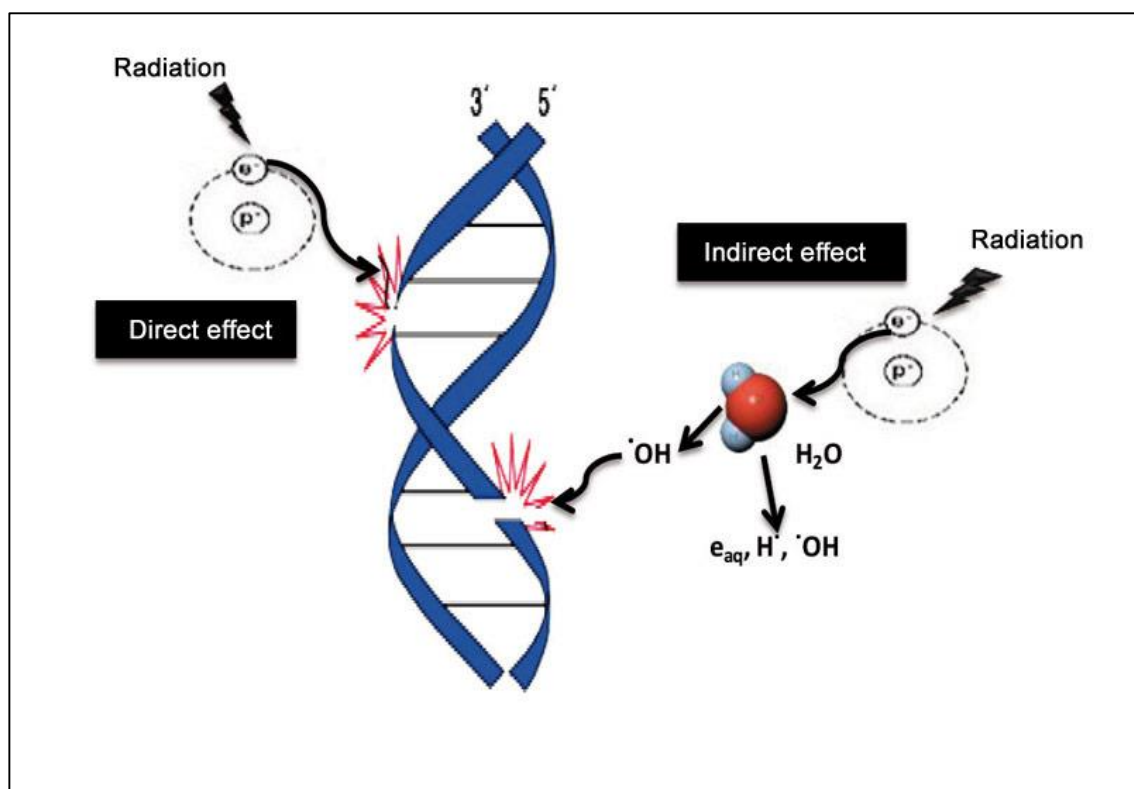


Figure 1.3 Illustration depicting the direct effect of ionizing radiation and the indirect effect on the DNA double helix structure and interaction with water molecules respectively. Image taken from Montoro *et al* <sup>71</sup>.

Non targeted effects of radiation include radiation induced bystander effects (RIBE) and genomic instability (GI). Abscopal and bystander mediated adaptive response (AR) are subdivisions of bystander effects<sup>72</sup> which although are of extreme importance are beyond the scope of this body of work.

#### 1.4.2. Types of DNA damage

As already discussed in the previous section, DNA is damaged and repaired daily in mammalian cells. Table 1.1 shows examples of the main DNA damage insults in terms of rate of occurrences of each. In the United States of America, 90% of lung cancer cases are attributed to smoking<sup>73</sup>. For example, a  $\beta$ -unsaturated aldehyde called Acrolein is thought to be the most important factor of cigarette smoke which can easily penetrate through the cell membrane and bind to the N<sup>2</sup> amine of deoxyguanine (dG) which is then

followed by cyclization of N<sup>1</sup> which forms DNA adducts  $\alpha$ -hydroxyl-1, N<sup>2</sup>-propano-2'-deoxyguanine ( $\alpha$ -HOPdG) which is a major DNA damage type responsible for mutagenesis of cells caused by smoking<sup>74</sup>. This is of relevance for this work as smoking has been included in the analysis from donors in chapter 2.

Table 1.1 Examples of rate of DNA damaging agents and rate of occurrences daily in human cells. Adapted from Bernstein and Prasad<sup>60</sup>.

<u>DNA Damages</u>	<u>Reported Rate of Occurrences</u>
Oxidative	10 - 11500 per cell per day in humans
Specific oxidative damage products: 8-hydroxyguanine, 8-hydroxydeoxyguanosine, 5-(hydroxymethyl) uracil	2,800 per cell per day in Humans
Depurinations	10,000 per cell per day
Depyrimidinations	Up to 700 per cell per day
Single Strand Breaks	55,200 per cell per day
Double Strand Breaks	up to 50 per cell cycle in Humans
O <sup>6</sup> Methylguanine	3120 per cell per day
Cytosine Deamination	192 per cell per day

Of the types of DNA damage mentioned, the most relevant is SSB and DSB which are caused by IR. The SSB is the most common form of DNA damage occurring from endogenous (replication errors) and exogenous agents (Chemotherapeutic drugs, UV), with upwards of 55,000 events per cell per day (Table 1.1). This form of DNA damage is not as serious in terms of cellular fate, as the SSB repair (SSBR) system deals with the insult quite efficiently using the non-damaged DNA strand as a template for repair (discussed more later).

However, the DSB is more fatal as it involves breakage of both DNA strands and can lead to genomic instability. The DSB is mostly formed by exogenous sources like IR (most

relevant to this thesis) or endogenous enzymatic processing of collapsed replication forks or inter/intra-strand crosslinks (usually in S phase)<sup>75</sup>. This one ended DSB which is caused in S phase, is usually repaired by HR with the Fanconi Anemia proteins and ATR pathways<sup>76,77</sup>. In response to DSB damage the cell has two major mechanisms built to attempt to repair the DSB, namely HR and NHEJ pathways.

#### 1.4.3. Damage Recognition and signal propagation

The initial events which follow a DSB have been under intense investigation for many years, with conflicting theories. It has now been recognised that the very earliest event (even before recruitment of sensor proteins to the site of damage) is relaxation of the chromatin, which through acetylation of histone H4 would allow for the recruitment of DNA damage sensor and repair proteins and allow for checkpoint functions<sup>78</sup>. Figure 1.4 shows a schematic of events which happen in the basal state. In normal conditions, histone H4 is kept inactive through deacetylation by a protein called males-absent on the first (MOF) and another 60kda tat interacting protein (TIP60) (histone acetylases). Levels of ATM are kept at a relatively low level through the action of dephosphorylation and downregulation of TIP60 and activating transcription factor 2 (ATF2).

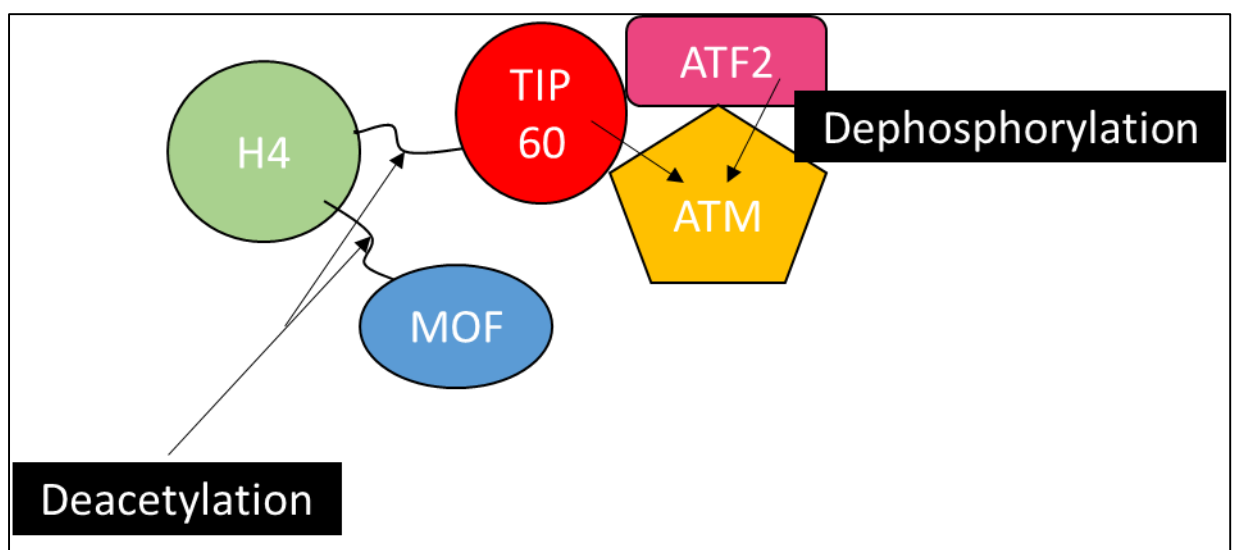


Figure 1.4 Interplay of factors in the basal state before DSB occurrence. Histone H4 (H4) is kept inactive through deacetylation by 60 kDa interacting protein (TIP60) and males absent on the first (MOF). Ataxia telangiectasia mutated (ATM) levels are kept low through TIP60 and Activating transcription factor 2 (ATF2).

Proteins involved in all cellular pathways undergo conformational changes when switched ON or OFF, through phosphorylation or dephosphorylation by kinases or phosphatases respectively. This allows for highly efficient and rapid cellular mechanisms<sup>79</sup>.

When a DSB occurs through IR, increase in H4 acetylation occurs which allows relaxation and mobilisation of heterochromatin protein 1 (HP1) bound to H3 (required by phosphorylation). Schematic of events are demonstrated in figure 1.5. Much like thread wrapped around a spool, cellular DNA is tightly bound to core histone proteins (H2A, H2B, H3 and H4) and linker (H1 and H5) histone proteins, which are subject to chemical modifications primarily through phosphorylation, methylation and acetylation but also ubiquitylation, SUMOylation and ribosylation (reviewed by Rothbart and Strahl<sup>80</sup>). Tip60 becomes activated when bound to unmasked H3 which is recruited into foci requiring the MRN complex. Poly ADP ribose polymerase (PARP) 1 and 2 are activated upon binding to SSB or DSB's and this allows for phosphorylation of ATM, collaboration of PARP with Ku and DNA protein kinases (DNA PK's). The recruitment of amplified in liver cancer 1 (ALC1) and nucleosome remodelling deacetylase (NURD) allow for chromatin remodelling<sup>81</sup>. ATM can be phosphorylated at very distant sites away from the DSB, through phosphorylation or autophosphorylation, which can then in turn phosphorylate the well-known histone H2AX (H2AX) becoming  $\gamma$ H2AX. Phosphorylation and activation of H2AX is one event of many which happens in response to DNA damage "sensor" activity. A large recruitment of proteins and protein complexes to the site of SSB or DSB are most commonly grouped into 3 pathways; 1) MRN – ATM protein pathway, 2) DNA – protein kinases (PKcs) – KU pathway and– 3) ATR - ATR interacting protein (ATRIP) pathways.

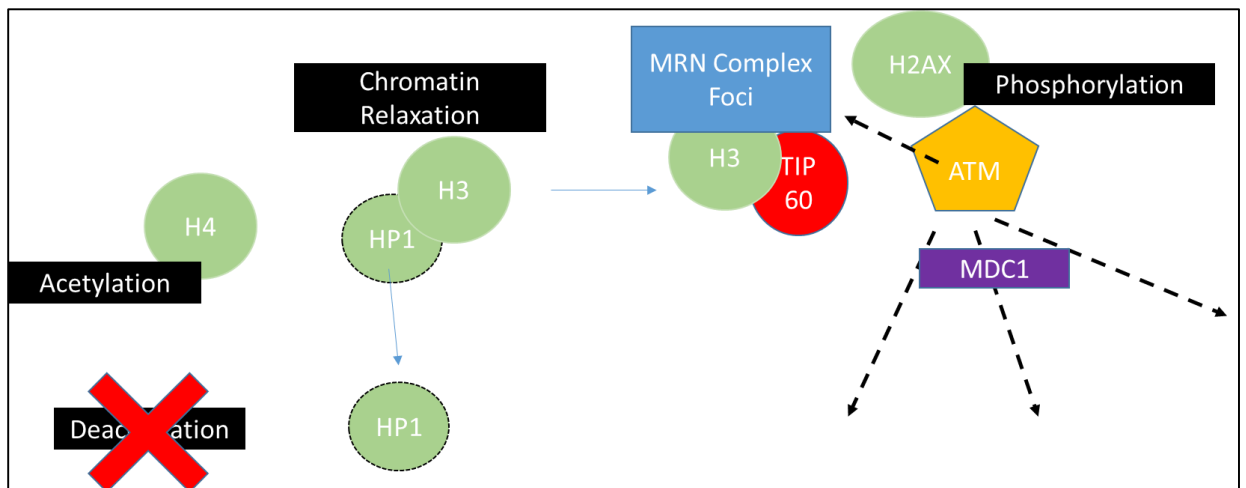


Figure 1.5 Sequence of signalling events after a DSB occurs. Histone H4 (H4) is acetylated which allows for chromatin relaxation and mobilisation of Histone protein 1 (HP1) bound to Histone H3 (H3). This allows for association of H3 with 60 kDa interacting protein (TIP60). H3 and TIP60 then become incorporated into the MRN complex (which consists of MRE11, RAD50 and NBS1) and this allows for recruitment of Ataxia telangiectasia mutated (ATM) and phosphorylation of Histone H2 A (H2AX). Recruitment of MDC1 allows for signal spread and propagation to distant sites.

#### 1.4.3.1. ATM - MRN

The first and most studied sensor pathway is the ATM – MRN pathway. The MRN complex is recruited to ATM, (through Tip60/ATF2 as previously mentioned) and consists of DSB repair proteins in a complex MRE11, RAD50 and NBS1. NBS1 has a key role of directly binding to ATM and takes it to the site of the DSB. The gene of the NBS protein was found to be mutated in Nijmegen Breakage Syndrome, and patients show similar symptoms to that of ATM patients<sup>82</sup>. Defects in DSB repair, radiosensitivity and immuno – compromise are some of the symptoms. Therefore, when NBS is mutated, defective or inactivated, the individual is found to be radiosensitive and lacks the appropriate DNA repair machinery required for efficient DNA damage sensing and repair. The MRN complex is important in sensing damage to DNA and recruiting ATM, but evidence suggests that it is also important in processing the DSB. It does this through digestion of incompatible ends of broken DNA that cannot be ligated. ATM is present in

every cell in its inactive form and becomes activated when it comes in contact with the DSB, brought by the MRN complex, which in turn causes the phosphorylation of signalling proteins such as H2AX. H2AX can be described as an “amplifier,” as this signal can spread over a relatively large area of chromatin in both directions of the DSB with the help of the MDC1 protein. This signal “spread” allows for recruitment of other repair machinery to become activated within the cell and localisation around the DSB<sup>83</sup>. How ATM is inactivated or why it is activated in response to non – DNA damaging events such as osmotic shock and chloroquine is not yet known, but reiterates that ATM is a core protein responsible for many functions of which are not yet known<sup>83</sup>. There are also reports of how ATM could be activated in three forms, ATM<sup>S367A</sup>, ATM<sup>S1893A</sup> and ATM<sup>S1981A</sup> corresponding to the serine phosphorylation sites on ATM, and evidence suggests that after IR, not all 3 forms are activated together (ATM<sup>S1983</sup> is less responsive to IR), suggesting yet further roles for ATM within the cellular response to irradiation<sup>84</sup>.

The importance of ATM in DNA damage checkpoints was clearly outlined with the discovery of ATM gene in ATM deficient patients. Without this protein, patients exhibit symptoms such as poor immunity, increased risk of cancer, and poor motor control of muscles. This showed that not only was the ATM checkpoint important in regulating the cell cycle and stalling cells, it was also important in the interaction between other checkpoints or proteins separate from the cell cycle<sup>85</sup>. AT patients exhibit symptoms of elevated radiosensitivity to the damaging effects of ionizing radiation.

#### 1.4.3.2. DNA – PKcs - KU

When ATM is inhibited, it has been shown that limited DNA repair can take place through an alternate pathway. This pathway, known as the DNA dependant protein kinase catalytic subunit (DNA – PKcs) interacts with Ku heterodimers to also activate a pathway which allows for phosphorylation of H2AX. The pathway is involved in DSB detection

and repair through the non-homologous end joining (NHEJ) pathway and is structurally similar to ATM. It has a similar role to the ATM pathway, and needs to recruit a further complex to “sense” damage. It does this through the Ku70/Ku80 complex which on binding to DSB ends allows recruitment of DNA – PKcs and phosphorylation of H2AX<sup>86</sup>.

#### 1.4.3.3. ATR - ATRIP

ATR – ATRIP is the third known kinase which is able to phosphorylate H2AX. So far it has not been implicated into the direct pathway associated with DSB, but it has been known to become activated in response to other forms of DNA damage, such as SSB and replication fork errors. When DNA polymerase enzymes stall in response to strand damage, replication continues along the single strand of DNA, a single strand binding protein replication protein A (RPA) binds to the DNA and recruits the ATR – ATRIP complex, which interacts in response to loading of proliferating cell nuclear antigen (PCNA) related 911 by cell cycle checkpoint protein RAD17 clamp loader<sup>83</sup>. ATR - ATRIP acts as the sensor of damage. Although not known to act in the earlier events of DSB, ATR is known to become activated with the MRN (MRE11/RAD/NBS1) processing of broken incompatible DNA ends. Therefore, ATM can activate ATR in a downstream pathway which can phosphorylate various other proteins to act in the DDR. ATR has also been shown to activate components of effector pathways and cell cycle checkpoints, therefore these actions are dependent on ATR activity<sup>83</sup>. Sensors such as MRN, PARP detect the damage at the damage site, and the signal is further propagated by transducers (to include ATM, DNA PK’s, ATR-ATRIP, BRCA etc.). When the signals of damage are propagated, effector proteins (XRCC4, RPA, retinoblastoma binding protein 8 (Ctip)) are phosphorylated to determine activation of effector pathways, whether it be cell cycle checkpoint activation, cell death or repair (Figure 1.6).

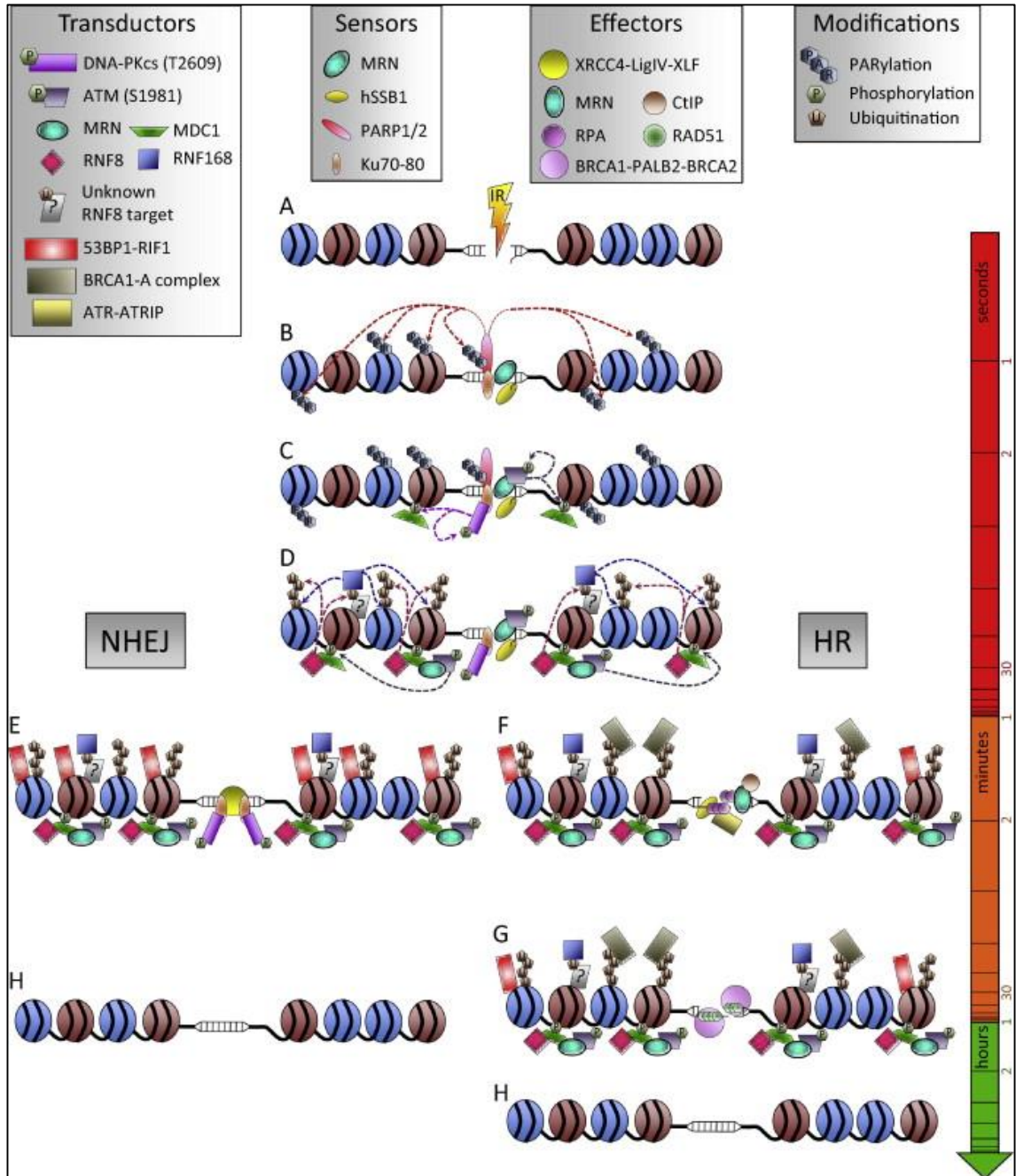


Figure 1.6 Overview of DSB signalling with a timescale of events which occur in the DDR cascade. Sensor proteins such as PARP recognise the DSB immediately, while the MRN complex is recruited and causes phosphorylation of ATM and  $\gamma$ H2AX. The signal is propagated to cause activation of cell cycle checkpoints and a decision is made for which type of repair will take place (either HR or NHEJ) which is influenced by many factors including cell cycle stage etc. (discussed in text later). Image taken from Vignard *et al*<sup>87</sup>. A-H outlines the process in terms of seconds to minutes and then hours.



#### 1.4.4. Cell Cycle Checkpoints

The DDR works by sensing and transducing signals of damage effectively to halt the cell cycle and allow for the appropriate repair mechanisms to occur. The cell cycle consists of 4 distinct phases (Figure 1.7). DNA is replicated during S phase, condensed into chromosomes in late G2 phase and then undergoes division in M phase. The S phase is sensitive to a DNA damage checkpoint, under the control of ATM/ATR, Chk1/2, cyclin dependent kinase inhibitor 1 (P21) and P53 (Figure 1.7). Two gap phases (G1 and G2) are present to prepare for both S and M phase respectively. During G1 phase, the cell grows and prepares proteins essential for DNA synthesis in S phase. In response to DNA damage, ATM/R is activated to phosphorylate p53 and activate p21 which inhibits the progression of the cell in the cell cycle through cyclin D – cyclin dependent kinase (CDK4) action. In G2 phase, the cell also grows and prepares for cell division in mitosis, when threshold levels of cyclinB1/CDK1 have been reached. There are two checkpoints associated with G2 – M cycle entry, an early and a late checkpoint.

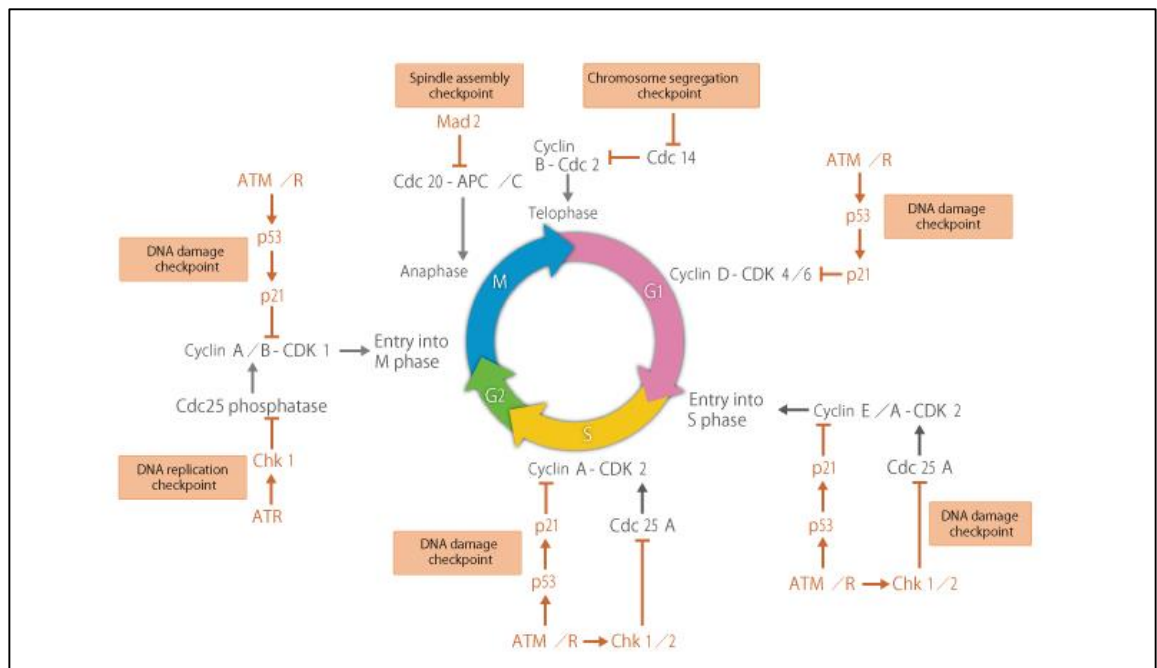


Figure 1.7 Overview of cell cycle checkpoints in response to various cellular stresses. The spindle assembly checkpoint, chromosome segregation, DNA damage, and DNA replication checkpoints are shown. Image taken from Makoto *et al*<sup>881</sup>.

There is also a quiescent phase G<sub>0</sub>, in which cells can exit the cell cycle and stay in this phase until resuming their proliferating capacity. Some cells may permanently stay in G<sub>0</sub> phase of the cell cycle until they or the organism dies. Of a 24hr cell cycle, interphase occupies 23/24hrs, while mitosis lasts approximately 1hr<sup>88</sup>.

The cell cycle is controlled by extracellular signals and the external environment of the cell. If conditions are favourable and the appropriate signals are in place, the cell will progress through the cell cycle. Cell cycle checkpoints are located in G<sub>1</sub>/S, intra S phase and G<sub>2</sub>/M phases of the cell cycle (figure 1.7). At each checkpoint, complexes of cyclin

proteins and partner cyclin dependant kinases (CDK's) are involved in maintaining and regulating the progression of a cell through each phase of the cell cycle.

The G1 phase checkpoint functions to facilitate the activation of checkpoints and progression of the cell through the G1 to S phase of the cell cycle and is brought about by the control of E2F transcription factor by the retinoblastoma protein (RB). The process begins through phosphorylation events of RB by G1 cyclin – CDK's. After irradiation, this can be prevented by ATM activity. ATM can activate p53, which can in turn up-regulate the gene CDK1 p21 (CDKN1A). This inhibits cyclin – CDK complexes in G1 phase, preventing phosphorylation of RB and therefore preventing the activation of E2F, which will in turn stop the cell at this checkpoint and phase in the cell cycle. Therefore, the cell will have delayed entry into S phase until repair and normal conditions are stabilised.

The S phase checkpoints are regulated by checkpoint genes CHK2 and CHK1. These can be activated by phosphorylation by ATM and ATR respectively. To prevent cells from progressing to G2 after S phase, the CDK2 kinase must be dephosphorylated. This is regulated by a protein known as cell division cycle 25A (CDC25A) and CDC25C phosphatases. CHK1 and CHK2 become activated and can phosphorylate CDC25A and CDC25C which leads to degradation of CHK1 and CHK2. When activated by ATM and ATR, an increase in CDK2 follows and this slows progression from S to G2 phase. Other proteins have been implicated into this response, including the well-known BRCA1 and BRCA2. ATM/ATR checkpoint regulation was recently reviewed by Reinhardt and Yaffe, 2009<sup>89</sup>, who describe an emerging third effector pathway that involves MAPK-activated protein kinase 2 (MK2) and shares substrate homology with CHK1/2 to arrest the cell cycle.

There are two G2 phase checkpoints; the early and late G2 checkpoints. The early G2 checkpoint is related to cells that are irradiated in the G2 phase of the cell cycle and can be activated by even low doses of irradiation. This results in a G2 block. It works through ATM – CHK2-CDC25A/C signalling and targets mitotic cyclin B – CDK1 complex. This complex must be dephosphorylated to become activated. This checkpoint stops progression of cells in G2 phase into mitosis and therefore explains why there is a drop in mitotic cells shortly after periods of irradiation<sup>90</sup>. The late G2 checkpoint (also known as the Sinclair checkpoint, after Warren Sinclair<sup>91</sup>) is a longer delay checkpoint and it applies to those cells which may have been irradiated in G1 or S phase that managed to progress in the cell cycle. These cells have a prolonged delay before mitotic entry and are a result of higher doses of irradiation<sup>92</sup>. In addition to higher doses of irradiation causing G2 inhibition, G2 block has been observed in cells irradiated with high LET irradiation. One of the earliest reports of prolonged G2 arrest following high LET irradiation was by Lücke–Huhle *et al* in 1979 who showed a much more perturbed cell cycle progression after high energy, high LET irradiation compared to x-ray irradiation<sup>93</sup>. This checkpoint is also ATM independent and utilises ATR – CHK1 – CDC25C signalling.

#### 1.4.5. Cell Fate after DNA damage

The fate of a damaged cell has various endpoints in response to radiation. A number of repair pathways are in place to help repair the damaged DNA when the cell cycle has been stopped by the appropriate checkpoint. These pathways include SSB repair mechanisms which include mismatch repair (MMR), base excision repair (BER), NER and DSB repair mechanisms which include NHEJ, HR, FA pathway (in response to intra strand crosslinking) and repair of bulky adducts using trans-lesion synthesis (TS) in response to production of thymidine dimers caused by UV irradiation. If the cell is too badly damaged and the correct repair mechanisms are not faulty, the cell will commit to a programmed cell death pathway such as apoptosis. Other forms of cell death include

Necrosis, Apoptosis, Mitotic catastrophe, autophagy and replicative senescence. If mutations exist in the repair or cell death machinery, problems such as genomic instability and carcinogenesis arise. Each cell fate pathway will be discussed in the following subsections.

#### 1.4.5.1. DNA Repair processes

As explained previously, there are a number of specialised repair mechanisms in place to repair the damaged cell and these mechanisms are specific to the different types of DNA lesions. The repair mechanisms employed for SSB are BER, MMR and NER. On recognition of chemically modified bases, the NER pathway involves glycosylases which can catalyse the cleavage of the base-sugar bond creating an apurinic/apyrimidinic (AP) site on the DNA structure to release the damaged base, and proceeds to repair either through short or long patch repair<sup>94</sup>. After DNA replication, MMR corrects mismatched bases on the newly synthesised strand by recognising strand specific “nicks” on the damaged site, which are recognised by the Mutator S (MutS) protein and form a complex with the MutL protein, further recruiting MutH forming a DNA loop, which allows for the excision of the incorrectly matched base along with several other bases and synthesis of a new strand by DNA polymerase and ligation<sup>95</sup>. NER is a specialised repair pathway capable of repairing damage which is caused by UV irradiation. CPD lesions (as described in previous sections) are firstly recognised by damage specific DNA binding protein 1 and 2 (DDB1 and 2), xeroderma pigmentosum complementation group c (XPC) and repair can take place via two pathways; global genomic repair (GGR) and transcription coupled repair (TCR) through the action of RNA polymerases which ultimately protects the genome from carcinogenesis from UV damage to an extent<sup>96</sup>.

Of primary relevance in this thesis with regard to DSB repair after IR, are two pathways; HR and NHEJ. Although figure 1.8 demonstrates the prime differences between NHEJ

and HR, it is important to note that there may be interplay between these pathways. It should not be assumed that all simple DSB are repaired by NHEJ and all complex damage is repaired by HR. Complex damage can be clustered (two or more lesions formed within two helical turns of the DNA by a single radiation track) or complex DSB (additional lesions close to the ends of the DSB)<sup>97,98</sup>.

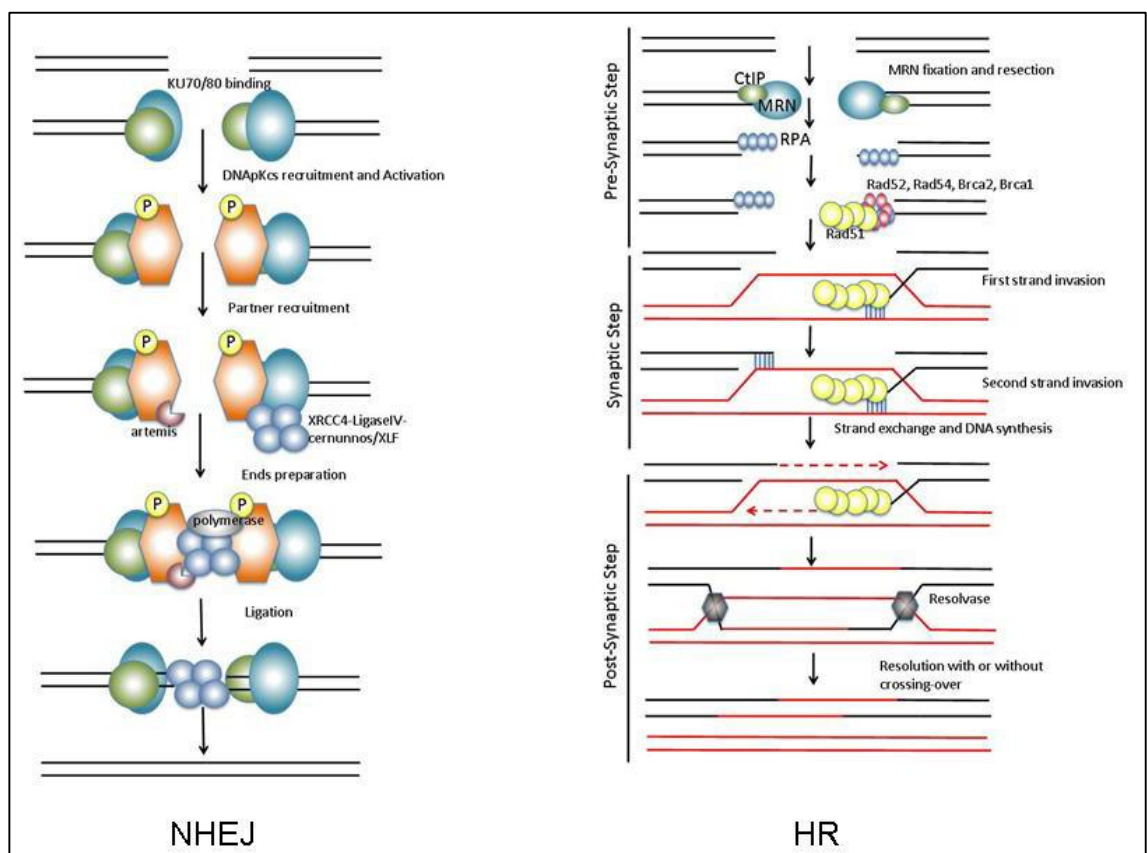


Figure 1.8 Non homologous end joining (NHEJ) and Homologous Recombination (HR) pathways. NHEJ is a rapid process, involving DNA protein kinases (DNA PKcs) and recruitment of factors such as XRCC4, Cernunnos and Artemis. The process ends with direct ligation of the two broken strands. HR is a more accurate pathway involving a base homology search on a sister chromatid through strand invasion and DNA synthesis of a new strand for repair. Image taken from Renodon-Cornière *et al*<sup>99</sup>.

Using a homologous sister chromatid as a template strand, HR can synthesise a new strand and ligate strands together to restore genomic stability, a process which is slower but much more accurate than NHEJ (Figure 1.8). In mammals, the process begins with sensing of the break by MRN and coating of the exposed single strand DNA (ssDNA) with RPA and recombination mediator proteins (RMP's) such as BRCA2, which allows for Rad51 to form a nucleoprotein filament on ssDNA, performing a base homology search and initiates strand invasion on sister chromatids<sup>100</sup>. After resection from 5' to 3' takes place by exonucleases, strand invasion, or a "D – loop" forms, and synthesis of a new strand takes place by DNA polymerases, identical to the sister chromatid sequence, and formation of a "holiday junction." How this holiday junction is resolved or cut is not fully known, but recent evidence suggests that BLM binds in a complex with topoisomerase III alpha ( TopIIIa) and BLM associated protein of 75kDa (BLAP75), which allows the complex to push the entangled holiday junction strands closer together and untangles DNA by TopIIIa, leaving only a small crossover region of DNA and ligation of broken ends are resolved by ligase1<sup>101</sup>.

NHEJ is a more rapid technique yet less accurate as there are no homology requirements and broken DSB ends are literally bound together (Figure 1.8). The choice of whether to use NHEJ rather than HR is still under intense investigation; however, the most plausible reason why NHEJ would be preferred is if a homolog is not available for HR to take place. It is known that HR is the preferred pathway for DSB repair in lower eukaryotes including yeast, but NHEJ is the preferred pathway in higher eukaryotes such as mammalian cells<sup>102</sup>. When NHEJ responds to a DSB, the initial event is the binding of Ku heterodimer and this (Ku70/80) is thought to bind to DSB ends within milliseconds after irradiation with a huge binding affinity for DNA ends<sup>103</sup>. When Ku is anchored to DSB ends, it serves as a scaffold for loading of DNA-PKc's X-ray cross complementing protein 4 (XRCC4), DNA ligase IV, XLF, aprataxin and PNK like factor (APLF)<sup>104</sup>. Evidence suggests that

in order for this Ku – DNA-PKc complex to become activated, it requires the presence of DNA and cannot be activated without DNA binding<sup>105</sup>. Non-specific processing of DNA DSB ends is protected also by Ku70/80 which is important as this could lead to chromosomal aberrations and genomic instability if allowed to proceed. A filament is created using XRCC4 and XLF which bridges the two ends of the DSB for stability and docking of further substrates<sup>106</sup>. After stabilisation occurs, the ends of DNA need to be stuck together and this is done with various enzymes depending on how much damage is caused. Factors that are recruited include artemis, PNKP, APF, Polymerases  $\mu$  and  $\lambda$ , Werner, Aprataxin and Ku<sup>104</sup>. Complexes of Artemis, Werners Syndrome gene (WRN) and APLF resect the DNA DSB ends which may require the phosphorylation of ATM and DNA PKc's by Artemis<sup>107</sup>. Finally, ligase IV can ligate the broken ends by becoming adenylated by XRCC4 which promotes ligase IV activity<sup>108</sup>.

#### 1.4.5.2. Cell Death mechanisms

If cell damage is substantial, cell death via a number of pathways can occur. Cell death pathways associated with various forms of cellular stress include Necrosis, Apoptosis, Mitotic catastrophe, autophagy and replicative senescence.

Necrosis is a more chaotic form of cell death, usually in response to cellular trauma which results in autolysis. Usually, necrosis results from extreme conditions, such as extreme temperature increase or decrease (frostbite), or exposure to extreme doses of IR radiation. At these high levels of IR, the damage is irreversible and often fatal<sup>109</sup>.

First noted by Hayflick in early 1960's using human fibroblasts, cellular senescence is a type of cell "ageing" described as an inability of proliferation regardless of nutrient abundance<sup>110</sup>. This is known as the Hayflick limit, in which cells reach their proliferative capacity through serial shortening of telomeres and either die through apoptosis or enter a senescent state, which is a protective mechanism against tumourigenesis<sup>111</sup>. Premature



senescence on the other hand can be induced by a variety of cellular stresses, such as ROS, IR and UV irradiation, which ultimately acts as a tumour suppressor mechanisms to prevent cellular damage from being carried through the progeny of cells<sup>112</sup>. It is thought that in response to DNA damage, two pathways can be activated to arrest cells in a senescent state; the first is the p53/p21 pathway and the second involves p16/pRB<sup>113</sup>.

Mitotic catastrophe should not be misinterpreted as a failure of the cell to complete mitosis, it is more likely a result of aberrant chromosome segregation or DNA damage during mitosis and it is most commonly associated with IR induced cell death<sup>114</sup>. 3 models of mitotic catastrophe have been presented; the first abnormalities in mitosis allows for increase of cyclin B1 levels and cell death machinery before the cell has exited mitosis, the second model allows for the cell to exit mitosis and then die in interphase of the next cell cycle (which can happen quickly or delayed, such like the radio-induced cell death years after RT), and finally the third model demonstrates activation of senescence irreversibly inactivating the damaged cell<sup>115</sup>. Mitotic catastrophe has been manipulated for therapeutic gain from the use of anticancer agents (such as taxanes and alkaloids) which bind to tubulin and disrupt the mitotic spindle<sup>116</sup>. The process aims to effectively disable or eliminate cells with aberrant chromosomal structures, thus preventing oncogenesis.

Autophagy is a metabolic process which functions in the destruction of cells within the body. The process is capable of regulating cellular homeostasis through recycling of proteins in the degradation process. Recently, a study demonstrating inhibition of autophagy showed a downscale of proteins involved in the homologous recombination and non-homologous end joining DNA repair pathways in response to nuclear irradiation<sup>117</sup>.

Finally, apoptosis is the last mentioned form of cellular death and is the most studied with relation to radiobiology and cancer research. P53 is a central player in initiating apoptosis, as it is regulated by mouse double minute homolog (MDM2). P53 is continually synthesised but degraded by ubiquitylation by the proteasome. When ATM is activated in response to DNA damage, P53-MDM2 is phosphorylated and stabilised. P53 can then up-regulate pro-apoptotic genes such as BCL2 associated X protein (BAX) and P53 upregulator of apoptosis (PUMA). Two pathways were originally described for the activation of apoptosis. First, the extrinsic pathway (binding of death ligands such as tumour necrosis factor receptor superfamily (FAS), tumour necrosis factor (TNF) and others to the death receptor is mediated through the death inducing signalling complex (DISC) and initiator caspase 8 activation to execute apoptosis by executioner Caspase 3. The second, 'intrinsic pathway' is initiated by a variety of toxicants including IR where the mitochondria are the direct target. Cytochrome C is released from the mitochondria which interacts with Apaf1 and initiator caspase 9 to form the Apoptosome complex which activates executioner caspase 3 for apoptosis. More recently, a third pathway called the Perforin granzyme pathway has been explained which involves a caspase-dependent and -independent pathway - primarily with the immune response<sup>118</sup>. Both pathways are outlined in figure 1.9.

The extrinsic pathway involves binding of an extracellular ligand to a transmembrane death receptor which is a member of the TNF superfamily. The most common and well characterised ligand which can bind and activate these receptors are FasL, TNF-alpha, Apolipoprotein (Apo) 3L and Apo2L to corresponding receptors FasR, TNFR1, Death receptor 3 (DR3) and DR4/5 respectively<sup>119-121</sup>. Upon binding of pro-apoptotic ligands to the corresponding death receptor, aggregation of receptors and recruitment of the Fas-associated death domain (FADD) occurs<sup>122</sup>. Assembly of the DISC complex and further cleavage and activation of initiator pro - caspases (8 and 10) follows which causes a

caspase cascade of events resulting in digestion of DNA by caspase activated DNase (CAD) and proteolytic degradation of cellular proteins by executioner caspases 3 and 7<sup>123</sup>.

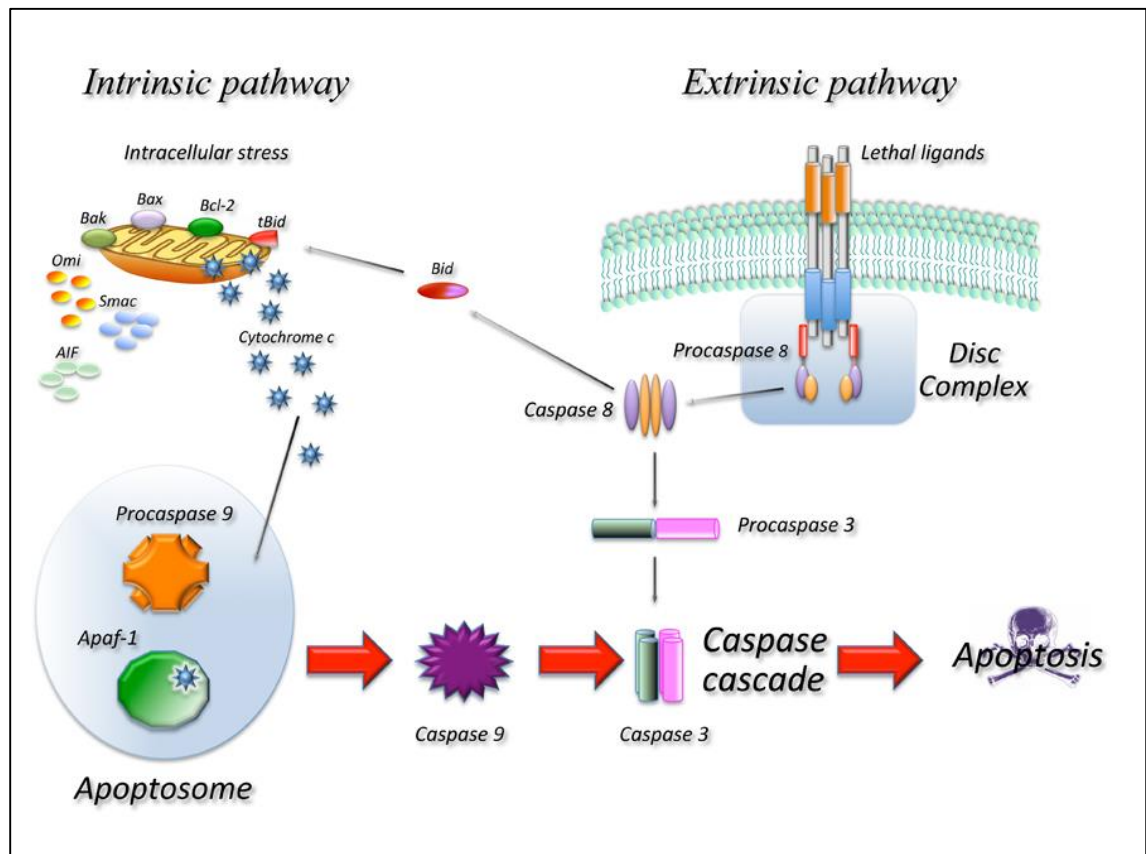


Figure 1.9 Simplified schematic of the intrinsic and extrinsic pathways of apoptosis. In response to intracellular stress (including Ionising radiation), release of apoptotic factors from the mitochondria which leads to formation of the apoptosome and cell death. The extrinsic pathway involves binding of an extracellular ligand such as TNF- $\alpha$ , FAS, Apolipoprotein (APOE). Following assembly of the death inducing signalling complex (DISC) and activation of procaspases, cell death occurs. Interplay between the two pathways has been studied. Image taken from Favoloro *et al*<sup>382</sup>.

The intrinsic pathway is initiated by signalling from various stress factors such as IR, which target the mitochondria and responds by releasing many apoptotic factors such as cytochrome c, apoptosis inducing factor (AIF), second mitochondria-derived activator of

caspases (Smac) from the mitochondrial intra-membrane space<sup>122</sup>. The pathway is dependent on the release of cytochrome C under the control of pro-apoptotic proteins BCL2, BCL2-associated – X protein (BAX) and Bcl2 homologous antagonist/killer protein (BAK) which operate in synergy with anti - apoptotic proteins Bcl2 and Bcl<sub>xl</sub>. Pro-apoptotic proteins initiate the release of cytochrome c from the mitochondria which binds to Apoptotic protease activating factor1 (APAF1) and pro – caspase 9 to produce the apoptosome (often referred to as the wheel of death). Caspase-3 is activated through the cytochrome-c/Apaf1/caspase-9 apoptosome complex<sup>122</sup>. Smac/DIABLO are antagonist proteins, released from the mitochondria in combination with cytochrome c and they promote caspase activation through inhibitory effects of IAPs by binding to inhibitors of apoptosis (IAP's) such as XIAP<sup>123</sup>.

In addition to the extrinsic and intrinsic pathways, a third pathway, the Perforin Granzyme pathway has been explained, which eliminates toxic cells by rapidly transporting perforin out of the cell to signal and deliver the pro apoptotic protease Granzyme into the cell to cause apoptosis<sup>118</sup>. The three pathways converge on the same terminal for the execution of apoptosis. One of the two subtypes of perforin-granzyme pathway; the granzyme B pathway is activated on cleavage of caspase 3, which results in DNA fragmentation, degradation of proteins, protein crosslinking, and expression of ligands for phagocyte uptake<sup>121</sup>. The granzyme A pathway has been shown to work independently from caspase activity, by nicking the DNA through DNase nucleotide diphosphate kinase (NM23-H1). NM23-H1 is important in immune surveillance which induces apoptosis therefore it is a tumour suppressor gene, which usually remains inhibited by the proto-oncogene SET. Granzyme A cleaves SET, which removes this inhibitory effect and leads to apoptosis through DNA fragmentation<sup>121</sup>.

Another apoptotic pathway was recently described that involves the endoplasmic reticulum (ER) responding to stresses such as pharmacological agents that block protein transports from ER to Golgi and inhibition of calcium uptake through sarcoplasmic/endoplasmic  $\text{Ca}^{2+}$ -ATPase<sup>124</sup>. Although poorly understood, one example of how this pathway regulates cell death is through the action of C/EBP homolog (CHOP)/ growth arrest and DNA damage (GADD)153 which can downregulate BCL2 and activate GADD34 and endoplasmic reticulum oxidoreductin (ERO)1 $\alpha$  encoding ER oxidase<sup>125</sup>. This stress can lead to the proteolytic cleavage of caspase 4 in human cells to activate apoptosis and evidence suggests crosstalk between this pathway and the mitochondria<sup>126</sup>, which would not be unusual due to the involvement of  $\text{Ca}^{2+}$ <sup>127</sup>.

#### 1.4.5.3. Genomic Instability and Carcinogenesis

Genomic instability (GI) is a hallmark of carcinogenesis which refers to the relative increase of genetic alterations or mutations within the cell lineage<sup>128</sup>. GI is subdivided into three categories, namely chromosomal, nucleotide, and microsatellite instability.

Most cancers display a form of genomic instability called 'Chromosomal instability' (CIN) which refers to the high rate of structural and numerical changes over time in cancer cells compared to normal cells. These changes were observed in cancer cells over 100 years ago<sup>129</sup>. CIN changes were sometimes found in all cells of a tumour, but not in all cells of other tumours, suggesting that the instability arises from one single unstable cell which acquires abnormalities over time<sup>130</sup>. 90% of human cancers exhibit CIN and aneuploidy, and are characterized by amplifications, deletions, loss of heterozygosity, translocations and inversions<sup>131</sup>. CIN develops early in cases of cancer, displays complex levels of heterogeneity among cell types and between individuals, and is associated with chemotherapeutic drug resistance which makes early detection of CIN important<sup>132</sup>. The molecular mechanisms of CIN are still poorly understood, as a large amount of instability

from a combination of genes within DNA damage and repair, chromosomal segregation and telomere maintenance can give rise to sporadic cancers.

Nucleotide instability (NIN) occurs as a result of replication errors and defects in the NER and BER DNA repair pathways. This type of instability is less common, and although subtle sequence changes in one or a few nucleotides (such as insertions and deletions) can occur, they can lead to a more drastic phenotype for e.g. Xeroderma pigmentosa which predisposes the individual to skin cancer<sup>133</sup>. Figure 1.10a demonstrates an example of NIN alongside Microsatellite instability (MIN) (Figure 1.10b).

MIN is a result of defects in the DNA MMR pathway which is responsible for correcting mismatched DNA bases. Cells with defects in this pathway are not able to carry out repair properly and therefore accumulate DNA matching errors. With accumulation of mismatched base errors, microsatellites are formed, which are short repetitive DNA sequences consisting of 1-6bp, scattered throughout the genome<sup>134</sup>. Microsatellites are most often GT/CA repeats, and lengths are highly variable between individuals<sup>135</sup>. Figure 1.10b shows an example of expansion or contraction of microsatellites.

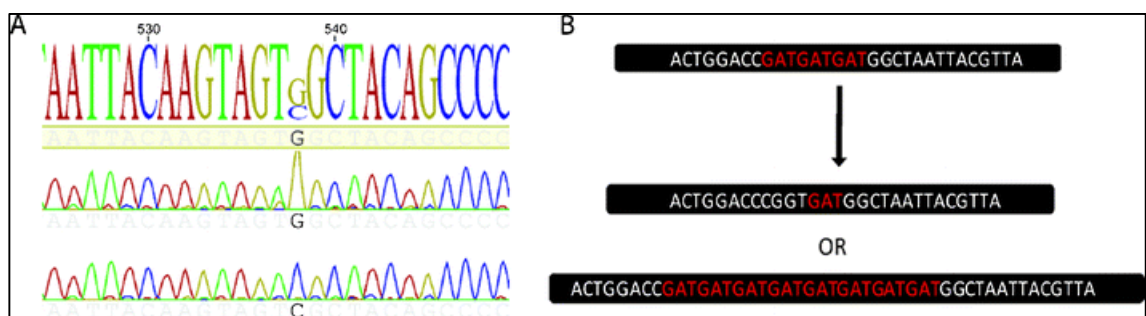


Figure 1.10 Example of a) Nucleotide instability (NIN) showing a GC variant encoding an amino acid change (Gly – Arg) and b) first contraction of a microsatellite sequence and expansion of the sequence which arise from defects in mismatch repair (MMR). Image taken from Pikor *et al*<sup>136</sup>.

A combination of mutation in DNA sequences that transcribe DNA damage sensing and repair genes, pro-apoptotic genes, cell cycle genes and other signalling substrates that alert the cell to defects in DNA repair contribute to genomic instability. Defects in spindle formation contribute largely to abnormal chromosome number and complement. All of the above mentioned cellular mechanisms in the DNA DDR function to eliminate damaged cells so that defects will not be continued in the progeny of irradiated cells. Much work has been done to find “driver” genes in genomic instability which could be targeted for therapeutics; some driver genes in relation to chromosome aberrations involve Birc5, BCL2 and the Androgen receptor which results in trisomy 17, gain of 17q gain of 20q11.21 and Trisomy X respectively<sup>137</sup>. Predictive biomarkers of radiosensitivity and cancer predisposition are still under intense investigation and the area warrants further research.

#### 1.5. Predictive Biomarkers of radiosensitivity

As physical models used for RT treatment planning are not accurate measurements for biological outcome, radiobiological based assays have been developed for prediction of biological outcome. Over the years many attempts for predicting response have been made based on the advancement of techniques from cell to molecular based radiobiological assay, with the later focusing on DNA damage and repair.

##### 1.5.1. Cell based assays

The first gold standard technique for measuring radiosensitivity was the *in vitro* clonogenic assay. West and colleagues used the clonogenic assay to predict patient outcome in 1993, and extended follow up time to 2 years, but poor growth of specimens for clonogenic analysis was observed and the group encouraged the development of other assays for a more successful prediction of radiosensitivity<sup>138</sup>. West *et al* also ruled out

correlation of patient age, grade and stage with radiosensitivity in cervical carcinomas<sup>139</sup> and when using lymphocytes they showed that survival fractions on peripheral blood lymphocytes from patients before receiving therapy was a good prognostic factor in predicting late tissue outcomes<sup>140</sup>. Tam *et al* took a step further in comparing the clonogenic assay with the adenosine tri-phosphate (ATP) Cell viability assay and showed no significant difference in survival fraction between both assays, and therefore suggested the use of the alternate assay to be a more representative measure of patient tumour response with high reproducibility<sup>141</sup>. However, limitations of these *in vitro* assays include how they are laborious and time consuming for routine clinical use on patient samples. The clonogenic assay is still used in many *in vitro* radiobiological assays on cell lines it requires approximately 2 weeks for colonies to form to obtain data. Many other attempts have therefore been made to develop a more rapid, accurate assay for radiosensitivity prediction using high throughput viability assays. Plate based assays such as (3-(4, 5-dimethylthiazolyl-2)-2,5-diphenyltetrazolium bromide) (MTT) and Alamar Blue have largely replaced clonogenic assays due to the rapid output. In the past decade, combinational plate assays such as the ApoTox™ triplex assay have taken over due to multi endpoint measures. For each well, three endpoints (cell viability, cytotoxicity and caspase activation) are measured in one, which reduces cost and experiment time.

#### 1.5.2. Cytogenetics Based Assays

The most researched cytogenetic based assays involve the micronucleus test (MN), the G2 chromosomal radiosensitivity assay and more recently fluorescent *in situ* hybridisation (FISH) analysis on chromosomes. Others include premature chromosome condensation, G0 and G1 chromosomal assays and other sub forms of FISH, but the primary 3 are mentioned as they are of most relevance to this work.



The Micronucleus (MN) test is another good reliable predictive assay of radiosensitivity. Developed and adapted for use by Heddle and colleagues<sup>142</sup>, the assay was further improved by Fenech *et al*<sup>143</sup> and it is used to detect bi nucleated cells scored as extranuclear bodies within the cell. As formation of extranuclear bodies is associated with defective DNA repair or replication, a link between radiosensitivity and the formation of micronuclei has been found. Vral *et al* observed high variability using the micronucleus assay in 2002, reporting that at one sampling time a person was considered to be radiosensitive, and when the assay was repeated was not considered radiosensitive<sup>144</sup>. This is not unusual as an individual's intrinsic radiosensitivity is said to fluctuate. The amount of extranuclear bodies is said to increase with radiation dose and thus is a reliable measure of radiosensitivity<sup>145</sup>, Encheva *et al* used the micronucleus assay to test radiosensitivity in cervical carcinoma patients and concluded that at doses > 1.5Gy difference between their tested control and cervical cancer cohort did not differ significantly, and they reported high inter individual variation values with outliers showing no side effects but a high micronucleus content<sup>146</sup>. These data are complicated and such confusion between sensitive and non-sensitive donors would not form basis for a reliable predictive assay to be used in the clinic. Further adding to this, early in 1999 Scott *et al* found the G2 chromosomal radiosensitivity assay to be more sensitive to detecting radiosensitivity of Breast cancer patients compared to the micronucleus test, as 40% were shown to be radiosensitive using the G2 assay vs 25% using the micronucleus test, however different molecular mechanisms are at work in both assays so it is important not to rule out any assay as it is dependent on the particular research endpoint<sup>147</sup>.

One of the most used predictive cytogenetic based assays to date is the G2 chromosomal radiosensitivity assay. The assay is a reliable predictor of radiosensitivity and correlates well with cancer predisposition<sup>148</sup>. All reports in the literature provide evidence of the predictive ability of the G2 chromosomal radiosensitivity assay, along with the different

donor control and patient cohorts. For example, Roberts *et al* used blood samples from healthy controls and breast cancer patients in 1999 to show inter and intra variation of 7%<sup>147</sup>. Baria *et al* used blood samples from healthy donors in comparison to breast, cervix, colorectal and lung carcinoma patients and found inter and intravariations of 15% and 10% respectively<sup>148</sup>. These reports are described in more detail in chapter 2 and 3 of this thesis. The previous assays mentioned are deemed to be time consuming with significant inter assay and cohort variability. In contrast, the G2 chromosomal radiosensitivity assay takes 3- 5 days to complete and shows good assay reproducibility between different cohorts. Therefore, the G2 chromosomal radiosensitivity assay has been shown to be a quick, reliable and reproducible marker of radiosensitivity and has the potential for use as a routine clinical test for predicting patient outcome before receiving RT.

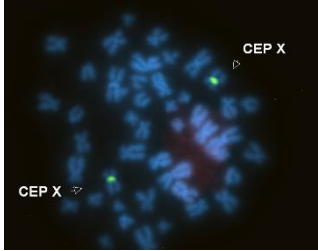
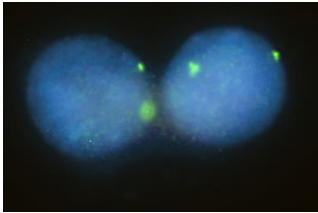
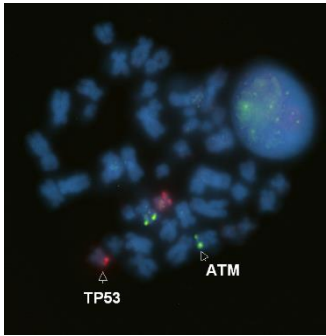
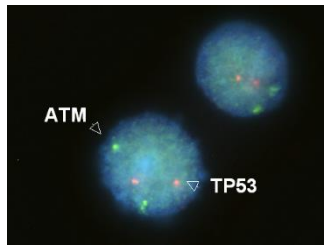
The G2 chromosomal radiosensitivity assay is a cytogenetic based assay which can be used on patient blood samples and has been shown to be reliable for predicting patient radiosensitivity. The G2 chromosomal assay has been used for many years now in studies for validating prediction of radiation response in control and cancer cohorts and has proved to be a reliable and reproducible assay. Shadley and Wolff in 1987 first reported increased aberration yield in blood samples after radiation<sup>149</sup>. This initial concept formed the basis of the G2 assay that was later developed by Sanford and Parshad in 1989<sup>58</sup> and was further adapted by Scott *et al* in 2003<sup>150</sup>. Early studies linking radiosensitivity and cancer predisposition showed increased chromosomal aberration yield using the G2 assay in those patients suffering from genetic instability syndromes, (as per section 1.3) such as Bloom Syndrome and FA<sup>58,151</sup>, Ataxia Telangiectasia individuals<sup>152</sup> and immunodeficient individuals<sup>153,154</sup>. These reports all observed an increase in chromosomal aberration yield after radiation, and increased sensitivity in those radiosensitive populations which found the ATM gene to be the main key player in radiation response and radiosensitivity. Other

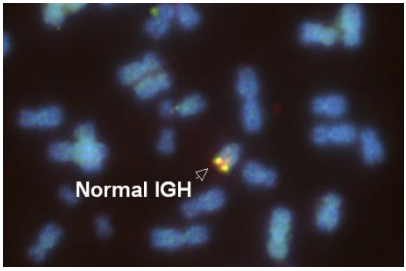
G2 studies have been complete using cancer cohorts such as; head and neck cancer cohorts<sup>155</sup>, retinoblastoma cases<sup>156</sup>, melanoma<sup>157</sup>, prostate<sup>158</sup>, breast cancer<sup>150,159-167</sup>, and general cancer studies<sup>148,168-171</sup>. Each report shows an increase in chromosomal aberration yields (more breaks, gaps and abnormalities) in cancer samples compared to healthy controls, and shows an extensive link between chromosomal radiosensitivity and cancer predisposition. A few reports have assessed reproducibility for the G2 assay by observing levels of variation in donor cohorts. In 1999 Scott *et al* reported inter variation (variation of G2 chromosomal radiosensitivity scores between individuals in a cohort) of between 15%-20%<sup>147</sup>, as did Baria *et al* in 2001 and 2002<sup>148,168</sup>. Smart *et al* reported no significant variation between donors<sup>170</sup> and Vral *et al* in 2004 reported very high variation values of above 39%<sup>164</sup>. A workshop held by Bryant *et al* in 2002 discussed experimental factors which affected G2 assay reproducibility<sup>169</sup>. These factors included regulation of temperature, pH and source of media for blood cultures. As published in a technical report by Bryant *et al*, variability in G2 aberration yield was associated with higher temperatures than 4°C, different media and serum batches, use of blood samples at more than 24hrs after extraction etc<sup>169</sup>. Although slight variability has been observed between laboratories (medium batch, FBS, usage of antibiotics within media<sup>58</sup>), the G2 assay is still a key radiobiological assay for predicting and monitoring radioresponse in patients cohorts.

Fluorescent *in situ* hybridisation (FISH) is also a cytogenetic based assay in which chromosomes are tagged with fluorescent probes which correspond to specific DNA sequences. FISH is a highly specialised medical technique in which genetic conditions such as Leukaemia and Downs syndrome are detected. Recently, FISH has been used to detect varying qualities of radiation which produce different complex chromosomal aberrations and rearrangements that would not otherwise have been able to be observed or analysed using classical m-Banding techniques<sup>172</sup>. Additionally, selected chromosomes can be probed using FISH to analyse specific rearrangements such as re-

joined chromosomal breaks, as Ritter *et al* detected distinct differences in chromosomal aberrations between low and high LET using FISH<sup>173</sup>. This technique is useful for detecting translocations of chromosomal material, which would not be identified fully using other cytogenetic techniques. Early in 1992, Lucas *et al* successfully detected higher levels of translocation frequency in chromosomes extracted from lymphocytes from atomic bomb survivors, decades after exposure. The results from both *in vitro* assays including dicentric frequency (using standard cytogenetic analysis) and translocation frequency (using FISH) were in excellent agreement<sup>174</sup>. There are a variety of probes available for FISH analysis, however the most relevant and used for this work include CEPX, ATM-TP53 and IGH (Table 1.2). FISH is a useful technique which can be interpreted directly and quickly without specialised training, as presented in Table 1.2. Presence of two green probes in a metaphase spread for CEPX indicates a karyotype of XX, which represents a female gender. Also, this can be easily and quickly observed in the interphase form. Dual colour probe ATM-TP53 is represented by two red copies (TP53) and two green copies (ATM) in normal karyotypes. In abnormal, a loss of one or both can be easily observed. Additionally, this can be quickly analysed using interphase FISH. Metaphase IGH break apart probe were also used to identify loss of or duplications of the probe. In normal karyotypes, two red dots in close proximity within the same chromosome are observed (Table 1.2). In abnormal cells, loss of one or duplication of this probe represents translocation or abnormality within the cells analysed. The FISH probes used for this work were of great benefit and show potential as an important biomarker of response (for e.g. patient response after radiotherapy). Use of the probes requires minimal training and processing time as abnormalities can be quantified quickly.

Table 1.2 FISH probes used for chapter 4 of this thesis. CEP X and ATM-TP53 probes were used in interphase and metaphase spreads. The IGH break apart probe was used only for interphase.

Name of Probe Used	Details	Example
Metaphase CEPX	Probe directed to the X chromosome for identification of the individual's sex	 <p>A metaphase spread of chromosomes stained with DAPI (blue). Two green fluorescent spots, labeled 'CEP X', are visible on the X chromosomes.</p>
Interphase CEPX	Same as above, only in interphase	 <p>Two interphase cells stained with DAPI (blue). Green fluorescent spots, labeled 'CEP X', are visible in the nuclei of both cells.</p>
Metaphase ATM-TP53	Probe directed for identification of ATM and TP53 in metaphase spreads	 <p>A metaphase spread of chromosomes stained with DAPI (blue). Green fluorescent spots are labeled 'ATM' and red fluorescent spots are labeled 'TP53'.</p>
Interphase ATM-TP53	Same as metaphase probe, only directed for use with interphase cells	 <p>Two interphase cells stained with DAPI (blue). Green fluorescent spots are labeled 'ATM' and red fluorescent spots are labeled 'TP53'.</p>

Metaphase IGH	Detection of IGH break apart probe in metaphase spreads	
---------------	---	---

### 1.5.3. DNA Damage Markers

DNA damage assays have been used to predict radiosensitivity. The most commonly used foci assay is the  $\gamma$ H2AX foci assay, which targets phosphorylated H2AX after radiation exposure by means of fluorescent labelling by confocal and flow cytometry analysis. One of the most central and important processes that occurs rapidly after DNA damage is the localisation and phosphorylation of histone H2AX (as explained in previous sections). Andrievski and Wilkins used the  $\gamma$ -H2AX assay on blood lymphocytes exposed between 0Gy – 10Gy of Caesium – 137 to detect foci by means of flow cytometry, reporting that although the assay provides good detection of foci in all lymphocyte subpopulations (CD19+ more so than CD4+ and CD8+), the assay could only be used as an indicator of exposure to ionizing radiation due to large inter variation between donors<sup>175</sup>. The importance of phosphorylation in the DDR was further outlined in knock out experiments of H2AX which results in increased radiosensitivity and genomic instability in mice, presenting with growth retardation and immunodeficiency<sup>176</sup>. In 2009 Redon *et al* used blood lymphocytes and fibroblasts exposed to 0.2 – 5Gy of  $\gamma$ -irradiation to show a linear dose –response pattern of  $\gamma$ H2AX at 24hrs and 48hrs after radiation exposure<sup>177</sup> which demonstrated good reproducibility and consistency of the assay. It was therefore suggested as a potential predictive assay of radiosensitivity or an assay of radiation exposure (reviewed by Scully and Xie, 2013<sup>178</sup>). Most recently, Bourton *et al* used a small number of 12 cancer patients (Pituitary, Thyroid, Larynx, Breast, Colorectal, Prostate and

Cervix) to show that flow cytometric analysis of prolonged  $\gamma$ H2AX correlated well with those patients experiencing acute and chronic tissue toxicity after radiotherapy. Although this study shows excellent potential for distinguishing those patients with toxicity compared to normal patient reactions, the assay was not sensitive enough to distinguish those patients with extreme sensitivity nor those patients with moderate severity of toxicity<sup>179</sup>.

The comet assay is another beneficial marker of DNA damage and potential marker of radiation response. Also known as ‘single cell gel electrophoresis,’ the method was first developed in 1984 by Östling & Johansson who suspended irradiated cells in melted agarose and cast on to microscope slides which were then lysed by detergent and electrophoresed<sup>180</sup>. After fluorescent staining, analysis reveals fragmented regions of DNA which form a comet shape, and is representative of the extent of DNA damage breaks. The intensity of the ‘comet’ tail in comparison to the head reveals how much DNA damage has occurred. Sophisticated automation of the assay and imaging techniques have propelled the comet assay to the forefront of DNA damage research (Figure 1.11). In this figure, many factors of measurement using the comet assay are shown, to include the most often used ‘tail moment’ and ‘tail length.’

The alkaline comet assay (ACA) is the most sensitive method for detecting SSB. It has been shown in early 1990’s to detect DNA damage after clinically relevant doses of radiation<sup>181</sup> and Jones’ *et al’s* group has also recently shown the ACA method beneficial for predicting bladder carcinoma cell sensitivity to irradiation<sup>182</sup>. However, in the original report by Östling & Johansson, a minimum dose of 0.5Gy is used and they explain how loss of sensitivity of the assay occurs at doses lower than this point. Therefore, the comet assay would be of no relevance to this work, as doses of 0.5Gy and lower are used throughout.

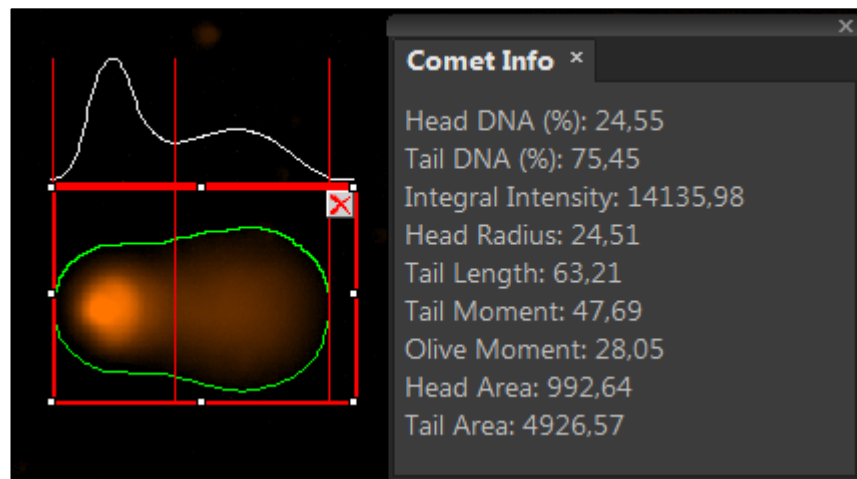


Figure 1.11 Informative results from comet assay analysis. Original reports analysed tail intensity to gain information about DNA damage. However more informative information is now given through automated software as described above. Image taken from Lucia Cytogenetics<sup>383</sup>.

#### 1.5.4. Genomic markers of radiation exposure

Recent work by Badie *et al* in 2011<sup>183</sup> suggest that using a new gene expression screening analysis technique could be a good predictor of individual radiation sensitivity because it was used to identify specific biomarkers of radiosensitivity. Of a panel of 800 genes simultaneously analysed, 5 key genes were selected to be key in the radiation response, these were phosphohistidine phosphatase (PHPT1), PUMA, cyclin G1 (CCNG1), DDB2 and MDM2 detected on an nCounter analysis system and Multiplex Quantitive Real Time PCR (MQRT-PCR). The nCounter technique was ideal for analysing 800 genes as it provides information on modification of a large number of genes without the need for enzymatic amplification of RNA prior to analysis, whereas the MQRT – PCR technique could only analyse a maximum of 6 genes. However, further work is required to investigate why different genes are radioresponsive at different times, and why radio responsive genes could be altered depending on the tissue sampling area; i.e. saliva, blood, tissue biopsy etc.



#### 1.5.5. Single nucleotide polymorphisms (SNP's)

Abbreviated to SNP's, single nucleotide polymorphisms are small alterations in nucleotide sequences in DNA that can account for 80% of individual variation in the population<sup>184</sup>. Relatively new for the prediction of radiosensitivity, it is thought that assays monitoring SNP's have the potential for routine use. SNPs are currently used for predicting human immunodeficiency virus (HIV) patient response to drugs such as Abacavir, in which SNP screening reduced the risk of hypersensitivity reaction to the drug<sup>185</sup>, but no current radio-toxic SNP's have been identified for radiosensitivity analysis and much more work needs to be done to verify this<sup>186</sup>. Many attempts have been made at analysing SNP variants in genome wide association studies (GWAS) to pick up common genetic variants between samples but a limitation of this system is that it may not detect rare genetic variants. As these methods are relatively new, further work needs to be done to validate and standardise the use of SNPs for detecting radiosensitivity

#### 1.5.6. Histone Modifications

Modification to histone proteins can alter the expression of genes in response to radiation by altering the overall structure and compaction of the chromatin. The most common alteration is the phosphorylation of histone H2AX, which has been described for its use in predictive assays in section 1.5.3. It is known that the alteration of histone modifications can be dose and time dependant after radiation insults due to the action of histone acetyl transferases (HAT's) and histone deacetyl transferases (HDAC's) but this is not fully understood<sup>187</sup>.

DNA methylation involves the addition of a methyl group to a cytosine residue on a CpG dinucleotide in the DNA sequence. These changes can be hereditary, and are termed the "epigenetic code." Changes most often lead to transcriptional repression, which can be a problem if a tumour suppressor gene (TSG) is repressed and would ultimately lead to a

mutation and genomic instability. Previous studies state that currently DNA methylation is not a good choice for radiosensitivity prediction because not enough studies have been done (especially in the low dose region) that elucidate all the mechanisms behind DNA methylation. Also much variability in methylation patterns has been noted in cohorts of individuals, which would also generate confusing results<sup>187</sup>.

#### 1.5.7. Micro RNA's Exosomes

Recently, the role of exosomal trafficking of functional micro RNA's (miRNA's) has gained increasing interest in cancer research and cell biology. The involvement of miRNA in the radiation induced DDR is a new and emerging field of investigation. miRNA's are small, non-coding RNA's capable of altering gene expression at the pre and post transcription level, through many mechanisms which are unclear and have not been fully outlined, but provide interesting insights into how aberrant DDR in tumorigenesis can be manipulated or controlled. In summary, miRNAs are formed via two pathways, intergenic (formed separate from genes with own transcriptional unit) and intronic/extronic (formed together with host genes). Figure 1.12 illustrates the biogenesis of miRNA from Pri-miRNA. Pri – miRNAs are recognised in the nucleus and cleaved by ribonuclease type iii (Drosha) – DiGeorge syndrome chromosomal region 8 (DGCR8) complex, generating a hairpin – like structure, and forming pre – miRNA. This hairpin pre – miRNA is exported from the nucleus in a Ras-related nuclear protein (RAN)–Guanosine triphosphate (GTP) dependant manner by Exportin 5. Dicer – Tar RNA binding protein (RBP) complex then cleaves the pre – miRNA to form a duplex, mature miRNA, which can then associate with Argonaute and RNA induced silencing complex (RISC), which can alter gene expression (reviewed by Wan *et al* 2011<sup>188</sup>, Metheetraitut and slack 2013<sup>189</sup>). A number of miRNA's have been discovered, with anticipation of discovering more. It has recently come to light that miRNA's can alter genes central in the DDR, one well known example is the tumour suppressor P53. miR -504 and miR-125b have recently been shown to negatively regulate

P53 and promote tumorigenicity of cells *in vivo*<sup>190</sup>. Another target, ATM has been shown to be inhibited by miR -421, which binds to ATM mRNA and leads to altered S phase cell cycle checkpoint and increased radiosensitivity<sup>191</sup>.

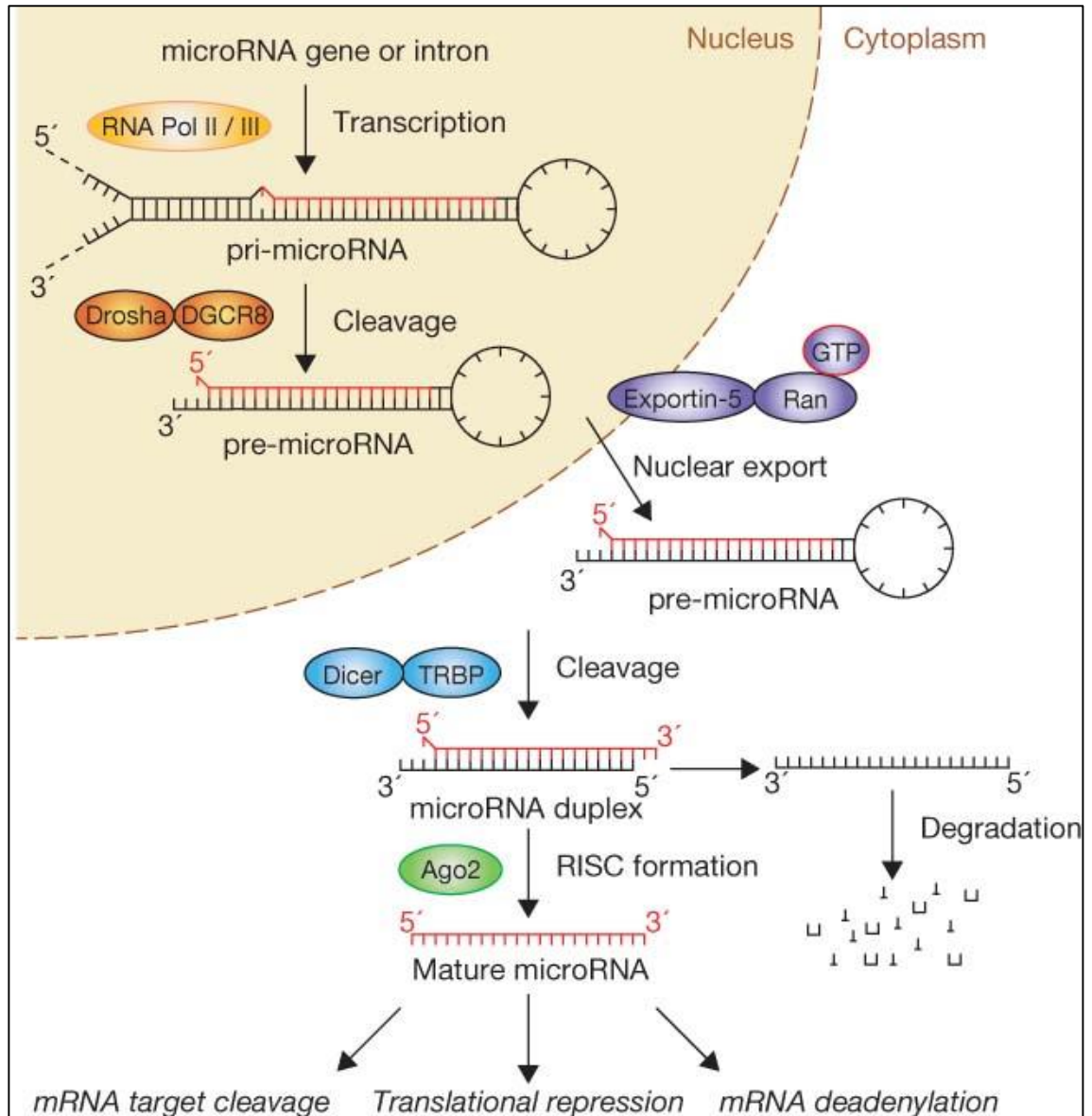


Figure 1.12 Biogenesis of miRNA and functions. Firstly, Pri-MIRNAs are cleaved in the nucleus by DROSHA-DGCR8. A hairpin pre-miRNA is formed and transported from the nucleus via a RAN-GTPase dependent manner by Exportin-5. The pre-miRNA is cleaved by DICER and TRBP to form a duplex, mature miRNA. Association of the duplex miRNA with Argonaute and RISC complex allows for the miRNA to interact with mRNA and leads to translational repression of many genes. Image taken from Winter *et al*<sup>192</sup>.

## 1.6. Novel tools for predicting radiosensitivity

As physical models used for RT treatment planning are not accurate measurements for biological outcome, radiobiological based assays have been developed for the prediction of biological outcome. Some of the original *in vitro* assays are too time consuming for routine clinical use and require invasive cellular extraction methods on patients such as biopsy extraction for laboratory testing. Many assays which involve less invasive cell extraction from blood have been developed and optimised for measuring patient radiosensitivity by modern genetic and/or molecular methods. However, limitations exist on all current assays and in some cases further experimentation is required to validate other methods (as described previously). Many other attempts have therefore been made to develop a more rapid, accurate measure of radiosensitivity prediction in patients. This includes the use of spectroscopy. Most non-biological methods of prediction of drug/therapy response use computational analysis which is based on data taken from biological endpoints. For example, Frank Emmert-Strieb *et al* were able to use agglomerative hierarchical clustering to assign haematuria patients into 5 subtypes based on the heterogeneity of the biomarker data, which was done on multiple biological measures previously taken from the urine of haematuria patients<sup>193</sup>.

### 1.6.1. Raman Spectroscopy

At our RESC laboratory in DIT, we are currently testing the hypothesis that Raman Spectroscopy may be a novel rapid method of predicting individual patient radiosensitivity. The Raman Effect, which is a term used to describe the inelastic scattering of photons from a material in response to a laser, was first described by CV Raman in 1930<sup>194</sup>. The method is based on measuring the vibrational profile of chemicals and substances in a sample. Raman spectroscopy does not alter or damage the biological material should it need to be used again. The process allows for the output of a biochemical profile, almost like a fingerprint, unique to the individual sample, where

peaks on the output graph represent a particular protein or molecule. Not only does the peak represent a particular protein or molecule, it also represents the content of protein present in the sample.

Raman spectroscopy has been successfully used to detect non cancer samples from cancerous samples in a variety of cancer types; Nijssen *et al* analysed skin cancer biopsy samples<sup>195</sup>, de Jong analysed bladder cancer tissue samples<sup>196</sup> and Tollefson *et al* used Raman spectroscopy to investigate whether Gleason 7 prostate samples could be used to detect those patients who would progress to metastatic disease<sup>197</sup>. As it has been successful in distinguishing between cancer and non-cancer, it would be of interest to observe if Raman spectroscopy could predict individual radiosensitivity.

The RESC has recently used Raman Spectroscopy for cervical smear screening. Lyng *et al* carried out an investigation in 2007 using Raman spectroscopy to distinguish between normal and abnormal cervical smear samples by screening macromolecules such as proteins, lipids, nucleic acids and carbohydrates<sup>198</sup>. The study validated the use of the Raman technique for screening different grades of smears in CIN. Raman spectroscopy has branched out to other fields, but with many factors still to be resolved (in house review on sample preparation considerations by Meade *et al* 2010 where the same fixation/preservative of samples and sample desiccation is required<sup>199</sup>, and problems associated with high background in measurements from samples which can be adjusted by biological means and not only mathematical manipulation of the data by Bonnier *et al*<sup>200</sup>). Meade *et al* conducted a study in 2007 using human keratinocytes which outlined the correlation between spectroscopic and biochemical analysis and identified the sensitivity and potential of use of Raman spectroscopy when used with appropriate spectroscopic substrates<sup>201</sup>. Raman spectroscopy was not carried out directly in the work for this PhD thesis. Raman studies were conducted by a colleague (Dr. Adrian Maguire) in parallel

with this work to validate the method of using Raman Spectroscopy for measuring radiosensitivity in individual donor samples.

### **1.7 Aims and objectives of Thesis;**

The primary aim of this project was to investigate if there was a reliable predictive method or biomarker to measure cellular radiosensitivity in blood samples from normal donors or patients. This work was carried out in parallel with Raman spectroscopic studies so that standard *in vitro* radiosensitivity measurements could be taken and compared to Raman data for validation and optimisation of Raman spectroscopy as a potential clinical predictive tool. Although biological validation was conducted for parallel analysis with Raman Spectroscopy, Raman data is not featured in this thesis.

#### Individual aims

1. To optimize and validate the G2 chromosomal radiosensitivity assay for correlation with other methods of radiosensitivity prediction in donor and patient samples in parallel with Raman Spectroscopy conducted by Dr. Adrian Maguire
2. To investigate the effects of low doses of ionizing radiation of different radiation energies on whole blood cultures from healthy donors
3. To investigate changes in radiosensitivity levels in Prostate cancer patients throughout their radiotherapy plan; at baseline, post hormone treatment, post radiotherapy, 2month and 8month follow up
4. Further explore biomarkers involved in radiosensitivity driven by mechanisms of ATM
5. To identify any potential genetic Biomarkers of radiosensitivity in normal, AT cells and prostate cancer cells which could be further explored
6. Attempt to find novel miRNA's in cell and exosome extracts from normal and AT Lymphoblastoid cell lines which could explain the mechanisms of radiosensitivity

## **2. OPTIMISATION AND VALIDATION OF THE G2 CHROMOSOMAL RADIOSENSITIVITY ASSAY ON HEALTHY DONOR BLOOD SAMPLES**

### **2.1 Introduction**

Conventional radiotherapy dose limits are based on the reaction of the most sensitive patients (those who develop acute severe reactions) and are prescribed to keep radiation response in all patients to a tolerable level<sup>16</sup>. If patient response could be predicted before radiotherapy, it would allow for a better individualised treatment plan, which would allow for dose escalation in radio resistant patients and dose alteration for radiosensitive patients. These problems could be addressed if an accurate individualised predictive assay was developed, and should ultimately be non – invasive, non – labour intensive, and time-efficient to deliver results after diagnosis during the therapy planning stage.

As described in section 1.5, attempts have been made to develop such an assay which include the clonogenic assay<sup>202</sup>, Micronucleus (MN) test<sup>143</sup>,  $\gamma$ -H2AX foci assay. One of the most extensively studied assays with clinical potential for predictive testing of radiosensitivity is the G2 chromosomal radiosensitivity assay. The G2 assay is used as a reliable predictor of *in vitro* radiosensitivity and has been optimised and validated for its efficacy by many groups (discussed more later). It is a cytogenetic based assay where donor/patient whole blood samples are cultured and synchronised in their cell cycle and irradiated at the G2 phase. Chromosomes are then extracted and fixed from the leucocyte population for microscopic analysis of radiation-induced chromatid damage that incurred *in vitro* in the G2 phase of the cell cycle as it is known to be the most sensitive phase before M phase and therefore ideal for measuring radiosensitivity<sup>11</sup>.

The assay was developed in 1989 by Sanford and Parshad<sup>58</sup> who used the assay on skin fibroblasts from radiosensitive patients (as described in chapter 1). The G2 assay was deemed to be a reliable assay for the prediction of individual radiosensitivity, but over many years the assay has been improved to reduce variability.

In the original studies by Sanford and Parshad the assay was carried out at room temperature and this was later adapted by Scott *et al*<sup>152</sup> who reduced temperatures to 0-4°C to prevent DNA damage repair mechanisms occurring during the cytogenetic preparation of chromosomes. A media change to the whole blood cultures was also performed 1 hr before irradiation but this was adapted by Howe *et al* to carry out the media change at least 24 hrs before irradiation, to allow whole blood cultures to settle before irradiation<sup>165</sup>. It is well known that strict conditions are needed for the successful use of this assay, with variations such as temperature and pH reported between different groups. The strict assay conditions were demonstrated by Sanford *et al* who showed an increased chromatid aberration yield in response to lowering the temperature and increasing the pH to pH 8 in the time immediately after X irradiation to 1Gy<sup>58</sup>. In a technical report published in 2002, Bryant *et al*<sup>169</sup> describes factors which do or do not influence G2 chromosomal radiosensitivity. The factors that do not appear to influence aberration yield are blood storage (once used within 24 hrs post extraction) and type of phytohaemagglutinin, PHA – M and PHA – P. Factors that do affect aberration yield include temperature, transport of blood samples and cultures (which is thought to depend on temperature fluctuations), types of irradiations and doses (with reduced mitotic index at doses over 0.5Gy), and serum batch in which the authors concluded that an experimental series using the G2 chromosomal radiosensitivity assay should be planned around using one batch of serum<sup>169,170</sup>.

In addition to experimental factors which cause variation, biological effects differ depending on cell and tissue type, dose and linear energy transfer (LET)<sup>68</sup>. LET represents



the energy transferred to the material by ionising radiation per unit track. Generally, higher relative biological effectiveness (RBE) is observed with increasing LET<sup>173,203–206</sup>, but at very high LET, the RBE begins to change, as shown by Barendsen *et al* comparing normal tissues, cultured cells and tumour samples<sup>207</sup>. Many studies have compared DNA double strand breaks, reproductive cell death and chromosome aberrations in cells irradiated *in vitro* with sparsely ionizing radiation of low LET or densely ionizing radiation of higher LET<sup>208–213</sup>. A number of radiobiological studies have also shown an increase in RBE with decreasing energy for low LET radiations, electrons and photons (reviewed<sup>214–216</sup>).

Chromosome damage has been reported in the literature as an effective endpoint for assessing radiation damage. The first study which demonstrated radiation damage to chromosomes using *Trudescantia* microspores, also showed a lower RBE of <sup>60</sup>Co gamma radiation compared to 250 kVp X – rays<sup>217</sup>, most likely as a result of a slightly higher RBE of 250 kVp X – rays as shown by Fowler<sup>218</sup>. Subsequent studies on human lymphocytes have shown that relatively high energy low LET radiation, such as gamma radiation, is several times less effective than relatively low energy low LET radiation, such as low energy X radiation<sup>215,219–223</sup>. Despite evidence from *in vitro* radiobiological data that the RBE of high energy low LET radiation is less than that of low energy low LET radiation, there is limited epidemiological data to show that cancer risk decreases as radiation energy increases for low LET radiations (reviewed<sup>215</sup>). Despite the radiobiological data suggesting that low LET radiations of different energy show different RBE, for radiation protection, the ICRP 2007 recommendations retain a weighting factor of 1 for all low LET radiations<sup>224</sup>. However an ICRU 1978 report states that absorbed dose values for 100-300 kV X-rays should be multiplied by 1.18, and not 1, when comparing effects to MV X- rays<sup>225</sup>. A recent study showed cluster patterns of energy deposition sites to differ up to 15% between low photon energy brachytherapy sources

( $^{103}\text{Pd}$  and  $^{125}\text{I}$  with mean photon energies of 0.021 and 0.028 MeV) and less than 2% for the high photon energy ( $^{192}\text{Ir}$  and  $^{137}\text{Cs}$  with mean photon energies of 0.36 and 0.615 MeV) brachytherapy sources with respect to  $^{60}\text{Co}$  <sup>69</sup> which correlated with reported RBE values for double strand break yields <sup>226</sup>.

This is of importance, as samples from the healthy control (HC) cohort of donors used to validate our assay were irradiated using  $\gamma$ -irradiation from a  $^{60}\text{Co}$  source which has been decommissioned from the hospital and our use. A linear accelerator (Linac) which delivers x-ray irradiation will be used on future cohorts, therefore it must be investigated if beam energy/source conveys additional radiobiological variation using the G2 assay.

To validate the G2 chromosomal radiosensitivity assay as a reliable predictor assay of individual radiosensitivity many studies describe a healthy donor control study prior to or in parallel with patient studies. Healthy control donor studies use mitotic index (mitotic inhibition) and G2 scoring to assess the inter- and intra- individual variation values between donor samples to ensure consistency within the assay.

The first measurement performed using the assay includes mitotic index. This is a quick measure of cell cycle checkpoint efficiency. Calculated by analysing the ratio of cells in metaphase to total cells, the mitotic index allows for a % checkpoint value to be assigned to each donor in response to that given dose of irradiation. The donors' mitotic inhibition is usually calculated and used for analysis (% mitotic index at 0Gy is subtracted from the % mitotic index at each radiation dose). The significance of this value is based on the mechanisms of cell cycle checkpoints in response to irradiation. When the donor cells are irradiated, the cell cycle checkpoints should function to halt the cell cycle to allow repair processes to occur before progressing to mitosis, and therefore would give a lower mitotic index value (or a higher mitotic inhibition value) during a cytogenetic analysis. Mitotic index and inhibition values were obtained in earlier G2 assay reports to analyse

checkpoint response in healthy controls, radiosensitivity populations such as Ataxia telangiectasia, Bloom's Syndrome, Fanconi's Anaemia or cancer patients. For example, in 1994 Scott *et al* reported mitotic index values in a range of 4-5% for healthy controls and 3% for Ataxia telangiectasia patients using 0.5Gy x-irradiation<sup>152</sup>. Howe *et al* found much lower mitotic indices (<1%) in irradiated blood samples of benign prostate hyperplasia and prostate cancer patients using 0.5Gy  $\gamma$  – irradiation<sup>158</sup>. This value is important for measuring donor checkpoint efficiency but also for validating the use of the assay on different donor cohorts to compare with previous reports in the literature.

G2 radiosensitivity scores form the basis of the G2 chromosomal radiosensitivity assay in donor samples. All chromatid aberrations (Figure 2.1) including gaps, breaks, fragments, deletions and dicentrics were totalled per 100 metaphase spreads analysed on each slide (0Gy, 0.05Gy and 0.5Gy). The spontaneous aberration yield at 0Gy is subtracted from the aberration yield at each dose to give a radiation induced G2 score. It is already well outlined that blood samples from patients with genetic disorders such as ataxia telangiectasia<sup>152</sup>, Bloom's syndrome<sup>50</sup>, Fanconi anaemia<sup>227</sup>, severe combined immunodeficiency syndrome<sup>53</sup> and patients with cancer show increased G2 chromatid aberration yield compared to healthy control samples (Table 2.1).

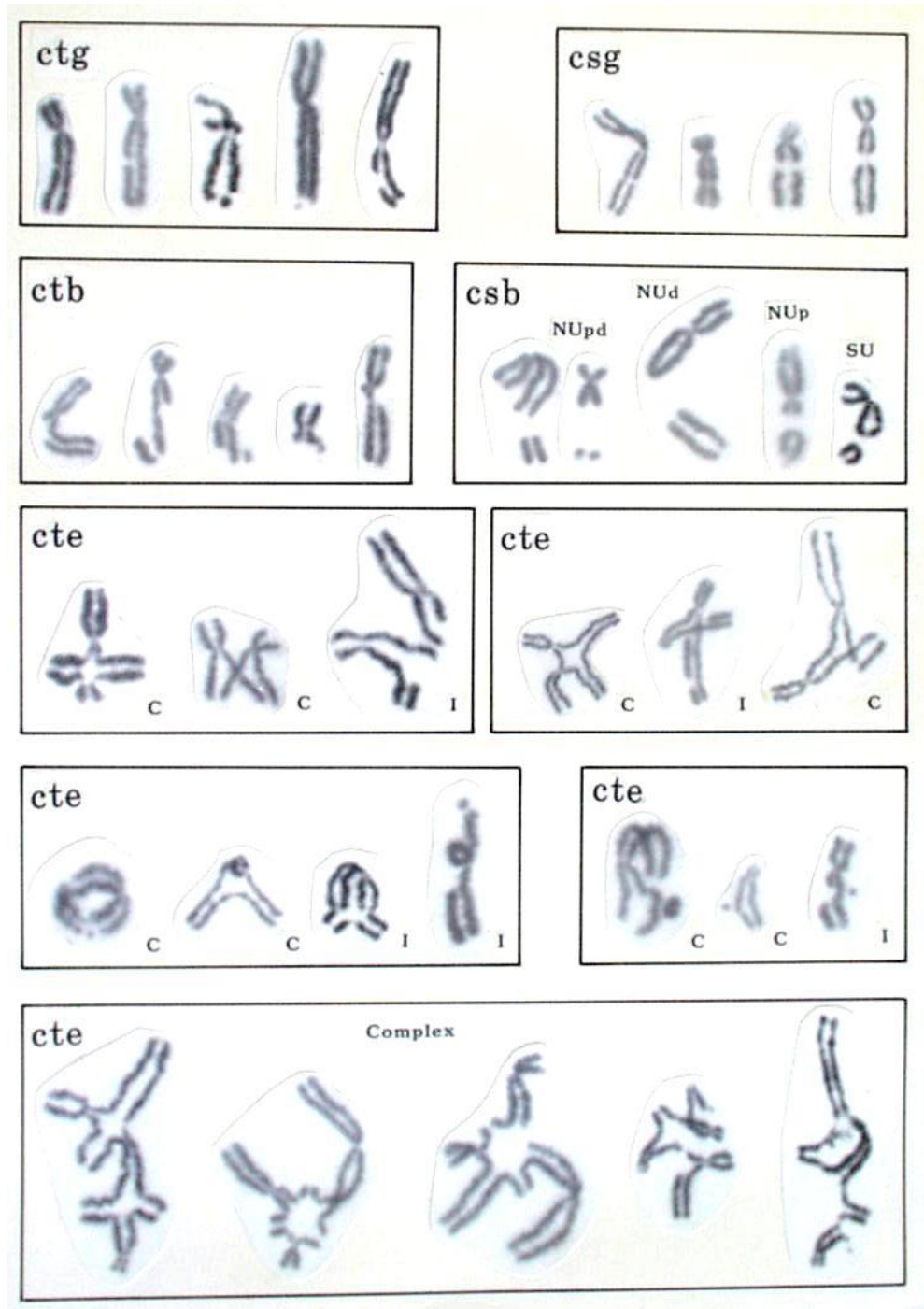


Figure 2.1 Chromatid type aberrations according to criteria 2 of the Radiation Biology Centre, Kyoto Japan. Chromatid gaps (ctg), chromatid breaks (ctb), chromatid exchanges (cte) and isochromatid gaps and breaks (csg and csb) are shown<sup>384</sup>.

Radiosensitivity cut off values represents another benchmark for the optimisation and validation of the G2 assay which express the data in terms of radiosensitive and non – radiosensitive patients. The G2 radiosensitivity cut off value is represented by calculating a 90<sup>th</sup> percentile from the range of radiation induced G2 scores in a number of donor control cohorts and it was first described by Scott *et al* in 1999<sup>147</sup>. The 90<sup>th</sup> percentile is the value at which 90% of the sampled population will fall below and be deemed normal or radio resistant. The upper 10% represents donors/patients who are considered to be radiosensitive. The 90% percentile value has been used in most of the G2 chromosomal radiosensitivity studies reported in the literature to date (discussed below and table 2.1). Individual G2 chromosomal radiosensitivity values are recorded as the total number of aberrations per 100 metaphases (written X abs/100 metaphases), and can vary between research groups from 80 to <200 aberrations per 100 metaphases for healthy donors. The 90th percentile is calculated from all of the G2 values from the healthy donor cohort. The radiosensitivity cut off value would generally rise if a cohort is based on cancer patients as these generally have higher G2 scores due to higher levels of intrinsic radiosensitivity. Published reports show slight variation in radiosensitivity cut off values using an array of cohort types, such as healthy controls, radiosensitive disorders and cancer cohorts with a minimum of 87 aberrations per 100 metaphases and a maximum of 175 aberrations per 100 metaphases (Table 2.1).

When the G2 radiosensitivity scores and radiosensitivity cut off values are determined, inter and intra-individual variation values can be obtained to compare control donor and cancer patient radiosensitivity by searching and obtaining values from the literature. This was deemed to be an important part of validating the G2 chromosomal radiosensitivity assay within our laboratory with new users. Inter variation is a measure of the variability in the G2 chromosomal radiosensitivity scores between a group of normal donors and intra – variation is a measure of the variability of the G2 chromosomal radiosensitivity

scores for the same donor sampled at multiple times. Many authors have reported validation of the G2 assay through inter-variability and intra-variability values (table 2.2). Using healthy control donors, the original published report was by David Scott and colleagues at the Patterson Institute of Cancer Research (PICR) in Manchester<sup>147</sup>.

Table 2.1 Summary of radiosensitivity cut off values, radiation type and doses used from previous reports in the literature. Cases of healthy controls (HC), breast cancer (BCa), Cervical cancer (CCa), colorectal cancer (CRCa), Lung cancer (LCa), benign prostate hyperplasia (BPH), prostate cancer (PCa), and head and neck cancer (HNCa) are presented.

<u>Author</u>	<u>Date</u>	<u>Donor &amp; Sample Type</u>	<u>Radiation Type</u>	<u>Dose (Gy)</u>	<u>Cut off</u>	<u>Ref</u>
Scott <i>et al</i>	1999	Bca	X - Rays	0.5	110	147
Roberts <i>et al</i>	1999	HC and BCa	X - Rays	0.5	110	160
Riches <i>et al</i>	2001	BCa	$\gamma$ -Rays	0.4	80	161
Baria <i>et al</i>	2001	HC, BCa, CCa, CRCa, LCa	X - Rays	0.5	100	148
Baeyens <i>et al</i>	2002	BCa	$\gamma$ -Rays	0.4	120	162
Thierens <i>et al</i>	2002	Radiation workers	$\gamma$ -Rays	0.4	130	228
Vral <i>et al</i>	2002	HC	$\gamma$ -Rays	0.4	135	144
Baria <i>et al</i>	2002	Young Donors	X - Rays	0.5	87	168
Smart <i>et al</i>	2003	HC	X - Rays	0.5	95	170
Vral <i>et al</i>	2004	HC	$\gamma$ -Rays	0.4	129	164
De Ruyck <i>et al</i>	2005	Cca	$\gamma$ -Rays	0.4	139	229
Howe <i>et al</i>	2005	BCa	$\gamma$ -Rays	0.5	110	165
Howe <i>et al</i>	2005	HC, BPH and PCa	$\gamma$ -Rays	0.5	110	158
Howe <i>et al</i>	2009	HC and CRCa	$\gamma$ -Rays	0.5	105 (HC) - 164 (CRC)	230
De Ruyck <i>et al</i>	2008	HC and HNCa	$\gamma$ -Rays	0.4	133	231
Borgmann <i>et al</i>	2010	Twins and PCa	X - Rays	0.5	164 (HC) and 172 (PCa)	232
Brzozowska <i>et al</i>	2012	HC & PCa	$\gamma$ -Rays	0.5-1	<70 (HC) and 150 (PCa)	233

Levels of inter and intra variation differ significantly between laboratories which emphasises the importance of assay validation by each new group adopting the assay for different cohorts. The assay has been validated through inter- and intra-variation values in numerous healthy donor cohorts and cancer cohorts showing inter individual values of between 7%-31% and intra individual values of between 1%-26% (Table 2.2). These authors used the G2 chromosomal radiosensitivity assay on either lymphocytes or whole blood samples from normal and/or patient donors and this specific experimental protocol (using whole blood) was adopted for the G2 studies described in this thesis. Variation could be attributed to the different radiation doses and types used, which varied between all studies. Most reports used a dose of 0.4 – 0.5Gy and either x or  $\gamma$ -irradiation with the odd report using either much lower doses (<0.1 Gy) or much higher doses (3Gy – 6Gy) (Table 2.2).

Table 2.2 Summary of inter-individual and intra-individual variation values by author. Radiation type and doses differ between cohorts used. Healthy control (HC), Breast cancer (BCa), Cervical Cancer (CCa), Colorectal Cancer (CRCa), Lung cancer (LCa), Benign prostate hyperplasia (BPH) and Prostate Cancer (PCa) cases are presented.

<u>Author</u>	<u>Date</u>	<u>Donor &amp; Sample Type</u>	<u>Radiation Type</u>	<u>Dose (Gy)</u>	<u>Inter variation</u>	<u>Intra Variation</u>	<u>REF</u>
Scott <i>et al</i>	1999	BCa	X - Rays	0.5	20	7	<sup>147</sup>
Roberts <i>et al</i>	1999	HCA and Bca	X - Rays	0.5	7	7	<sup>160</sup>
Riches <i>et al</i>	2001	BCa	$\gamma$ -Rays	0.4	19	8	<sup>161</sup>
Baria <i>et al</i>	2001	HC, BCa, CCa, CRCa, LCa	X - Rays	0.5	15.1	10.3	<sup>148</sup>
Baeyens <i>et al</i>	2002	BCa	$\gamma$ -Rays	0.4	20	15	<sup>162</sup>
Thierens <i>et al</i>	2002	Radiation workers	$\gamma$ -Rays	0.4	20	9	<sup>228</sup>
Vral <i>et al</i>	2002	HC	$\gamma$ -Rays	0.4	17	2 donors 14 and 16	<sup>144</sup>
Baria <i>et al</i>	2002	Young Donors	X-Rays	0.5	19.2	18.6	<sup>168</sup>
Smart <i>et al</i>	2003	HC	X-Rays	0.5		0.5 - 26	<sup>170</sup>
Vral <i>et al</i>	2004	HC	$\gamma$ -Rays	0.4	20	3 to 22	<sup>164</sup>
Howe <i>et al</i>	2005	BCa	$\gamma$ -Rays	0.5	30.5	4.6 to 5.1	<sup>165</sup>
Howe <i>et al</i>	2005	HC, BPH and PCa	$\gamma$ -Rays	0.5	30.5	4.6 to 5.1	
Borgmann <i>et al</i>	2007	HC	X-Rays	0.5	31	NONE	<sup>234</sup>
Borgmann <i>et al</i>	2008	BCa	X-Rays	3 or 6	17	NONE	<sup>235</sup>

Intra-variation is also assessed to validate the G2 assay and ensure consistency in the experimental conditions (Table 2.2). It was reported that checkpoint response and G2 radiosensitivity levels vary between individuals particularly at higher radiation doses, as reported in the technical meeting in 2002<sup>169</sup>. The groups here reported good assay reproducibility with regard to their achieved intra-individual values which ranged from 4.6% to 15%. The range (1%-30%) in intra-variation values were proposed to be due to G2 assay experimental conditions but specific donor cases pointed to the fact that repeated



sampling at different times affected radiosensitivity possibly due to immune status, medication, hormone status and other intrinsic conditions and more studies examining these factors were encouraged<sup>164</sup>.

The main objective of this chapter was to optimise and validate the G2 chromosomal radiosensitivity assay using the experimental parameters and criteria reported in the published studies for radiosensitivity cut off values and variation values, in addition to investigating the factors which may influence donor radiosensitivity such as blood culturing techniques, smoking status, season of blood sample extraction and radiation type (i.e.  $\gamma$  or x ray irradiation).

The desired aims of this study was to obtain inter-variation values which lie in the range of other published work to validate the use of the assay in our laboratory (between 7%-30.5% and intra-variation between 4.6%-15% with a G2 radiosensitivity cut off 90% percentile value ranging from 80-135 aberrations/100 metaphases) in a healthy donor control sample cohort. Once these parameters were obtained to prove validity of the G2 chromosomal radiosensitivity assay, then the same G2 radiosensitivity values could be adopted for a parallel study validating and testing Raman Spectroscopy as a potential predictive tool of radiosensitivity<sup>236</sup>.

Furthermore, because blood samples from cohorts were being obtained, several subtypes of cells from whole blood could also be extracted and further investigated for their radiobiological response specifically related to immunity. Whole blood is made up of erythrocytes (red blood cells), leucocytes (white blood cells) and plasma. Erythrocytes are the most abundant cell type in whole blood (approximately making up 40 – 45% of all cell subtypes), which are biconcave in structure and contain haemoglobin which is responsible for the physiological functioning of oxygen transport throughout the body. As erythrocytes do not possess a nucleus, this cell type is not of importance within our studies and was eliminated through haemolysis using potassium chloride (KCl) early in

the G2 chromosomal assay. White blood cells (WBC's) however, delineate into a number of cellular subtypes involved in an immune response elicited by DNA damage. The most abundant white blood cell (WBC) type are the neutrophils, which make up approximately 60% of the white cell content, but only survive between 6 – 10 hrs, the next most abundant WBC subtype are lymphocytes (30%) (which are currently used for the assay) and monocytes which incorporate only 5% of the white cell content<sup>237</sup>. Lymphocytes can be further subdivided into T and B cells, with T cells even further divided into helper, cytotoxic, regulatory, natural killer subtypes. In response to cellular stress or injury, these cells are part of a coordinated immune response which respond to the invasion of foreign material or cellular damage. The chromosomes analysed in the G2 chromosomal radiosensitivity assay are of lymphocyte origin, and are easily obtained through blood sampling from the individual. These are separated out from the whole blood in the G2 assay protocol. However, sub-population of lymphocytes were also extracted from a ficoll gradient (using Histopaque) and analysed for both G2 and Raman studies in parallel. Whole blood was used for the G2 chromosomal radiosensitivity assay as this is the best method which incorporates all elements of the blood sample. However, the abundance of contaminating RBC's made Raman spectroscopic analysis difficult as the WBC population of lymphocytes could not be directly analysed which is the cell type of interest in this work. Steps were taken to remove RBC's but pre-extraction of lymphocytes from whole blood was deemed to be the best option. Therefore, optimisation of this technique to ensure no major differences between whole blood and pre-extracted lymphocytes from 3 donors was done using the G2 chromosomal radiosensitivity assay. To come to the conclusion of using extracted lymphocytes for Raman studies, optimisation was done using whole blood vs extracted lymphocytes with different doses of radiation. The methods are described here as part of the blood processing protocol for donor and cancer

patient samples (discussed later in chapter 3), but the results specifically on Raman spectroscopy are outlined in another PhD thesis at our Institute by Dr. A Maguire<sup>236</sup>.

## **2.2 Materials & Methods**

### **2.2.1. Blood samples and Ethics**

Blood samples were donated from 42 volunteers at our Institute (Dublin Institute of Technology, Kevin St, Dublin). 19 donors were male and 23 were female, with an age range from 21- 64 and 6 of the donors were smokers. 20 ml of circulating peripheral blood was extracted from donors and placed into heparinised vacutainers (Sarstedt). Ethical approval for this study was granted by the DIT Research Ethics Committee.

### **2.2.2 Whole blood cultures**

Whole blood cultures were set up using 2 ml of whole blood and 18 ml of pre-warmed (37°C) pre-gassed (5% CO<sub>2</sub>) RPMI medium (Sigma) supplemented with 12.5% FBS (Sigma), 2 mM L-glutamine (Sigma) and 0.2 ml (45mg Phytohaemagglutinin (PHA) PAA Laboratories). Cultures were incubated at 37°C with 5% CO<sub>2</sub> for 72 hours prior to radiation exposure. Whole blood cultures were stimulated with the mitogen PHA to induce and synchronise cultured lymphocytes into a cell cycle. 24hrs prior to irradiation, 15mls of media was removed from each culture and replaced with fresh pre-warmed and pre-gassed RPMI media supplemented as described above.

### **2.2.3 Histopaque Lymphocyte Isolation**

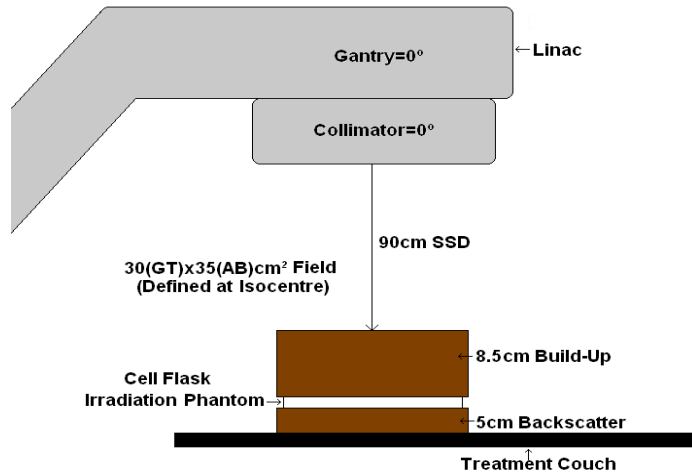
3 mL of whole blood was layered on to 3ml of Histopaque-1077 in a 15ml conical centrifuge tube and centrifuged at 400g for 30mins at room temperature with the brake off. After centrifugation, a plastic Pasteur pipette was used to carefully remove the opaque interface containing mononuclear cells which were transferred to a clean conical

centrifuge tube and washed 3 times with 10mls of PBS. The cell pellet was resuspended in 5 mL of RPMI (Sigma) and cultures were incubated for 72hrs. After 24hrs of incubation, media with lymphocytes were removed and placed in a fresh flask, while monocytes (adhered to the bottom of the flask) were removed by scraping, were then centrifuged and cultured in separate flasks.

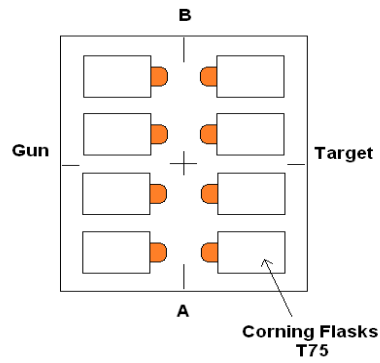
#### 2.2.4 Irradiation procedure

At 72 hours, whole blood cultures were irradiated in G2 phase of the cell cycle at 0.05 Gy and 0.5 Gy using linac 6MV Photons. The dosimetry was performed with Gafchromic film to ensure that each flask was irradiated with the actual dose required<sup>238</sup>. The film was calibrated against a Farmer type ionization chamber using the triple channel dosimetry method and the film was scanned using the single scan protocol<sup>239</sup> on an Epson Expression 10000 XL scanner using the recommended scanning resolution of 72 dpi in a 48-bit RGB format in a single scan<sup>240</sup>. Glass was placed over the calibration and test film during scanning to minimize ringing artefacts. The film was analysed using FilmQAe Pro (Ashland Inc.). This calibration technique was needed to ensure that all flasks for the study were irradiated at the exact doses required, and that each flask (all 42 donors with 6 flasks each) was irradiated in exactly the same conditions.

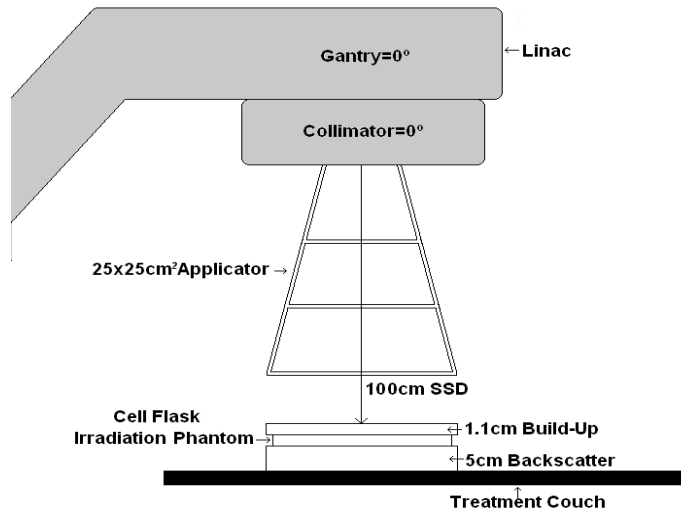
For investigation of radiobiological responses in cells between radiation sources, three sets of cultures were set up per donor with 20 donors investigated in total. The first set were irradiated using  $\gamma$  irradiation from the <sup>60</sup>Co Teletherapy unit (Theratron 780 E, MDS Canada). The second set was exposed to a 6 MV x-ray photon beam and the third set to a 12 MeV electron beam on an Elekta Precise Linac. Irradiation procedures were set up as per figure 2.2.



(a)



(b)



(c)

Figure 2.2 Irradiation procedure set up. Figure (a) 6MV Photon irradiation set-up, (b) Cell Flask Irradiation Phantom, (c) 12 MeV Electron irradiation set-up

### 2.2.5 Post irradiation Cytogenetics

After irradiation, cultures were incubated for 30 mins and then incubated with 200 $\mu$ l of colcemid (1 $\mu$ g/ml stock) (Gibco) at 37°C with 5% CO<sub>2</sub> for 60mins to arrest cells in metaphase. Samples were centrifuged at 1200rpm for 10mins at 0°C and an ice cold hypotonic solution was added (5mls of 0.075mM KCL) to lyse red blood cells. Samples were incubated on ice for 20mins to prevent chromatid damage repair. All further centrifugation steps were carried out at 0°C at 1200rpm for 10 minutes. The extracted chromosomes were fixed with 3:1 methanol: acetic acid twice and then stored at 4°C until slide preparation

For slide preparation, slides were pre-cleaned in methanol 24hrs prior to use and stored in deionised water until needed. Cell suspensions were centrifuged at 1200rpm for 10mins and resuspended in 1ml of fixative. Cell suspension was dropped on to 3 slides per dose and per donor. Slides were gently flamed over a Bunsen burner to fix cells onto the slide and were left to cool. Slides were then stained with 3% Giemsa (Gibco) prepared in pH 6.8 buffer (BDH Chemicals) for 15mins. All slides were then mounted in DPX.

Microscopy was carried out to obtain mitotic indices and G2 radiosensitivity scores. The mitotic index was calculated by counting the ratio of metaphase spreads among interphase cells from a total number of 1000 cells. G2 radiosensitivity was determined by analysing 100 clear metaphase spreads at x 100 magnification for chromatid aberrations which mainly consisted of chromosome breaks and gaps. Chromosomes were also counted for any numerical abnormality (e.g. alteration in chromosome number from 46). Figure 2.1 outlines examples of the types of aberrations analysed. Most metaphase aberrations included chromatid gaps or breaks, little to no exchanges (cte) or complex aberrations were observed in the healthy control donor cohort.

The data was recorded for all slides of the same donor (0Gy, 0.05Gy and 0.5Gy). Aberrations found in the 0Gy control are known to be spontaneous aberrations and a G2 score was calculated for the number of aberrations per 100 metaphases scored and this acted as the control for the set of samples per donor. These control G2 scores were subtracted from the G2 scores recorded at the different radiation doses 0.05Gy and 0.5Gy and are recorded as radiation-induced G2 scores for a particular dose per donor.

#### 2.2.6 Statistical Analysis

All statistical analysis was carried out using Microsoft Excel 2010 and GraphPad Prism 5<sup>241</sup>. Coefficient of variation (CV) was calculated by dividing the mean by the standard deviation and multiplying by 100 to obtain a % variation value. The 90<sup>th</sup> percentile was calculated on each dose by using the “percentile” function in Microsoft Excel in the following formula; =percentile (A1:A42, 0.9) where A1 – A42 represent the excel cells with each donor value at that dose and 0.9 represents the 90<sup>th</sup> percentile.

Non-parametric statistics were used as no assumptions were made about the sampling population distribution and how many donors would need to be sampled. This analysis was carried out using Graphpad prism 5. Analysis of variance (ANOVA) was used to compare donors and doses to the control.

### 2.3 Results

The mitotic index and G2 radiosensitivity scores were calculated per donor to obtain radiation induced mitotic inhibition (MIn) and radiation induced G2 scores (RIG2). These values were then used to obtain inter- and intra-individual variation and 90<sup>th</sup> percentiles to assess assay reproducibility and validity. Brief details of optimisation of blood culturing and conclusion of techniques chosen for analysis are provided.

### 2.3.1 Mitotic index

The mitotic index is the ratio of cells in metaphase to all other cells present on the slide and it was calculated from each dose (0, 0.05 and 0.5Gy) per donor. Analysis from 42 healthy control donor samples revealed a decrease in mitotic index value with increasing dose (Figure 2.3). The highest mitotic index value was found to be 4.4% at 0.05Gy from HC41, and the lowest value was 0.1% at 0.5Gy from donor HC37. A large distribution in mitotic index was observed across all donors.

Cell cycle checkpoint response was assessed by calculating a mitotic inhibition value (MIn), which is the mitotic index at each dose (0.05 and 0.5Gy) subtracted from the control (0Gy) mitotic index value. An increase in mitotic inhibition (decrease of mitotic index) was observed in all donors and values lay below 5%. Comparison of MIn values between 0.05Gy and 0.5Gy compared to the control was significantly different ( $p < 0.001$ ) demonstrating efficient checkpoint response after ionizing radiation. Comparison of MIn between 0.05Gy and 0.5Gy were also significantly different ( $p \geq 0.002$ ) showing a dose response. The largest MIn (difference between irradiated and non-irradiated) was found to be a difference of 2.8% from donor HC22 at 0.5Gy, and the smallest MIn was found to be 0.1% from donor HC25 at 0.05Gy.



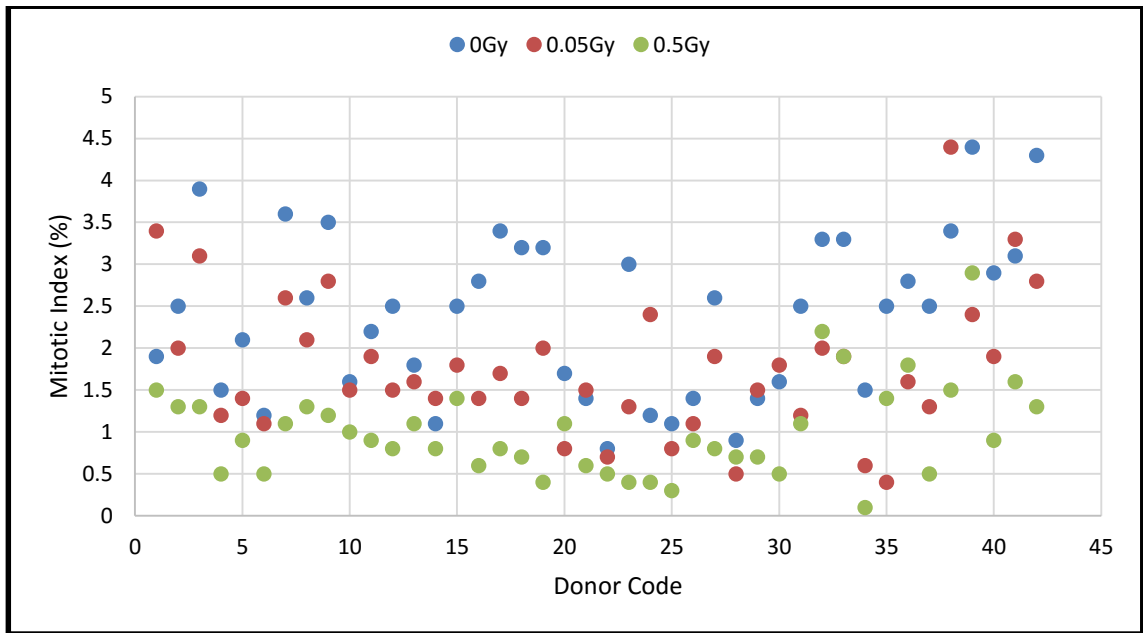


Figure 2.3 Distribution of mitotic index values from 42 healthy donors. Non-irradiated, 0Gy control samples are presented in blue, 0.05Gy samples in red and 0.5Gy samples in green.

### 2.3.2 G2 chromosomal radiosensitivity scores

The G2 chromosomal radiosensitivity score was derived from calculating the total number of structural aberrations (chromatid breaks and gaps) in 100 metaphase cells per dose per donor (Figure 2.4). This ranged from a minimum of 0 at 0Gy in a number of donors to a maximum of 218 at 0.5Gy from donor HC18.

A radiation-induced G2 chromosomal radiosensitivity score was calculated by subtracting the 0Gy control (non-irradiated spontaneous aberrations) from the irradiated (0.05Gy or 0.5Gy) G2 scores per donor. The distribution of G2 radiosensitivity scores for all 42 healthy donors per dose (0, 0.05 and 0.5Gy) were varied (Figure 2.4). It was evident that G2 scores were dependent on dose based on the discrimination between the values per dose and donor in Figure 2.4.

A significant increase in G2 scoring at 0.05Gy and 0.5Gy samples was observed compared to the non-irradiated control ( $p < 0.001$ ). Also, a significant increase in G2

scoring from 0.05Gy to 0.5Gy was observed ( $p < 0.001$ ) with scores doubling or more between dose indicating a dose dependent response.

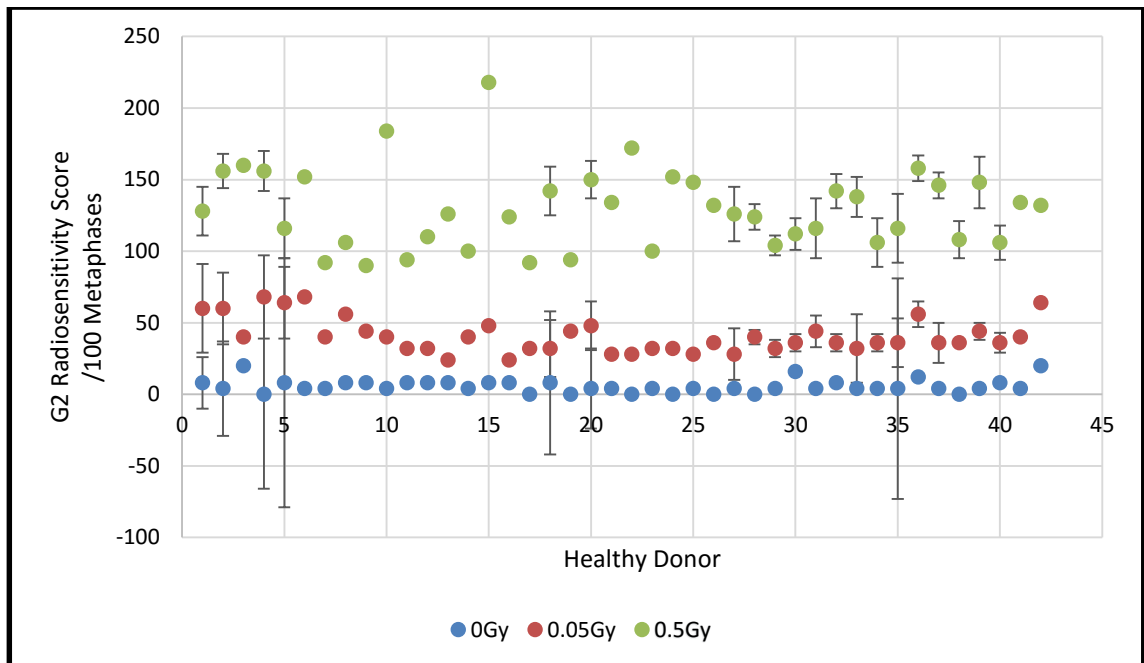


Figure 2.4 Distribution of individual G2 radiosensitivity scores from 42 healthy donors. 0Gy non irradiated controls are presented in blue, 0.05Gy represented in red and 0.5Gy represented in green. Error bars have been added to those donors which were sampled more than once.

### 2.3.3 Validation of the assay – Variation and Radiosensitivity Cut off

The blood samples from 42 normal individuals were obtained for irradiation at two doses (0.05Gy and 0.5Gy) and a sham-irradiated control (0Gy). The mean ( $\mu$ ), standard deviation (SD), and coefficient of variation (CV) were calculated per dose per group ( $n=42$ ) (Table 2.3). Using all 42 donors, inter- individual variation values were calculated (CV as described in methods section) as a measure of assay reproducibility from the radiation induced G2 scores assigned per donor. An inter-variation value of 34% was obtained for 0.05Gy and a value of 22% was obtained at 0.5Gy. Intra-individual variation was calculated using 3 donors, sampled at multiple times over the course of 4 years (table

2.3). From table 2.3, the mitotic index and G2 radiosensitivity score is given for the 3 donors coded HC3, HC8 and HC38. Intra- variation fell below a value of 30% at 0.05Gy and below a value of 26% for 0.5Gy. All values in the present study were comparable, but slightly higher than previous studies which report ranges of 4%-15% for intra-variation (explained in table 2.2)<sup>144,148,158,234</sup>.

Table 2.3 Intra individual variation values for three healthy donors who consented for multiple samples over a period of 4 years. Raw G2 Radiosensitivity scores are presented. The intra variation at 0.5Gy is highlighted as this measurement is routinely used at a dose of between 0.1-0.5Gy.

	Mitotic Index			G2 Radiosensitivity Score		
	0Gy	0.05Gy	0.5Gy	0Gy	0.05Gy	0.5Gy
Sample No.	HC3					
1	2.5	2	1.3	4	60	156
2	1.6	1.7	0.7	4	40	116
3	2.7	1.9	0.4	4	32	132
4	2	1.1	1.1	4	32	134
5	3.6	2.7	1.6	0	32	126
6	3.6	2	0.7	4	36	124
Intra-variation				49%	30%	10%
	HC8					
1	2.1	1.4	0.9	8	64	116
2	1.2	0.5	0.1	0	44	170
3	2.8	2.1	1	12	28	138
4	1.6	0.4	0.4	8	56	188
5	1.5	1.4	0.7	8	44	156
Intra-variation				60%	29%	18%
	HC38					
1	2.5	0.4	1.4	4	36	116
2	3.6	1.7	0.6	4	32	122
3	1.7	1.5	0.8	16	44	208
4	4	4.4	2.2	4	48	160
5	3.9	2.9	4.2	4	28	128
Intra-variation				84%	22%	26%

A radiosensitivity cut off value was defined by calculating the 90<sup>th</sup> percentile of each group at each dose (Table 2.4). This value represents a threshold of which 90% of the donor population fall below. The radiosensitivity cut off value can also be represented graphically, as shown in figure 2.5. Donors who lie to the left of this dashed line (which represents a radiosensitivity cut off) are considered normal while those donors who lie to the right of the line are considered slightly radiosensitive. As 0.5Gy is considered the most radiosensitive dose, 7 donors were considered radiosensitive as their G2 values lay above the cut off for 0.5Gy.

Table 2.4 Summary of statistics from G2 scoring of 42 healthy controls. The radiosensitivity cut off values are represented by the 90<sup>th</sup> percentile values.

	0.05Gy	0.5Gy
Mean	35 aberrations/100 metaphases	124 aberrations/ 100 metaphases
St. Dev	12	27
90 <sup>th</sup> Percentile	51	152
C.V (%)	34%	22%

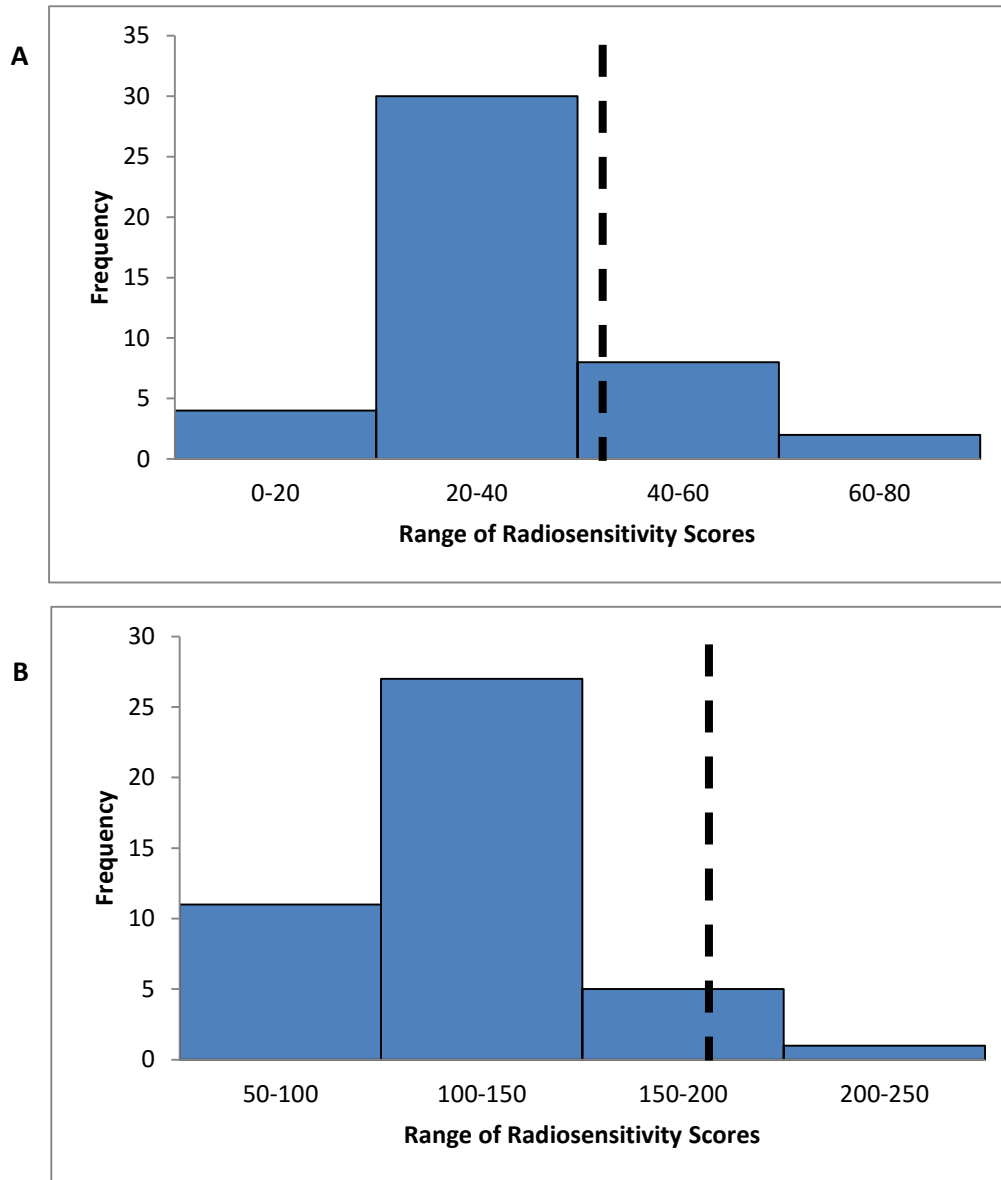


Figure 2.5 Range of radiosensitivity scores from 42 healthy donors at 0.05Gy (a) and 0.5Gy (b). Radiosensitivity cut offs are represented by a dashed line on each graph for each dose. Spontaneous aberrations from the control were subtracted from each dose to give radiation induced G2 sensitivity scores.

No significant difference was observed in radiosensitivity scores between male and female samples at any dose ( $P > 0.17$ ). A higher aberration frequency was observed in all of the donors who smoked compared to non-smokers except for one pair of donors which showed the opposite, only at 0.05Gy (Figure 2.6) ( $p=0.019$ ).

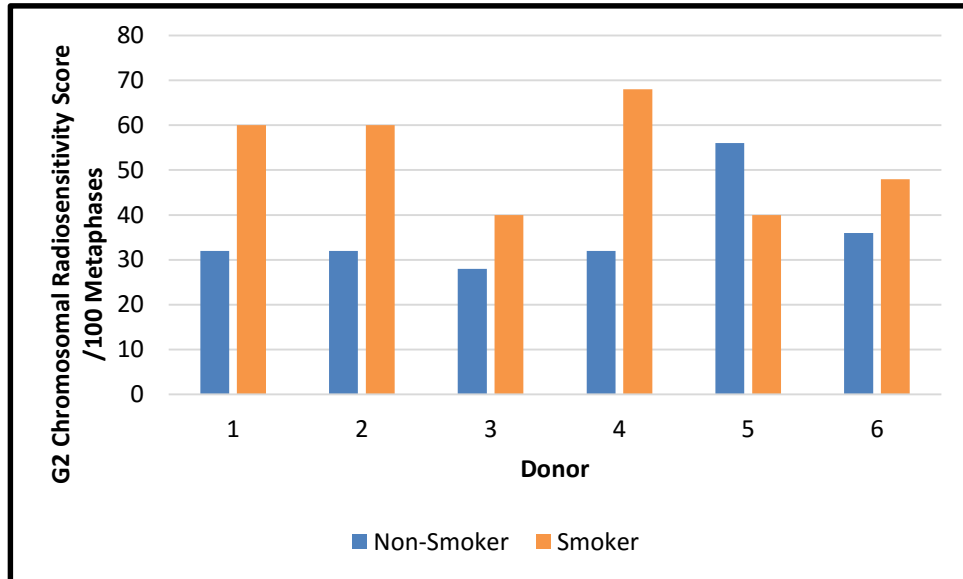


Figure 2.6 Differences in G2 chromosomal radiosensitivity between smoker and non-smoking donors. Donors were sex matched before statistical analysis.

#### 2.3.4 Correlations

Investigation of links between MIn and radiation induced G2 scoring in addition to age, and season of blood sampling was done (Figure 2.7). A small significant ( $P = 0.049$ ) ( $R = -0.31$ ) negative correlation was found at 0.05Gy between age and MIn. As age increased, the MIn decreased. This was not significant at 0.5Gy ( $P = 0.054$ ) ( $R = -0.3$ ).

A significant negative correlation was found with age and radiation induced G2 scores at 0.05Gy (Figure 2.7). As age increased, radiosensitivity score decreased significantly ( $P = 0.0009$ ) ( $R = -0.5$ ). This was not significant at 0.5Gy ( $P = 0.42$ ) ( $R = -0.13$ ).

No significant correlation of MIn and radiosensitivity score was observed at 0.05Gy (Figure 2.8) ( $P = 0.4$ ) ( $R = 0.13$ ). However, a significant negative correlation was observed between MIn and radiosensitivity score at 0.5Gy (Figure 2.8) ( $P = 0.0077$ ) ( $R = -0.41$ ).

A significant correlation between season of blood sampling and mitotic index was observed at 0Gy ( $P = 0.0065$ ) ( $R = -0.4285$ ) and 0.5Gy ( $P = 0.0001$ ) ( $R = -0.5760$ ) but

not at 0.05Gy ( $P = 0.3881$ ) ( $R = -0.142$ ). The mitotic index was lower toward December, and highest in January.

Additionally, a significant correlation was found between season of blood sampling and G2 radiosensitivity scoring of donors at 0.05Gy ( $P = 0.0428$ ) ( $R = -0.3260$ ) but not at 0Gy ( $P = 0.3$ ) ( $R = -0.1711$ ) or 0.5Gy ( $P = 0.9$ ) ( $R = -0.020$ ). With the significant correlation at 0.05Gy, G2 scores were slightly higher in January and lower toward the following December.

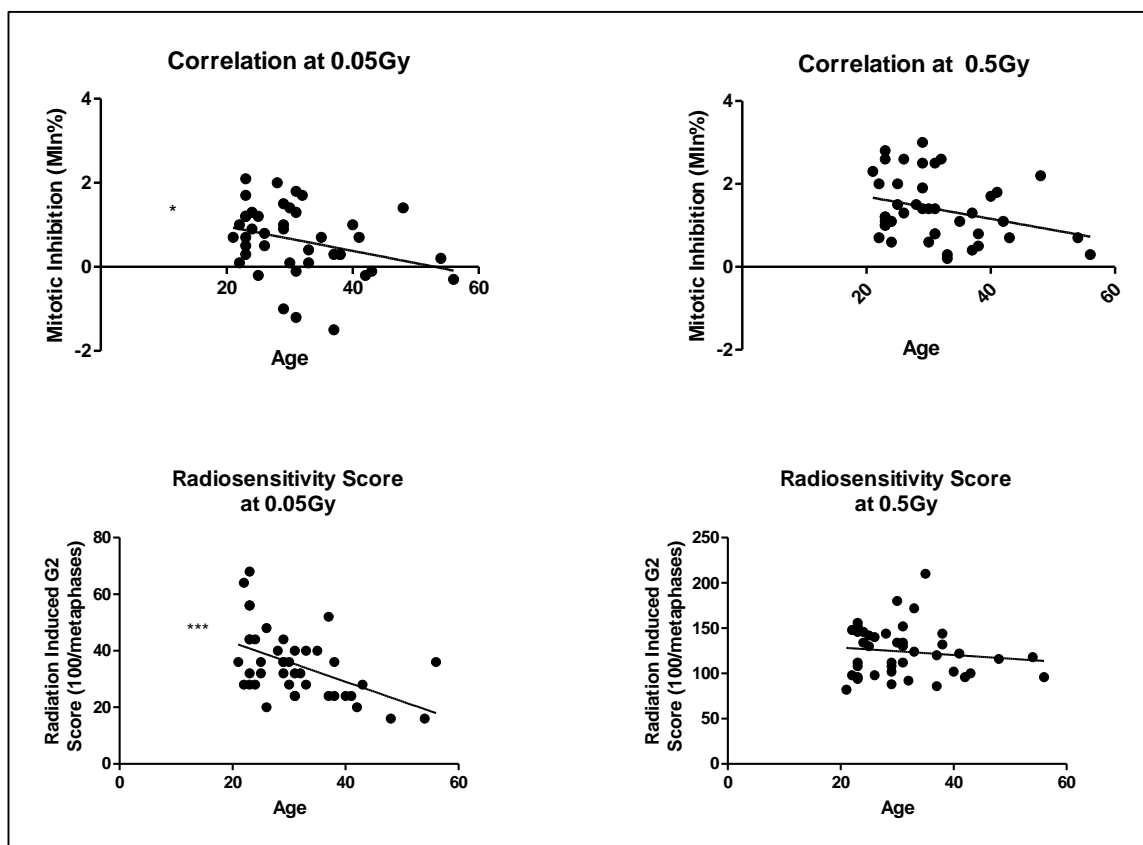


Figure 2.7 Pearson R correlation of age with mitotic inhibition (MIn) and Radiosensitivity score. Correlation of age with MIn at 0.05Gy and 0.5Gy are presented in the top panel. Values at each dose have been subtracted from the 0Gy non-irradiated control. Correlations of Age with Radiosensitivity score at 0.05Gy and 0.5Gy are presented in the bottom panel. The 0Gy non-irradiated control has been subtracted from both doses.

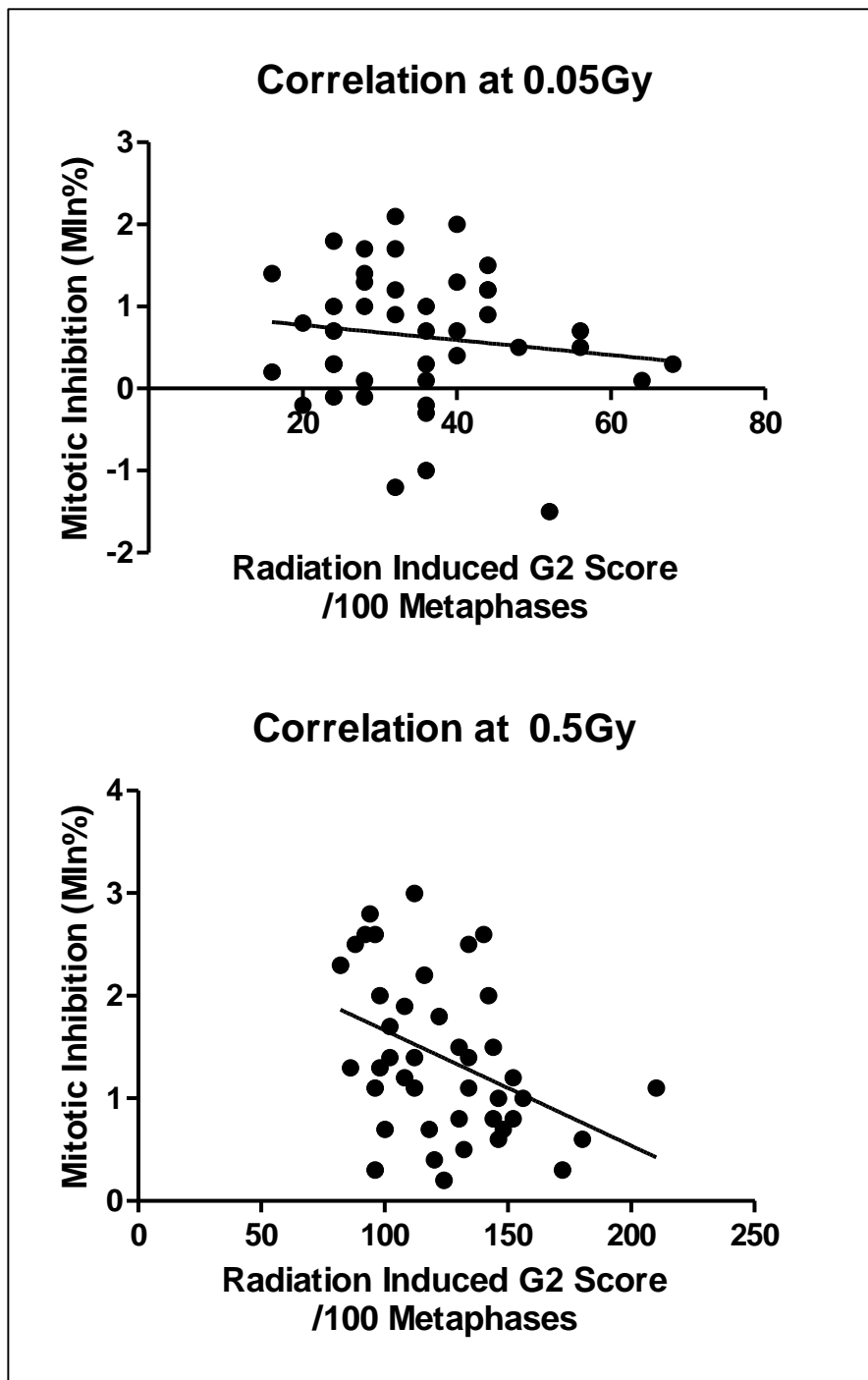


Figure 2.8 Pearson R correlation of Mitotic inhibition (MIn) with Radiosensitivity score. The top panel represents no correlation at 0.05Gy, and the bottom panel represents a negative correlation with MIn and Radiosensitivity Score.



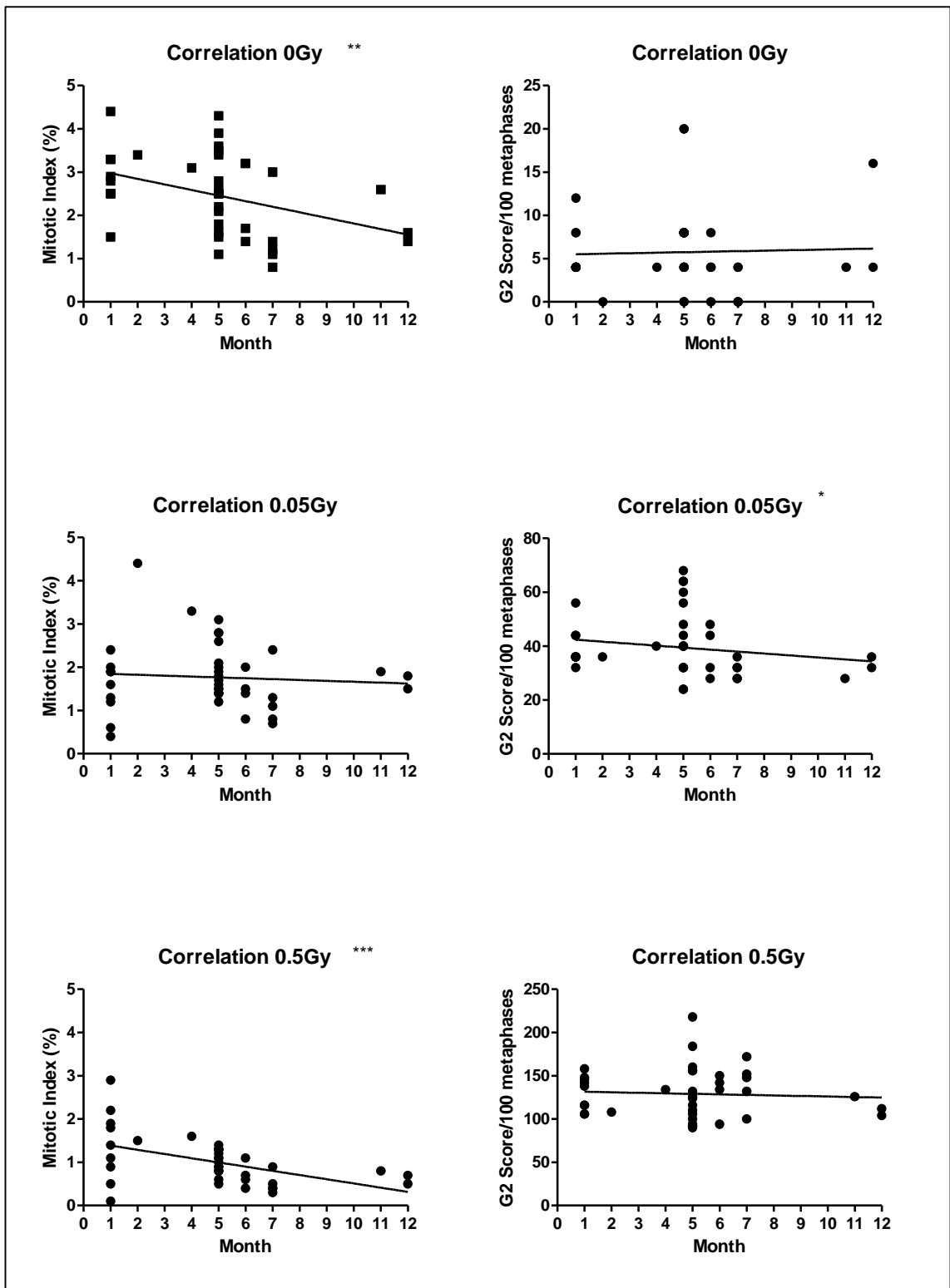


Figure 2.9 Correlations between month of blood sampling from healthy donors and Mitotic Index values (left panel) and G2 radiosensitivity Scores (Right panel). \* Denotes significant correlation i.e.  $P \leq 0.05$ .

### 2.3.5 Culturing Effects

A slight but not significant difference in G2 scores between whole blood and pre-extracted lymphocytes was observed in 3 donors (Figure 2.10) ( $p=0.6531$  at  $0.05\text{Gy}$  and  $p=0.2$  at  $0.5\text{Gy}$ ). Doses of  $2\text{Gy}$  were also investigated using the G2 radiosensitivity assay (Raw Data, appendix 10.4) and high aberration frequency along with high inhibition was observed. Aberrations were in excess of  $>300$  per 100 metaphases.

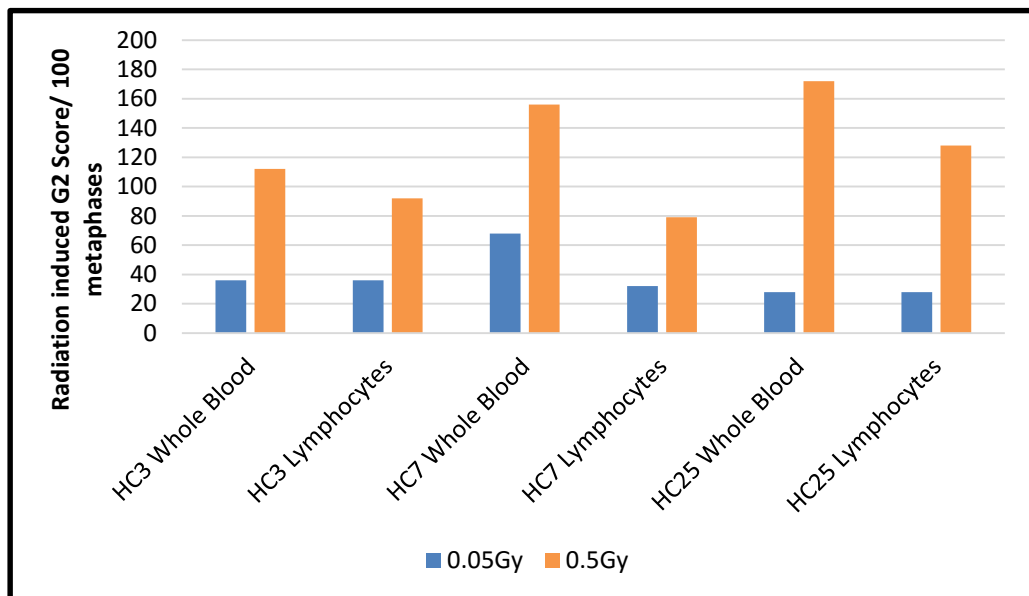


Figure 2.10 Comparison of radiation induced G2 scores from whole blood vs pre extracted lymphocytes. Blue bars represent values obtained at  $0.05\text{Gy}$  and orange represent  $0.5\text{Gy}$ . Spontaneous aberration yield at  $0\text{Gy}$  was subtracted from each dose.

### 2.3.6 Beam energy effect

Cell cycle checkpoint response was assessed by calculating a radiation induced mitotic inhibition value (MIn) (explained in section 2.3.1). MIn values per dose and radiation type are shown in figure 2.11.

Comparison of means showed that inhibition was observed in all donors as MIn values fell below 5%. MIn values between control and irradiated samples were significantly different ( $P < 0.001$ ). MIn values were compared between radiation source (Co-60, Linac Photon and Linac Electron) by using ANOVA. Inhibition was observed in all donors across all sources, but no statistically significant difference was observed between sources ( $p = 0.8835$ ). Considerable inter – individual variation of mitotic index was observed within the donor group, but consistent across radiation source for each donor (Table 2.5).

Table 2.5 Summary of statistics for radiation induced G2 scores for all beam sources at 0.05Gy and 0.5Gy. Mean, standard deviation (St. Dev), coefficient of variation (CV) and radiosensitivity cut offs (90th percentile) are shown

		<b>Co60 Photon</b>	<b>Linac Photon</b>	<b>Linac Electron</b>
<b>0.05Gy</b>	Mean ( $\mu$ )	32.6	32.8	34.5
	SEM	1.45	1.682	1.857
	CV (%)	20.01%	22.93%	21.54%
	90th Percentile	40	44	42
<b>0.5Gy</b>	Mean ( $\mu$ )	124.6	113.3	116.4
	SEM	5.016	3.937	5.742
	CV (%)	18%	15.54%	19.74%
	90th Percentile	147	132	144

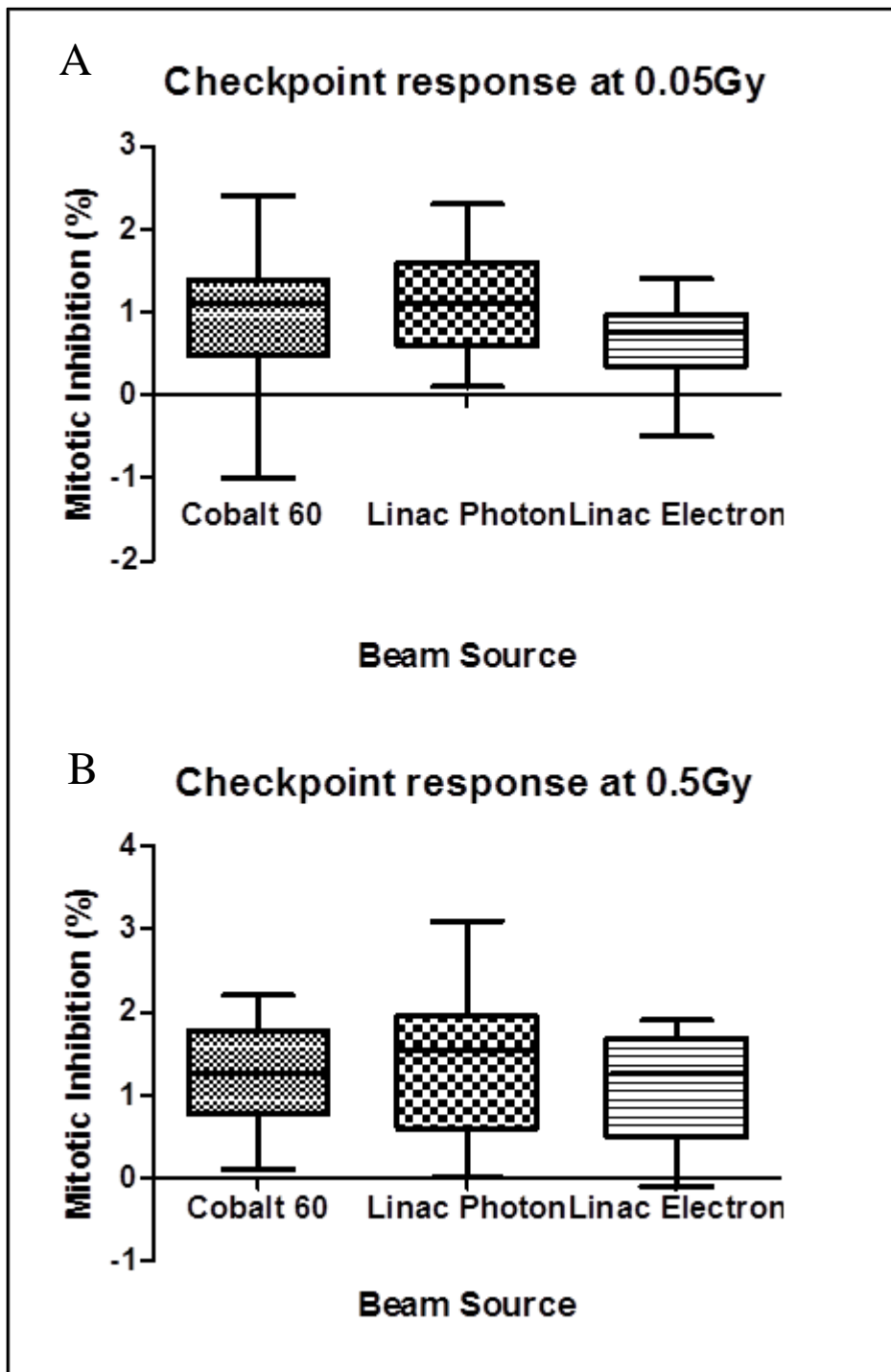


Figure 2.11 Checkpoint response as calculated from radiation induced mitotic inhibition at a) 0.05Gy and b) 0.5Gy. Mitotic index values for each dose point were subtracted from the 0Gy control to give a mitotic inhibition value. Data from 6MV photons (Linac) and 12MeV electrons (Linac) are presented compared to Cobalt 60. Error bars represent upper and lower values.

Distribution of G2 radiosensitivity scores are illustrated as boxplots in Figure 2.12 for each dose and each source. No statistically significant difference between radiation sources ( $^{60}\text{Co}$ , linac photon and linac electron) was observed ( $P=0.2305$ ).

A significant difference in G2 score between 0Gy control and irradiated (0.05Gy and 0.5Gy) samples was observed ( $p < 0.001$ ). In addition, a significant difference between each dose (0.05Gy and 0.5Gy) was observed ( $p < 0.001$ ) with G2 scores increasing at least three fold. Comparison of G2 scores between radiation sources was performed using ANOVA. No statistically significant difference in G2 scores between sources was observed ( $p > 0.05$ ).

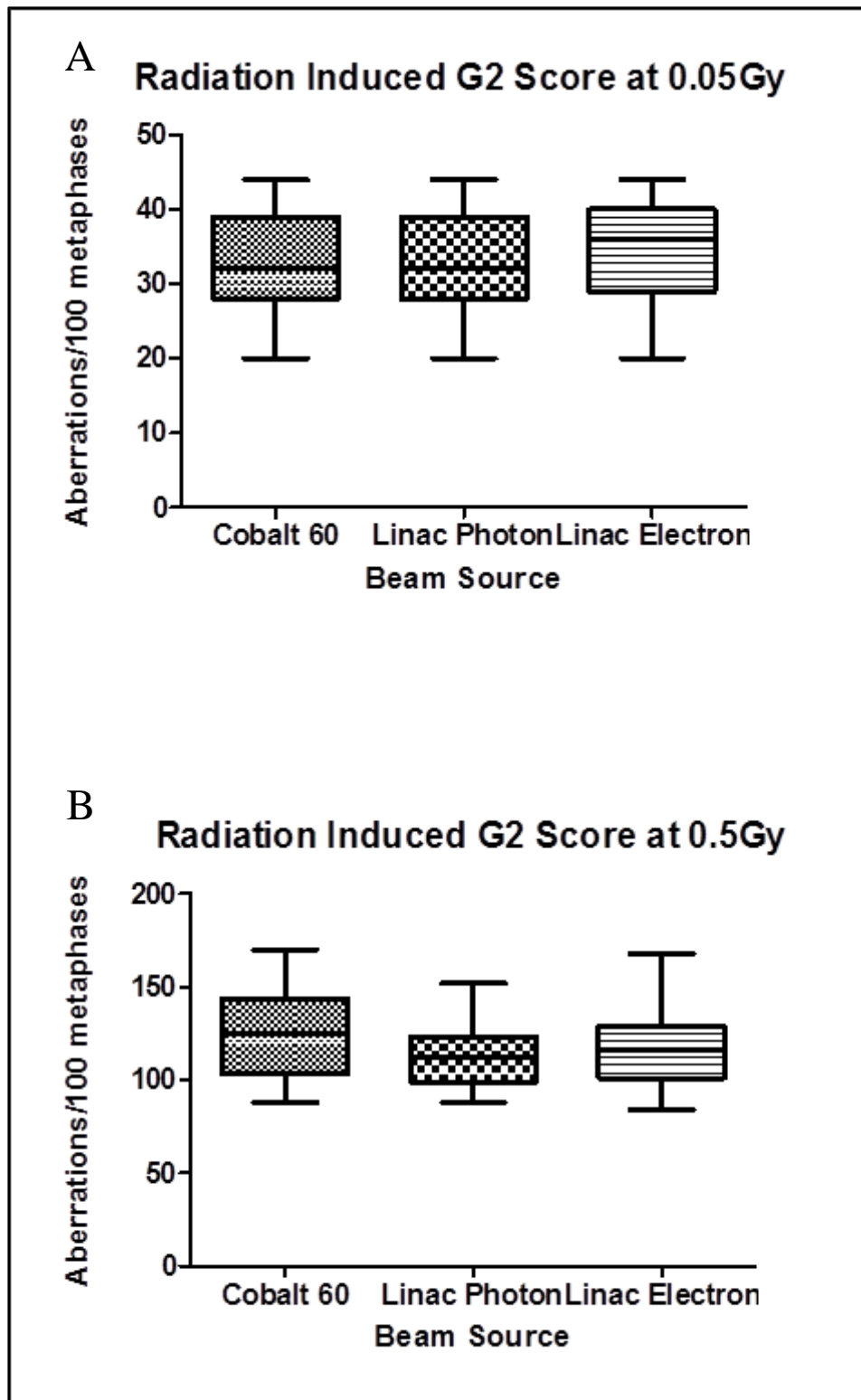


Figure 2.12 G2 Chromosomal radiosensitivity at low doses from clinical sources (Linac photon 6MV and Linac electron 12MeV). Boxplots show G2 radiosensitivity scores from blood samples taken from 20 Healthy control donors irradiated to a) 0.05Gy and b) 0.5Gy. The spontaneous aberration yield from the 0Gy control was subtracted from each dose to give a radiation induced G2 radiosensitivity score. Error bars represent upper and lower values.

## 2.4 Discussion

### 2.4.1 Checkpoint Response

Mitotic index is a measure of individual checkpoint response, which should respond quickly and effectively to radiation insults. Significant drops in mitotic index were observed in control donors as shown with a decrease in mitotic cells (from a maximum of 4.4% to a minimum of 0.1%) indicating good cell cycle checkpoint efficacy. The mitotic inhibition is derived from subtracting the mitotic index at each dose from the control, non-irradiated sample value. A significant increase in mitotic inhibition was observed in irradiated samples (both 0.05Gy and 0.5Gy) compared to control samples. There was also significant mitotic inhibition between 0.05Gy and 0.5Gy. It was expected that mitotic inhibition would increase following ionizing radiation exposure in a molecular DNA damage response to radiation. This suggests an inhibition of cyclin-CDK complex (cyclin B – CDC2), which prevents the cell from progressing into mitosis. Therefore, blood lymphocytes exposed to radiation (0.05 and 0.5Gy) through the G2 chromosomal radiosensitivity assay would have a reduced number of cells in mitosis compared to the control (0Gy). For very low doses of 0.05Gy this has not been done previously, and for 0.5Gy values of up to 15% were obtained in some early reports<sup>152,242</sup>.

This increase in mitotic inhibition was discovered in early reports in response to irradiation and lower mitotic inhibition was observed in a cohort of breast cancer patients<sup>150</sup>. A reduced mitotic inhibition is expected in samples from cancer cohorts, as mutations in the tumour suppressor genes (such as P53) controlling cell cycle progression are key factors in carcinogenesis. In 2005, another report using blood samples from healthy controls and prostate cancer patients demonstrated a lower mitotic inhibition in response to irradiation in the cancer cohort<sup>158</sup>. The response to irradiation described here suggests a contribution of the two G2 phase checkpoints. The ATM independent and dose dependent checkpoint which is thought to be activated in response to doses of 0.5Gy and

responds to accumulation of cells damaged in G1/S. This checkpoint inhibits progression in the cell cycle in response to doses between 1Gy and 10Gy. In normal conditions, the G2 checkpoint involves activation and stabilisation of CDC25 which inhibits CDC2 and allows progression as normal in the cell cycle. However, in response to activation of CHK1 by ATM, Wee1 is phosphorylated, activated and stabilised which inhibits CDC25 activity and therefore cannot associate with CDC2 and prevents progression of the cell in the cell cycle through a stable G2 arrest<sup>243</sup>. The ATM dependent and dose independent checkpoint, causes upregulation of p21 which inhibits CDK1 – cyclin B complex and therefore results in G2 arrest<sup>244</sup>. It is well known that radiosensitive populations exhibit a delayed mitotic inhibition, with reports dating back to 1994. Those reports used skin fibroblasts from AT patients to demonstrate an increased G2 chromosomal radiosensitivity concluding that there is a defective G2 checkpoint in AT patients<sup>152</sup>. This defect, is rather described now as a “delayed” checkpoint in AT patients relating back to the absence of ATM and cell cycle inhibition by other checkpoints (CDC2 – CDC25)<sup>245</sup>. This is now well documented and ATM is known to be a key player in the DNA damage response which transduces the damage from radiation exposure so that CDK1 – Cyclin B is inhibited and cell cycle progression is halted.

#### 2.4.2 G2 Chromosomal Radiosensitivity

G2 aberration analysis involves recording the amount of chromatid aberrations in 100 metaphase cells in each sample, at each dose, and assigning a G2 score to each individual. The G2 score is indicative of individual radiosensitivity, and varies between doses. Here, spontaneous aberration yields in samples from healthy controls were minimal at under 20 aberrations/100 metaphases analysed. This was a little higher than previous reports, which is most likely due to the subjectivity of G2 aberration scoring, as the radiosensitive cut off values in this study were slightly higher than previous reports<sup>150,165</sup>. A significant



increase in aberration yield between 0.05Gy and 0.5Gy was observed, as well as significant differences between doses and controls ( $P < 0.002$ ). Again, a higher aberration yield was expected in response to radiation. A natural variation in aberration yield was observed between the 42 healthy donors, which represents variation in intrinsic radiosensitivity in the individual donors.

After obtaining a range of G2 radiosensitivity scores for the 42 healthy controls, a 90<sup>th</sup> percentile was calculated which represents the radiosensitivity cut off value within the cohort. This was done for 0.05Gy and 0.5Gy, and a cut off value of 51 and 152 was found for each dose respectively. The value at 0.5Gy was used as this represents the most sensitive dose for the G2 assay<sup>150,158,246</sup>. This value represents a cut off for radiosensitive donors, samples with values that fall above this point are considered radiosensitive (figure 2.3b). From the data generated 7 donors were deemed radiosensitive, but surprisingly were not the same 7 donors for each dose i.e. those who are considered radiosensitive at 0.05Gy may not be radiosensitive at 0.5Gy and vice versa). This could suggest that different molecular mechanisms are initiated at each dose. The 7 donors' samples considered radiosensitive would be candidates for further investigation, if variation induced by extrinsic factors were ruled out (e.g. smoking, hormone status, age). This is consistent with a recent radiobiological report conducted in our laboratory that demonstrated a significant upregulation of critical apoptotic genes at the lower dose of 0.05Gy compared to 0.5Gy and therefore different mechanisms of arrest, repair or cell death in biological systems is possible for low doses of radiation<sup>247</sup>. This response at lower doses was further shown in a recent report that showed differing cellular response pathways at low doses of radiation concluding that directly irradiated cells undergo apoptotic, necrotic and some mitotic cell death compared to bystander cells which predominantly undergo mitotic cell death<sup>248</sup>. Furthermore, Beels *et al* recently showed a hyper sensitivity response at lower doses (<0.5Gy) using whole blood and isolated T

lymphocytes, in response to x-irradiation, in which the hypersensitivity response at lower doses was not observed after  $\gamma$ -irradiation at low doses<sup>249</sup>. The radiosensitive cut off value obtained in this healthy control cohort is of importance in chapter 4 using cancer and AT cohorts as it provides a radiosensitivity benchmark to report which patients are considered more radiosensitive in response to radiotherapy.

### 2.4.3 Correlation Analysis

Previous reports have suggested a correlation between mitotic inhibition and G2 radiosensitivity<sup>158</sup>. It was expected that radiosensitive patients who have a higher aberration yield (G2 radiosensitivity score) would also have a higher mitotic inhibition. A Pearson's Rank correlation was performed between checkpoint response (MIn) and radiation induced G2 chromosomal radiosensitivity. A slight, significant negative correlation between MIn and G2 scoring was observed ( $p = 0.0077$ ) ( $R = -0.41$ ). This result is surprising, as it is expected that an increase of radiation induced damage would cause a more pronounced MIn checkpoint response. In previous cancer patient reports a correlation was found between mitotic inhibition and G2 radiosensitivity using a prostate cancer cohort<sup>158</sup>. The correlation may not be as evident in normal healthy donors compared to more radiosensitive cancer populations. In 1994, Scott *et al* reported significant mitotic delay in radiosensitive subpopulations by describing a highly variable mitotic inhibition in AT patients in comparison to controls<sup>152</sup>.

A significant correlation was observed with age and MIn at 0.05Gy. As age increases, MIn decreases. In early reports, Scott *et al* also showed a reduced mitotic inhibition with increasing age<sup>152</sup>. Altered mitotic inhibition values represent defects in cell cycle checkpoint control and efficiency. The effect of age on cell cycle could be a result of telomere shortening which is known to be associated with the ageing process and involved

in genomic instability. A significant correlation of age and G2 radiosensitivity was also observed at 0.5Gy, which showed a reduced aberration yield with increasing age. The opposite was observed in an early study by Ramsey *et al* in 1995 who showed an increase in aberration yield with increasing age using chromosomal painting techniques. But in this report, variables such as exposure to asbestos, diet/intake of sweeteners, suffering from a major illness and smoking were recorded, which would contribute to accumulation of cytogenetic damage<sup>250</sup>. The variables examined in the mentioned report were not recorded in this work, and there are limited reports within the literature therefore more investigation of factors affecting individual radiosensitivity are encouraged.

A correlation of MIn and G2 radiosensitivity was also previously shown by Howe *et al* in 2005<sup>158</sup> using control and prostate cancer and benign prostate hyperplasia patients. A small positive correlation was found between mitotic inhibition values and radiation induced G2 scores in the prostate cancer patient cohort, but no significant correlation between the endpoints was found in control or benign prostate hyperplasia patients.

In the data presented, a small significant correlation with MIn and season of blood sampling was found at 0Gy and 0.5Gy. The MIn reduced toward December and was at its highest in January. There has been no reference to this finding in other reports, but it has been suggested that diet can affect cell cycle kinetics, such as caffeine intake. For e.g. an early study by Lau *et al* showed that caffeine in combination with DNA damaging agents increased the potency of the drug and therefore induced a more pronounced cell cycle inhibition.

#### 2.4.4 Assay Validation

Two measures used to validate the assay successfully were inter individual variation and intra- variation. Previous reports have calculated inter-individual variation values in cohorts of various donors/patients of 15% - 39% (Chapter 2 section 2.2). The inter-

individual variation values were calculated from the radiation-induced G2 scores for both dose points 0.05Gy and 0.5Gy in this study were 34% and 22% respectively. These results fall within the acceptable range according to the literature. It is of interest that higher variation was observed at the lower doses, further adding speculation about the different molecular events that possibly occur at very low doses. It has been reported that female hormonal status has an effect on G2 scoring with increased variation in female donors<sup>251</sup>. There have been other physiological conditions attributed to variation such as smoking, medication, immune and hormonal status<sup>251</sup> although in this work only a significant difference in smoker vs non-smoker at 0.05Gy was found, with no differences between male and female donors. Significantly lower aberrations were observed in the non-smoking donors compared to smokers' which is not surprising as these cells would have more DNA damage occurring daily in response to carcinogen exposures, therefore leading to a higher damage rate. The intra - variation values (samples obtained 5 or 6 times) per individual for each dose 0.05Gy and 0.5Gy, fall below values of 29% and 10% respectively, which is also comparable with the literature for 0.5Gy. Inter-individual differences in samples are expected and are what makes a radiosensitive assay successful as a patient's radiosensitivity status should be determined based on the measurement taken directly that day and date in the clinic. Due to fluctuations in the intra-variation of patient sampling it was previously suggested by Smart *et al*<sup>170</sup> that more than one sample should be taken if the G2 assay is incorporated for use within the clinic.

#### 2.4.5 Beam Energy Effect

Another factor which was previously described to affect G2 radiosensitivity was radiation beam energy. Although most reports described differences between low and high LET, it was not known if little differences in beam energy of similar LET but delivered from different sources would be observed. In the current work, the distribution of G2 scores

and mitotic index values between sources showed similar minimum and maximum values and overlapping error bars which demonstrates no significant difference in G2 radiosensitivity or mitotic inhibition between sources. Therefore, regardless of beam source, the same effect was observed. To the best of the authors knowledge, no previous reports investigating this exist.

## **2.5 Aims of chapter and conclusions**

To summarise, the G2 chromosomal radiosensitivity assay was optimised and validated at our laboratory for further use on patient cohorts, with good assay reproducibility and reliability. The values obtained in the current work were in accordance with other published studies in the area. This was confirmed by expected levels of mitotic indices representing G2 checkpoint efficacy, G2 scores and 90% percentile for the donor control study consisting of 42 donors. Furthermore, variation was assessed between donors for inter-variation of all 42 donors and intra-variation of 3 donors sampled 5/6 times. This was also in accordance with published studies. Additionally, our study shows no significant difference in radiobiological response with beam energy as measured by chromosomal radiosensitivity. This data therefore allowed for the progression of work using a linear accelerator for irradiation of samples instead of the  $^{60}\text{Co}$  unit which was used for the current healthy control cohort. The  $^{60}\text{Co}$  unit was decommissioned so the subsequent experiments were completed using a linear accelerator.

### **3. CYTOGENETIC ANALYSIS OF RADIOSENSITIVITY OF PROSTATE CANCER PATIENTS THROUGHOUT THEIR RADIOTHERAPY REGIME AND FOLLOW UP**

#### **3.1 Introduction**

The work described in this chapter is part of an on-going All-Ireland Cooperative Oncology Research Group (ICORG) clinical trial, ICORG08-17. The mission of ICORG is to bring early access of new cancer treatments to Irish cancer patients. So far, approximately 340 research protocols have been opened to allow research treatments to more than 14,000 cancer patients since ICORG was established in 1996, encompassing 95% of Ireland's oncology consultants as members. ICORG08-17, A Prospective Phase II Dose Escalation Study using IMRT for High Risk N0M0 Prostate Cancer, is a prospective, phase II non-randomised controlled clinical study where the primary endpoint is to determine if dose escalation up to 81 Gy using IMRT for high risk localised prostate cancer can provide prostate specific antigen (PSA) relapse-free survival. The associated translational study described in this chapter was funded by Science Foundation Ireland and the FP7 Network of Excellence, Low Dose Research toward Multidisciplinary Integration (DoReMi). This programme investigates effects of radiation in multiple areas which spans biology, chemistry and physics, to examine non targeted effects of radiation, low dose effects, cancer-dose risks, dosimetry, individual variation in radiation sensitivity, radiation quality and non-cancer effects.

Enrolment for the ICORG08-17 translational study involved recruiting patients from the St Luke's Radiation Oncology Network of St Luke's, The Beacon, St. James' and Beaumont hospital. The first patient sample for DIT was collected in August 2014. In brief, patients with newly diagnosed PCa of Gleason score >8, Prostate Specific Antigen (PSA) levels of >20ng/ml and Karnofsky Performance Status (KPS) greater than or equal

to 60 were chosen for participation in the trial (full details of inclusion and exclusion criteria are detailed in appendix 10.1). KPS is a measure of the ability of the patient to do everyday tasks and ranges from 1-100. The estimated primary completion date is 2017 with a complete study end date of September 2026 and with an estimated overall enrolment of 190 PCa patients. Clinical details, including PSA levels, are being recorded prior to treatment and at follow up. KPS and toxicity, using the National Cancer Institute Common Terminology Criteria for Adverse Events (NCI-CTCAE) grading system, version 3.0, are being recorded prior to treatment, weekly during treatment and at follow up. Patients are being followed up regularly at 2 months' post radiation therapy (RT), 8 months' post RT and at 6 monthly intervals until Year 9. Radiotherapy volume/dose metrics are being recorded for planning target volumes (PTVs) and organs at risk (OARs) together with details on duration of treatment, treatment breaks etc. Details regarding medications (disease / trial-related) are captured on an on-going basis. The aim of this chapter was to investigate radiosensitivity in PCa patients recruited to the ICORG08-17 translational study throughout their radiotherapy treatment, i.e. at baseline (before RT), post hormone treatment, last day of radiotherapy, 2 month follow up and 8 month follow up.

### 3.1.1 Prostate Cancer detection, diagnosis and staging

PCa is the second most commonly diagnosed cancer in Ireland, with over 150,000 new cases each year (National Cancer Registry Ireland)<sup>252</sup>. Risk factors for PCa include increasing age, ethnicity (African men with high Gleason score presenting with a higher PSA level than Caucasian men with the same Gleason score)<sup>253</sup> and heredity, with doubling of risk if a first line relative was previously diagnosed <sup>254</sup>.

On presentation of symptoms, (urinary frequency, painful urination and blood in urine or semen), a full digital rectal examination (DRE) and blood sampling is performed to

determine abnormality within the prostate or detection of prostate specific antigen (PSA) in the individual's blood. Usually an elevated PSA ( $>4\text{ng/mL}$ ) is considered abnormal but could indicate non-malignant disorders such as prostatitis and benign prostate hyperplasia (BPH) (National Cancer Institute (NIH)<sup>255</sup>). The PSA value has been under intense investigation, as it is not unusual but uncommon if a patient with PCa presents with levels of PSA lower than  $4\text{ng/mL}$ <sup>256</sup>. However, PSA detection is still deemed to be the most clinically effective predictor of PCa.

If abnormality is detected in the DRE or PSA test, further investigation is warranted via biopsy. Ultrasound-guided trans-rectal biopsy is the method of preference for prostate biopsy<sup>257</sup> followed by histopathological staging using the Gleason Score. The system was first described by Dr. Gleason<sup>258</sup> in which he described 5 pathological patterns; pattern 1 showing well differentiated, normal tissue with a range up to pattern 5 which shows poorly differentiated abnormal tissue. Figure 3.1 shows the original illustration by Donald Gleason depicting the 5 different histological patterns that are used to derive a Gleason Score. This is a histological score deduced by adding the primary pattern throughout the sample (primary grade pattern) and the second most common pattern throughout the sample (secondary grade pattern) to give a score between 2 and 10. Sometimes, a third or tertiary grade pattern is included in histological analysis but not thoroughly used worldwide<sup>259</sup>. The specimen is analysed for tumour/node/ metastasis (TNM) status which evaluates the size of the tumour, if there is any nodal involvement or if there are any distant metastasis evident. Table 3.1 displays the TNM system which groups the histological outcome into one of 3 stages, localised, locally invasive or metastatic and these outcomes determine the type of treatment available for the individual<sup>260</sup>. TX to T2C represents evaluation of the tumour itself, size, location and if both lobes of the prostate are involved. T3a to T4 represents if the tumour locally extends to immediate structures



close to the prostate gland, and N1 to M1 represents the involvement of lymph nodes, and metastatic disease.

Table 3.1 Tumour, node, metastasis (TNM) staging system. Localised disease is denoted as Tx to T2c, local extension is T3a to T4 and Metastatic disease is represented by N1 for nodal involvement and M1 for distant metastasis. Table adapted from the AJCC Cancer Staging manual, Edge *et al* <sup>260</sup>.

<b>Localized Disease</b>	
Tx	Primary tumour cannot be assessed
T0	No evidence of primary tumour
T1	Clinically apparent tumour neither palpable nor visible by imaging
T1a	Tumour incidental histologic finding in $\leq 5\%$ of resected tissue
T1b	Tumour incidental histologic finding in $\geq 5\%$ of resected tissue
T1c	Tumour identified by needle biopsy (e.g., because of elevated PSA level)
T2	Tumour confined within prostate
T2a	Tumour involves one-half of one lobe or less
T2b	Tumour involves more than one-half of one lobe but not both lobes
T2c	Tumour involves both lobes
<b>Local extension</b>	
T3a	Extracapsular extension (unilateral or bilateral)
T3b	Tumour invades seminal vesicles
T4	Bladder invasion, fixed to pelvic side wall, or invasion of adjacent structures
<b>Metastatic disease</b>	
N1	Positive regional lymph nodes
M1	Distant metastasis

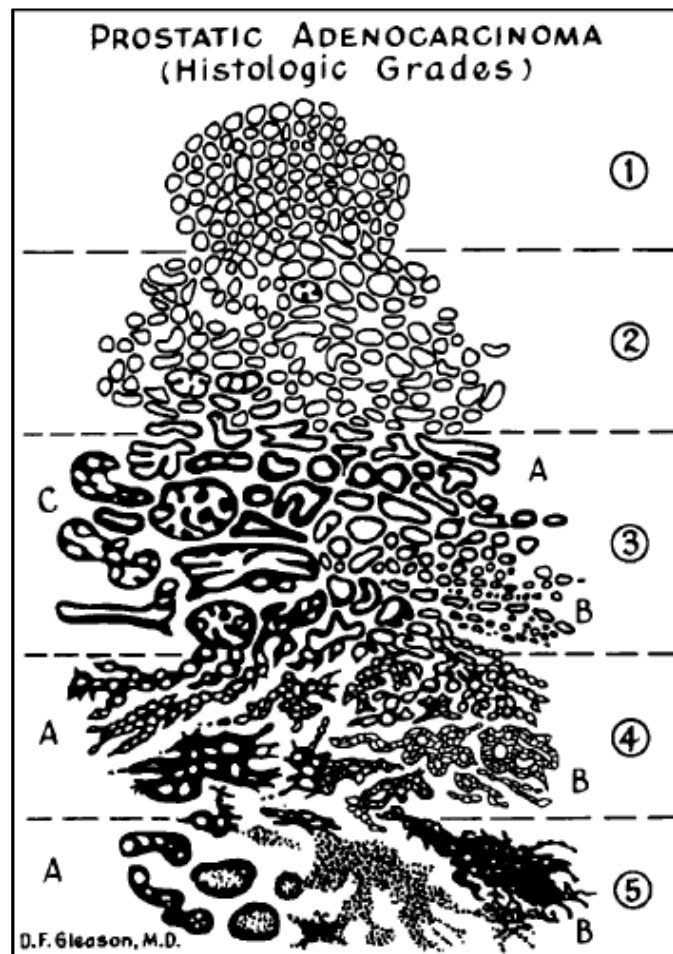


Figure 3.1 Gleason histological staging drawn by D.F. Gleason, illustrating grades 1 to 5. Image taken from P. Humphrey<sup>259</sup>.

### 3.1.2 Types of therapy for PCa and outcomes

Therapy for PCa is dependent on grade and stage of the tumour. To determine the type of treatment for an individual the stage and grade of the tumour is considered and the patient is classified into low, intermediate and high risk groups. Options for treatment include the following, which can be stand-alone treatment options or combined depending on the extent of tumour progression;

i. Deferred treatment – watchful waiting or active surveillance

Deferred treatment or “watchful waiting” is an older approach which is used while waiting until local or systemic progression of the PCa occurs<sup>261</sup>. Sometimes hormone therapy or radiation therapy were used as a palliative treatment for metastasis. A more recent (post 1990) approach has been adopted which is to actively decide not to treat the PCa but to keep a close follow up to deduce if the PCa is progressing and this is termed active surveillance. If treatment is needed with active surveillance, then it is with a curative intent. The purpose of deferred treatment is to avoid unnecessary overtreatment of localised PCa, it is most often prescribed to older patients who have a shorter life expectancy or less aggressive tumour. Often, increasing grade/stage correlate with lower disease specific survival with a deferred treatment approach<sup>262</sup>. Low Gleason scores of <7, confined PCa (T1-T2), and PSA levels of <20ng/ml are some of the criteria which are used to select patients for an active surveillance treatment approach<sup>263</sup>. During active surveillance, other criteria are used to define a cancer “progression” such as PSA doubling between 2 and 4 years and progression of Gleason score >7 in less than 4 years<sup>263</sup>. For T3 – M0, deferred treatment is rare as patients with locally advanced PCa are candidates for hormone deprivation therapy. For metastatic PCa treatment is usually only deferred if the patient feels strongly against it, as median survival with metastatic PCa is less than 2 years<sup>261</sup>.

ii. Radical Prostatectomy

This surgical method involves complete removal of the prostate gland and seminal vesicles, often with assessment of pelvic lymph nodes and sometimes removal of the lymph nodes. This is an advantageous treatment option for localised PCa in patients with a predicted survival of >10 years<sup>264</sup>. Two surgical methods were originally used in the beginning of the 20<sup>th</sup> century; Young used a perineal approach (between anus and

scrotum)<sup>265</sup> while Memmelar and Millin used a retropubic approach (incision in the abdomen)<sup>266</sup>. The latter method is more commonly used to limit faecal incontinence, whereas the perineal approach leads to a faster recovery time and limited loss of blood during surgery compared to the retropubic approach<sup>267</sup>. Radical prostatectomy through the retropubic approach is favoured as more minimally invasive laparoscopic radical prostatectomy (LRP) and robot assisted radical prostatectomy (RARP) have been developed. No evidence in the literature suggests that one technique is superior to the other when used alone, and more work is needed to determine which is best. However both LRP and RARP have been described as the superior techniques for radical prostatectomy in localised PCa as lymph nodes can be checked during the surgery, it requires less operative time and surgical 'skill,' less mean blood loss through surgery, and a hospital stay of 24hrs in more than 96% of patients<sup>268</sup>. Intermediate risk PCa patients (T1-3) are counselled and guided toward a radical prostatectomy approach. If any lymph node involvement is found with intermediate risk and often with high risk patients, surgery alone is not sufficient to provide disease control and survival and often multiple modalities are necessary<sup>261</sup>. With lymph node involvement, extended lymph node dissection (eLND) should be done if the estimated risk of positive lymph node involvement exceeds more than 7%, which is often the case in intermediate risk and high risk PCa patients<sup>269</sup>. Neoadjuvant hormonal therapy and radical prostatectomy has been used and no overall significant improvement in disease free survival was observed, but adjuvant hormonal therapy after radical prostatectomy has been reported as favourable for disease free survival, although not significant<sup>261</sup>.

Most often, radical prostatectomy can be done with limited side effects. Mortality rate for this procedure remains low at 0-1.5%<sup>270</sup> with urinary incontinence the most common side effect which affects 7% of patients undergoing radical prostatectomy<sup>271</sup>.

The combination of, timing of and exact types of treatment needed for PCa differs between individuals and often expertise from a multidisciplinary team of urologists, histopathologists, radiologists and oncologists is needed to decide the treatment plan best suited for the individual.

iii. Definitive radiation therapy

External Beam Radiotherapy (EBRT) specifically Image Guided Intensity Modulated RT (IMRT) and 3 dimensional conformal radiotherapy (3D-CRT) are the most standard form of Radiotherapy (RT) for treatment of PCa worldwide<sup>261</sup>.

Image guided radiotherapy (IGRT) is the most used form of RT as it allows for planar images of the patient to be taken on a daily basis prior to RT at each session, as a linear accelerator is equipped with an on board imaging system (OBI). A sophisticated form of IGRT is cone beam RT which rotates the OBI to obtain volumetric images of the patient for better control of treatment<sup>272</sup>.

3D-CRT is based on image guidance through computed tomography scanning and provides a 3D image of the internal anatomy of the patient and tumour site. Highly advanced computer software has been developed to shape and contour radiation beams to deliver a high dose of radiation to the target volume of the tumour, while allowing margins which spare normal healthy tissue<sup>19</sup>. Intensity modulated RT (IMRT) is vastly becoming the most used type of 3D-CRT for PCa, as use of a multileaf collimator allows for intensity of radiation to be controlled (increased or decreased) while treating a particular tumour. Early reports using patients with clinically localized PCa demonstrate the safe use of high dose IMRT for treatment, which also decreased the incidence of rectal bleeding up to 8 years to <2%<sup>273</sup>. In PCa trial studies, evidence suggests that disease free survival is significantly higher in cases where >72Gy are used compared to those with less than 72Gy of irradiation in localised (T1-2c, N0, M0) PCa<sup>274</sup>. With intermediate risk

(T1c-T3) PCa, dose escalation was shown to provide a better 5 year biological outcome without hormonal therapy<sup>275,276</sup>. With a high risk (T2c, Gleason Score>7) PCa, dose escalation that is predominantly used as phase III trials have shown an overall better disease free survival compared to lower doses<sup>277</sup>. Additionally, determined by phase III clinical trials, neoadjuvant hormonal therapy (6 months of ADT) resulted in a 13% improvement on survival of high risk PCa patients<sup>276</sup>.

Innovative techniques for the treatment of PCa with RT involving IMRT have predominantly attempted to escalate doses of up to 86Gy aimed homogeneously to the target volume of tumour. The ICORG clinical trial aims of this chapter are based on the work by the Memorial Sloan-Kettering Cancer Centre. In the first cohort using >500 PCa patients, use of 81Gy resulted in PSA relapse free survival rates of 85%, 76% and 72% in the favourable, intermediate and unfavourable risk groups respectively<sup>278</sup>. Later, using 478 PCa patients, doses of up to 86Gy were used to show PSA relapse free survival rates of 98%, 85% and 70% for the low, intermediate and high risk groups respectively<sup>279</sup>. The ICORG08-17 study aims to investigate the overall survival and disease free survival of patients treated with a maximum dose escalation of up to 81Gy and report the toxicity data associated with such dose escalation methods.

Low risk PCa patients can be effectively treated with low dose rate brachytherapy. Small radioactive seeds are implanted into the tumour and left for weeks – months to allow slow release of irradiation to the prostate<sup>280</sup>. High dose rate brachytherapy (HDR) is usually combined with EBRT or neoadjuvant hormonal therapy to treat higher risk PCa patients<sup>281</sup>. In patients with organ confined PCa, a significant increase in disease free survival was reported when HDR brachytherapy in combination with EBRT was used compared to EBRT alone<sup>282</sup>.

For extracapsular invasion in pT3, NO and MO, post-operative (after RP) EBRT is a recommended option. If EBRT is used after surgery before PSA levels rise again, more than 60% of patients achieve a progression free rate of 80% at 5 years after therapy<sup>261, 262</sup>.

iv. Locally Advanced PCa (Hormone Therapy)

Incidence rates of advanced PCa are decreasing due to the vast screening of PSA in individuals with symptoms. In patients with advanced disease, EBRT alone provides poor prognosis<sup>285,286</sup> due to the dependence of hormones from PCa tumours. Therefore ADT (hormonal therapy) is used in combination with RT to reduce progression of the disease and metastasis as well as reducing local recurrences<sup>287</sup>. Trials have been completed using hormone treatment in combination with EBRT such as neoadjuvant ADT (hormone treatment for a period of time before RT), neoadjuvant and concomitant ADT (hormone treatment before RT and during), concomitant and adjuvant (during RT and after) and long term adjuvant ADT (hormone treatment for a long period of time after RT). With neoadjuvant (2 months prior to RT) and concomitant hormonal therapy, a higher (but not significant) 10 year overall survival was shown in EBRT + ADT compared to ADT alone<sup>288</sup>. Using concomitant and long-term adjuvant therapy and comparing to EBRT alone, the combined ADT and EBRT demonstrated significant survival compared to EBRT alone<sup>289</sup>. Furthermore, long term adjuvant therapy in combination with EBRT has also shown a significantly higher 10 year survival rate in the adjuvant therapy group compared to standalone EBRT<sup>290</sup>. In one trial using neoadjuvant, concomitant and long term adjuvant treatment, significant improvements were demonstrated such as local control and disease free survival in the long term treatment compared to short term ADT, but a lower 10 year overall survival was found in the long term ADT patients<sup>291</sup>. Moreover, comparison of short term adjuvant ADT with long term adjuvant ADT demonstrated a lower survival rate with short term adjuvant ADT<sup>292</sup>. As previously

mentioned in the Memorial Sloan-Kettering Cancer Centre report, dose escalation in combination with hormonal therapy has proved significantly advantageous. Although the main aim of the study was directly on dose escalation and not comparing any type of ADT, it still provides an opportunity for investigating the effect of dose escalation in combination with ADT, yielding a higher survival rate in patients receiving 86Gy compared to 81Gy<sup>273</sup>. Again, this work forms the basis of the ICORG 08-17 study in this chapter.

### 3.1.3 Patient toxicity and side effects

Although radiation treatment for early stage tumours is effective, it is not without unwanted side effects or toxicity. Toxicity grading is categorised depending on Patients with acute toxicity of > Grade 2 represents about 5-10% and about 35% of those patients will continue to have toxicity at 10 years after radiotherapy<sup>278</sup>. With radical prostatectomy, side effects vary depending on which surgical approach is adopted. As explained in section 3.1.2, the retropubic approach reduces faecal incontinence, but less blood is lost during the actual surgery of a perineal approach<sup>268</sup>. According to the Irish Cancer Society, normal and common side effects related to RT include tiredness, nausea/vomiting, hair loss, constipation and/or bouts of diarrhoea<sup>293</sup>. Specifically, for PCa, side effects recorded in the demographics of our study include urinary frequency/retention/pain, rectal bleeding, cystitis, proctitis, nocturia, diarrhoea or constipation and hot flushes. Acute toxicity such as those described can be damaging to quality of life for the patient, but could potentially predict occurrence of late toxicity<sup>278</sup>. In this study, toxicity is recorded using the National Cancer Institute Common Terminology Criteria for Adverse Events (NCI-CTCAE) grading system, version 3.0, prior to treatment, weekly during treatment and at follow up.



### 3.1.4 Assays for measuring PCa Patient Toxicity

As explained in the general introduction of this thesis in section 1.5, attempts have been made to predict patient response to irradiation specifically in PCa cohorts. In 2009 Mitchell *et al* tried to predict patient response through radiotherapy regimes in PCa patients by measuring excreted exosomes in patient urine. They found a decrease in exosomes following hormone therapy, but only a clear decline through all hospital visits in one of eight patients, and the number of and quality of exosome purification was highly variable<sup>294</sup>. Additionally, Schnarr *et al* found lower apoptotic responses in lymphocytes from PCa patients with late toxicity compared to those who had no toxicity after therapy, using an apoptotic assay in response to much higher *in vitro* doses (8Gy)<sup>295</sup>. Most recently, Brzozowska *et al* investigated the predictive capacity of  $\gamma$ H2AX induction, G2 chromosomal radiosensitivity and apoptosis by annexin V assay to distinguish between PCa patients with and without severe acute side effects, and found no significant correlations between toxicity and each endpoint. Although they found a marked increase in aberration induction in PCa patients compared to age and sex matched controls, they conclude that the predictive capacity of each endpoint for severe toxicity is doubtful<sup>233</sup>. It is well known that dicentric chromosomes are formed in response to irradiation and are therefore a good predictor for biodosimetry<sup>296</sup>. It is also known that a higher baseline level of dicentrics are present in PCa patients and could potentially be an indicator of radiosensitivity<sup>297</sup>. Similar to this work, in 2010 Hille *et al* conducted a study investigating dicentric occurrence before, in the middle, at the end and at 1 year follow up after radiation therapy. They found a high level of baseline dicentrics at first sampling from patients, which persisted up to 1 year after therapy indicating high genomic instability in those patients<sup>298</sup>. Therefore, in addition to  $\gamma$ H2AX induction and G2 chromosomal radiosensitivity, dicentrics could provide an insight into toxicity in PCa during and after radiotherapy.

To date, there are still no accurate predictive tests for measuring patient toxicity response to their radiotherapy treatment. This would be beneficial at the treatment planning stage so that treatment regimens could be individualised according to the patient's response and needs. Chapter 2 described the standardisation and validation of the G2 chromosomal radiosensitivity assay using patient blood samples as a potential predictive test. Furthermore, this work was carried out in parallel with a Raman Spectroscopy study which has the potential to be a predictive tool of response in the clinic. The G2 chromosomal radiosensitivity assay was applied to prostate cancer patient samples taken at baseline (V1), post hormone treatment (V2), last day of radiotherapy (V3), 2 month (V4) and 8 month follow up (V5) stages of their radiotherapy treatment. *In vitro* irradiation was performed to low doses of 0.05Gy and 0.5Gy. No study has currently used multiple sampling times to investigate patient sensitivity throughout a treatment regime using low doses of irradiation.

An additional set of patients who experienced long term grade 2+ toxicity (>2years after treatment) were recruited toward the end of this study. Only 3 patients were recruited while this thesis chapter was written, along with controls who experienced no long term toxicity, grade 0, but who received radiotherapy at the same time as those patients who experienced long term toxicity. This recruitment and investigation is currently ongoing in RESC, DIT.

The novelty in this work lies in the investigation of individual radiosensitivity in patient blood samples using low doses of ionizing radiation. To the best of the author's knowledge this is the first report investigating individual sensitivity using low doses at each sampling point (V1 – V5) with chromosomal radiosensitivity endpoints.

## **3.2 Methods**

Radiosensitivity was analysed in 22 PCa patients and compared to a subset of 19 male healthy controls from the previous healthy control cohort presented in chapter 2. Blood samples were collected from a total of 22 Prostate Cancer patients who were sampled at 1-5 different visits; 22 at baseline (V1), 15 at post hormone treatment (V2), 10 at the last day of irradiation (V3), 7 at the two month follow up (V4) and 3 at the eighth month follow up (V5). On each visit, 20 ml of circulating peripheral blood was extracted into heparinised vacutainers (Sarstedt). Ethical approval for the acquisition of whole blood for the ICORG 08-17 translational study was granted by the research ethics committees of St Luke's, St. James' and Beaumont hospitals (DIT Ethics Ref. 15-32).

### **3.2.1 Blood culture set up**

Whole blood cultures were set up as per section 2.2.2 of this thesis.

### **3.2.2 Histopaque Lymphocyte Isolation**

The methodology for the isolation of lymphocytes was described in chapter 2, section 2.2.3. These cultures were used for Raman spectroscopy

### **3.2.3 Irradiation Conditions**

At 72 hrs, whole blood cultures and lymphocyte cultures were irradiated in G2 phase of the cell cycle at 0.05 Gy and 0.5 Gy using a 6 MV photon beam on an Elekta Precise Linac. Irradiation conditions and calibration from section 2.2.4 were used.

### **3.2.4 G2 chromosomal radiosensitivity assay**

The assay was carried out as previously described in chapter 2 section 2.2.5 of this thesis. Microscopy was carried out to obtain mitotic index and G2 radiosensitivity scores as described in chapter 2.2.5.

### 3.2.5 Statistical Analysis

Statistical comparison of mitotic index between doses was done using the non-parametric Kruskal-Wallis test in Graphpad Prism 6. G2 radiosensitivity scores which were obtained through totalling the number of aberrations per 100 metaphases on each slide per dose per donor were also compared between doses using the Kruskal-Wallis test. Comparison of radiation doses per donor for checkpoint response, radiosensitivity scoring and  $\gamma$ H2AX were done using a grouped two-way ANOVA on GraphPad Prism 6 to determine any significant changes between all doses or different endpoints. Analysis of donor and dose for each hospital visit (V1 pre hormonal, V2 post hormone treatment, V3 last day of RT, V4 2 month follow up and V5 8month follow up) for each endpoint was also done using a two-way ANOVA. A p value was derived and a significance level of 0.05 was used. This was done using Microsoft Excel 2016 and is explained in detail in chapter 2 of this thesis. Radiosensitivity cut offs calculated from a male subset of the healthy control cohort in chapter 2 were used to determine radiosensitive individuals.

## 3.3 Results

Radiosensitivity was analysed in 22 PCa patients and compared to a subset of 19 male healthy controls from the previous healthy control cohort in chapter 2. Additionally, radiosensitivity was investigated in PCa patients throughout their radiotherapy treatment regime – V1 represents baseline, V2 after hormone treatment, V3 last day of radiotherapy, V4 2month follow up and V5 8month follow up. G2 Checkpoint response and G2 chromosomal radiosensitivity were analysed.

### 3.3.1 G2 Checkpoint response

Mitotic index was obtained by counting the ratio of cells in metaphase (on each slide at each dose per donor) compared to all other cells on the slide (interphase). No significant difference in non-irradiated, baseline values from PCa and healthy controls was observed

at both dose points ( $p > 0.1$ ) The mitotic index value at each dose was then subtracted from each individual's non irradiated control value to obtain a radiation induced mitotic inhibition value (MIn). This is a value representative of the individual's response to each particular dose of irradiation. Figures 3.2-3.4 show the G2 checkpoint response data in healthy controls (figure 3.2), pre-therapy/baseline PCa (figure 3.3) and all 5 visits for 3 PCa patients at 0.05Gy compared to 0.5Gy (figure 3.4).

A significant increase in MIn was observed in the subset of male healthy controls at 0.5Gy ( $p = 0.0004$ ) (figure 3.2) as was observed in the PCa patients ( $P = 0.02$ ) (figure 3.3). A drop in mitotic inhibition at both doses was observed after hormone treatment (V2) (Figure 3.4) which then increased significantly after last day of radiotherapy (V3) and 8month follow up (V5). There was little to no inhibition at the 2month follow up. At 0.5Gy, little change was observed after V2, with only a significant drop from V1 to V2 from 3% to 1% ( $P = 0.048$ ) (Figure 3.5).

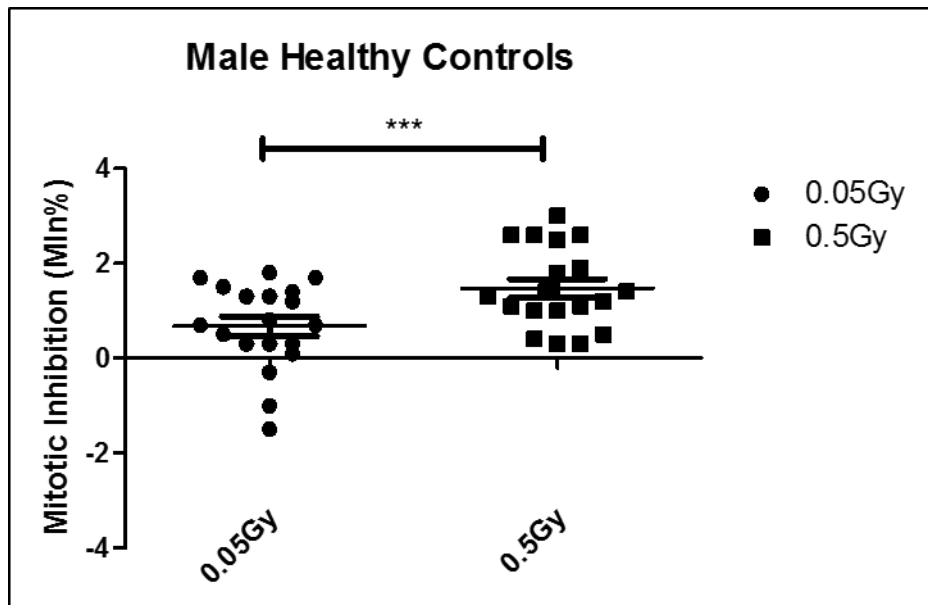


Figure 3.2 Checkpoint response from the male subset of a healthy control donor cohort as represented by Mitotic Inhibition (MIn) at 0.05Gy and 0.5Gy. P =0.0004.

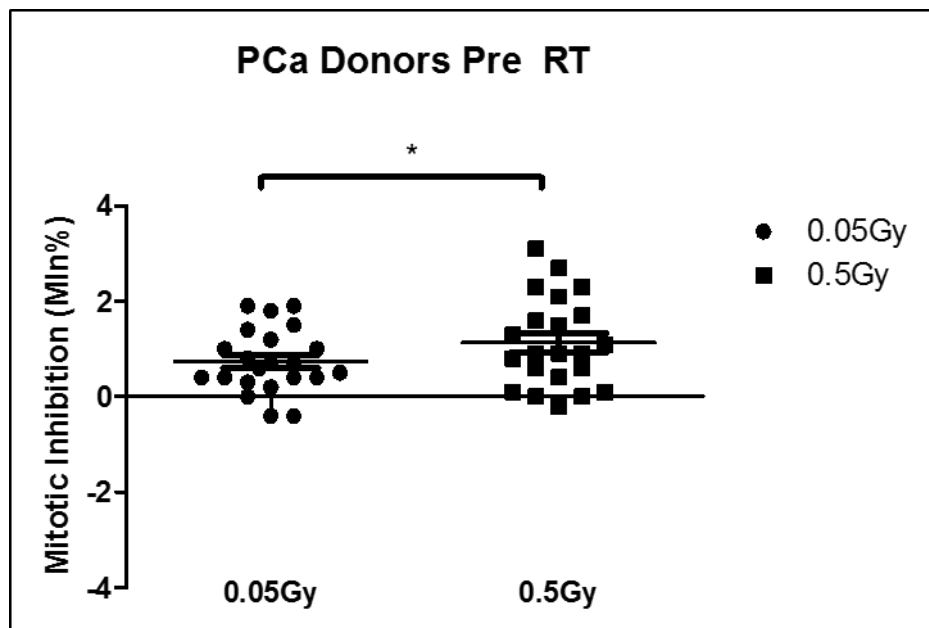


Figure 3.3 Baseline (V1) checkpoint response in Prostate Cancer (PCa) donors as represented by mitotic inhibition (MIn) values. The MIn value was obtained by subtracting the mitotic index for each dose from the individuals non irradiated control.

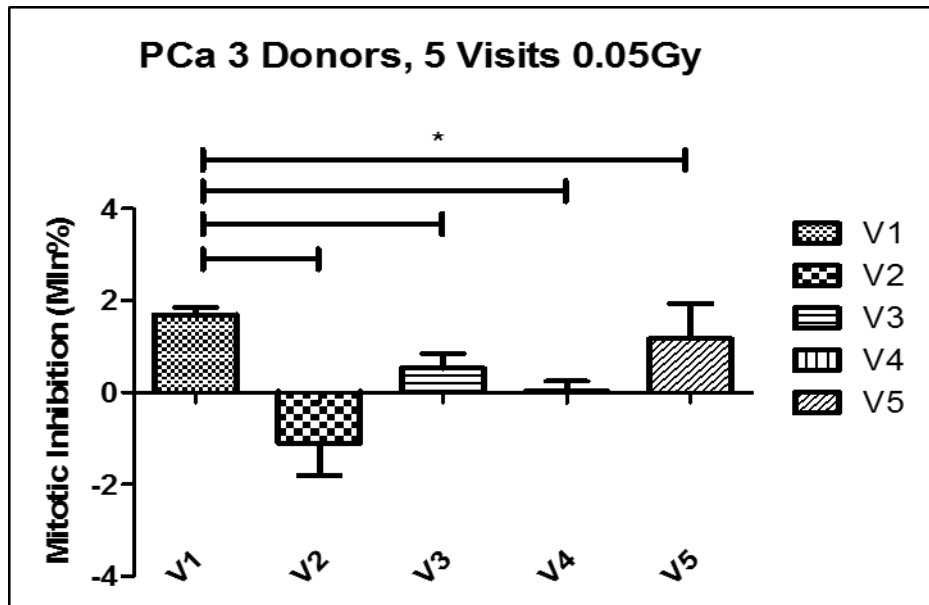


Figure 3.4 Checkpoint response as represented by mitotic inhibition (MIn) from 3 PCa donors for all 5 hospital visits. V1 represents baseline, V2 after hormone treatment, V3 last day of RT, V4 2month follow up and V5 8month follow up.

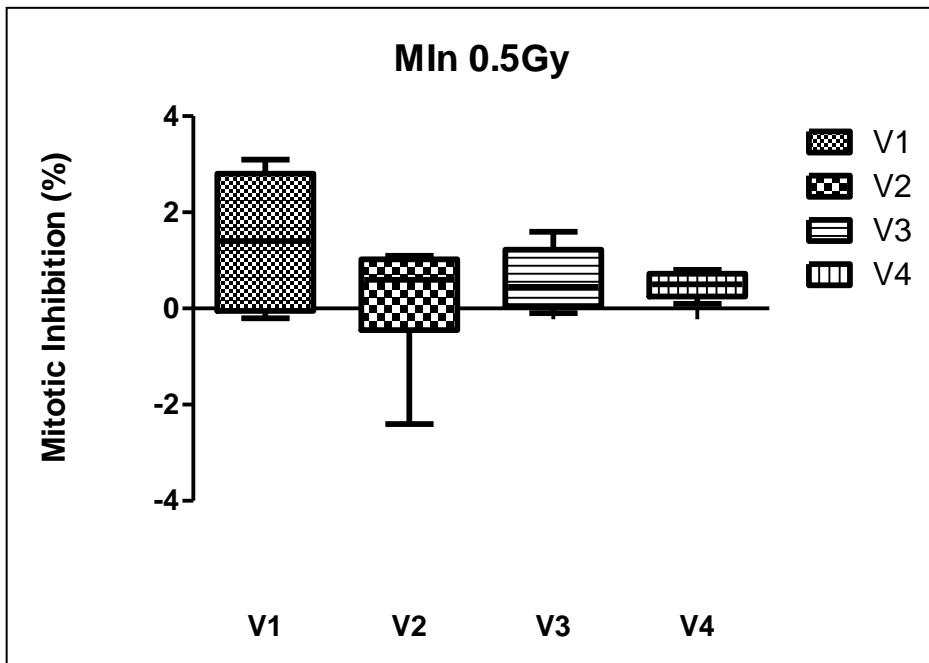


Figure 3.5 Checkpoint response as represented by mitotic inhibition (MIn) from 3 PCa donors for 4 hospital visits. V1 represents baseline, V2 after hormone treatment, V3 last day of RT, V4 2month follow up.

### 3.3.2 G2 Chromosomal Radiosensitivity

G2 chromosomal radiosensitivity was analysed in PCa patients for all types of structural and numerical aberrations (described previously in the methods section and examples shown in figure 3.6). 100 metaphase spreads were analysed per dose, per donor and a G2 score was assigned to each donor.

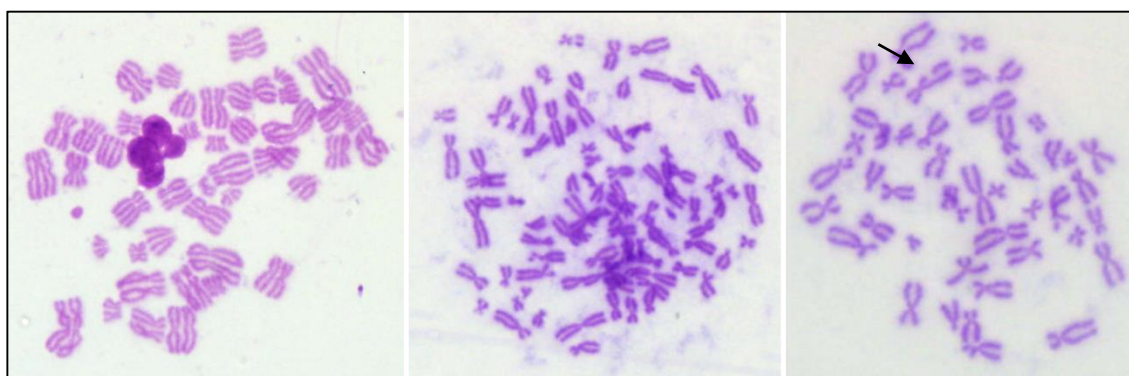


Figure 3.6 Examples of chromosomal aberrations recorded by microscopy in this chapter. The first image represents endoreduplication, the second tetraploidy, and the third shows an example of a break.

The radiation induced G2 score was calculated by subtracting spontaneous aberrations in the non-irradiated control away from the dose points. A radiosensitive cut-off value was used from a male subset of the healthy donor cohort which was validated in chapter 2. This cut-off represents a point where 90% of the sampled population lie, and donors above this point are considered to be radiosensitive. This was previously used in a number of chromosomal radiosensitivity studies. For this thesis, the radiosensitive cut-off was 159 aberrations/100 metaphases as derived from the validation study in chapter 2 using the healthy control cohort. Figures 3.7 – 3.12 represent G2 radiosensitivity data of HC, PCa and comparison of hospital visits for PCa patients. Figure 3.7 represents ranges of G2



scores at 0.5Gy from donors in each category; a subset of 19 male healthy donors from the 42 healthy control donor cohort in chapter 2 and V1 baseline G2 scores from 22 PCa patients. The radiosensitivity cut off has been routinely used to identify radiosensitive subgroups in previous studies (chapter 2).

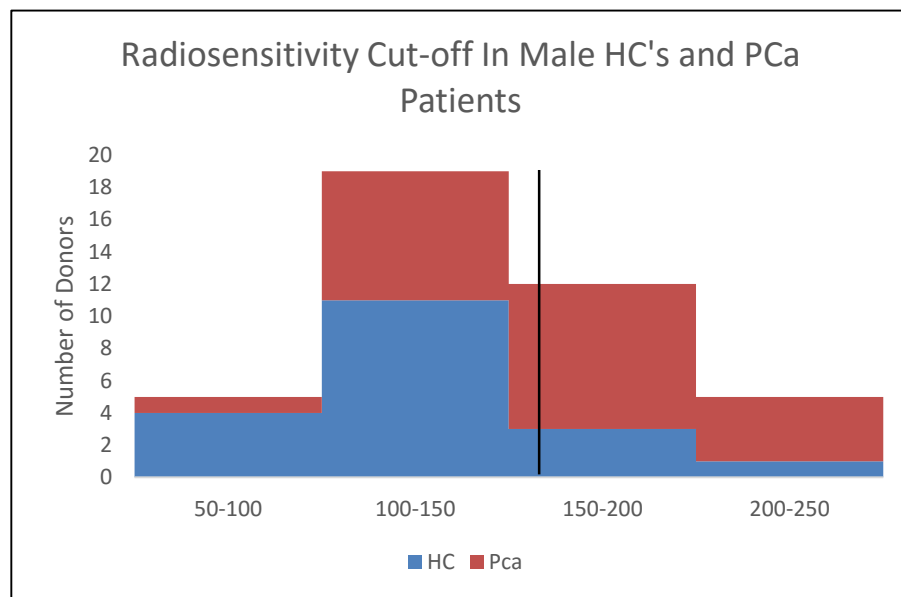


Figure 3.7 Range of Healthy controls (HC's) and Prostate Cancer (PCa) patients in each category of G2 scores at 0.5Gy. Radiosensitivity cut-off is represented with a solid dark line at 159 aberrations/100 metaphases.

A significant increase in aberration yield was observed between spontaneous aberrations in the controls compared to aberration yields at 0.05Gy and 0.5Gy in both HC and PCa patients (Figure 3.8) ( $P < 0.001$ ). Additionally, a significant increase in aberration yields was observed in PCa compared to HC at 0Gy and 0.5Gy ( $P = 0.002$ ), but not at 0.05Gy where aberration yields were slightly higher in HC ( $P > 0.01$ ).

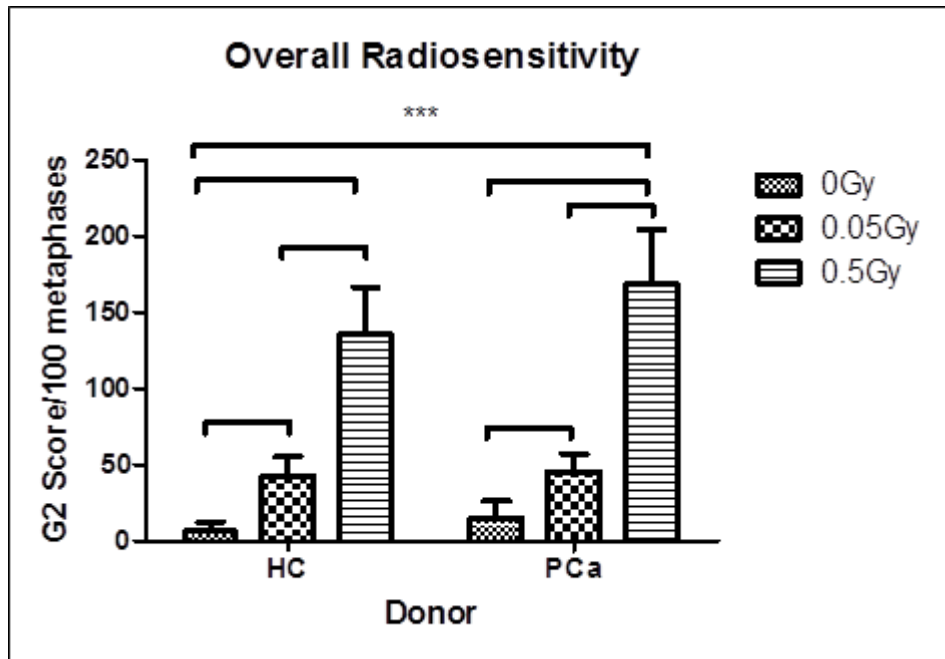


Figure 3.8 G2 Radiosensitivity in Healthy controls (HC) compared to Prostate Cancer patients (PCa) at 0Gy, 0.05Gy and 0.5Gy

For 3 donors at all 5 follow ups, a trend was observed in aberration yields between follow up visits, with a significant drop in radiosensitivity scores between visit 2 and visit 3 ( $p = 0.038$ ) (Figure 3.9). A drop in aberration yield was observed from baseline until last day of radiotherapy, but by 2 month follow up the aberration yield had increased, with more aberrations observed by the 8 month follow up at 0.05Gy (Figure 3.9).

At 0.5Gy a significant trend was observed in radiosensitivity through follow up visits (Figure 3.10). A drop in aberration yield was observed between baseline and post hormone treatment, but an increase in aberration yield followed at last day of radiotherapy, which dropped again at the 2 month follow up only to increase at 8 month follow up (Figure 3.9) ( $P=0.0428$ ). The same was observed for four visits with 13 donors.

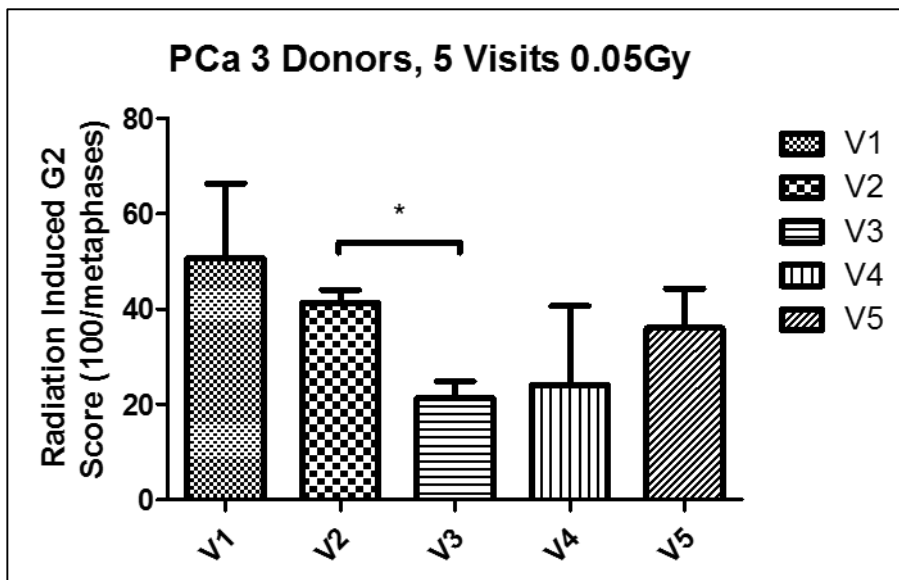


Figure 3.9 Radiosensitivity scores at 0.05Gy for Prostate Cancer (PCa) patients through their radiotherapy regimes. V1 represents baseline, V2 after hormone treatment, V3 last day of Radiotherapy, V4 2month follow up and V5 8month follow up.

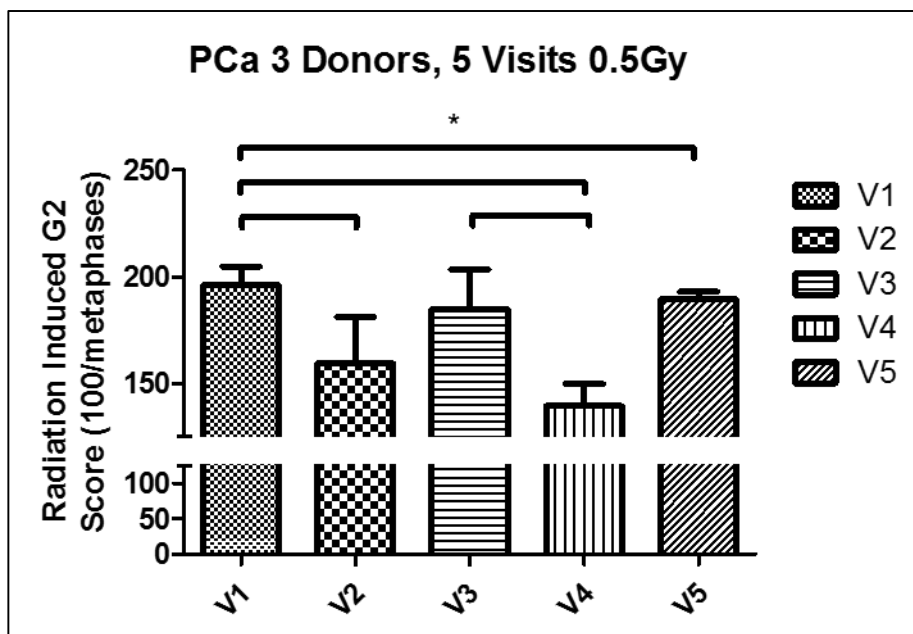


Figure 3.10. Radiosensitivity scores from Prostate Cancer (PCa) patient blood samples irradiated at 0.5Gy throughout radiotherapy visits. V1 – V5 corresponding to hospital visits as described previously. Spontaneous aberration yield was subtracted from each dose.

As more patients were recruited for sampling in 4 out of 5 follow ups, those 13 patients were analysed to determine the trend over pre-therapy (V1), post-hormone treatment (V2), last day of radiotherapy (V3) and 2 month follow up (V4). Similar trends were observed as per Figure 3.8 and 3.9 and no significant change between any follow up was observed at both dose points ( $P > 0.056$ ). Additionally, no significant change in aberration yield was observed between the first two follow ups in 13 donors (pre therapy and post hormone therapy) at both dose points ( $P > 0.5$ ).

### 3.3.3 Radiosensitivity and Toxicity

From the subset of PCa patients (N=22), no donor showed extreme radiosensitivity as compared to other radiosensitive disorders using the assays mentioned. Therefore, patients with long-term side effects were recruited as part of the study. These individuals were sampled at 2 years after radiotherapy with side effects (grade 2 late toxicity) and compared to control patients who received radiotherapy at the same time as those individuals but did not display long term side effects. 3 of those patients were used in this study, as patient recruitment and sampling is currently ongoing for an extension of this study. No significant change in checkpoint response or radiosensitivity was observed, apart from one of the 3 patients who had an abnormally low G2 radiosensitivity score at 0.5Gy at 85 aberrations/100 metaphases compared to healthy controls and other prostate cancer patients.

Using the Spearman – Rank correlation test, correlations were done using each endpoint – MIn, RIG2 and Toxicity grading at each dose and each visit. The correlation was performed in Graphpad Prism 6 by sorting values in ascending order. The test gave a correlation coefficient of between 0 and 1 as an output, with values closer to 1 representing a positive correlation. All the mentioned endpoints were analysed together

to observe if any correlations existed, but no significant correlation was found between all the experimental endpoints ( $R > 0.2$  for all).

### 3.4 Discussion

G2 checkpoint response and radiation induced G2 chromosomal aberrations data are discussed with reference to dose, patient visit and toxicity gathered from the ICORG clinical trial (explained in section 3.1).

Significant checkpoint inhibition was observed at 0.5Gy but not 0.05Gy for both the subset of male HC's and PCa patients. This was expected as it represents efficient checkpoint activation in response to the doses of radiation used. A radiosensitivity score was assigned to all donors throughout their radiotherapy visits (as previously explained). PCa patients showed a significantly greater level of aberrations per 100 metaphases compared to a subset of male healthy controls as expected. This was found to be true in a number of other studies on G2 radiosensitivity of PCa and BPH patients, for example Howe *et al* found a significant increase in aberration yield in both PCa and BPH patients compared to healthy controls<sup>158</sup>. A radiosensitivity cut off of 159 aberrations per 100 metaphases was derived by the 90<sup>th</sup> percentile calculation of healthy controls in chapter 2 of this thesis. A significant proportion of PCa donors (represented in blue) are to the right of this cut off, which represents that this subset of donors is considered radiosensitive. Similar work was shown by Howe *et al* using PCa and BPH patients<sup>158</sup>, and again using breast cancer<sup>165</sup> and colorectal carcinoma cohorts<sup>230</sup>. In this prostate study, a higher aberration yield was observed at 0.5Gy compared to 0.05Gy at all radiotherapy hospital visits (V1-5) which is not unusual. The highest aberration yield was observed at baseline. A significantly higher level of aberrations was observed in PCa donors at 0.5Gy compared to male healthy controls, and although not significant but interestingly, the opposite pattern was observed at 0.05Gy, which suggests that

aberrations are produced through differing molecular mechanisms at the lower dose point as discussed in chapter 2<sup>299</sup>. At 0.05Gy, the lowest aberration yield is after radiation therapy (V3), and aberration yield increases at 2 months and 8 month follow up. This may be due to cell death mechanisms after radiotherapy. At 0.5Gy, the opposite is observed, with the highest level of aberrations shown after radiotherapy at V3. Baseline levels (V1), after radiotherapy (V3) and 8 month follow up (v5) aberration yields are all similar, with a drop in aberrations after hormone treatment and at 2 month follow up. This could be due to hormonal effects in response to hormone therapy at V2, and possibly redistribution of cells in the cell cycle after radiotherapy. Recently, a long term follow up in PCa patients who received radiotherapy showed that even from 2 years to 15 years after radiotherapy, side effects such as urinary leakage, bowel problems and erectile dysfunction still exists therefore an increased aberration yield at 8 month follow up in the data compared to the 2 month follow up presented here could possibly predict future side effects or complications<sup>300</sup>.

18 patients were recruited as part of the study who exhibited grade 2 toxicity up to 2 years after radiation treatment. Using 3 of these donors, no significant change in checkpoint response or radiosensitivity was observed compared to controls, apart from one of the three donors who showed extremely low levels of aberrations at 85/100 metaphases at the higher dose point. No differences in toxicity using G2 chromosomal radiosensitivity is not unusual, as Brzozowska *et al* found exactly the same results using lymphocytes from PCa patients with and without acute side effects after 0.5Gy or 1Gy of *ex vivo* irradiation<sup>233</sup>. Cesaretti *et al* found that ATM sequence variants could predict adverse reaction to brachytherapy in PCa patients, so further exploration of ATM and target genes could provide more information for identifying a biomarker panel for toxicity testing<sup>40</sup>. In their findings, many more patients were tested (>2000) over a 15 year period for 20 ATM variants and they found that those patients with a variant substitution were

candidates for further investigation as they tended to be more prone to developing toxicity after treatment with brachytherapy.

### **3.5 Chapter Conclusions and Summary**

To the best of the author's knowledge, this is the first piece of work which investigates prostate cancer patient radiosensitivity using a chromosomal aberration approach at the low doses used at 5 different stages of radiotherapy treatment. The data presented in this chapter supports the idea of potentially using the G2 chromosomal radiosensitivity assay as an accurate predictor of radiotherapy response. This is evident by the response presented in this chapter at the doses of 0.05Gy and 0.5Gy compared to 0Gy control. Although the picture is complicated at 0.05Gy for all techniques, using this dose was able to show higher aberration frequency in Grade 0/1 toxicity compared to Grade 2 toxicity in 2 PCa donors. However, further work is needed with a larger number of patients and toxicity data to draw any conclusions from this.

## **4. FURTHER EXPLORATION OF BIOMARKERS OF RADIOSENSITIVITY DRIVEN BY CELLULAR MECHANISMS**

### **4.1 Introduction**

Ataxia Telangiectasia (AT) is an inherited autosomal recessive disorder in which carriers (AT heterozygotes) constitute approximately 1% of the population<sup>160</sup>. It is the most thoroughly studied radiosensitive phenotype and was first described clinically in 1926 by Syllaba *et al* who reported the clinical observations of AT (then known as Louis-Barr syndrome)<sup>36</sup>. These observations were ocular telangiectasia, cerebellar ataxia, chorea, cerebellar atrophy and thinning of the cerebellum and slurred speech. The name Louis-Barr comes from Madame Louis-Barr who reported a case of AT in a nine year old boy in 1941, who presented with cerebellar ataxia and cutaneous telangiectasias<sup>301</sup>. There were no further reports until the late 1950's when AT was then established as a disease entity after a study of eight unrelated cases of AT and six familial cases by Boder and Sedgwick, who termed the disease Ataxia Telangeectasia<sup>37</sup>.

Symptoms of the disease develop in children before the age of 6 with the most common symptom reported as slurred speech and loss of balance and then progressive neurodegeneration leads to wheelchair confinement before the age of 10 years<sup>32</sup>. The median survival rate ranges from 19 – 25 years of age<sup>302</sup>. Chronic lung disease is the most frequent cause of death among AT patients due to recurrent sino-pulmonary infections and immune disorders<sup>32</sup>. AT patients demonstrate characteristic cellular features of immunodeficiency, radiosensitivity and present a high predisposition to cancer (most often leukaemia's or breast cancer). These characteristics are all common cellular features of a variety of radiosensitive syndromes described in section 1.3 of this thesis. These syndromes are caused by an underlying genetic mechanism most often associated with the DNA damage and repair response.



In addition to the clinical features of AT, patients have diminished cellular immunity with little to no immunoglobulin A (IgA)<sup>303</sup>. Additionally, Waldmann and McIntire reported a higher level of alpha fetoprotein specific to AT patients and not in patients from other immunodeficient syndromes. Interestingly, it was found to be elevated in pregnant women, the molecular link of which is not yet known<sup>304</sup>. Other elevated blood proteins in AT patients include cancer antigen 125 (CA125) which is also a marker of ovarian cancer and is used to help diagnose AT<sup>305</sup>. AT patients are monitored periodically due to their diminishing lung function. Recently, an association between elevated interleukin-6 (IL-6) levels and lower forced vital capacity (FVC) has helped to monitor AT patients within the clinic<sup>306</sup>. Additionally, significantly increased levels of copper and decreased levels of zinc were identified in the blood from AT patients compared to control donor blood copper and zinc levels using mass spectrometry<sup>307</sup>.

Chromosomal radiosensitivity was one of the first cellular features described in AT patients. Higurashi *et al* found a higher level of chromosomal aberrations in AT patients and other associated immunodeficient syndromes in response to 0.1-1Gy of  $\gamma$ -rays delivered to leukocytes<sup>308</sup>. Taylor *et al* further described higher chromosomal radiosensitivity of cells from AT patients compared to controls and fluctuations of radiosensitivity in AT cells through the stages of the cell cycle<sup>309</sup>. They also described how histone modifications prevented AT cells from repairing DNA damage, as healthy cells readily utilised histone remodelling to promote DNA repair in response to DNA damage<sup>289, 290</sup>. Bender *et al*<sup>312</sup> and Parshad *et al*<sup>151</sup> also described higher aberration frequencies in LCLs and fibroblasts from AT patients and AT heterozygotes compared to age matched controls. These observations came before identification and mapping of the ATM gene.

In 1988, Gatti *et al* mapped the gene responsible for AT to chromosome 11 on the q arm and position 22-23<sup>34</sup>. This was later identified by Savitsky *et al* who identified the gene as ataxia telangiectasia mutated (ATM)<sup>33</sup>. The ATM gene is a member of the phosphatidylinositol-3-kinase (PI3K) family of kinases and is 150kb which comprises 69 exons encoding a protein of 3056 amino acids<sup>313</sup>. Kinases catalyse the addition of phosphates to other proteins in the process of phosphorylation. This can activate or deactivate other proteins and operates in tandem with dephosphorylation (removal of a phosphate).

Several mutations have been associated with AT with the most common being truncating mutations, resulting in the total absence of ATM kinase activity. In contrast, Missense or splice site mutations of ATM result in limited kinase activity<sup>314</sup>. According to the Ataxia Telangiectasia Mutations database website, 459 unique DNA sequence variants have been discovered as of 15 Feb 2016<sup>315</sup>. Over 33 allelic variants of ATM mutations have been found. For example, Savitsky *et al* observed a loss of serine 152 resulting from a deletion of 3 base pairs in one allele in a case of AT complement A in a Dutch family. They went on to describe two siblings diagnosed with AT complement group E and found both were homozygous for a deletion of 9 base pairs resulting in a loss of amino acids 1198-1200 in the gene product. On analysis of the ATM gene in two AT patients with English/Indian ancestry, a complementation group D was defined showing a deletion of 6bp in one allele resulting in deletion of 2 amino acids in the gene product<sup>33</sup>. Whether truncating, splice or missense mutations, mutations in ATM result in loss of amino acids leading to diminished or altered ATM levels and perturbed response to DNA damage and repair.

The role of ATM is to coordinate a cascade of molecular events by phosphorylation mechanisms in the DNA damage response (DDR)<sup>316</sup>. ATM is the central coordinator in

the DNA damage response for recognition and transduction of signals so that the cell cycle is halted to allow for repair mechanisms to occur. The cell does this via two pathways, namely ataxia telangiectasia rad 3 related (ATR) and ATM. Single strand breaks (SSB's) caused by replication errors in DNA synthesis activate ATR which in turn inhibits cell cycle progression at G2/M through CHK1. Double strand breaks (DSB's) are the most common break associated with ionizing radiation induced damage. DSB's are sensed by ATM and downstream signalling causes the activation of CHK2 and G1/S checkpoint arrest. ATM signalling is described in detail in section 1.4.3.

The radiosensitivity phenotype of AT cell lines along with the characterised molecular role of ATM in the DNA damage response to radiation has been adopted by many radiobiologists as the best biological model for studying cellular radiosensitivity. The work described in this chapter aims to investigate cellular radiosensitivity and the role of ATM in lymphoblastoid cell lines (LCL's) from healthy controls versus AT patients. The cell lines were established from lymphocytes taken from healthy controls (2139 and 2145) and AT patients (AT2Bi and AT3Bi) and immortalised with the Epstein Barr virus. This allowed for multiple experiments and replicates to be conducted which was in contrast with the studies done on whole blood cells directly from donors.

The normal cell lines were established before 1990 using healthy controls and characterised as normal for AT comparison analysis based on cell survival, cell cycle analysis and ATM gene expression<sup>317</sup>. The AT2Bi cell line was established from a 19-year-old Caucasian female affected by AT who exhibited increased chromosomal radiation sensitivity and increased chromosome breakage induced by bleomycin. From the repository of Coriell Institute of Medical Research, genetic characterisation of AT2Bi showed one allele which carries an insertion of TT at nucleoside 6404 (6404insTT) in exon 46 which leads to a frameshift beginning at codon 2073 and a truncation at codon

2135 (L2073fsX2135)<sup>318</sup>. AT3Bi cell line was collected and established from a donor affected with AT. No other genetic information was supplied or found for this cell line but it was characterised as radiosensitive among other radiosensitive syndromes using cell survival as an endpoint<sup>319</sup>.

Characterisation of the normal and AT cells was performed to investigate if a molecular cytogenetic probe could distinguish AT from the healthy control cell lines and be potential cytogenetic biomarkers for cellular radiosensitivity. The target probes employed were ATM, CEPX (for centromere), TP53, and immunoglobulin heavy chain (IGH). The ATM and TP53 probes were used to determine any gene deletions in the AT cells. CEPX was a chromosomal marker used to determine the sex of the donor and IGH was used to determine any rearrangements in chromosome 14 due to its association with blood based cancers i.e.: Leukaemia. IGH rearrangements have been associated with a wide range of leukaemias and lymphomas including non-Hodgkin's lymphomas (NHL), chronic lymphocytic leukaemia, Multiple Myeloma and acute lymphoblastic leukaemia (ALL) which AT patient have been known to be susceptible to.

The aim of this chapter was to investigate the normal cellular response to irradiation using healthy cells and cells lacking in ATM using an array of radiobiological assays, doses, time-points and endpoints. These included cell survival, viability, cytotoxicity,  $\gamma$ H2AX induction, cytogenetics (to include chromosomal aberration analysis, G-Banding and fluorescent *in situ* hybridisation).

## **4.2 Methods**

### **4.2.1 Cell lines and Cell culture and Irradiation setup**

LCL's generated from lymphocytes taken from two healthy donors (2145 and 2139) were donated from Dr Janet Hall at the Institute d' Curie, Paris, France. LCL's from donors with confirmed Ataxia telangiectasia (AT) (AT2Bi and AT3Bi) were donated from

Professor Malcolm Taylor from the University of Birmingham. These lymphocytes were immortalised with Epstein-Barr virus. LCL's are cells which grow in suspension and do not attach to surfaces of their environment. They were maintained in standard RPMI medium (Sigma) supplemented with 10% Foetal bovine serum (FBS), L-Glutamine and incubated at 37°C with 5% CO<sub>2</sub>. Each cell line was kept at a density of 1x10<sup>5</sup>/ml and split by 1:5 dilutions every 24-48 hrs. Prior to irradiation, 5 mls of cells at a density of 1x10<sup>6</sup>cells/ml were seeded per flask, per cell line and per dose for each of the biological endpoints described below. Flasks were irradiated at 0 Gy, 0.05Gy, 0.5Gy and 2Gy using a Linear Accelerator (setup and dosimetry described in Chapter 2).

#### 4.2.2 Cell viability and Cytotoxicity

Cell viability, cytotoxicity and caspase activation was analysed 1 hr and 24 hrs post irradiation using the ApoTox – Glo Triplex assay (Promega). To determine viability and cytotoxicity, two differential protease biomarkers were measured by the addition of a non-lytic reagent with two peptide substrates. The live cell portion was analysed for viability with a fluorogenic cell permanent peptide substrate (GF-AFC substrate) which restricted uptake of the dye into live intact cells only. A second, non-permanent fluorogenic peptide substrate (bis-AAF-R110) was used simultaneously to measure dead cell protease activity which was released from cells with ruptured membranes.

#### 4.2.3 Cell Survival

Cells were plated at a density of 1x10<sup>6</sup> cells/ml for each cell line. After irradiation the cells were incubated for 72 hrs. Cell counts were conducted from suspensions taken at 72 hrs post irradiation using a Coulter Counter. The data collected was used from three independent experiments which were carried out for cell survival analysis.

#### 4.2.4 DNA Damage

Twenty-four hours prior to irradiation, LCL's were seeded into T25 flasks at a density of  $1 \times 10^6$  cells/ml. 1 hr and 72 hrs post irradiation, cells were fixed with 70% ethanol (Sigma, Laboratory Grade).

#### 4.2.5 Cytogenetics and Microscopic analysis

The G2 Chromosomal radiosensitivity assay as described previously in Chapter 2 section 2.2. was also conducted to measure cell cycle checkpoint response by mitotic indices and radiation-induced mitotic inhibition, as well as G2 chromosomal radiosensitivity. The mitotic index was calculated by counting the ratio of cells in metaphase to all cells on the slide up to 1000 cells in total for each dose and cell line. Mitotic inhibition was calculated by subtracting the mitotic index at each dose away from the control. A G2 radiosensitivity score was assigned to each of the cell lines and per irradiation dose by calculating the total number of aberrations in each. All numerical aberrations (aneuploidy/polyploidy/endoreduplication) and structural (gaps/breaks/terminal deletions/fragments/dicentrics etc.) were totalled for each dose per 100 metaphase cells. The spontaneous aberration yield in the non-irradiated control (0Gy) for each cell line was subtracted from each dose (0.05Gy and 0.5Gy) to calculate a radiation induced G2 radiosensitivity score. For LCL's, incubation of colcemid was increased from 1hr to 2hrs for chromosome harvest. Low chromosome harvest was observed compared to whole blood cultures used previously.

#### 4.2.6 G-Banding

After metaphase preparation on glass slides, slides were aged for 1 minute in the UV box. They were then placed on the slide rack and covered with 30% hydrogen peroxide solution for one minute. After rinsing with 0.9% NaCl solution the slides were placed in

trypsin solution for the 2 mins. Slides were rinsed with Gurr buffer and were then stained in 1ml of 1:2 Leishmann: Gurr buffer mix for 1min. After 1 minute, slides were rinsed with Gurr buffer and immediately with distilled water. The excess water was drained from the slide on to tissue and the slide was placed on to a slide to allow the surface to dry thoroughly. The slides were then mounted with DPX with air bubbles removed. Each slide was evaluated under the microscope set up for bright-field use, noting conditions of under or over banding or staining. 25 metaphases were analysed under the microscope for G-Banding and karyotyping.

#### 4.2.7 Fluorescent *In Situ* Hybridisation (FISH) cytogenetics

Slides were soaked in sodium chloride and sodium citrate buffer (SCC) for 2mins at 37°C, before being soaked in protease solution for 30-40 seconds at 37°C. Slides were then washed in 1xPBS at room temperature. Slides were dehydrated in an ethanol series (70%, 85% and 100%) for 2 minutes each at RT and air dried before hybridisation. Hybridisation probes were used to identify deletions or rearrangements in ATM-TP53 (Cytocell), CEPX (Abbott) and IGH (Abbott). Probes for ATM-TP53 were used to show if ATM was deleted in the AT cells. CEPX is a probe for the X chromosome and was used to identify the sex of the donor of each cell line. IGH break apart probes were used to detect breakage of IGH, which is observed in the t(14;14) (q11;q32) translocation (or in(14)(q11q32) rearrangement) and is usually found in T-cell leukaemia associated with AT. IGH Break Apart Probes are designed to detect the translocation involving the immunoglobulin heavy chain (IGH) locus on chromosome 14q32. In normal situations, two colours represent the 3' and 5' ends of IGH. In disease break apart of the probe colours represent duplications or deletions of one or more colours of the probe indicating abnormality. Probes were mixed according to the manufacturers protocol (Appendix 3) and the required amount was added to each slide. Slides were transferred to a Hybrite machine

which was programmed to 37°C. Hybridisation program 1 was selected (75°C for 2 min, 37°C for 20 hours). On removal from the Hybrite, coverslips were removed and slides were immersed in wash solution (0.4xSSC/0.3% NP 40, Appendix 3) for 2 minutes. Slides were then transferred into a solution of 2xSSC/0.1% NP40 for a minimum of 1 minute and excess liquid was removed from each slide. 20µl of DAPI stain and then coverslips were added to the slide preparations. For FISH microscopy 25 metaphases were recorded.

#### 4.2.8 Statistical Analysis

Statistical analysis was completed using Graphpad Prism 6 for all cellular assays. For each assay, ANOVA was done for all doses (0Gy, 0.05Gy, 0.5Gy and 2Gy) and cell lines (normal 2145 and 2139, and radiosensitive AT2Bi and AT3Bi). A significance level of 0.05 was assigned for each output. Coefficient of variation (%) for cytogenetic results was calculated using Microsoft Excel and was described in chapter 2 section 2.2. This formula was as follows;  $\text{Variation} = (\text{standard deviation of the mean}/\text{mean}) \times 100$ .

### 4.3 Results

#### 4.3.1 Cell Growth and DNA Damage Post Irradiation

Relative growth of cells after irradiation was measured by cell counts at 72 hrs post irradiation. No significant difference was observed with dose using the normal 2145 cell line, however a dose response effect was observed with the control cell line 2139 and both AT cell lines (Figure 4.1) ( $p < 0.05$ ). A higher cell survival (between 50,000 and 100,000 cells) was observed with the 2139 and both AT cell lines compared to the 2145 cell line which showed low levels of cell survival (less than 50,000 cells) and no differences between any dose. A higher level of variation of triplicates was observed for the non-irradiated control in AT2Bi, and a higher cell survival was observed at the lower dose point (0.05Gy) with this cell line compared to all other cell lines and doses.



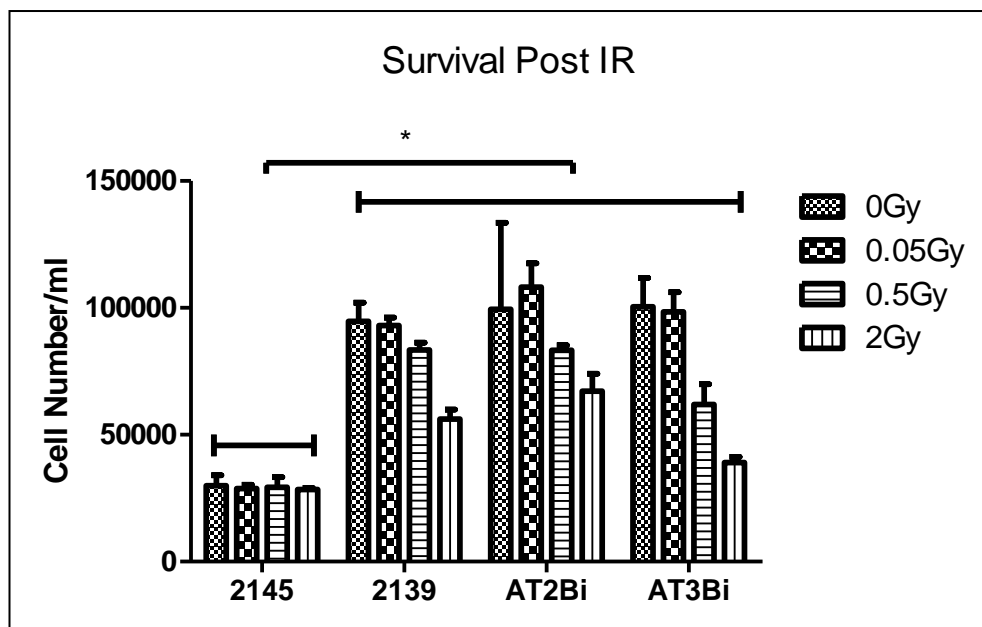


Figure 4.1 Survival after irradiation of LCL's measured by their relative growth at 72hrs post irradiation. Cell survival for normal cell lines (2145 and 2139) were compared to AT cell lines (AT2Bi and AT3Bi) N=3.

#### 4.3.2 Cell viability and Cytotoxicity

Figures 4.2 and 4.3 represent cell viability and cytotoxicity which was measured using the ApoTox -ProGlo™ triplex assay kit from Promega at 1 hr and 24 hrs following irradiation. There was no significant change in viability between cell line, dose or time point. However, a large difference in viability was observed in AT2Bi for the 3 doses at

24 hours indicating a varied response compared to the other cells lines (Figure 4.2) ( $p > 0.05$ ).

For cytotoxicity, little difference was observed across dose or time point for the control cell lines, except for 2Gy at 24 hrs for the 2139 cell line (Figure 4.3). A significant increase in cytotoxicity was observed at 24 hrs post irradiation in AT2Bi compared to 1 hr, as well as a significant increase in cytotoxicity at 1 hr for AT3Bi compared to 24 hrs for the irradiated cells only ( $p=0.04$ ). With deficient ATM, AT cells cannot recognise DNA damage or inhibit cell cycle progression for repair. AT cells undergo aberrant repair despite lacking ATM, but this is chaotic and involves lowering the threshold of p53 activation due to spontaneous DNA damage (not involving ATM). This could be why the AT2Bi cell line here showed an immediate spike in cellular cytotoxicity (immediate recognition of damage not involving ATM) and also why AT3Bi showed a delayed response (delay until p53 is activated). Both cell lines differ due to their heterogeneity (separate individuals) and therefore would be predicted to show differences in radioresponse.

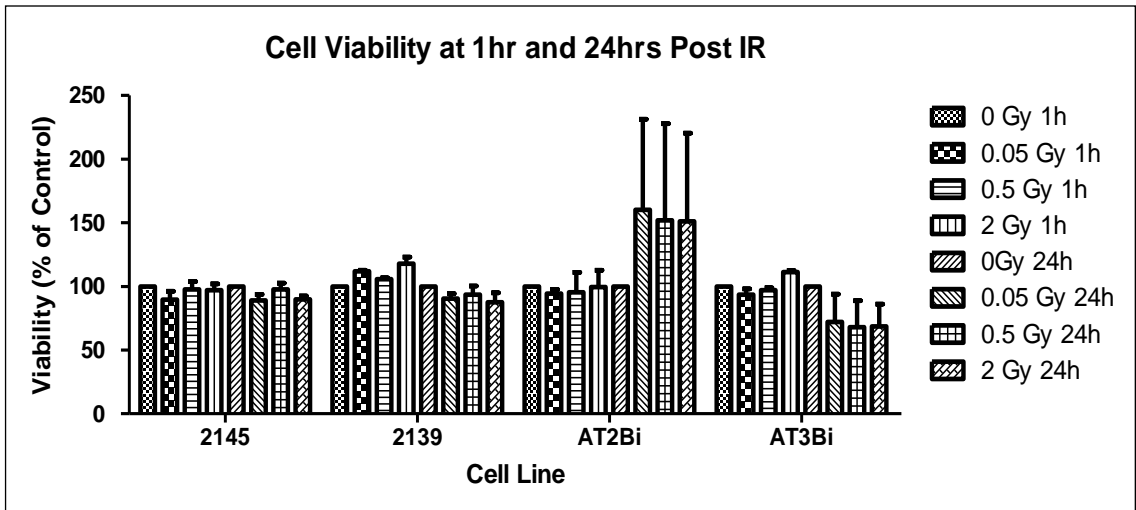


Figure 4.2 Cell viability as a percentage of the non-irradiated control. Cells from Ataxia Telangiectasia individuals (AT2BI and AT3BI) in comparison to cells from normal healthy donors (2145 and 2139) (N=2).

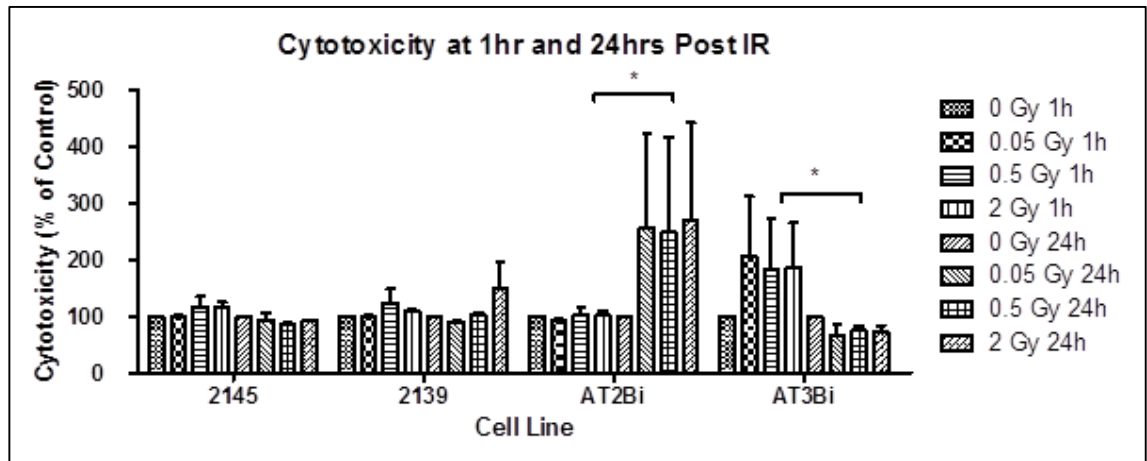


Figure 4.3 Cytotoxicity at 1hr and 24hrs post irradiation. Values for each dose and cell line were expressed as a percentage of the non-irradiated control. n=2

### 4.3.3 DNA Damage

DNA damage was investigated by means of  $\gamma$ H2AX. This was performed using flow cytometry (mean fluorescence intensity (MFI)) and foci induction using confocal microscopy. Using flow cytometry, MFI was plotted for each of the doses as a percentage of their control for 1 hr post irradiation (figure 4.4) and 72 hrs post irradiation (figure 4.5). At 1 hr, the two control cell lines are very different at the lower dose point (0.05Gy) and the higher dose point (2Gy) as a higher level of  $\gamma$ H2AX is observed in the 2139 cell line for both of these doses compared to a much lower level in the 2145 cell line. The highest overall intensity of  $\gamma$ H2AX was observed at 2Gy in the normal cell line 2139. Both AT cell lines show a similar response apart from a much higher baseline  $\gamma$ H2AX induction in the non-irradiated control of AT3Bi, which indicates a level of damage present before irradiation exposure. Additionally, large variation was observed at 2Gy with the AT3Bi cell line, indicated by large overlapping error bars.

An overall reduced response of  $\gamma$ H2AX induction was observed at 72 hrs (Figure 4.5). A lower level of  $\gamma$ H2AX was observed at 0.05Gy and 2Gy in the normal 2145 cell line, compared to little or no  $\gamma$ H2AX in the irradiated samples of 2139. No  $\gamma$ H2AX was observed at 0.5Gy and 2Gy in the AT2Bi cell line, compared to a much higher level of  $\gamma$ H2AX at 0.05Gy and 2Gy with the AT3Bi cell line. A large variation in  $\gamma$ H2AX induction was observed in AT3Bi at 2Gy again, represented by large error bars.

There was an overall reduced response of  $\gamma$ H2AX at 72 hrs post irradiation compared to 1 hr, which highlighted that  $\gamma$ H2AX foci are presented instantly in the DNA damage response and that cell cycle response and DNA repair mechanisms are central to this response so that damage foci would indeed be reduced by 72 hours. A reduced expression of  $\gamma$ H2AX was observed in the 2145 cell line at the lower dose points at 72 hrs, compared to the high level at 1 hr.

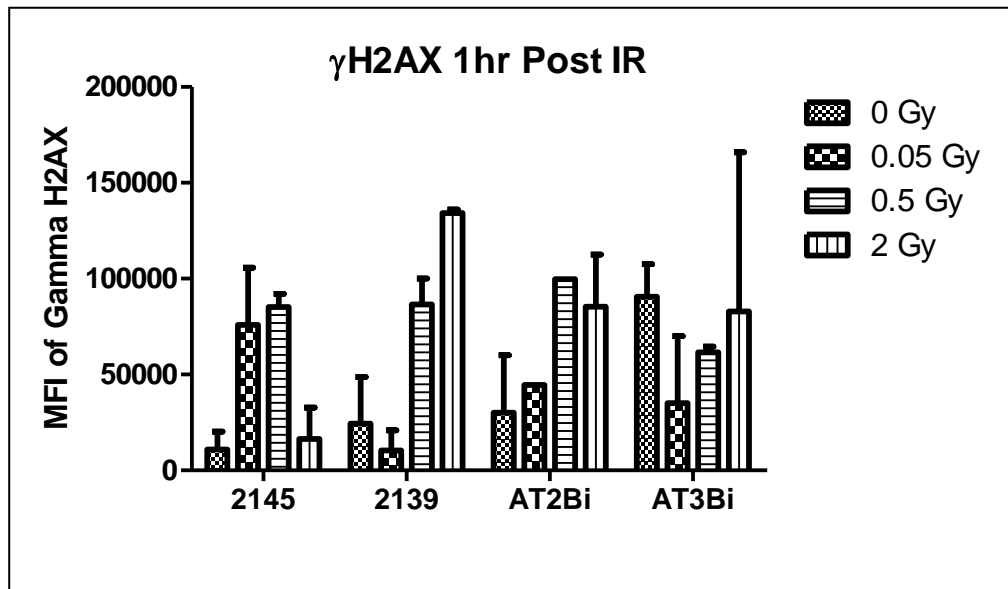


Figure 4.4 Mean fluorescence intensity (MFI) of  $\gamma$ H2AX at 1hr after irradiation for each of the cell lines and doses. n=2

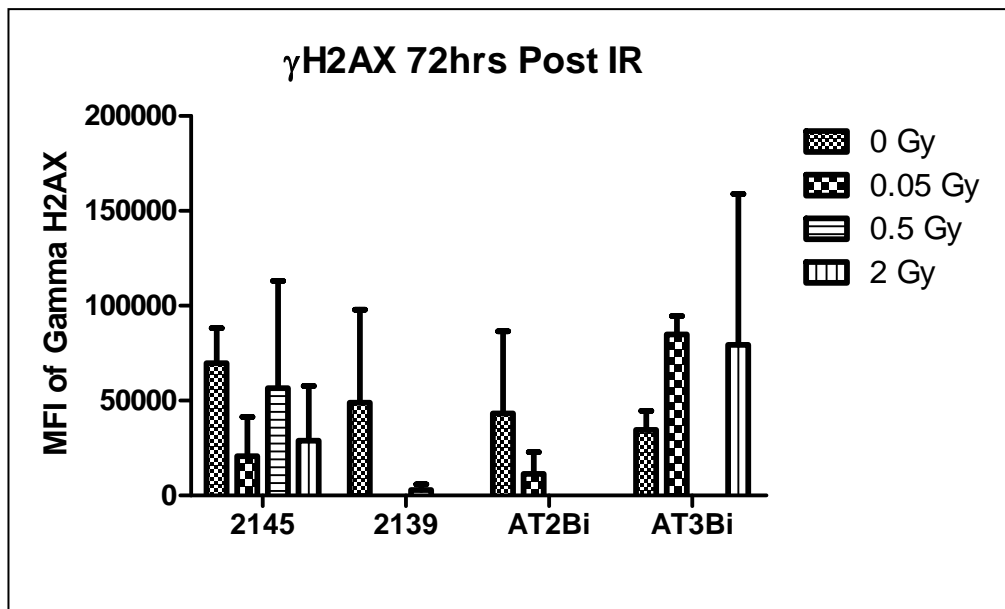


Figure 4.5 Mean fluorescence intensity (MFI) of  $\gamma$ H2AX at 72hrs after irradiation for each cell line and dose. n=2

Using confocal microscopy, average foci per cell were calculated for each of the cell lines and doses at 1 hr and 72 hrs. This was done to observe if measuring another endpoint in parallel for  $\gamma$ H2AX could confirm results of flow cytometry induction of  $\gamma$ H2AX or obtain additional information to distinguish radiosensitivities of each cell line per dose and time point. A dose response was observed in all cell lines, between each dose for 1 hr (Figure 4.6) (not distinguishable for the lower dose points with AT3BI cell line). At 72 hrs the average number of foci per cell had dramatically decreased at the higher dose points (Figure 4.7). This most likely represents a reduction of  $\gamma$ H2AX foci around the site of DNA damage break as the damage has had time to repair. A dose response was observed in 2139, and AT3Bi, and a higher level of foci observed at 0.5Gy for AT2Bi ( $p < 0.05$ ). Similar levels of  $\gamma$ H2AX foci remained from 1hr to 72hrs for the lower dose points (0.05Gy and 0.5Gy) and a reduction was observed from 1hr to 72hrs for the higher dose of 2Gy. A high level of background foci was observed in the non- irradiated controls for both flow cytometry and confocal microscopy  $\gamma$ H2AX endpoints.

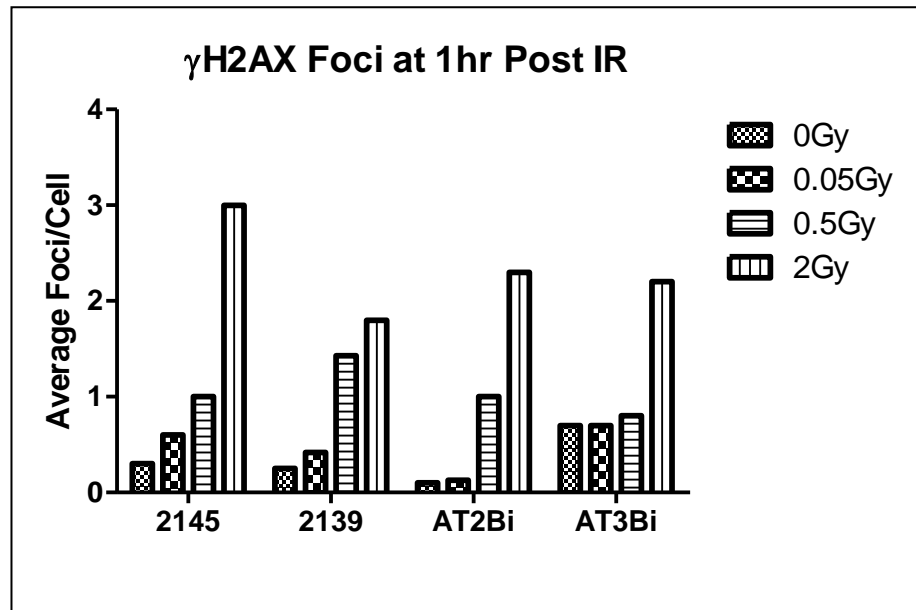


Figure 4.6 Average foci per cell of normal (2139 and 2145) cell lines compared to AT (AT2BI and AT3BI) cell lines. n=1

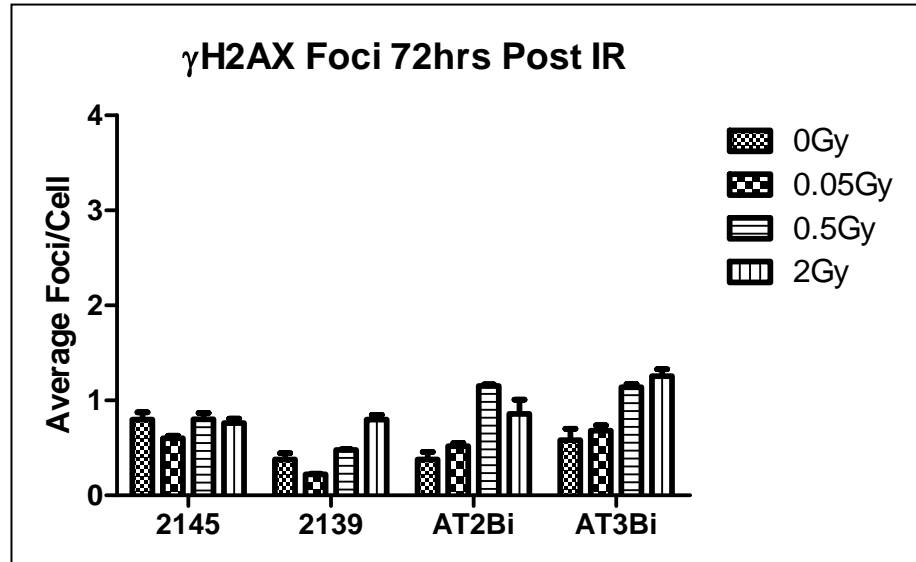


Figure 4.7 Average foci per cell observed in normal (2145/2139) vs AT (AT2Bi and AT3Bi) cell lines. n=3

#### 4.3.4 G2 Chromosomal Radiosensitivity

Checkpoint and G2 radiosensitivity analysis was performed by measuring the mitotic index and G2 radiosensitivity scoring respectively as described in the methods of Chapter 2 and 3.

##### 4.3.4.1 Radiation induced Mitotic Inhibition and G2 Radiosensitivity

A higher cell cycle checkpoint radiation-induced mitotic inhibition was observed in the 2145 and 2139 cell lines at each dose (except for 2Gy in the 2145 cell line which was lower than at 0.5Gy) compared to the AT cell lines, indicating that the cell cycle checkpoint response was functioning normally in the underlying DNA damage response. No inhibition was observed at the lowest dose point for both AT cell lines, (represented by negative inhibition in Figure 4.8). A lower inhibition was observed in all other doses in each of the AT cell lines (figure 4.8). Mitotic inhibition represents checkpoint response to the given dose of irradiation. Inhibition is the result of activation of ATM which in turn regulates inhibition of cell cycle progression through CHK1 and CHK2. Therefore, more inhibition represents a delay in progression of cells in the cell cycle to allow for DNA damage repair in the normal DDR. The normal cell lines were expected to show more checkpoint inhibition and more sensitivity to radiation because the DDR is working normally. However, if ATM was depleted, an alteration in checkpoint response (mitotic inhibition) would be expected and was observed in the AT cells

A significant increase in radiation induced G2 chromosomal aberration frequency was observed with increasing dose in all cell lines (Figure 4.9) with a significant change observed in all doses compared to the control, and between each dose ( $p < 0.05$ ). No significant difference was observed between control cell lines and AT cell lines at any dose point. Therefore, all cells showed similar chromosome damage induced by the same low doses of radiation.



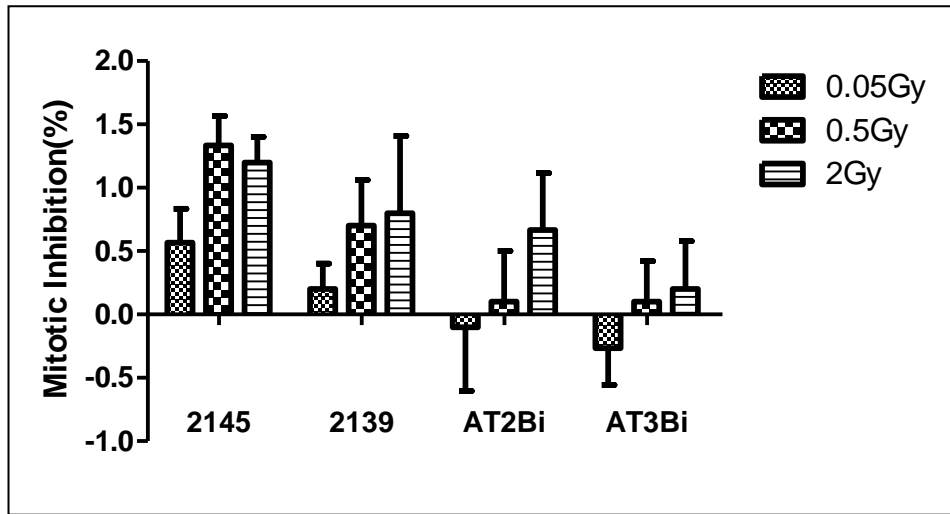


Figure 4.8 Mitotic inhibition was calculated by subtracting the mitotic index value at each dose point from the value at the respective cell line's 0Gy control value. This is represented as a percentage for each of the cell lines. n=3

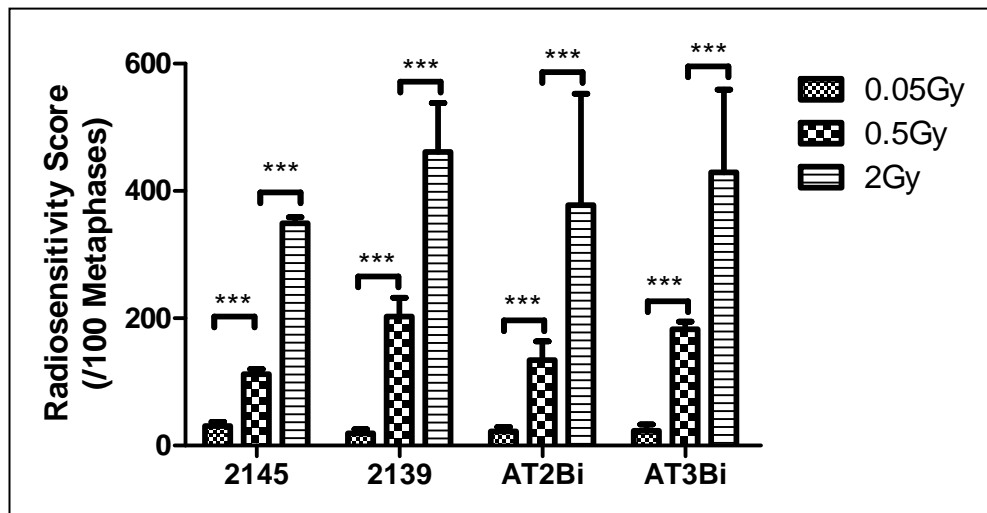


Figure 4.9 Radiation induced G2 score was calculated by subtracting the spontaneous aberration score in the 0Gy controls for each cell line from the dose value in each cell line. n=3

#### 4.3.4.2 LCL variation in radiosensitivity response

Coefficient of variation was calculated on the healthy control cohort from chapter 2 for optimisation and validation of the G2 chromosomal radiosensitivity assay. From the variation results in chapter 2, it was clear that less inter variation is observed with increasing radiation dose (chapter 2, section 2.3.3). Here, variation was calculated between normal healthy cells (HC) (2145 and 2139) and compared to AT cells (AT2Bi and AT3Bi) since all cells were derived from individual donors and similar to the inter variation analysis performed on donor and patient blood cohorts. A higher variation was observed with dose in the healthy control cells and compared to the AT cells (Figure 4.10). The highest variation (38%) was observed at the dose of 0.5Gy for both healthy and AT cell lines, indicating that there were different radiation responses between the healthy and AT cell lines at the most radiosensitive dose, but surprisingly that some underlying factor was responsible for radiosensitivity observed in the healthy controls. In contrast, minimal difference between the healthy controls and AT cell lines was observed at 0Gy highlighting that radiation exposure was a critical instigator of the DNA damage response in all cell lines and that the DNA damage response involving ATM was a key player. Although a difference was observed between the doses and cell lines, this was not significant due to the high levels of variation ( $P=0.08$  for cell lines and  $P=0.111$  for dose).

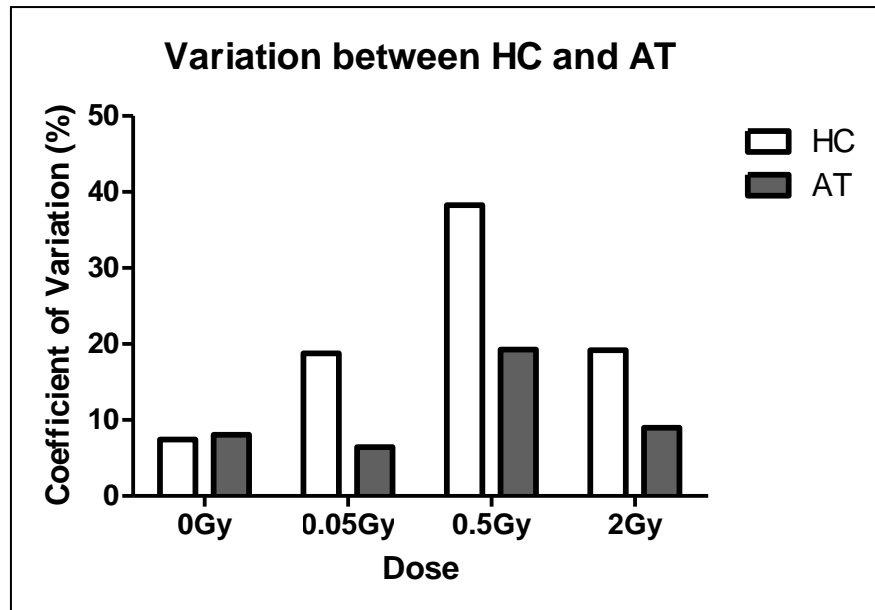


Figure 4.10. Coefficient of variation (%) was calculated by dividing the standard deviation of the mean by the mean for the Healthy cells (HC) (2145 and 2139) and the AT cell lines (AT2Bi and AT3Bi).

#### 4.3.5 G-Banding

For cytogenetic characterisation and analysis, G-Banding was completed on the 4 lymphoblastoid cell lines. This work was carried out in collaboration with Dr Natasha Coen at the Crumlin Hospital Genetics Department. The cell line 2145 repeatedly failed to produce any metaphase to carry out a G-band analysis and therefore no conclusive results were given and experiments continued with the 2139 control cells for comparison.

Clonal or recurrent aberrations are a hallmark of carcinogenesis found in nearly all cancer types. Clonal chromosomal aberrations are defined as follows; a chromosomal aberration which can be detected at least twice within 20 to 40 randomly examined mitotic figures<sup>320</sup>.

Therefore, the frequency of detecting a clonal aberration should be above 10 – 15%, and the frequency of detecting a non-clonal aberration should be below 5%.

Non clonal aberrations were first considered as genetic noise and spontaneous aberrations which are not induced by outside factors. More recent reports suggest however that non-clonal aberrations are a main feature of heterogeneity and most of the aberrations detected after chemo or radio therapy are non-clonal and unbalanced (>75%)<sup>320</sup>. Therefore, these types of aberrations can serve as an indicator of genomic instability and were characterised in the cytogenetic G-banding analysis.

The cytogenetic analysis on 2139 cells surprisingly showed a loss of a sex chromosome in all of cells analysed (Table 4.1/ Figure 4.11 for karyotype). There was no other single cell or non-recurrent aberrations detected (Table 4.2). The loss of a sex chromosome is associated with the constitutional diagnosis of Turners syndrome in females. FISH analysis using ATM (11q22)/TP53 (17p13.1) probe set showed no deletions or numerical aberrations involving these loci in the 100 cells analysed (Table 4.3). Cytogenetic analysis of the AT2B1 cell line detected loss of chromosome X (monosomy X) in 9 out of the 50 cells examined and so demonstrating that it was clonal (Table 4.1/ Figure 4.12 for karyotype). There were non-clonal aberrations detected in 4 out of the 50 metaphases examined (Table 4.2). 2 out of these cells showed a marker chromosome of unknown origin which were seen in both the normal clone and the clone with the monosomy X, this marker was not clonal as it was different in both cells. The 3<sup>rd</sup> cell showed a complex hyper-diploid (chromosome number 51-65 ) karyotype containing both numerical and structural aberrations including addition of material of unidentifiable origin to the long arms of both chromosome 1 homologues and to chromosome 2 (there was an additional chromosome 1 containing additional material on unidentifiable origin on the long q arm but at a different breakpoint) and there were also gains of numerous chromosomes

including chromosomes 4, 6, 11, 13, 14, 15, 18, 19, 20 and 21. The 4<sup>th</sup> cell showed an apparently balanced translocation between the short arms of chromosomes 12 and 19.

Table 4.1 Results of the G-band analysis of each of the cell lines showing recurrent and clonal cytogenetic aberration. Addition denoted by (add).

<b>Cell Line</b>	<b>Karyotype</b>	<b>Comments</b>
<b>2145</b>	Fail	Failed to produce metaphases for G-banding
<b>2139</b>	45,X[50]	Loss of a sex chromosome in all cells (Turners Syndrome)
<b>AT2B1</b>	45,X,-X[9]/46,XX[39]	Monosomy X in 9 out of 50 cells
<b>AT3B1</b>	46,XX,add(14)(q32),add(15)(p13)[25]/46,XX[14]	Addition of material of unknown origin to the long arm of chromosome 14 and to the short arm of chromosome 15

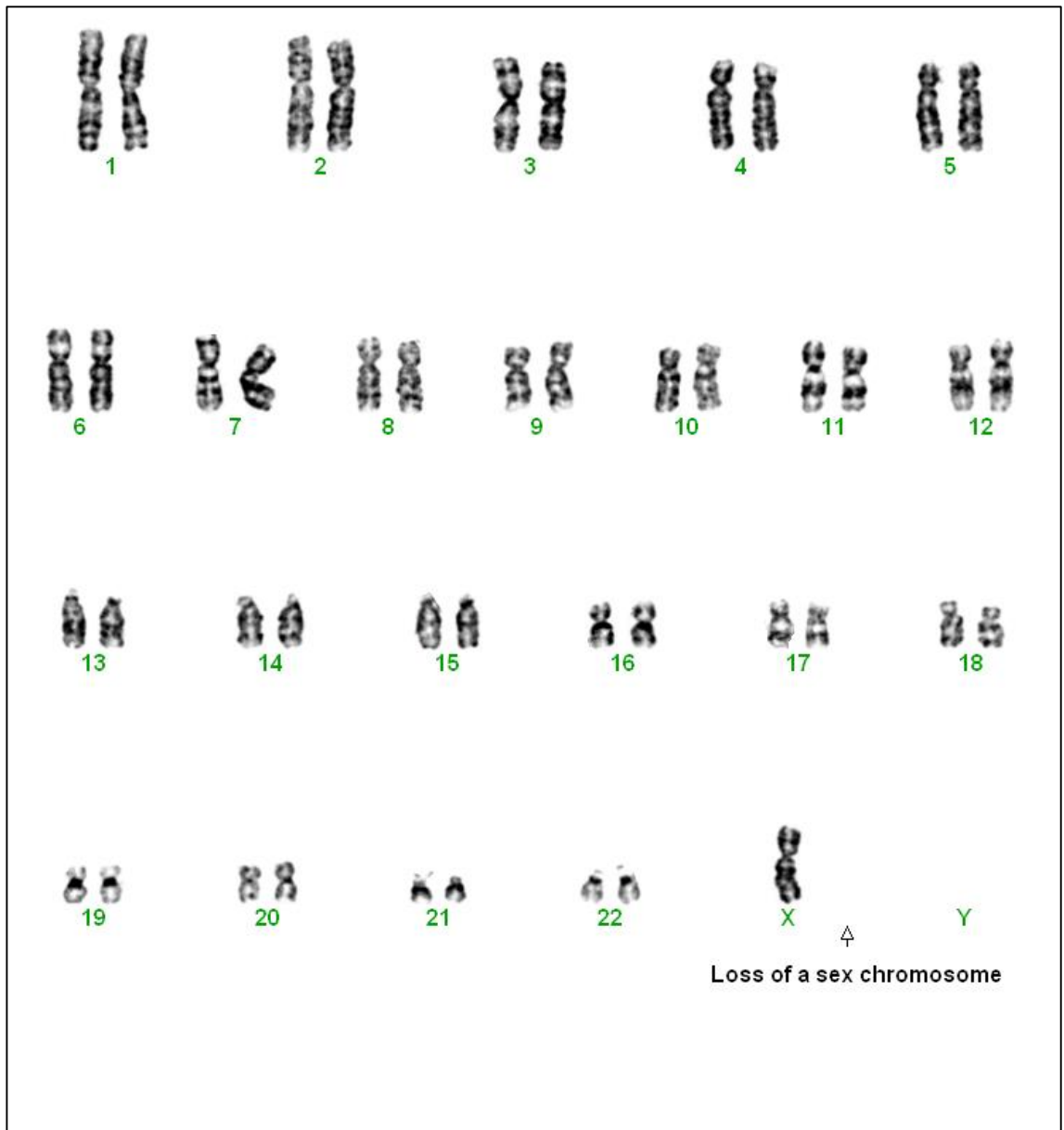


Figure 4.11 G-Banding of the 2139 cell line showing an abnormal karyotype. Loss of X chromosome was found in all 50 metaphases analysed.

Table 4.2 Non-clonal aberrations that were detected by G-band analysis. Note that normal cell line 2145 did not yield enough metaphases for analysis and no aberrations were found in the 2139 karyotype. Deletion (Del), marker (mar), addition (add)

<b>Cell Line</b>	<b>Karyotype</b>
<b>2139</b>	None Found
<b>AT2B1</b>	47,XX,+mar
	46,X,-X,+mar
	56,X,-X,del(1)(q12q42)x2,+add(1)(q44),+add(2)(q37)x2,- 3,+4,+4,+4,+6,+6,-7,-8,-9,+11,+13,+14,+15,-16,16,- 17,+18,+19,+20,+21,+2mar
	46,XX,t(12;19)(p13;p12)
<b>AT3B1</b>	46,X,add(X)(p11.2)
	46,X,del(X)(q21q26)
	39,XX,-4,-7,+8,-9,-10,-12,-13,-16,-16,dic(19;?)(q13;?)
	44,XX,-10,-11,dic(19;?)(q13.3;?)
	46,XX,add(11)(q25)
	43,XX,del(1)(q12),-3,-5,-5,-16,+mar
	45,XX,del(1)(q11q44),del(5)(q11.2q35),add(6)(q13),add(14)(q32),add(15)(p13), add(16)(q11.2),add(20)(q11.1)

The cytogenetic analysis of the AT3B1 cell line showed addition of material of unidentifiable origin to the long arm of chromosome 14 and to the short arm of chromosome 15 in 25 out of the 50 metaphases analysed (Figure 4.13 for cell line karyotype). There were 7 metaphases found with non-clonal aberrations out of the 50 metaphases. These included 2 cells found with aberrations involving the X chromosome, the first had addition of material of unknown origin to the short arm and the second had an interstitial deletion in the long arm. There were 2 cells found containing a dicentric chromosome 19 where breakage and reunion occurred between the long arm of chromosome 19 and a chromosome of unidentifiable origin, both these aberrations were different in morphology and the breakpoints were also different, and therefore they were classified as non-clonal. There was a cell found containing an aberration in the long arm of chromosome 11. The final 2 cells contained deletions in the long arm of chromosome 1 but with different breakpoints, the first of these cells also contained loss of chromosomes 3, 5 and 16 as well as a marker chromosome. The second cell also contained numerous other structural aberrations including a deletion in the long arm of chromosome 5 and addition of material of unidentifiable origin to the long arms of chromosomes 6, 16 and 20 as well as the clonal add(14q) and add(15p) previously described.



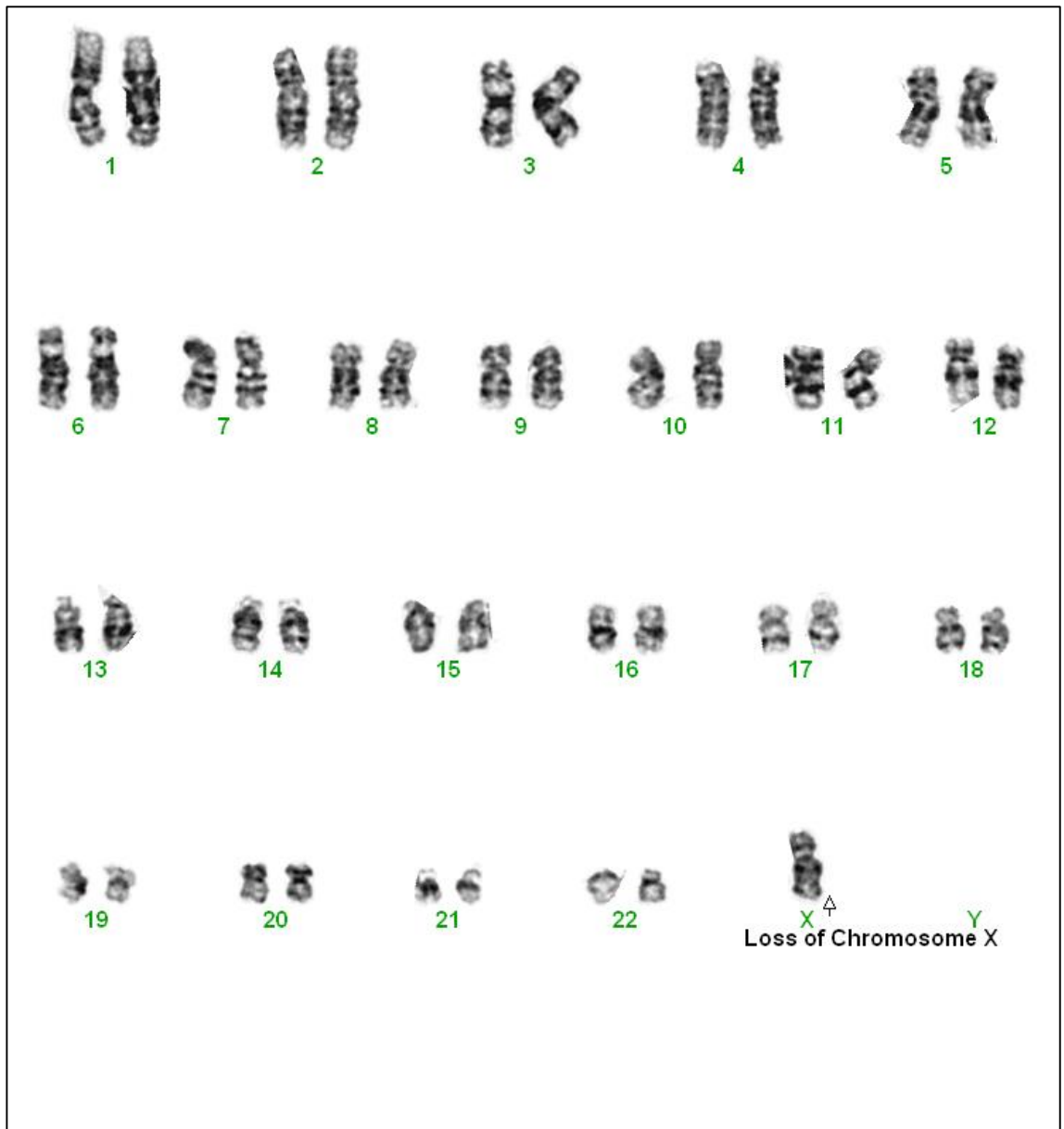


Figure 4.12 G-Banding and karyotype of AT2Bi showing loss of X chromosome. This was found in 9 out of 50 cells analysed.

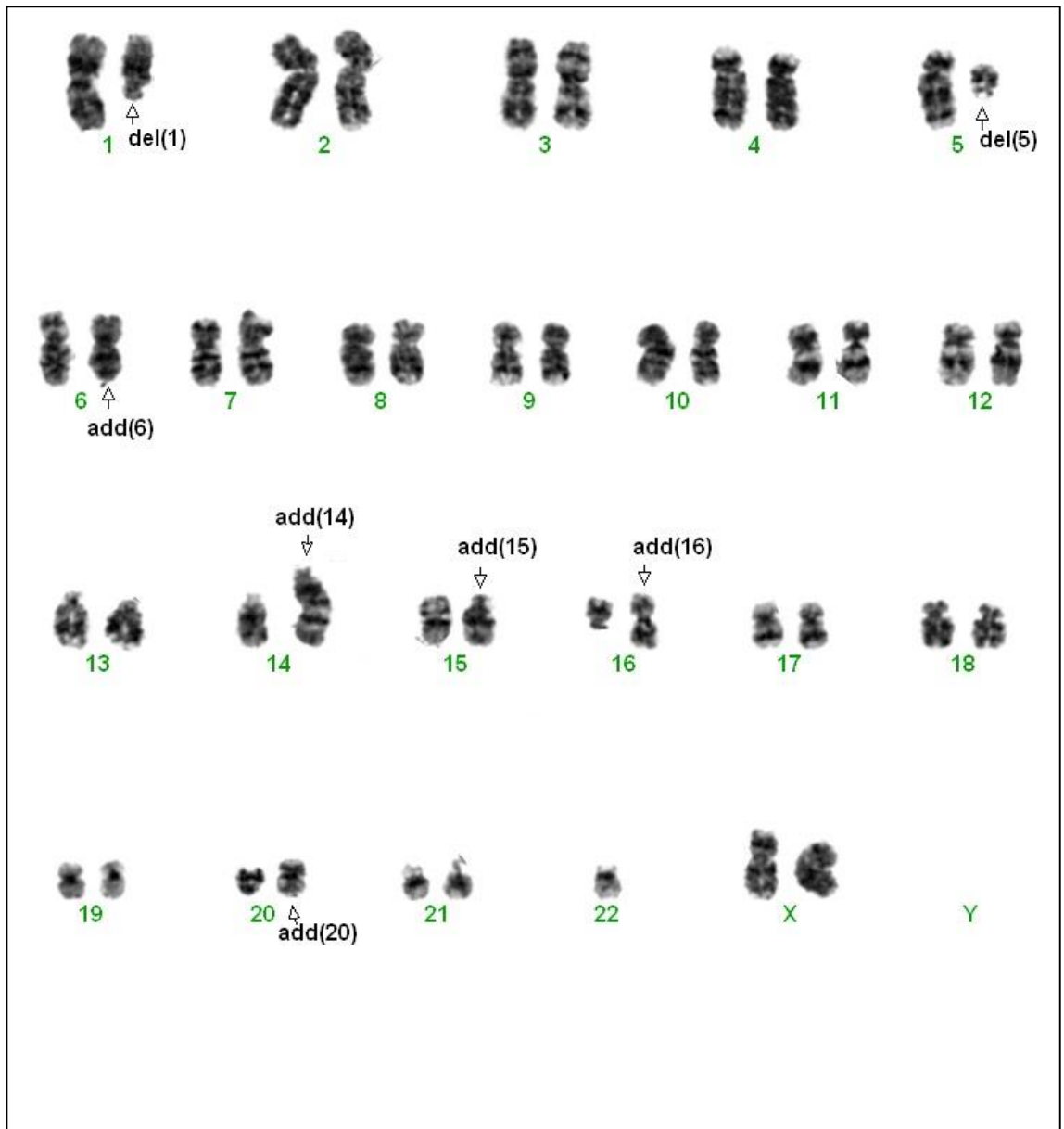


Figure 4.13 G-Banding and karyotype of AT3Bi showing numerous addition and deletions of chromosomal material on/from the wrong chromosomes.

#### 4.3.6 Fluorescent *in situ* Hybridisation (FISH)

FISH analysis using the ATM (11q22)/TP53 (17p13.1) probe set showed no deletions or numerical aberrations involving these loci in the 100 cells analysed (Table 4.3). Further FISH with centromere specific probe (CEPX) to chromosome X showed a low level loss in 14 out of 100 cells examined and thus confirming the G-band finding of monosomy X for 2139 cells (Table 4.1).

Table 4.3 FISH analysis of each of the cell lines to include probes for CEPX, IGH, TP53 and ATM. Note normal cell line 2145 did not yield enough metaphases for a conclusive analysis. Addition is denoted by 'add.'. Nuclear *in situ* hybridisation denoted as (Nuc ish).

Cell Line	FISH Probe	Karyotype
<b>2139</b>	TP53/ATM	.nuc ish (ATM,TP53)x2[100]
<b>AT2B1</b>	TP53/ATM	.nuc ish(ATM,TP53)x2[100]
	CEPX	.nuc ish(DXZ1x1)[14/100]
<b>AT3B1</b>	TP53/ATM	.nuc ish(ATM,TP53)[100]
	IGH (Break apart)	.ish add(14)(q32)(5'IGH +,3'IGH-,5'IGH+)[10]

In normal cells, break apart probes depict two colours which represent the 3' and 5' end of the IGH locus on chromosome 14q32. Further metaphase FISH with an IGH (14q32) break apart probe showed a population of cells with loss of the 3'IGH and a duplication

of the 5'IGH end of the probe that has been shown to be on the derivative chromosome 14 by metaphase FISH (Figure 4.15). This result would represent a rearrangement of the IGH locus with the 5'IGH promotor region been retained on the critical chromosome 14 and loss of the 3'IGH region. Unfortunately, interphase FISH was not possible due to the high level of FITC (green) background making it difficult to read the signals in the nuclei. There was a t(14;14) aberration that is classical to AT patients but the aberration observed was different as it showed foreign chromosomal material and the orientation of the second 5'IGH is proximal to the native 5'IGH. This indicated a duplication of the 5'IGH region post translocation of the IGH locus. There was also a more complex rearrangement present that involved another unidentifiable chromosome resulting in loss of the 3'IGH.

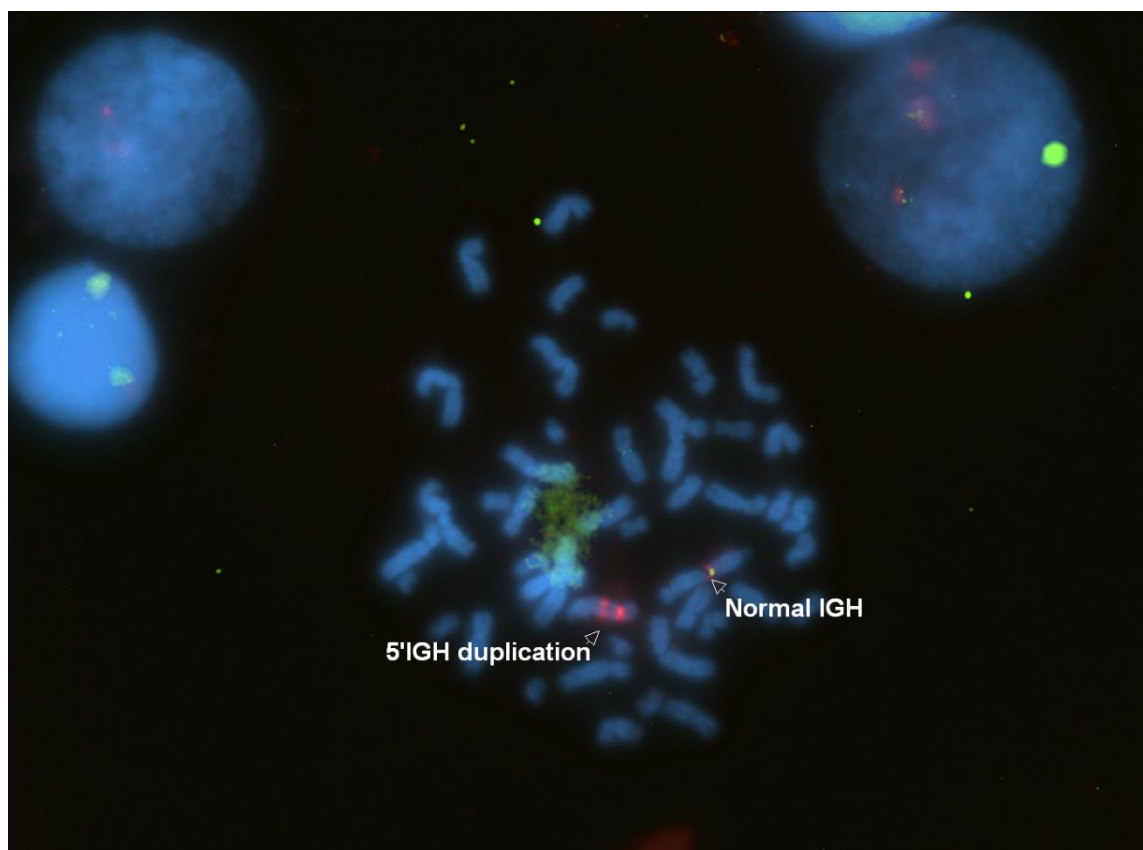


Figure 4.14 FISH analysis using the ATM probe set for AT3Bi cell line showing loss of the 3'IGH and duplication of the 5'IGH end of probe.

Interphase FISH was done on each cell line with a probe used for detection of ATM and TP53 presence or absence. Both ATM and TP53 were observed in all cell lines in two copies (Figure 4.15).

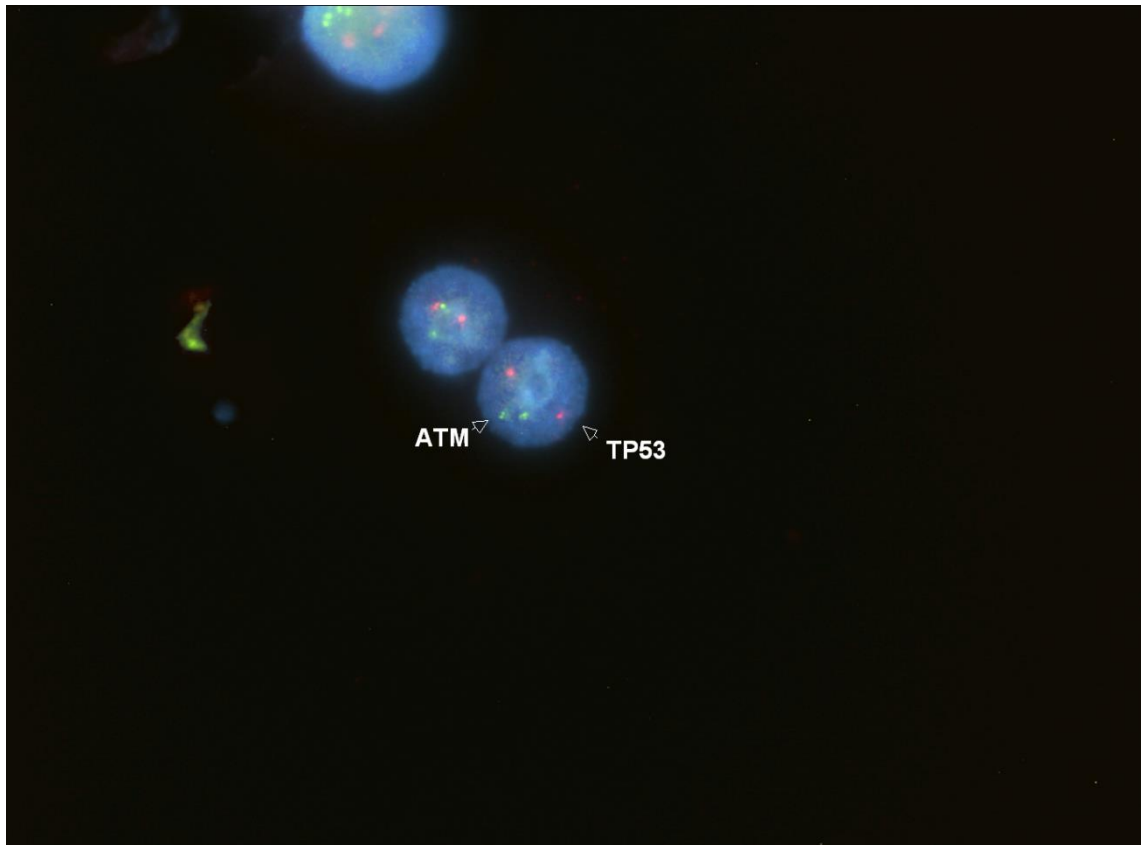


Figure 4.15 Interphase FISH using dual ATM-TP53 probe. A normal ATM and TP53 presence is indicated here by two red dots (TP53) and two green dots (ATM).

#### 4.4 Discussion

Epstein Barr virus immortalised lymphoblastoid cell lines from normal (2145 and 2139) and AT (AT2Bi and AT3Bi) were used as radiobiological models to investigate extreme cellular radiosensitivity and the underlying genetic mechanisms incorporating ATM and the DNA damage response.

Overall with cell survival, viability, cytotoxicity and caspase activation, a small difference was observed between normal cell lines and AT cell lines. For  $\gamma$ H2AX there was a marked response at 1 hr which was dramatically reduced by 72 hrs, which indicates that repair mechanisms are still in place for up to 72 hrs after irradiation. These results confirm findings by Porcedda *et al* who also found residual  $\gamma$ H2AX foci present in AT cells up to 72hrs after 2Gy of irradiation<sup>321</sup>.

It was expected that a different radio-response would be observed in the normal cell lines compared to the AT cell lines which was cited by a number of groups using cell survival assays for AT radiosensitivity<sup>32</sup>. Results for the 2139 cell line were surprising as they responded quite similarly to the AT cell lines with cell survival experiments. There was a large variation within the control cell lines and AT cell lines, which is not unusual as they were extracted at one stage from human donors and cells were cultured and immortalized. This in addition to the variation of responses in healthy controls at 0.5Gy emphasise the underlying genetic mechanisms and factors which may be involved.

Due to conflicting results between assays, the 4 cell lines were sent to the Cytogenetics Department in Crumlin Hospital, Dublin for cytogenetic characterisation by G banding and FISH analysis using several selected probes. Of huge interest was the “normal” cell line 2139 which was found to have a loss of X chromosome in all cells analysed, and therefore characterised as Turners syndrome. Although, it can only be confirmed as Turners syndrome if the results are not a consequence of culturing techniques, which have

acquired instability over rigorous culturing and time. A radiosensitivity study conducted in 2012 using two groups of Turners syndrome patients, each with different variants (45 X complement and 46 XX gonadal dysgenesis) and compared to age and sex matched controls demonstrated significantly higher levels of chromosomal radiosensitivity after 3Gy of irradiation<sup>322</sup>. Therefore, the conflicting data which was obtained with the radiobiological assays specifically between the two control cell lines is in agreement with previous groups findings. The 2139 cell line in the cellular survival studies shows the exact delayed dose response as recorded for the AT cells compared to the normal cellular response in the normal 2145 cell line.

Additionally, G2 aberration scoring from the G2 chromosomal radiosensitivity assay demonstrated a higher (although not significant) aberration frequency in the 2139 cell line compared to the control 2145 cell line. However, a huge difference in radiosensitivity between normal and radiosensitive cell lines was not observed. This is not unusual, as Bender *et al* explained in 1985 reports that no difference was observed in sensitivity between normal peripheral blood lymphocytes and peripheral blood lymphocytes from AT patients<sup>312</sup>. It could be worth using fresh whole blood for future experiments, however as AT is so rare (<1% of the population) this could be difficult to obtain sufficient numbers of donors for analysis. In addition, ATM sequence variants play a huge role in heterogeneity and could be one of many factors affecting results in this work. As discussed in the previous chapter, Cesaretti *et al* found over 20 ATM sequence variants that contributed to toxicity after brachytherapy for prostate cancer<sup>40</sup>. As the immortalised cell lines were extracted from different donors, the lack of determination of radiosensitivity between the cell lines in this work could be attributed to donor heterogeneity.

Although the cytogenetic findings were in excellent agreement with the data presented for cell survival and G2 radiosensitivity, the remaining normal cell line 2145 failed to produce enough metaphases for conclusive karyotyping. This cell line (2145) had an extremely slow doubling time (approx. 64 hrs) which proved difficult in synchronising the experiments with the short doubling time of the three other cell lines (all <20hrs). This also indicated that the 2145 cell line had reached its Hayflick limit and was in replicative senescence.

The cytogenetic analysis using G-Banding and FISH clearly indicated that 2139, AT2Bi and AT3Bi were genetically unstable cell lines. A high level of clonal and non-clonal aberrations was found in the AT cell lines, and additional chromosomal material from unidentifiable origin were found on a number of chromosomes (specifically on chromosome 14). In the initial chromosomal reports (pre ATM mapping) on cells from AT patients, chromosome 14 rearrangements were often identified and mapped to the q arm of the chromosome between area 31-32<sup>303</sup>. FISH probing showed a number of cells with loss of the 3'IGH end of the probe and duplication of the 5'IGH end of the probe, which confirms genetic instability associated with radiosensitive syndromes. As a common breakpoint for chromosomes in patients with AT (14q32), this represents an increased risk (38%) for neoplasia, and young AT children have been described to be prone to acute lymphoblastic leukaemia and older AT patients at risk of T cell leukaemia<sup>323</sup>.

Interphase FISH probes were particularly useful for detecting presence or absence of ATM-TP53. These could possibly be used in a clinical setting as they require very little training to analyse results, and do not take a lot of time for conclusive results.

The cytogenetic probes which were used here yielded more information about the cell lines used than the radiobiological assays showed. The data presented confirms the crucial



central role of ATM in the DNA damage response as deduced from the different cell cycle (mitotic inhibition) response. As previously explained, cell cycle checkpoints are activated by ionising radiation and are under control of ATM thus altered ATM in AT cells would be expected to result in higher mitotic inhibition. This was observed from the mitotic inhibition data for the normal cell lines but not for the AT cell lines which showed a reduction in mitotic inhibition. Although one of the 'normal' cell lines (2139) showed a normal cell cycle response in terms of inhibition, it is important to remember that this donor's ATM was not mutated and the radiosensitivity of those cells are due to different underlying genetic mechanisms than those which cause radiosensitivity in the two AT cells. No deletion in ATM or TP53 was shown in the normal cell line 2139 or both AT cell lines. However, loss of the 3' end of the IGH break apart probes and duplication of the 5' IGH in chromosome 14q32 which is associated with radiosensitive syndromes and a t(14q14) which is a classical AT aberration<sup>303</sup> was found here.

#### **4.5 Chapter Conclusions and Summary**

In Summary, ATM is the key gene involved in coordinating the cellular response to ionising radiation. It is responsible for downstream signalling and activation of cell cycle checkpoints to inhibit progression of damaged cells in the cell cycle and to promote DNA repair. In summary, it is clear that ATM, the cell cycle and DNA repair mechanisms in the DDR are key genetic mechanisms underlying radiosensitivity and should be considered for investigating potential biomarkers for radiosensitivity prediction. Additionally, the cytogenetic probes used (TP53, ATM, CEPX and IGH) were useful indicators of abnormalities, therefore would be useful as potential biomarkers of radiosensitivity. The IGH break-apart probe was particularly useful and easy to examine samples quickly.

## **5. POTENTIAL OF A FOUR-GENE SIGNATURE FOR THE PREDICTION OF RADIOSENSITIVITY IN HEALTHY DONOR AND PROSTATE CANCER PATIENTS COMPARED TO ATAXIA TELANGIECTASIA SAMPLES**

### **5.1 Introduction**

Intrinsic individual variation is a key aspect involved in the prediction of radiosensitivity. Factors affecting radiosensitivity include sex, age, tissue type, medication, smoking or alcohol intake and hormones<sup>59</sup> (described in section 2.1). It is thought that the mentioned factors do not account for all factors which influence radiosensitivity, and genetic and epigenetic mechanisms play a major role<sup>324</sup>. In addition to the factors mentioned, target dose, anatomical variation, tumour or tissue volume treated and field size may account for inter individual differences in radiosensitivity variation after radiation treatment<sup>325</sup>. Although the many factors mentioned have been suggested to play a role in inter and intra individual variability in radiosensitivity, evidence suggests involvement of a more profound underlying biological mechanism. This evidence points toward a genetic underlying cause of radiosensitivity and comes from early studies showing that first degree relatives of those suffering breast cancer (BCa) showed a higher level of radiosensitivity compared to healthy controls using a micronucleus assay approach<sup>326</sup>.

Genetic alterations associated with radiosensitivity have been further investigated in depth through the finding of radiosensitive syndromes such as Ataxia Telangiectasia (AT), Nijmegen Breakage Syndrome (NBS) and Bloom's syndrome (BS) in which all patients suffer cellular and clinical radiosensitivity due to mutations in DNA damage and repair response genes<sup>327</sup>.

Furthermore, large intra individual variations within radiosensitivity genes have been attributed to single nucleotide polymorphisms (SNP's) that make up approximately 90% of naturally occurring sequence variations<sup>328</sup>. Hall *et al* outlined in a review that polymorphisms in DNA damage and repair response genes such as ATM, XRCC1, hHR23 and TGF- $\beta$  are positively associated with increased late tissue reactions, with one ATM polymorphism showing a radioprotective effect<sup>329</sup>.

As the genetic basis of radiosensitivity is still unfolding, more complex gene expression studies in the form of micro-arrays are being investigated to identify more accurate predictors of radioresponse. Genome wide association studies are currently ongoing; for example the Gene-PARE project (Genetic predictors of adverse radiotherapy effects) utilizes large scale population cohorts to identify genetic signatures and sequence variations in radio-responsive genes which could be of use in radiosensitivity monitoring<sup>330</sup>.

In 2010, Kabacik *et al* successfully identified radio-responsive genes for dose estimation and individual radio-response, in which peripheral blood lymphocytes from healthy controls were exposed to either 2Gy or 4Gy of x-irradiation using a multiplex quantitative real time polymerase chain reaction (MQRT-PCR) method<sup>331</sup>. After micro-array analysis of over 800 genes, key genes such as sestrin 1 (SESN1), cyclin-dependent kinase inhibitor 1 a (CDKN1A) (also known as p21), ferredoxin reductase (FDXR) and proliferating cell nuclear antigen (PCNA) were among the key radio responsive genes upregulated at 2 hr and 24 hrs after irradiation. CDKN1a and SESN1 were upregulated for a longer time after irradiation (up to 48 hrs).

Using a multiplex polymerase chain reaction (PCR) approach, multiple gene targets can be used within one reaction tube allowing for the analysis of several genes of interest in one reaction and greatly minimizing costs and time needed for gene analysis. As multiple

healthy donors and prostate cancer patient samples as well as AT specific lymphoblastoid cell lines were used for the radiosensitivity studies described previously, this multiplex PCR approach was adopted to assess radiosensitivity gene candidates from all of the different cellular samples.

Four specific genes are of interest in this work. Figure 5.1 outlines the main functions and interactions of each gene with the others. The first, p21 (**CDKN1A**) is a Cyclin Dependent Kinase Inhibitor which binds to and inhibits cyclin – CDK1, CDK2 and CDK4/6 complexes to regulate or halt cell cycle progression at G1 and S phase<sup>332</sup>. This is done through p21 regulation of p53 which up-regulates ATM and activates the cell cycle checkpoints in response to ionizing radiation. In addition to the role of p21 within the cell cycle, it has also been found to possess a strong affinity for binding with Proliferating Cell Nuclear Antigen (PCNA), another of the genes found to be highly radioresponsive<sup>332</sup>.

**PCNA** is a DNA clamp that helps binding of DNA polymerase  $\delta$  in eukaryotic cells and is essential for replication. PCNA also has a direct role in the DNA damage response (DDR) as it is placed at replication forks and coordinates DNA replication and DNA repair. It also acts as a loading clamp for additional DDR proteins to recruit to the site of DNA damage and bind<sup>333</sup>. P21 is also highly expressed in senescent cells, and inhibition of p21 has been found to increase radiosensitivity in prostate cancer cells<sup>334</sup>. The interaction of p21 with PCNA was also of interest because this interaction and binding facilitates the inhibition of DNA synthesis in response to irradiation. This promotes cell checkpoint arrest until DNA repair is complete through trans lesion synthesis, promoting genetic stability<sup>335</sup>. Additionally, the interaction of p21 and PCNA causes G1 and G2 cell cycle arrest in the absence of p53 in human colon cancer cells<sup>336</sup>.

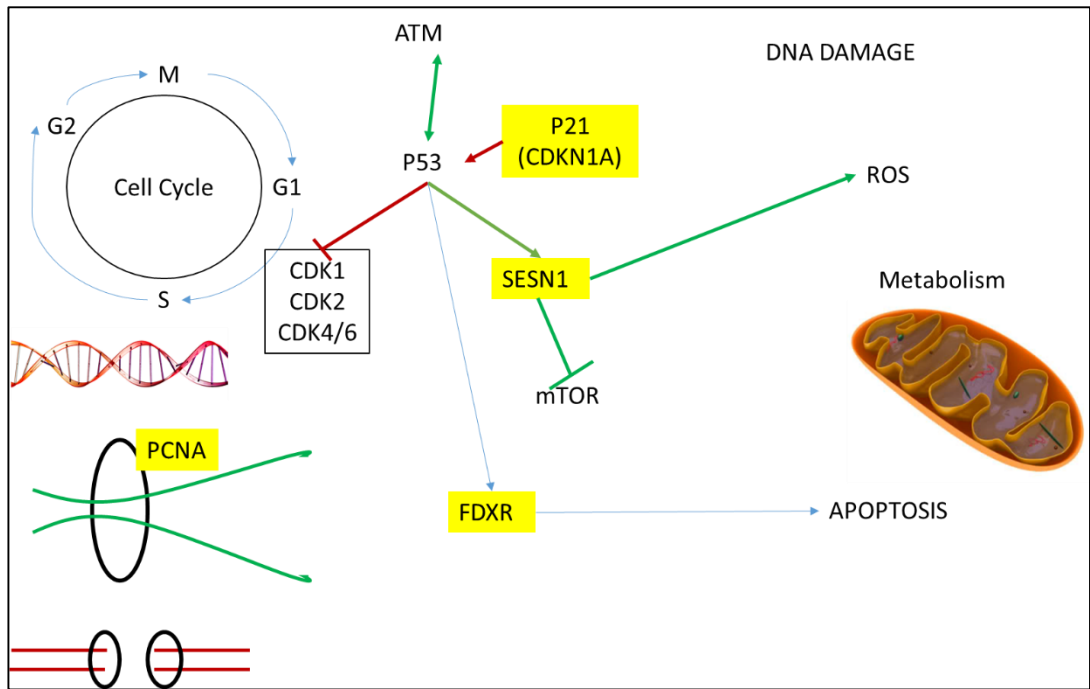


Figure 5.1 Overview of the 4 genes used in this chapter for radiosensitivity prediction. The first, CDKN1A (P21) regulates P53 inhibition of CDK complexes for cell cycle inhibition in response to stress. PCNA is a DNA synthesis clamp which facilitates loading of factors for DNA replication, but also loading of DDR genes in the event of a DSB. SESN1 is regulated by p53 for metabolism of peroxiredoxins, but the SESN family are important negative regulators of MTOR which promotes tumorigenesis. SESN1 can also regulate ROS levels in response to ionising radiation. FDXR is also regulated by p53 in response to ROS production, but favours an apoptotic approach as a fate to cellular stress.

**SESN1** has been identified as a p53-dependent target gene (solely activated by p53) which functions to regenerate over oxidized peroxiredoxins in response to ionizing radiation among other members of the sestrin family such as SESN2<sup>337</sup>. SESN1 and SESN2 has also been found to negatively regulate mTOR and its signalling, in which mTOR functions to promote tumorigenesis through proliferation and chemoresistance<sup>338</sup>.

**FDXR** was of interest to these studies because it was found to be highly responsive to radiation and useful for bio dosimetry, but has also recently shown evidence of a heritability factor for its expression. Correa and Cheung demonstrated a higher variability in FDXR and p21 expression among a number of twin pairs as opposed to within individual twin pairs<sup>339</sup>. Therefore genetic stability and radiosensitivity are strongly linked in the stress response to ionizing radiation through the actions of p21, PCNA, SESN1 and FDXR which have been highly expressed in previous studies<sup>331</sup>. Furthermore, given that p21 and SESN1 are linked to critical regulators of the cell cycle, they are of interest in the present work to investigate if they are potential biomarkers of radiosensitivity using healthy donors compared to prostate cancer patients and cell lines from AT patients.

From the original 800 gene studies by Kabacik *et al*, genes involved in metabolism have surfaced<sup>331</sup>. Of the four genes used for this study both SESN1 and FDXR are involved in regulating cellular fate after oxidative stress. It is known from previous work that repression of the SESN family of genes (SESN1, 2 and 3) leads to an upregulation of ROS through the action of RAS, which can lead to genomic instability and is of importance in research for cancer therapy<sup>340</sup>. In addition, FDXR is known to regulate normal metabolism and mitochondrial function but has been found to be transcriptionally regulated by p53 in response to ROS production, favouring an apoptotic pathway approach<sup>341</sup>. Therefore, as these two genes have important roles in metabolism related to ROS and ionising radiation produces a large amount of ROS within the cellular microenvironment, they could be useful biomarkers for radiosensitivity prediction.

The aim of the current chapter was to use a panel of genes in multiplex (P21, PCNA, SESN1 and FDXR) to determine if they would be suitable predictive biomarkers or indicators of patient radiosensitivity. The current work aimed to investigate levels of

radiosensitivity in a cohort of healthy donors and prostate cancer patients which are of unknown and variable levels of radiosensitivity, and compare the gene expression to that obtained from a cellular radiosensitivity phenotype in Ataxia telangiectasia patients which are known to display extreme radiosensitivity. The work presented in this chapter was carried out in collaboration with Public Health England (PHE) who has expertise in the bio dosimetry field for monitoring and prediction of radiation exposure. The group have used genome wide association studies to elucidate key radio-responsive genes and have refined the nCounter and MQRT-PCR techniques for radiation bio dosimetry applications<sup>183</sup>. Therefore, four of the highly expressed radio-responsive genes found through their genome wide studies on healthy cohorts were used here as a possible panel of genes for prediction of individual radiosensitivity among healthy controls and prostate cancer patients with reference to LCLs from AT patients.

## **5.2 Methods**

### **5.2.1 Samples and Cell Culture**

Blood samples were used from the healthy control (HC) cohort described in Chapter 2 and the Prostate Cancer (PCa) cohort in chapter 3 of this thesis. 15 HC's were used for MQRT-PCR analysis and 6 PCa patients were used. For investigation of effect of hormone therapy on gene expression, 6 PCa patients were used at visit 1 (baseline) and visit 2 (post androgen deprivation therapy (ADT)). A larger cohort of PCa samples could not be analysed as they were not available at the time. Whole blood was obtained from healthy control donors and prostate cancer patients and cultured as per section 2.2.2. Whole blood cultures were irradiated at 0.05Gy and 0.5Gy compared to a non-irradiated control (section 2.2.4).

Lymphoblastoid cell lines (LCL's) obtained from 2 clinically characterised Ataxia telangiectasia (AT) patients from chapter 4 were used for this study and were coded AT2Bi and AT2BI. The cells were kindly donated from the University of Birmingham. Culturing and maintenance described in section 4.2. For experimental set up,  $1 \times 10^6$ /ml cells for each cell line were seeded into T25 flasks per dose (at doses of 0Gy, 0.05Gy, 0.5Gy and 2Gy) and (Irradiation procedures and set up as described in section 2.2).

### 5.2.2 RNA extraction and Quantification

At 1 hr post irradiation (1 hr and 24 hrs for AT cells), samples were centrifuged at 300g for 5 mins and pellets were resuspended in 1ml of TriReagent (Sigma) (supplemented with 3N Acetic Acid) for RNA extraction. 200 $\mu$ l of Chloroform (Sigma) was added to each sample for 10 – 15 seconds with shaking and allowed to stand for 5 mins at room temperature. After centrifugation at 12,000 rpm for 15mins at 4°C, the upper aqueous phase containing RNA was collected and transferred to a clean Eppendorf tube with 500 $\mu$ l of isopropanol (Sigma) and stored for 5-10 mins at room temperature. Samples were then centrifuged at 12,000g for 10 mins at 4°C. After centrifugation, the RNA pellet was washed with Ethanol (Sigma) and centrifuged at 7,500g for 5 mins at 4°C. Ethanol was removed and RNA pellets were air dried for 10 mins and then resuspended in 30 $\mu$ l of RNase free water (Ambion). Samples were stored at -80°C until reverse transcription and real time PCR.

RNA was quantified on a Nanodrop spectrophotometer and 1 $\mu$ g of RNA with RNase free water and loading buffer was loaded on to 1.2% agarose (Sigma) gels with 4 $\mu$ l of GelRed (Sigma) for quality analysis. Gel electrophoresis was set up for 30 mins at 80 volts and gels were subsequently visualized using the SynGene G: BOX chemi XX6



transilluminator system. Only samples with complete intact 18s and 28s RNA bands were used for cDNA synthesis and MQRT-PCR analysis.

### 5.2.3 CDNA Synthesis

Reverse transcription reactions were performed using High Capacity cDNA Reverse transcription kit, (Applied Bio- systems, Foster City, CA, USA) according to the manufacturer's protocol with 700ng of total RNA and as previously described by Manning *et al* <sup>183</sup>.

### 5.2.4 Multiplex Quantative Real Time PCR

Real-time PCR was performed using Rotor-Gene Q (Qiagen, Hilden, Germany). Reactions were run in triplicate using PerfeCTa ® MultiPlex qPCR SuperMix (Quanta Biosciences, Inc. Gaithersburg, MD, USA) with primer and probe sets for each of the target genes at 300 nM concentration each and 2.5 µl of cDNA in 30 µl reaction volume (Table 5.1). 3 ' 6-Carboxy fluorescein (FAM), 6-Hexachloro fluorescein (HEX), Texas Red and CY5 (Eurogentec Ltd, Fawley, Hampshire, UK) were used as fluorochrome reporters for the hydrolysis probes analysed in multiplexed reactions between the 5 genes (p21, PCNA, SESN1 and FDXR in combination with the housekeeping gene HPRT1) per run. Cycling parameters were 2 min at 95 ° C, then 45 cycles of 10 secs at 95 ° C and 60 secs at 60 ° C. Data was collected and analysed by Rotor-Gene Q Series Software. Gene target Ct (cycle threshold) values were normalized to a Hypoxanthine-Guanine phosphoribosyl transferase 1 (HPRT1) internal control. Ct values were converted to transcript quantity using standard curves obtained by serial dilution of PCR-amplified DNA fragments of each gene. The linear dynamic range of the standard curves covering six orders of magnitude (serial dilution from  $3.2 \times 10^{-4}$  to  $8.2 \times 10^{-10}$ ) gave PCR efficiencies between 91% and 103% for each gene with an efficiency score of  $R^2 > 0.998$  (PCR efficiency graphs can be found in appendix 10.4). Fold change in gene expression

levels are presented. Raw data was entered into a pre-programmed Microsoft Excel worksheet which calculated average gene expression per triplicate wells and normalized each gene expression to the housekeeping gene and 0Gy non-irradiated control. Statistical analysis and graphical outputs were carried out using ANOVA on Graphpad Prism 5.

Table 5.1 Primer and probe sequences used in this work for genes analysed with MQRT-PCR. The primers were designed within Public Health England specifically for use with MQRT-PCR for bio dosimetry and as per Kabacik *et al* <sup>331</sup>.

Gene	PCR Primers, Fwd., Rev	Probes
<b>HPRT1</b>	TCAGGCAGTATAATCCAAAGATGG AGTCTGGCTTATATCCAACACTTCGT	CGCAAGCTTGCTGGTGAAAAGGACCC
<b>P21</b>	GCAGACCAGCATGACAG TAGGGCTTCCTCTTGGA	TTTCTACCACTCCAAACGCCGGCT
<b>FDXR</b>	GTACAACGGGCTTCCTGAGA CTCAGGTGGGGTCAGTAGGA	CGGGCCACGTCCAGAGCCA
<b>PCNA</b>	CTCAAGGACCTCATCAACGA GGACATACTGGTGAGGTTCA	CCGCTGCGACCGCAACCTGG
<b>SESN1</b>	GCTGTCTTGTGCATTAATTGTG CTGCGCAGCAGTCTACAG	ACATGTCCCACAACCTTGGTGCTGG

## **5.3 Results**

### **5.3.1 Healthy Controls**

Higher expression levels of all genes analysed was observed after 0.5Gy compared to 0.05Gy. Considerable inter individual variation between the healthy controls was observed at both doses, but most notably at 0.5Gy (Figure 5.2). Significant fold increases were observed in only a small number of donors (if fold change was  $> 2$ ). A gene expression fold change of 2 was considered significant when using a small donor cohort (as with the present work) and with considerable PCR triplicate variation of gene expression.

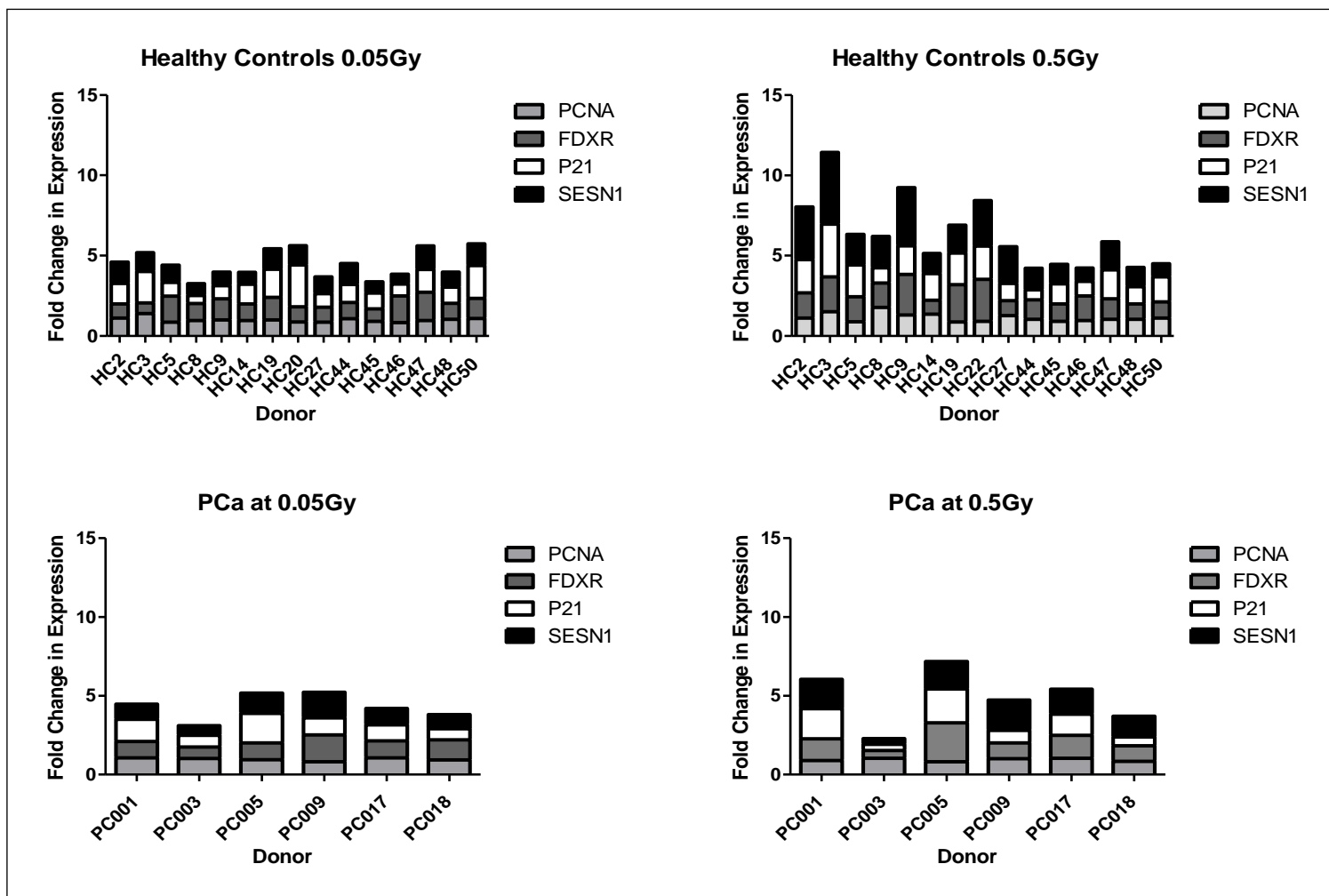


Figure 5.2. Combined relative gene expression in healthy controls (HC) compared to Prostate Cancer (PCa) patients. The top panel represents HC's and the bottom PCa patients at each dose at 1hr post irradiation. Gene expressions were normalized to a housekeeping gene and to a non-irradiated control. Note that all genes except SESN1 for the HC's were not above 2-fold change in gene expression.

All genes were analysed to observe if they differed significantly according to dose. Overall, a significantly higher expression was observed after 0.5Gy compared to 0.05Gy for SESN1 only (P=0.0028). The remaining three genes were not significantly changed in response to irradiation; PCNA (P=0.0564), FDXR (P= 0.1057) or P21 (P= 0.1354).

Gene expression of PCNA, FDXR, P21 and SESN1 were analysed relative to a housekeeping internal control and to a non-irradiated control (0Gy) for each of the healthy control (HC) donors. Inter variation was calculated for each gene and dose, by dividing the standard deviation of gene expression for all donors at each dose by the mean and multiplying by 100 to get a percentage variation value. This ranged between 14%-40% at 0.05Gy and 22%-54% at 0.5Gy (Table 5.2).

Table 5.2 Inter individual variation in Healthy controls. 0Gy is not displayed as the 0Gy control is used to normalize gene expression data for overall fold changes in gene expression at each dose. The inter individual variation was calculated for each gene at each dose for a cohort of healthy controls. The variation was calculated by dividing the standard deviation by the mean and multiplying by 100 to get a percentage variation level.

<b>Healthy Control Inter Individual Variation (%)</b>				
	PCNA	FDXR	P21	SESN1
<b>0.05Gy</b>	14.14	29.86	39.90	26.26
<b>0.5Gy</b>	22.68	38.36	41.32	53.28

### 5.3.2 Prostate Cancer

Expression of four genes (PCNA, FDXR, P21 and SESN1) were analysed relative to a non-irradiated control (Figure 5.3). Few significant fold change in gene expression (of >2 fold) were observed, so gene expressions were analysed according to dose. No significant change in gene expression between 0.05Gy and 0.5Gy was observed for PCNA (P= 0.4848), FDXR (P= 1), P21 (P= 1) or SESN1 (P= 0.1320). Significantly higher inter individual variation was observed at 0.5Gy compared to 0.05Gy (Table 5.3) over the range of all genes, indicating a more varied gene response at the most radiosensitive dose and as expected.

Table 5.3 Inter individual variation of gene expression in 6 Prostate cancer patients. Each value represents a percentage variation. Variation was calculated for each gene at each dose by dividing the standard deviation by the mean and multiplying by 100 to get a percentage variation value. Gene expressions were normalized to a control housekeeping gene (HPRT1) and normalized to the non-irradiated control.

<b>Prostate Cancer Inter Individual Variation (%)</b>				
	PCNA	FDXR	P21	SESN1
<b>0.05Gy</b>	9.9487	28.01354	38.77959	32.55822
<b>0.5Gy</b>	10.93878	51.91584	61.19946	39.72864

### 5.3.3 Cells from Ataxia Telangiectasia Donors

The AT2Bi and AT3Bi cell lines were used for comparison to HC's and PCa as they are known to show extreme radiosensitivity in biological assays (Chapter 4). However, no significant fold change in gene expression was observed for any of the genes (Figure 5.3) (fold change >2). A higher dose point and additional time-point for AT cells was then used for a further investigation as more LCL cells were available for analysis compared

to the limited availability of whole blood (only 0.05Gy and 0.5Gy were used compared to a 0Gy control). No significant change in gene expression was observed between doses at 0.05Gy, 0.5Gy and 2Gy at 1 hr ( $P= 0.8473$ ) but gene expression had significantly increased at each dose for the 24 hr time-point ( $P= 0.0158$ ). This was interesting as it demonstrated that time was a critical factor for the underlying genetic response to radiation.

#### 5.3.4 Combined Cohort Analysis

Only SESN1 was sensitive enough using HC's to be "significantly" up-regulated ( $> 2$ -fold change compared to control) (Figure 5.3). However, to analyse if a dose effect was observed using the combination of genes investigated, a significant change in expression was evident between 0.05Gy and 0.5Gy for HC's ( $P < 0.0001$ ), but not for PCa donors ( $P= 0.2821$ ) or AT cell lines ( $P= 0.8473$ ). Investigation of all genes between donors was carried out to conclude if radiosensitivity in the cohort type could be determined by the panel of MQRT-PCR genes analysed. When all cohort types were investigated together using a two-way ANOVA in Graphpad Prism, a significant change in radiosensitivity between HC, PCa and AT was observed at 0.5Gy ( $P= 0.0297$ ) but not after 0.05Gy ( $P= 0.7114$ ). This again was expected since 0.5Gy is known to be the most radiosensitive dose.

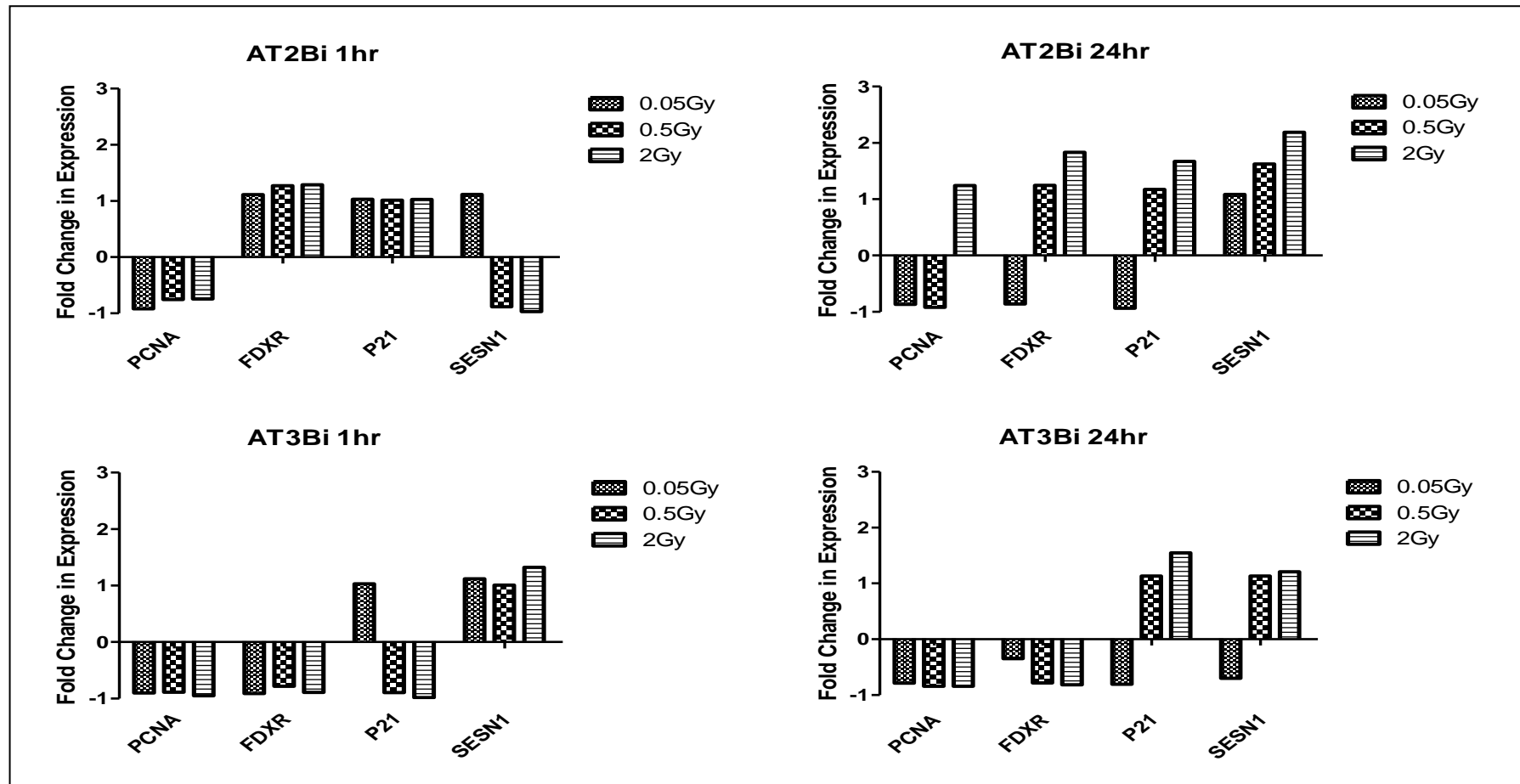


Figure 5.3 Gene expression in two AT cell lines. The top panel represents one AT cell line at 1hr and 24hrs after radiation exposure, and the bottom panel represents expression in the other AT cell line at 1hr and 24 hrs after exposure. (Details of AT cell lines in section 4.2)



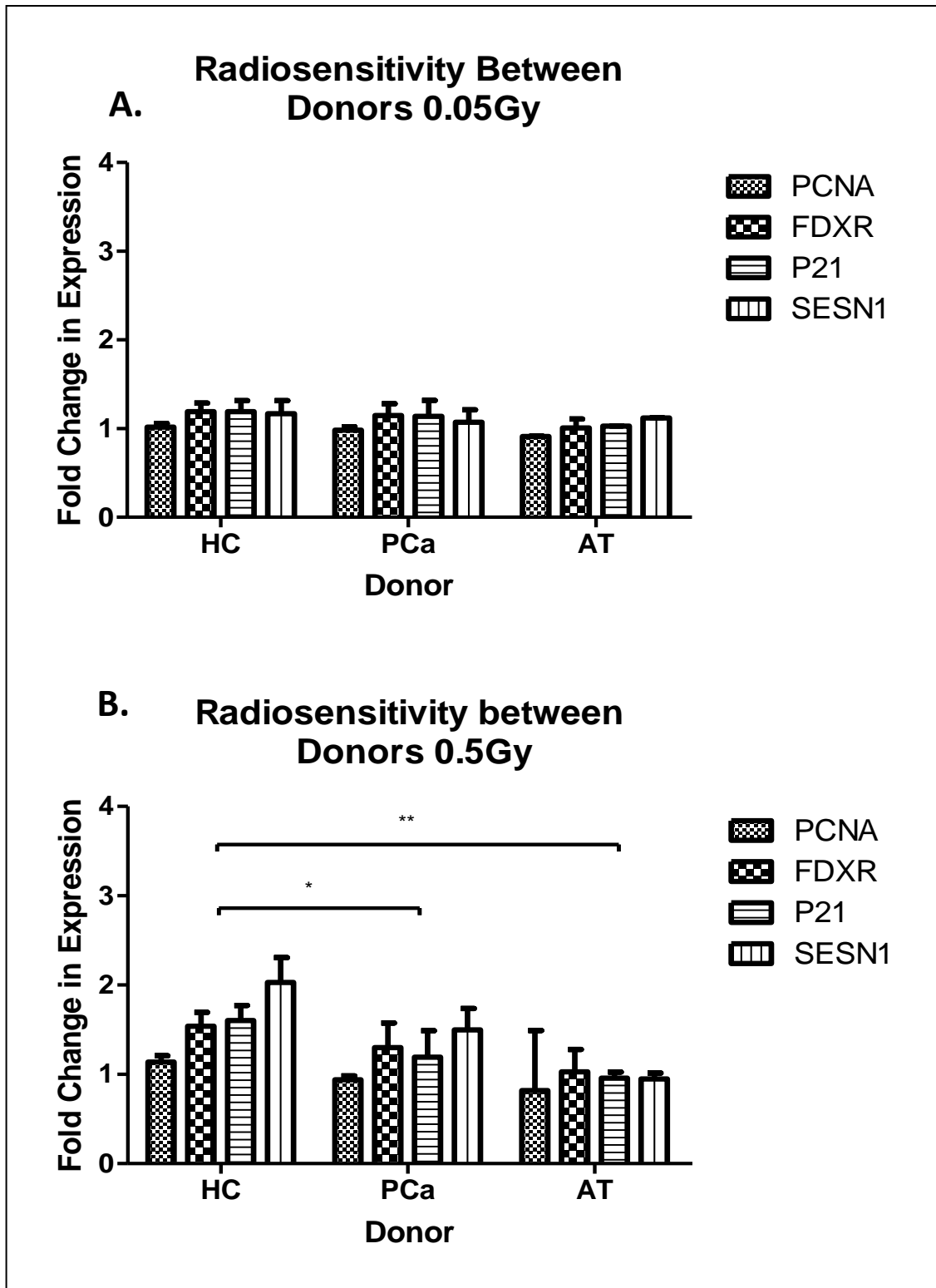


Figure 5.4. Differential gene expression between Healthy controls (HC), prostate cancer (PCa) and Ataxia Telangiectasia (AT) cell lines at 0.05Gy and 0.5Gy at 1hr post radiation exposure.

As an additional time point of 24 hrs was used for AT cells, this was compared between donor cohorts (Figure 5.4). A more pronounced gene expression was observed across all genes analysed for AT at 24 hrs however these were not significantly different from gene expression in HC or PCa patients as was observed in figure 5.3.

#### 5.3.5 Use of MQRT-PCR panel through PCa treatment visits

Further investigation of the 6 PCa donors through hospital visits (and as described in chapter 3) was carried out to observe if any change in gene expression correlated with PCa donors before hormone and after hormone treatment. Relating back to chapter 3, V1 represents first sampling of PCa donor blood, and V2 is after hormone therapy, pre radiotherapy. Similar levels of gene expression were observed at both doses, but again no significant fold change in gene expression ( $> 2$  fold) was observed in any particular gene/dose or visit (Figure 5.6). No significant change of expression in any gene analysed was observed between doses for either visit (Figure 5.6) ( $P>0.3$ ). However, the sample number was small for this analysis.

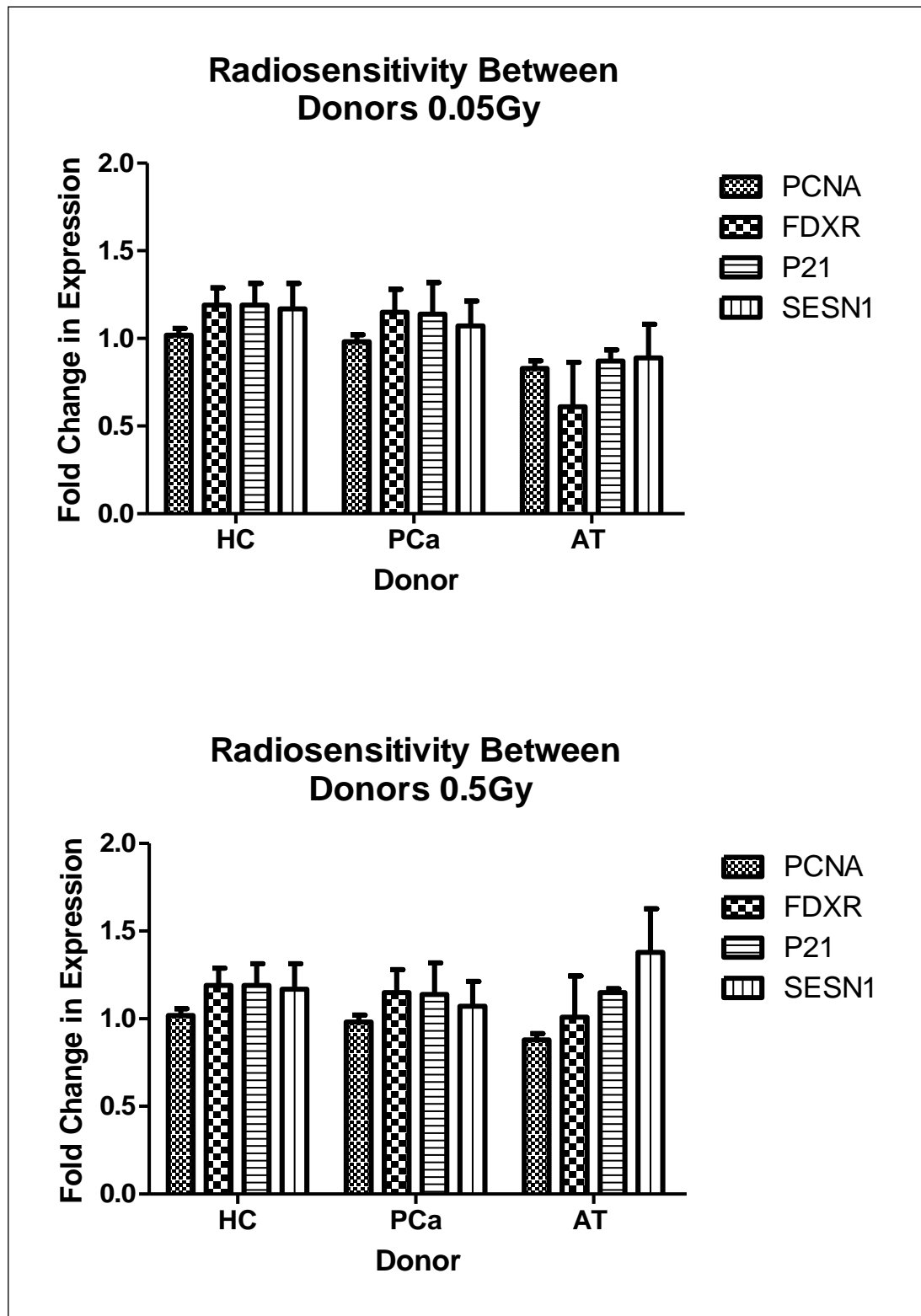


Figure 5.5. Gene expression in healthy controls (HC), prostate cancer (PCa) patients and cells from Ataxia Telangiectasia (AT) donors for 0.05Gy and 0.5Gy. AT cells at 24hrs post irradiation. Gene expression was normalized to a housekeeping gene (HPRT1) and a 0Gy non-irradiated control.

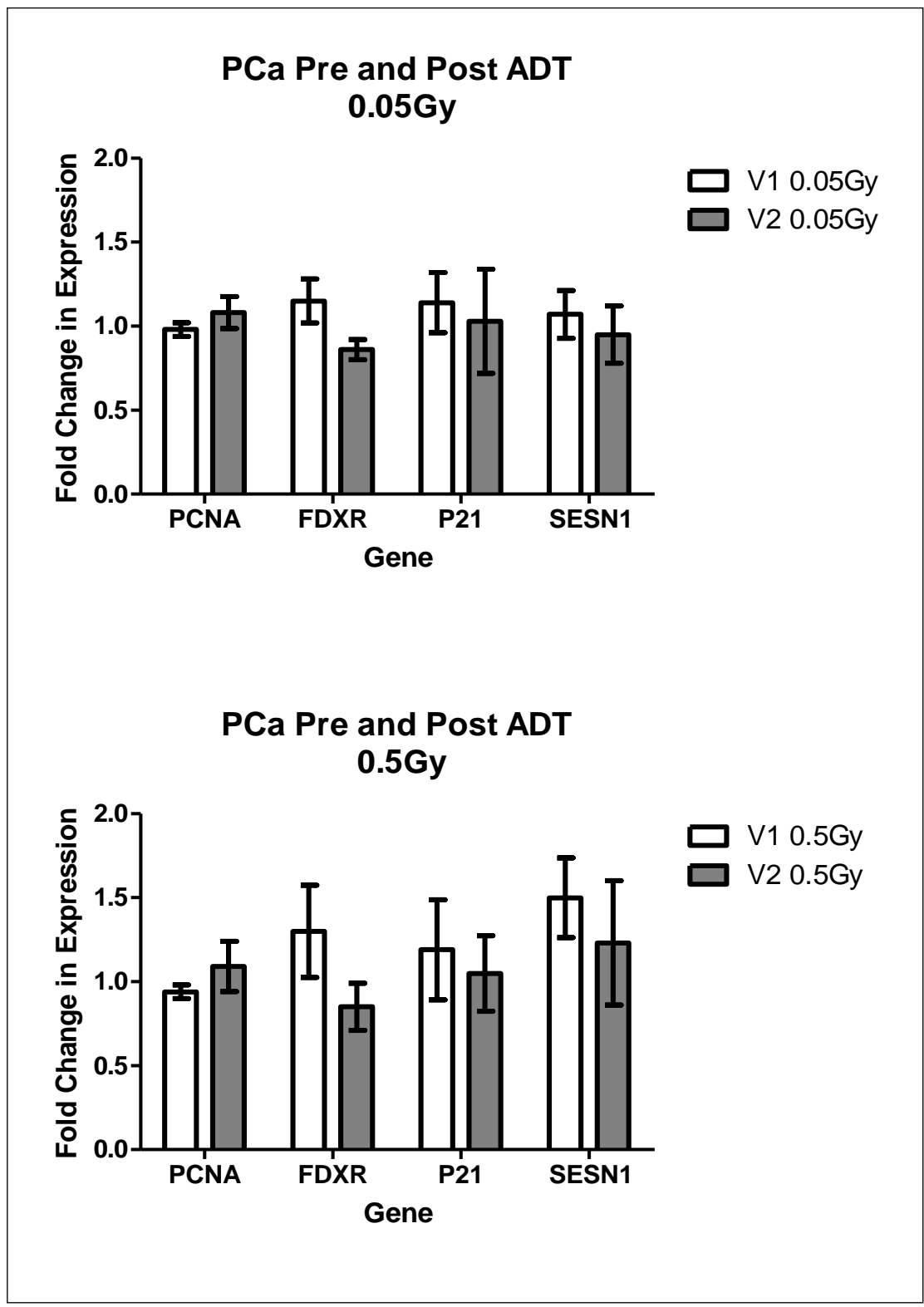


Figure 5.6. Gene expression in Prostate Cancer (PCa) patients pre and post hormonal androgen deprivation therapy (ADT) treatment. Gene expression levels after 0.05Gy and 0.5Gy are represented. N = 6 patients

## 5.4 Discussion

The aim of the current chapter was to investigate the underlying genetic response of radiosensitivity and discover any potential genetic biomarkers of radiosensitivity that could be incorporated into future predictive testing using HC's, PCa patient samples and cells from AT patients.

In all cohorts; healthy controls, prostate cancer and Ataxia Telangiectasia a higher variation of gene expression was observed at 0.5Gy at 1 hour for all genes p21, PCNA, SESN1 and FDXR. This was as expected, as 0.5Gy is the most radiosensitive dose (as this dose is sufficient to induce DNA repair<sup>244</sup>). Cells were analysed at 1 hr because G2 chromosomal radiosensitivity studies were performed at this time-point in parallel. LCLs could be tested at many doses and time-points because they are immortalized cell lines and plentiful, therefore 2 Gy and 24 hr were also incorporated as an additional dose and time-point to the study. However, 2Gy did not show significant results (only 0.5Gy as it is considered most radiosensitive like the variation above) but the later time point of 24 hrs showed a higher gene expression (although not significant) indicating that the genetic radiosensitivity response may be later than 1 hour for particular genes and donor types.

Kabacik *et al* and Manning *et al* found the current genes used in this work (p21, FDXR, PCNA and SESN1) to be highly radioresponsive to doses of >1Gy as they are key regulators in the response to irradiation<sup>164, 316</sup>. P21 is a key Cyclin Dependent Kinase Inhibitor which is under tight regulation of p53 to control progression of damaged cells within the cell cycle through CDK1/CDK2 and CDK4/6 activity. Previous evidence suggests a threshold which would need to be reached before this inhibition could occur, for example Marples *et al* described how the early G2 checkpoint is activated in response to irradiation immediately, dependent on ATM and requires an activation threshold (doses

>1Gy)<sup>244</sup>. It is possible that, from this data complete activation of p21 was not observed as a high enough dose was not used.

PCNA's interaction with p21 was of interest as the high binding affinity of p21 for PCNA in response to irradiation has been shown to inhibit DNA synthesis. The two genes interact to inhibit cell cycle progression at G1 and G2 phase in response to DNA damage therefore would be of interest for radiosensitivity analysis. No correlation was observed between both genes in the current work, but again more doses and time-points would determine the use of either or both genes as a radiosensitivity predictor. PCNA shows potential for prediction of radio-response as it has been shown to be involved in an array of processes including (but not limited to) DNA replication, repair, chromosome segregation and cell cycle progression, but after much higher doses than were used in this study (>2Gy)<sup>342</sup>.

An interesting theme involving metabolomics biomarkers has come through strongly from the data presented. Both SESN1 and FDXR were strongly expressed, and both are involved in the cellular maintenance of ROS production and/or peroxiredoxins. SESN1 shows the most potential for radiosensitivity prediction as it is the most highly expressed in all cohorts within this work. This is not unusual as it is activated by p53 in response to ionizing radiation and evidence suggests that inhibition of protein synthesis in breast cancer cells results from inhibiting SESN1 activity<sup>343</sup>. As the cell cycle is controlled by p53 and P21, PCNA and SESN1 are in turn regulated by p53, the genes are important for analysing the cellular response to irradiation. In addition, SESN1 has been found to regulate ROS through studies which inhibit SESN1 expression. Kopnin *et al* found that repression of SESN1 levels substantially increased levels of ROS in response to cellular stress<sup>340</sup>.

It was identified in microarray data of previous reports by Kabacik *et al* who explain that FDXR is of major interest for bio dosimetry as they found a near 15 fold increase of expression at 2 and 24 hrs after irradiation<sup>331</sup>. This could be why much of a response was not observed as the samples used were processed at 1 hr after irradiation and this time point could have been too early to identify an appropriate response. Found solely within the mitochondria and interacting with TP53, it could be a good predictor of radio-response as it could be a marker of apoptosis. It is not evident from this data how beneficial it could be as a predictor of radiosensitivity, and further work is needed to investigate this. However, Hwang *et al* found that total destruction of FDXR showed that this gene is essential for cellular viability and oxidative stress regulation. Partial destruction showed that FDXR favoured cell death through p53 regulation of apoptosis<sup>341</sup>.

For combined gene expression a slightly higher (but not significant) increase in general gene expression was observed for all genes in both HC and PCa donors at 0.5Gy compared to 0.05Gy. This is not unusual as the radio-responsive genes analysed were originally found to be activated at doses of >1Gy<sup>331</sup>, therefore the dose points used may not have been high enough to activate the selected genes completely. This is not surprising as a large number of radio-responsive genes require a “threshold” dose in order to change. The present study confirms work by El-Saghire *et al* in 2013 who identified activation of chemokine signalling and activation (GNG11 and CCR4) at lower doses (<0.05Gy) and DNA damage and checkpoint related gene activation (p53 related) at doses of >1Gy using peripheral blood lymphocytes from healthy donors<sup>344</sup>. The expression of SESN1 is of interest as it showed the highest change in expression and highest variation between donors of each cohort. It is of note that donors with the most change in gene expression from 0.05Gy to 0.5Gy (HC3 and HC9) show much higher levels of SESN1 also. However, no correlation of gene expression with G2 radiosensitivity of these donors was found.

P21 in the PCa cohort showed the highest variation. As most PCa tumours are p53 deficient and p21 regulates p53 in the response to ionizing radiation, this result is also not unusual. The highest variation for HC's was observed for SESN1, which was also the gene expressed with the highest fold increase compared to non-irradiated controls. As SESN1 plays a key role in the cellular response to oxidative stress, this result is not unusual for healthy cells.

Variation in gene expression is difficult to assess as it is altered between cell types, stage of the cell cycle and within different cohorts. For instance Whitney *et al* investigated over 300 gene expression profiles in 75 healthy donors and found blood cellular subtype specific alterations in gene expression as well as gender, age and time of day which played a huge role in genetic variation<sup>345</sup>. Finnon *et al* failed to correlate lymphocyte radiosensitivity with normal tissue response to radiotherapy using gene expression arrays despite finding changes in over 800 genes. Although it did not predict radiosensitivity, the technique showed potential for biodosimetry<sup>346</sup>.

No significant regulation of gene expression was observed in AT cells. Given that ATM drives the expression or regulation of the genes analysed, this data is not unusual. There was a clear change between the two AT cell lines which represents the heterogeneity of LCL's as they came from individual donors. From chapter 4 it is now known that both of these LCL's show inter individual variation which could explain the differences in gene expression patterns shown here, but analysis such as denaturing High Performance Liquid Chromatography (dHPLC) would be needed to genetically determine these. AT2Bi shows more differences in time-points than AT3Bi, as there is a complete gene expression reversal in FDXR and P21 at 0.05Gy, SESN1 at 0.5Gy and PCNA and SESN1 at 2Gy. It is interesting that a complete change in FDXR was observed between the two AT cell lines, with upregulation in AT2Bi and downregulation in AT3Bi (not significant), and



SESN1 was the only gene which was significantly upregulated in AT2Bi at 24 hrs as FDXR and SESN1 are the only two genes studied that are known to be not directly regulated by ATM. Zhou *et al* investigated changes in gene expression in 3 AT cell lines in response to 1.5Gy of irradiation and found that most genes were attenuated or delayed – therefore suggesting that longer time points and higher doses would need to be investigated to find a significant change in gene expression<sup>347</sup>.

Interestingly, no change in gene expression for any of the genes was observed pre and post hormone therapy by dose. This would suggest that radiation dose does not make a huge difference to the expression of the genes analysed in combination with hormone treatment. This would be beneficial for predicting radiosensitivity of PCa patients, as their radiosensitivity could be monitored throughout their radiotherapy treatment regime knowing that hormone treatment would not cause variation of the result. However, further work is required to conclude this hypothesis.

Using the panel of genes for donors of different radiosensitivity levels, combined analysis showed that HC could be significantly distinguished from PCa and AT cell types at 0.5Gy only. This has not been shown before with the given genes. The data shows potential for predicting radiosensitivity using a MQRT-PCR technique, and future work would include higher dose points (1Gy) as well as longer time points to determine the most sensitive dose/ gene expression for clinical radiosensitivity prediction. From the current work it is clear that SESN1 was highly responsive in all cohorts and doses and highly expressed in AT cells at 24 hrs post irradiation, therefore this family of genes would be of further interest to investigate.

## **5.5 Chapter Conclusions**

The present data show that expression of the panel of genes p21, PCNA, SESN1 and FDXR in combination or alone show potential as biomarkers for predicting

radiosensitivity in patient cohorts. The analyses of these 4 genes also led to further understanding of the underlying genetic mechanisms of cellular radiosensitivity.

## **6. A PANEL OF EXOSOMAL MIRNA'S CAN DISTINGUISH EXTREME RADIOSENSITIVITY FROM NORMAL CONTROLS**

### **6.1 Introduction**

Exosomes are small (30 – 120nm) membrane derived endocytic vesicles involved in cellular trafficking and communication and they contain active components such as proteins, DNA, mRNA and miRNA<sup>348</sup>. Exosomes were first described by Trams *et al*<sup>349</sup> as enzymatic vesicles. This work was developed further by Harding and Stahl who explained that exosomes could take up particles such as colloidal gold and release them in rat reticulocytes<sup>350</sup>. Evidence suggests that exosomes may carry functional molecules from the endosomal sorting complex required for transport (ESCRT machinery) for their own biogenesis<sup>351</sup>. These include ESCRT components I-III and accessory proteins apoptosis-linked gene 2 interacting protein X (ALIX) and tumour susceptibility gene 101 (TSG101) which are now used as markers for exosomal identification. It is now known almost all cells in the human body (including bacterial) are capable of excreting exosomes, such as red and white blood cells<sup>352</sup>, platelets<sup>353</sup> and endothelial cells<sup>354</sup>. These have major research implications in pathogenic diseases as a blood sample can be taken with ease and numerous subcellular components can be analysed. Over the past decade, the role of exosomes has become more diverse. This was demonstrated by Montecalvo *et al* who found that exosomes contained and delivered functional microRNA (miRNA's) between dendritic cells<sup>355</sup>. Therefore, exosomes play a role in delivering miRNA's that can influence the expression of genes through interference with gene translation. As of June 2014, 28,645 entries have been made to the micro RNA database (miRBase) representing individual miRNA discoveries<sup>356</sup>. Each miRNA has more than one target, greatly increasing the influence of miRNA on gene expression.

MiRNA's are small non coding RNA's that can interfere with translation through degradation or inhibition of target mRNA's<sup>357</sup>. For biogenesis of miRNA see figure 1.12 in section 1.5 of this thesis. The role of miRNA's influencing various cancer types has been under intense investigation; a 5 miRNA panel has shown early success in non-small cell lung carcinoma as a biomarker for cancer identification across races<sup>358</sup>. Cohort studies on blood from breast cancer patients revealed the importance of two expressed miRNA's (miR-195-5p and miR-495) as a potential molecular signature for early case breast cancer<sup>359</sup>. Differential expression of miRNA's in colorectal cancer compared to healthy controls with an overall downregulation of miRNA in colorectal cancer further implies an anti-tumour role of miRNA's<sup>360</sup>. Inhibition of proliferation of bladder cancer cells was found through the regulation of p21 by miR-370, miR-1180 and miR-1236<sup>334</sup> and the implications of miR541 for inhibiting cancer metastasis or invasion in prostate cancer has also been documented<sup>361,362</sup> and reviewed by Cheng *et al* <sup>363</sup>. As well as oncogenesis, miRNA's transported via exosomes have also been implicated in the propagation of non-targeted bystander effects and their roles in influencing radiation sensitivity. For example, Jella *et al* found an increasing quantity of exosomes in keratinocytes exposed to 0.005Gy up to 5Gy in a dose dependent manner, and when transferred to fresh media from non-irradiated samples, a radiation-induced bystander response was evident through reactive oxygen species and calcium imaging<sup>364</sup>. Al-Mayah reported that the manipulation of miR-26a could cause radiosensitivity or radioresistance through overexpression or knockout of the gene respectively, using human glioblastoma cell lines<sup>365</sup>.

A number of additional reports have investigated how miRNA's influence cellular radiosensitivity. Ye *et al* showed that miR-145 was consistently downregulated in cervical cancer tissue samples and was correlated with advanced cancer stage, poor differentiation and large tumour size. Further analysis showed that its target mRNA

HTLF was inversely correlated with miR-145 and was involved in chromatin remodelling which enhanced radiosensitivity overall<sup>366</sup>. Upregulation of miR-25 was found to act on the downregulation of BTG2 in radioresistant NSCLC patients, therefore modulation of this radiosensitive miRNA could have implications for radiotherapy patients<sup>367</sup>. Furthermore, Lee *et al* found that increased expression of miR-7 attenuated EGFR and akt expression which radiosensitized larynx, breast, lung and glioma cancer cell lines<sup>368</sup>. Recently, miR-26a enhanced radiosensitivity in U87 cells by reducing the repair capacity of DNA damage after 4Gy of Caesium137 irradiation<sup>369</sup>, and miR-223 has already been shown to act on ataxia telangiectasia mutated (ATM) through downregulation of the ATM gene causing radiosensitivity in U87 cells both *in vitro* and *in vivo*<sup>370</sup>.

As miRNA's excreted from exosomes have previously shown roles in affecting radiosensitivity, the purpose of this study was to isolate exosomes from cell culture media of the lymphoblastoid cell lines from chapter 4. Two normal (2145 and 2139) and two ataxia telangiectasia (AT) cell lines were used for this work. The isolated exosomes were then characterised using TEM and by a protein marker known as TSG101. Analysis was then done on differentially expressed miRNA's to investigate if miRNA's could be used as a biomarker to predict individual radiosensitivity and be applied to patient cohorts with future therapeutic implications

## **6.2 Methods**

### **6.2.1 Cell Culture**

Lymphoblastoid cell lines (LCL's) described in the previous chapter 4 and 5 were used and were maintained in standard RPMI medium (Sigma) supplemented with 10% Foetal bovine serum (FBS), L-Glutamine and incubated at 37°C with 5% CO<sup>2</sup>. The cells in suspension were sub cultured by 1:5 dilutions every 24-48hrs. 1x10<sup>5</sup> cells/ml were added to T25 flasks (5ml total) using cell culture media that was exosome depleted FBS (10%)

in RPMI medium. Cells were cultured for 72 hrs before media harvesting for isolation of exosomes.

### 6.2.2 Isolation of Exosomes

Cells were pelleted by centrifugation at 300g for 5 mins and conditioned medium was removed. The conditioned medium was then centrifuged at 2000g for 10 mins at 4°C to remove debris, and then filtered through a 0.22µm pore filter. This was then ultracentrifuged at 110,000g for 75mins at 4°C to isolate the exosomes. Exosome pellets were then washed in PBS and ultracentrifuged at 110,000g for 75mins at 4°C to purify the exosome fractions. Half of the sample was stored in PBS and transported to the Centre for Microscopy and Analysis (CMA), Trinity College Dublin for characterisation by transmission electron microscopy (TEM) and half was resuspended in RIPA buffer (Sigma) for protein lysis and subsequent Western blot analysis.

### 6.2.3 Characterisation by Transmission Electron Microscopy (TEM)

TEM of exosome fractions was conducted by technical support staff at the CMA in Trinity College Dublin. The protocol as previously published<sup>371</sup> was applied.

### 6.2.4 Protein extraction and analysis of Cell and Exosome Extracts

1ml of RIPA buffer (Sigma) was added to each sample containing exosomes (approx. 100µl), vortexed and stored on ice for 5 mins. Samples were then centrifuged at 8000g for 10 mins at 4°C to pellet cell debris, while the supernatant (protein) was transferred to an Eppendorf and frozen at -80°C until quantification. The Biorad DC protein estimation kit was used for protein quantification against protein standards which were previously made up from 2mg/ml up to 12mg/ml in 2mg/ml increments and frozen. Protein standards and protein samples for SDS-Polyacrylamide Gel Electrophoresis (the Westerns are just a mirror image of the separation on the gels) were pipetted into a 96 well plate in triplicate

wells. An appropriate volume of Solution A and S (from the Biorad DC assay, appendix 3) were mixed in a 5:1 ratio and 25µl of this mix was added to each well. 200µl of reagent B was added to each well and the plate was incubated for 5mins with a gentle shake before spectrophotometric reading at a wavelength of 595nm. An average was taken from each triplicate of each protein reading. The values for the standards were plotted and a line of best fit was calculated forming a standard curve. The unknown protein quantities were then calculated with reference to the standard curve. Protein loading quantities can be found in appendix 10.4, section for Chapter 6 Raw data on page 308.

#### 6.2.5 Sodium Dodecyl Sulphate-Polyacrylamide Gel Electrophoresis (SDS-PAGE) gel electrophoresis

After protein quantification, 30µg of protein for each sample was resolved on 10% SDS-PAGE gels in a Bio-Rad mini Protean system. These were made up by a separating gel and stacking gel and were composed as demonstrated in table 7.1. TEMED and APS were added to the gels at the last minute as they cause the gel to solidify. The separating gel was first poured into the gel rig and topped with isopropanol and left for 10-20minutes to allow solidification. After solidification, stacking gel was made up according to table 7.1 and poured over the separating gel (with TEMED and APS last). The comb for protein wells was added quickly to the gel rig and it was left for 20mins. During this time, 30µg of protein from each sample was prepared with approximately 10µl of loading buffer (Laemelli) (dependent on amount in µl for each protein to make up to 20µl total sample volume for loading). The samples were boiled at 100°C for 3mins to linearize proteins before loading.

Table 6.1 Components and concentrations used for SDS-PAGE. Water (H<sub>2</sub>O), TrisHydroxymethylaminomethane (Tris), Sodium Dodecyl Sulphate (SDS), Ammonium persulfate (APS), Tetramethylethylenediamine (TEMED).

Separating Gel		Stacking Gel	
PERCENTAGE SOLUTION	10%	PERCENTAGE SOLUTION	4%
Deionised H <sub>2</sub> O	4.1	Deionised H <sub>2</sub> O	3.6
30% Acrylamide	3.2	30% Acrylamide	0.65
1.5M Tris (pH8.8)	2.5	1M Tris (pH 6.8)	0.63
10% SDS	0.1	10% SDS	0.05
10% APS	0.1	10% APS	0.075
TEMED	0.01	TEMED	0.007

30µg of each protein sample (approximately 20ul volume) was loaded into relevant wells. 10µl of prestained BenchMark protein ladder (Invitrogen) was loaded into the first well/lane. The SDS-PAGE gel loaded with the protein samples was placed into a BioRad electrophoresis tank and filled up with 1X SDS-PAGE running buffer (Tris base, acetic acid and Ethylenediaminetetraacetic acid, appendix 3). Gels were electrophoresed at 80-100milliamps for 1.5hrs or until the protein dye was visible at the bottom of the gel.

#### 6.2.6 Western Blotting

After electrophoresis, the SDS-PAGE gel was carefully transferred to a nitrocellulose membrane -with blotting paper sandwiched either side of the gel and membrane for western blotting transfer. Each 'sandwich' was placed in a BioRad transfer cassette and transfer tank. The tank was topped up with pre-cooled 1X High molecular weight (HMW) transfer buffer made using 100mls of 10X HMW transfer buffer (Tris, Glycine, SDS and H<sub>2</sub>O, Appendix 3) with 200mls of methanol and topped up to 1liter with deionised H<sub>2</sub>O. and run at 100volts for 1hr. The membrane was recovered from the BioRad apparatus



when finished and transferred to a dish for subsequent antibody probing. (Information for all buffers can be found in appendix 10.2).

#### 6.2.7 Antibody Probing

Membranes were blocked in 5% low fat powdered milk in Tris buffered saline and tween (TBS-T) (appendix 3) for 1hr to limit unspecific binding of antibody. The membranes were incubated overnight with primary antibody TSG101 (Abcam) for detection of the presence of exosomes and it was prepared in 1:1000 in 3% low fat powdered milk in TBST. Membranes were then washed 3 x 10mins in TBS-T. They were then incubated with secondary horseradish peroxidase (HRP) tagged antibody prepared in 1:5000 in 3% low fat powdered milk for 1hr. This was done to detect the antigen-antibody reaction on the membrane. After an additional 3 x 10min TBS-T washes the membranes were processed using chemiluminescent detection.

#### 6.2.8 Chemiluminescent Detection and Imaging

Membranes were incubated with enhanced chemiluminescent (ECL) detection kit (Pierce). This was done according to the kit specifications, with equal volumes of reagent 1 (Peroxide solution) mixed with reagent 2 (Luminol enhancer). After 1 minute of incubation, Western blots were imaged on a Syngene g-Box Chemi XR5 system.

#### 6.2.9 Real Time PCR Panel Analysis (Exiqon)

RNA was extracted, quantified and qualified as described in the protocol from section.5.2.2. RNA samples were then sent to Exiqon services in Denmark who collaborate with Companies, Research Institutes and Pharmaceutical Industries to deliver top quality, novel molecular diagnostics for early detection of disease. They analysed samples for detection of a) 5 known miRNA's ((miR-142, miR-451, miR-23a, miR-30c and miR-103a) and then to subsequently determine whether to proceed with b) profiling

a full miRNA panel of 752 miRNAs'. The following procedures were carried out by Exiqon in Denmark.

#### 6.2.9.1 Detection of 5 known miRNA's in Cells and Exosomes

For a) 10µl RNA was reverse transcribed in 50µl reactions using the miRCURY LNA™ Universal RT microRNA PCR, Polyadenylation and cDNA synthesis kit (Exiqon). Each RT was performed including an artificial RNA spike-in (UniSp6). cDNA was diluted 100x and assayed in 10µl PCR reactions according to the protocol for miRCURY LNA™ Universal RT microRNA PCR; each microRNA was assayed once by qPCR using assays for miR-23a, miR-30c, miR-103, miR-142-3p, and miR-451. In addition to these miRNA assays, the RNA spike-ins were assayed. Negative controls excluding a template from the reverse transcription reaction was performed and profiled like the samples. Amplification was performed in a LightCycler® 480 Real-Time PCR System (Roche) in 384 well plates. The amplification curves were analysed using the Roche LC software, both for determination of Cp (by the 2nd derivative method) and for melting curve analysis. The raw data was extracted from the Lightcycler 480 software. An average Cp was calculated for the duplicate RT's, and evaluation of expression levels was performed based on raw Cp-values.

#### 6.2.9.2 Full miRNA Panel analysis of Cell Extracts

50ng RNA was reverse transcribed in 50µl reactions using the miRCURY LNA™ universal RT microRNA PCR, Polyadenylation and cDNA synthesis kit (Exiqon). cDNA was diluted 100 x and assayed in 10ul PCR reactions according to the protocol for miRCURY LNA™ Universal RT microRNA PCR; each microRNA was assayed once by qPCR on the microRNA Ready-to-Use PCR, Human panel I+II using ExiLENT SYBR® Green master mix. Negative controls excluding template from the reverse transcription reaction was performed and profiled like the samples. The amplification was

performed in a LightCycler® 480 Real Time PCR System (Roche) in 384 well plates. The amplification curves were analyzed using the Roche LC software, both for determination of Cq (by the 2nd derivative method) and for melting curve analysis.

#### 6.2.10 Data Analysis

The amplification efficiency was calculated using algorithms similar to the LinReg software. All assays were inspected for distinct melting curves and the T<sub>m</sub> was checked to be within known specifications for the assay. Furthermore, assays must be detected with 5C<sub>q</sub>s less than the negative control, and with C<sub>q</sub><37 to be included in the data analysis. Data that did not pass these criteria were omitted from any further analysis. C<sub>q</sub> was calculated as the 2nd derivative. Using NormFinder the best normalizer was found to be the average of assays detected in all samples. All data was normalized to the average of assays detected in all samples (average – assay C<sub>q</sub>).

Data is presented in two forms using a hierarchical clustering heat map and a principle component analysis plot. Hierarchical clustering is a form of data analysis which clusters data by individual means firstly, and gradually reduces the number of clusters based on similarities within the data. For example, each miRNA here begins in its own cluster based on its expression, then miRNA's with similar expression become one cluster, and gradually until the heat map is generated to classify each of the cell lines based on miRNA expression profiles. Principal Component Analysis (PCA) is a method used to reduce the dimension of large data sets and thereby a useful way to explore the naturally arising sample classes based on the expression profile. The method is simply a way to identify any particular pattern that arises in the data by highlighting similarities or differences. It orders data on the basis of variance so here the cell lines can be classified on the plot based on variance of the miRNA data for each cell line.

Additionally, T-Tests were used to determine if miRNA profiling differed significantly between each cell line and between normal (2145 and 2139) and radiosensitivity AT cell lines (AT2Bi and AT3Bi).

## 6.3 Results

### 6.3.1 Characterisation

Characterisation of exosomes was performed through transmission electron microscopy and protein Western blot analysis. The exosomal marker TSG101 was positively identified in exosomes isolated from all lymphoblastoid cell lines which consisted of 2 normal (2145 and 2139) and 2 AT (AT2Bi and AT3Bi) cells (figure 6.1). A small band was observed at 43kDa where TSG101 is present.

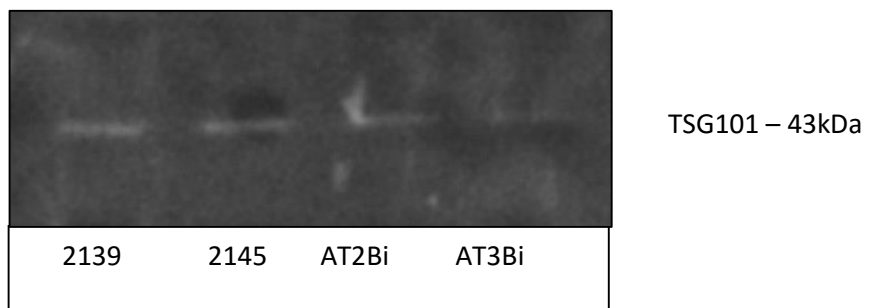


Figure 6.1 Western Blot identification of exosomal marker TSG101 present at 43kDA (N=7). In the normal cell lines (2145 and 2139) and AT cell lines (AT2Bi and AT3Bi).

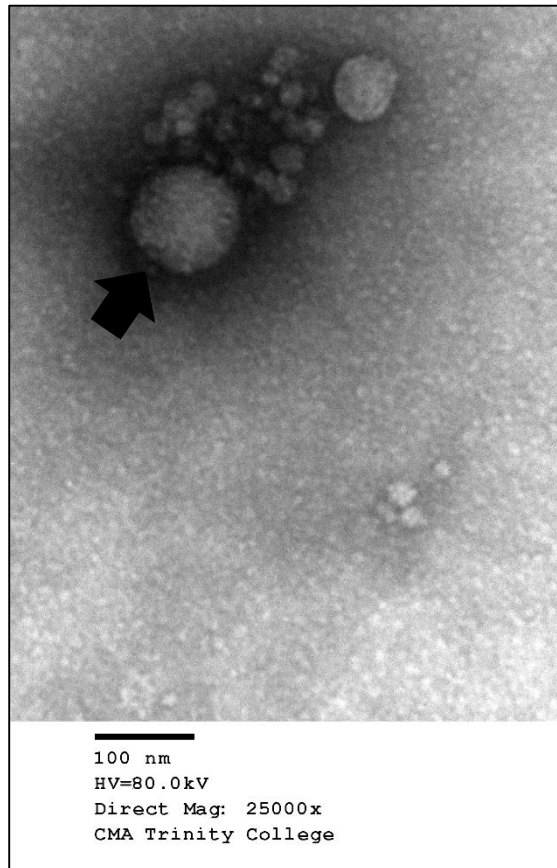


Figure 6.2 Identification of exosomes in samples by transmission electron microscopy. This image was taken from AT2Bi from the marked example (arrowhead) the crystal type outer structure of the exosome can be observed which appears grainy here.

Exosomes were positively identified using TEM in all extracts from media filtered from all cell lines including the two normal (2145 and 2139) and two AT cell lines (AT2Bi and AT3Bi) (Figure 6.2). The exosomes were sized from 30nm-100nm.

### 6.3.2 Detection of miRNA in Cell and Exosome samples

Before full miRNA panel profiling, cell extracts and exosome extracts from two seemingly normal cell lines and two AT cell lines were sent to Exiqon in Denmark to detect the presence of 5 common miRNA's which were miR-142, miR-451, miR-23a,

miR-30c and miR-103a (Figure 6.3). 4 of the 5 microRNAs (miR-142, miR-23a, miR-30c and miR-103a) were detected in the cell samples, but only 1 of the 5 microRNAs (miR-451) were detected in 1 of the 4 exosome samples (AT2Bi). Figure 6.3 shows the quantity of total miRNA from each cell and exosome sample for each cell line. Only miR-451 was detected in one exosome sample for AT2Bi (cell extract miRNA is represented to the left of the graph, which is highlighted in a red box). From the Exiqon preliminary report for detection of miRNA in cell and exosome extracted from each cell line, the expression levels of the detected microRNAs in the cell fraction were good quality and comparable with samples used within the company. The signal in the exosomes samples was extremely low for the detection of only one miRNA (miR-451) in AT2Bi, therefore company reports suggested the exosomes samples would not perform well in a profiling experiment. Therefore, full miRNA profiling was continued using cell fractions only, and not exosomes isolated from those fractions. miRCURY LNA™ Universal RT microRNA PCR Human panel I+II were used for each cell line 2145, 2139, AT2Bi and AT3Bi, which were commercially available due to their high sensitivity and specificity for profiling analysis. In general terms of miRNA content, of the 752 miRNA's for each cell line, 106 were detected in all cell samples and on average 216 miRNA's were detected for each sample (Figure 6.4). Figure 6.4 demonstrates a general quantity of miRNA's detected in each cell line, with the lowest number of miRNA's detected in the 2145 cell line. This cell line also performed poorly in previous work for cytogenetic analysis (chapter 4).

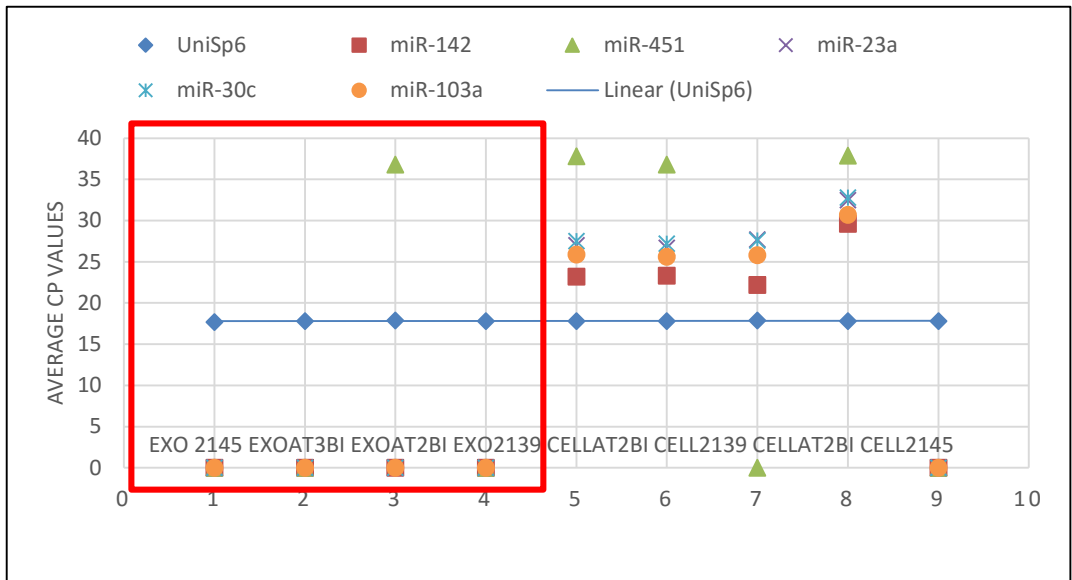


Figure 6.3 Average Cp values of common miRNA's in each sample. Steady cp of the cDNA synthesis control in blue (UniSp6) indicates that both cDNA synthesis and qPCR were successful. Little to no miRNA's were detected in the exosomal extracts (depicted in the red box), but 4 out of 5 miRNAs' were detected in all of the cell extract samples.

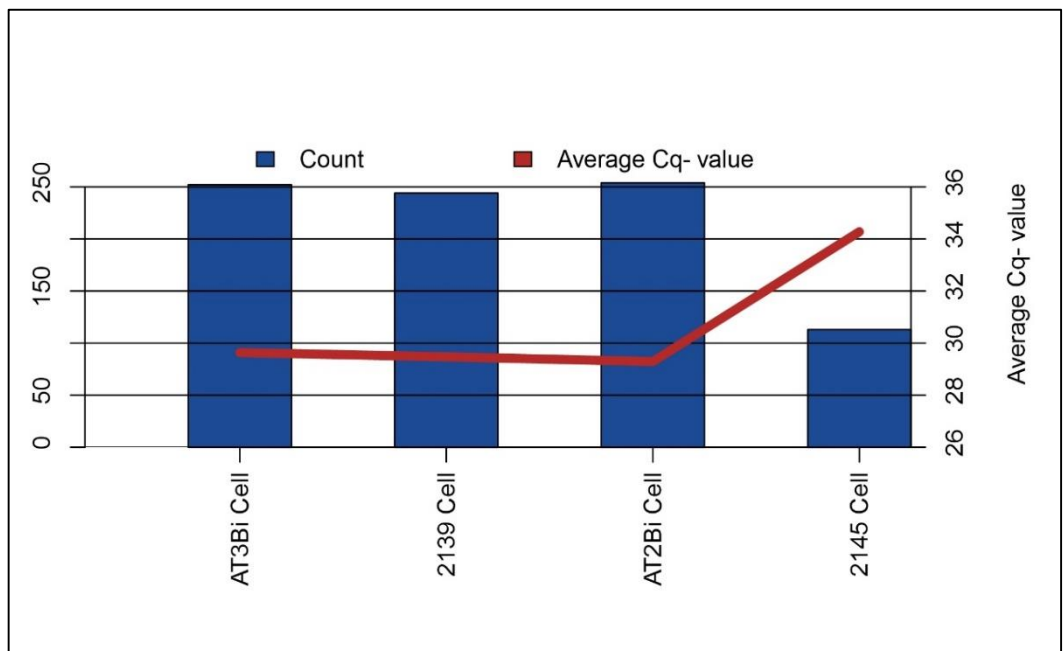


Figure 6.4 Graphical illustration of the microRNA content. The blue bars represent number of microRNAs detected and the red line shows the average Cq value for the commonly expressed microRNAs. On average, 216 microRNA were detected per sample

### 6.3.3 Heat map and unsupervised clustering from Exiqon

Exiqon in Denmark handle and represent large datasets with heat map analysis as it allows for an initial, immediate summary of the data. Exiqon prepared a heat map of the miRNA data obtained from the outsourced cell samples. Here, a two-way hierarchical clustering of miRNA's is represented based on sample type (Figure 6.5). Hierarchical clustering is a method used with large datasets to cluster data based on similarities within the data. For this data, this is represented by similar levels of miRNA expression being clustered together. Figure 6.5 shows a representation of this using the top 50 expressed miRNAs within the data. Each row represents a miRNA while each column represents the sample type. The expression level of each miRNA is represented by a colour, green indicating an expression level below the mean, whereas red represents expression levels of miRNAs above the mean. From figure 6.5 it is clear that different expression profiles of miRNA can be observed between the cell lines which are represented by horizontal panels. The normal 2145 cell line looks to be completely different from the remaining three cell lines (2139, AT2Bi and AT3Bi). This indicates differences in miRNA expression based on cell line alone. From heat map clustering, normal cells could clearly be distinguished from radiosensitive cells based on the latest data about the 2139 lymphoblastoid cell lines (chapter 4) that the donor of these cells was shown to have Turners syndrome and is also considered to be radiosensitive.



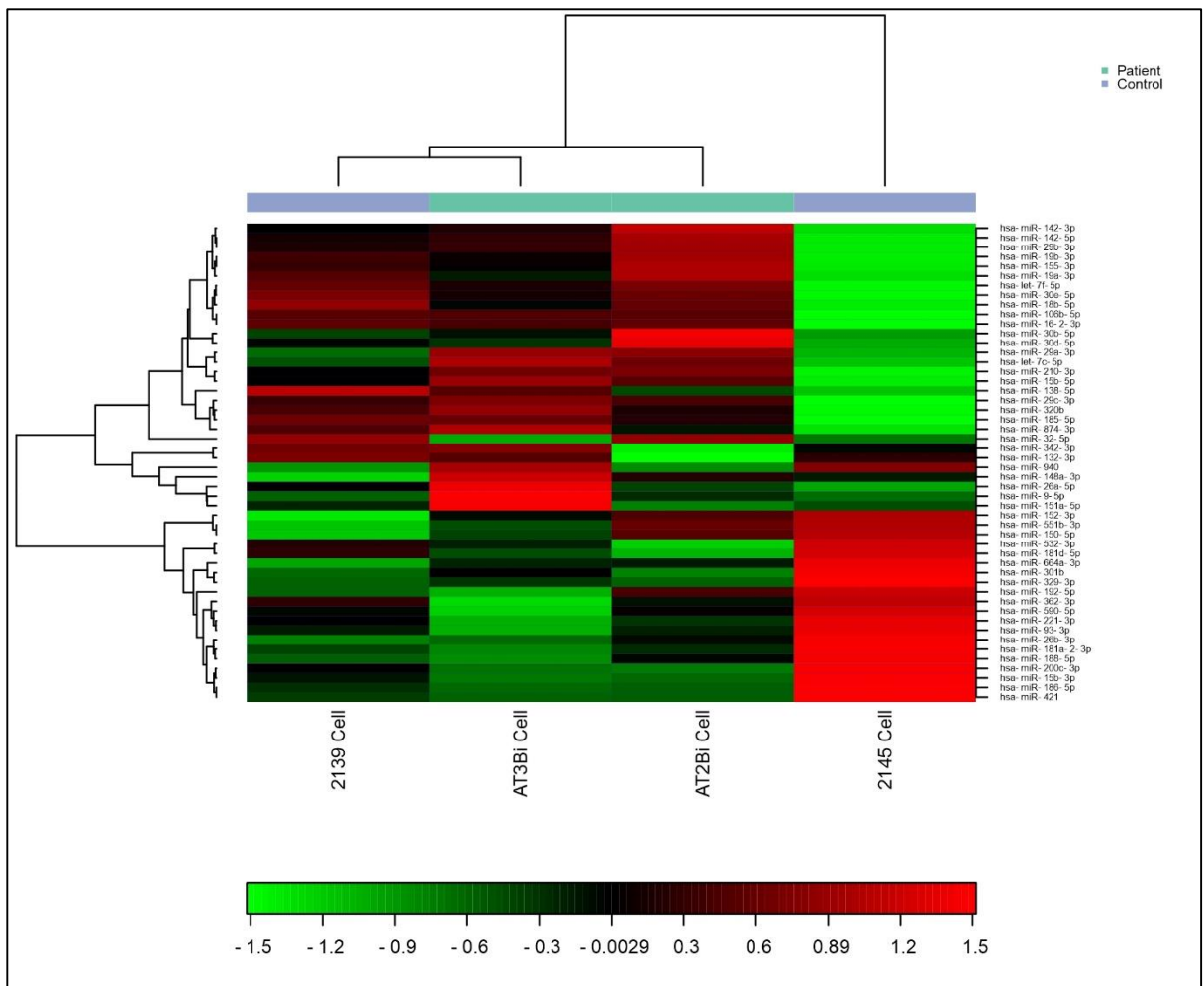


Figure 6.5 Heat map and unsupervised hierarchical clustering. The clustering is performed on all samples, and on the top 50 microRNAs with highest standard deviation. The normalized (dCq) values have been used for the analysis. The horizontal bar shows how the data is clustered based on the mean of expression of each miRNA. Green represents expression of miRNA that fall below the mean whereas red represents expression of miRNA that fall above the mean.

#### 6.3.4 Differential Expression of miRNA between Normal and Radiosensitive

Exiqon carried out PCA analysis using the top 50 microRNA that have the largest variation across all samples, in which an overview of how the samples cluster based on this variance is obtained (Figure 6.6). Figure 6.6 shows a PCA plot of each cell line based on the variance of miRNA expression within each cell line using only the top 50 highest expressed miRNA's. From the PCA it would seem that good classification was made between normal and radiosensitive LCLs. This is based on what was known from the

“normal” 2139 at the time of sample processing, which was later discovered to have Turner’s syndrome and is considered radiosensitive (Chapter 4 findings).

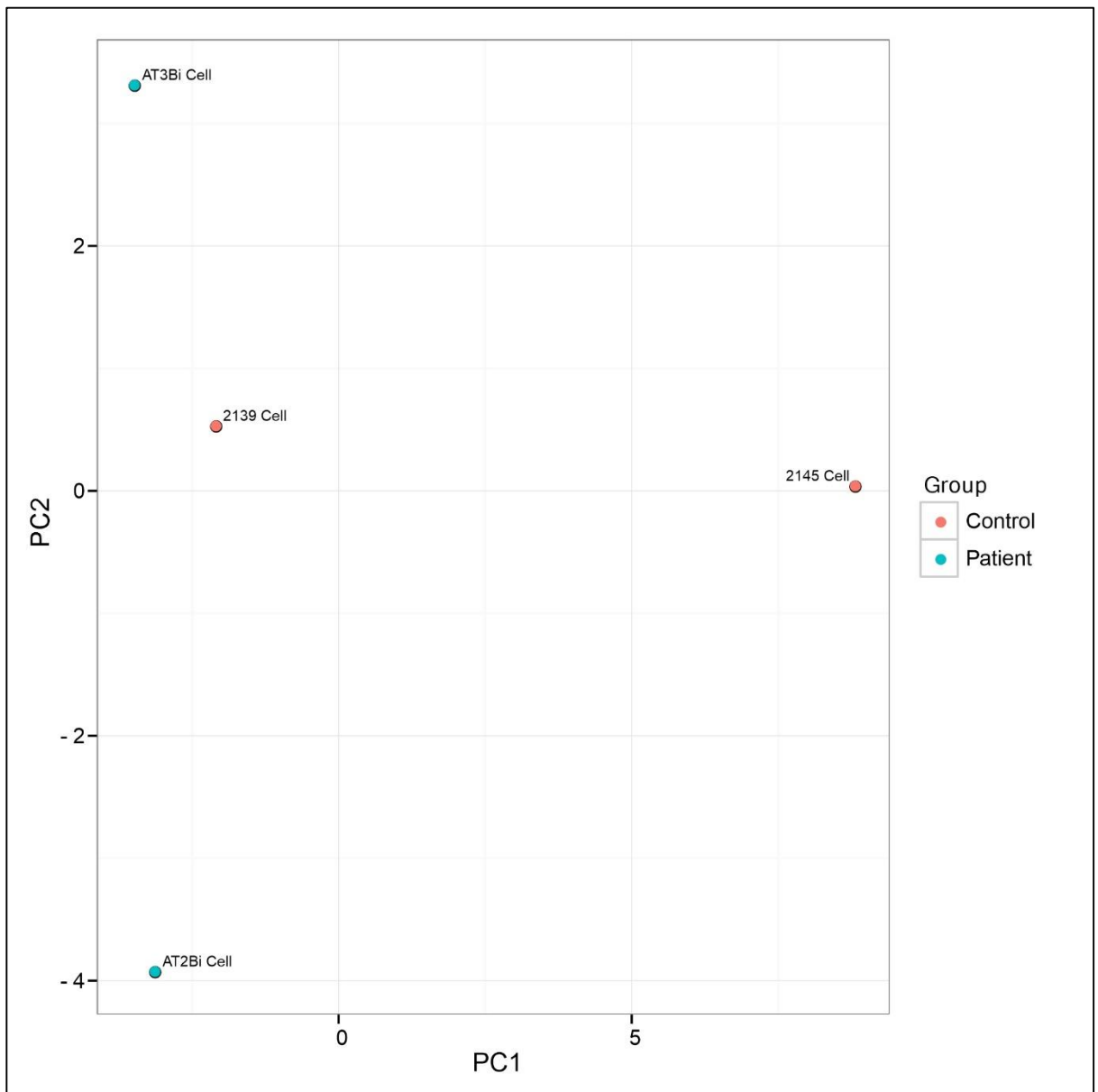


Figure 6.6 PCA plot of miRNAs from AT and normal cell lines. The principal component analysis is performed on all samples, and on the top 50 microRNAs with highest standard deviation. The normalized (dCq) values have been used for the analysis. No outliers were detected.

### 6.3.5 Differentially expressed miRNA's

A full list of 88 detected miRNAs' in *all four cell* samples is presented in Table 6.2 in descending order of highest standard deviation between the samples. From Table 6.2, the majority of miRNA's expressed seem to be higher in the normal cell line (2139) and lower in the two AT cell lines (AT2Bi and AT3Bi) and the 2139 cell line (Turners). This would imply that radiosensitivity may involve downregulation of certain miRNA's. In Table 6.2 a few miRNAs' which have been shown to influence radiosensitivity are highlighted in pink. These are miR-21-5p, miR-26a-5p, miR-7-5p, miR-25-3p. Additionally, miR-125b was highly expressed in one of the AT cell lines, and was not expressed in the normal 2145 cell line. This miRNA has been shown to influence radiosensitivity and radioresistance<sup>372</sup>. This was not represented here as only the miRNA's are shown which were expressed in all of the cell lines. See appendix 3 for full list of miRNA's expressed in each cell line.

From Table 6.2, miRNA's involved with radiosensitivity and the let-7 family of miRNA's are highlighted (The let-7 miRNA's are highlighted in yellow). The let-7 family of miRNA's were the first miRNA's to be discovered. A lower let-7 miRNA expression has been previously linked to poor differentiation and development of aggressive carcinomas. Additionally, Let-7 (a, c, d, g, f and I) have been found to bind to and regulate CDKN1A (p21) and PCNA. It is interesting here that all of the mentioned let-7 miRNA's involved with cell cycle and DNA synthesis control (p21 and PCNA) are expressed in the top 88 of 752 miRNA's analysed within these cell lines (2145, 2139, AT2Bi and AT3Bi) (Table 6.2). It is interesting that a higher expression of let-7 miRNAs was found in the control cell line 2145 and reduced in the radiosensitive cell lines; 2139 with Turners and AT2bi and AT3Bi with AT. Therefore, the data suggests a reduction in overall miRNA expression is associated with disease.

Table 6.2 Differentially expressed miRNAs in each cell line. miRNAs are represented in an order from highest standard deviation between the cell lines to the lowest standard deviation. A few miRNAs' which have been investigated for radiosensitivity analysis in the literature have been highlighted in pink and the let-7 miRNA's are highlighted in yellow.

<b>Target miRNA</b>	<b>AT3Bi</b>	<b>2139.00</b>	<b>AT2Bi</b>	<b>2145.00</b>	<b>Standard Dev.</b>
hsa-miR-138-5p	28.13	26.79	29.66	36.08	4.111835
hsa-miR-210-3p	28.03	28.69	27.58	35.34	3.650165
hsa-miR-142-5p	27.94	27.98	26.71	34.71	3.629733
hsa-miR-29b-3p	28.88	28.90	27.79	35.53	3.543452
hsa-miR-320b	29.02	29.29	29.42	36.15	3.459292
hsa-miR-155-3p	30.52	30.06	29.17	36.68	3.427411
hsa-miR-142-3p	23.86	23.89	22.55	30.10	3.390336
hsa-miR-29c-3p	27.95	28.18	27.88	34.62	3.312354
hsa-miR-106b-5p	28.13	27.90	27.71	34.48	3.286748
hsa-miR-15b-5p	29.27	29.85	29.22	35.79	3.183962
hsa-miR-19a-3p	26.85	26.15	25.53	32.43	3.17148
hsa-miR-18b-5p	29.46	28.59	28.63	35.15	3.15468
hsa-miR-30e-5p	29.81	29.21	29.11	35.62	3.140427
hsa-let-7f-5p	27.75	27.30	27.04	33.48	3.074023
hsa-miR-9-5p	29.75	32.05	31.45	36.90	3.066573
hsa-miR-19b-3p	25.16	24.80	24.22	30.80	3.059394
hsa-miR-185-5p	30.02	29.83	29.94	36.05	3.059229
hsa-miR-16-2-3p	30.97	30.71	30.51	36.83	3.055473
hsa-miR-29a-3p	26.46	27.53	26.16	32.67	3.0357
hsa-miR-30b-5p	29.55	29.63	27.95	34.85	3.006985
hsa-miR-874-3p	30.54	30.72	30.91	36.62	2.949477
hsa-let-7c-5p	29.47	30.29	29.37	35.52	2.935857
hsa-miR-21-5p	23.91	24.05	23.36	29.60	2.929886
hsa-miR-20a-5p	25.60	25.04	24.81	30.94	2.914006
hsa-miR-32-5p	31.52	29.84	29.66	35.91	2.910561
hsa-miR-26a-5p	29.70	30.50	30.59	35.96	2.878848
hsa-miR-30d-5p	30.89	30.55	29.51	35.95	2.874756
hsa-let-7d-5p	28.28	28.24	28.20	33.98	2.873581
hsa-let-7a-5p	26.07	26.78	26.13	31.94	2.827859
hsa-miR-15a-5p	27.89	27.63	26.95	33.05	2.807802
hsa-miR-484	31.52	31.49	30.72	36.70	2.755886
hsa-miR-103a-3p	26.57	25.97	26.34	31.78	2.755582
hsa-miR-101-3p	30.51	29.77	29.26	35.25	2.747172
hsa-miR-16-5p	24.16	24.28	23.90	29.56	2.72668
hsa-miR-22-3p	30.20	30.09	29.98	35.54	2.725949
hsa-let-7g-5p	26.59	26.45	26.22	31.86	2.725185
hsa-miR-155-5p	22.55	22.79	22.08	27.89	2.724615
hsa-miR-151a-5p	30.46	31.65	31.90	36.62	2.717459
hsa-let-7i-5p	27.87	27.99	27.72	33.27	2.705802
hsa-miR-423-3p	28.02	27.80	27.95	33.32	2.700826

hsa-miR-331-3p	29.66	29.75	29.79	35.12	2.696144
hsa-miR-24-3p	27.49	27.04	27.82	32.75	2.669208
hsa-miR-107	27.95	27.98	27.93	33.28	2.662738
hsa-miR-27b-3p	30.85	31.07	30.20	35.95	2.645943
hsa-miR-27a-3p	30.33	30.50	30.57	35.75	2.644047
hsa-miR-146a-5p	25.53	24.91	25.31	30.50	2.638056
hsa-miR-320a	27.54	27.82	27.63	32.93	2.636105
hsa-miR-17-3p	29.51	29.72	29.65	34.86	2.616154
hsa-miR-342-3p	27.73	27.65	29.66	33.22	2.608903
hsa-miR-454-3p	31.59	31.03	31.10	36.42	2.603605
hsa-miR-106a-5p	26.01	25.54	25.58	30.89	2.59768
hsa-miR-18a-5p	29.21	28.36	28.29	33.71	2.578466
hsa-miR-140-3p	29.69	29.76	29.07	34.58	2.554523
hsa-miR-34a-5p	26.89	26.54	26.72	31.80	2.547093
hsa-miR-148a-3p	27.68	28.97	27.90	33.11	2.52892
hsa-miR-1260a	26.78	26.81	26.47	31.68	2.501639
hsa-miR-92a-3p	25.50	25.98	25.55	30.62	2.482241
hsa-miR-361-3p	30.77	31.65	30.91	35.96	2.457265
hsa-miR-365a-3p	27.70	27.30	27.70	32.45	2.451102
hsa-miR-148b-3p	29.89	29.97	29.93	34.81	2.439152
hsa-miR-339-5p	28.48	28.50	28.05	33.20	2.436424
hsa-miR-30c-5p	27.49	27.51	27.36	32.29	2.416767
hsa-miR-320c	31.09	30.86	31.03	35.79	2.401571
hsa-miR-26b-5p	31.30	31.48	31.17	36.10	2.3938
hsa-miR-132-3p	29.82	29.45	31.16	34.68	2.383593
hsa-miR-193b-3p	26.05	25.56	26.13	30.65	2.383491
hsa-miR-7-5p	32.32	31.54	31.43	36.45	2.379498
hsa-miR-98-5p	31.79	30.65	31.06	35.83	2.379198
hsa-miR-23a-3p	27.48	27.11	27.80	32.11	2.34128
hsa-let-7i-3p	32.15	32.68	32.15	36.91	2.304812
hsa-miR-23b-3p	29.53	29.47	29.62	34.14	2.301586
hsa-miR-181b-5p	29.78	28.38	28.79	33.37	2.269711
hsa-miR-191-5p	28.11	27.96	28.66	32.66	2.226295
hsa-miR-222-3p	28.78	27.92	27.60	32.41	2.212354
hsa-miR-181a-5p	27.07	26.06	26.44	30.87	2.210726
hsa-miR-339-3p	31.83	31.27	31.20	35.80	2.205092
mmu-miR-378a-3p	28.37	27.01	27.69	31.90	2.176159
hsa-miR-93-5p	27.86	27.56	27.79	32.00	2.137058
hsa-miR-146b-5p	31.08	31.03	31.15	35.34	2.127614
hsa-miR-425-5p	28.67	29.07	29.01	33.15	2.1257
hsa-miR-423-5p	29.49	29.54	29.64	33.77	2.107572
hsa-miR-940	30.84	32.32	32.10	35.66	2.058938
hsa-miR-197-3p	31.60	31.31	31.19	35.46	2.054514
hsa-miR-25-3p	28.75	28.22	28.21	32.45	2.04617
hsa-miR-660-5p	32.47	31.67	31.35	35.80	2.039174
hsa-miR-128-3p	31.82	30.96	30.86	35.17	2.023652

<b>hsa-miR-362-3p</b>	33.11	31.84	31.93	36.05	1.965652
<b>hsa-miR-150-5p</b>	33.30	33.88	32.06	36.53	1.886441

Table 6.3 illustrates the function of the highlighted miRNAs from Table 6.2. The let-7 family of miRNA's (which include hsa-miR-98) are in the top 88 expressed miRNA's in this work and have been found to regulate cell cycle control genes and DNA synthesis genes such as p21 and PCNA. Additional miRNAs of interest include miR-21, 26 and 451 which have various roles in carcinogenesis and resistance to chemotherapeutic drugs.

Additionally, two miRNAs were expressed in the normal 2145 cell lines and not the radiosensitive cell lines (miR-411-5p and miR545-3p). A few miRNAs were expressed in both AT cell lines (AT2Bi and AT3Bi) and not the normal control cell lines as shown in Table 6.4. None of the miRNA's in table 6.4 has been detected in radiosensitivity cohorts from the literature but could be a novel signature for radiosensitivity prediction.

Table 6.3 Summary of the roles of miRNAs of interest. The chromosome number and examples of the roles of each miRNA are depicted.

<b>miRNA Name/cluster</b>	<b>Chromosome location</b>	<b>Functions</b>	<b>Reference</b>
<b>hsa-let-7a-5p</b>	Chromosome 9, 11 and 22	Let-7 family of miRNA's were first miRNA's discovered. Roles in embryogenesis, metabolism and oncogenesis, cell cycle control, proliferation and apoptosis. Found to bind to and regulate cell cycle control genes such as P21 and DNA synthesis clamp PCNA. Interacts with oncogenes such as RAS and MYC.	373
<b>hsa-let-7c</b>	Chromosome 21		
<b>hsa-let-7d</b>	Chromosome 9		
<b>hsa-let-7f</b>	Chromosome 9 and X		
<b>hsa-let-7g</b>	Chromosome 3		
<b>hsa-let-7i</b>	Chromosome 12		
<b>hsa-miR-98</b>			
<b>hsa-miR-21-5p</b>	Chromosome 17	Encodes for a gene TMEM (a vacuole membrane protein). Most targets are tumour suppressors. High levels detected in B cell lymphoma & cervical cancer. Increased expression found in heart failure of humans and murine models	374,375
<b>hsa-miR-26a-5p</b>	Chromosome 3	Induced in response to hypoxia. Downregulated in hepatocellular, nasopharyngeal, lung and breast cancer. Upregulated in glioma, pituitary and bladder carcinoma	376,377
<b>hsa-miR-451</b>	Chromosome 17	Regulates drug transporter protein P-glycoprotein which could regulate resistance to chemo drug Paclitaxel	378,379

Table 6.4 Potential radiosensitivity miRNA's. The miRNA's presented here are highly expressed in both AT cell lines (AT2Bi and AT3Bi) but not expressed in controls (2145 and 2139). No expression is denoted as Not determined (ND)

<b>Target MiRNA</b>	<b>AT3Bi</b>	<b>AT2Bi</b>	<b>2139</b>	<b>2145</b>
hsa-miR-450a-5p	35.01261997	32.8176891	ND	ND
hsa-miR-99b-5p	33.7923948	35.76875706	ND	ND
hsa-miR-363-3p	31.6732785	30.29645028	ND	ND
hsa-miR-513c-5p	33.9027518	35.07598372	ND	ND
hsa-miR-542-5p	34.64203508	35.64230108	ND	ND
hsa-miR-708-5p	35.60798058	34.73660205	ND	ND
hsa-miR-20b-5p	34.90190879	34.03990372	ND	ND
hsa-miR-618	34.76197598	33.93939199	ND	ND
hsa-miR-320d	32.0163168	32.50126174	ND	ND
hsa-miR-10a-5p	36.01983424	35.60760192	ND	ND
hsa-miR-503-5p	33.59965861	33.71171554	ND	ND
hsa-miR-424-5p	31.93660052	32.02640131	ND	ND
hsa-miR-96-5p	35.07064865	35.15061287	ND	ND
hsa-miR-550a-3p	34.92316622	34.98927438	ND	ND

## 6.4 Discussion

To date, much work has been done to date investigating the use of miRNA signatures for cancer detection and to enhance radiosensitivity by regulating genes which cause radioresistance for treatment purposes. To our knowledge, no study has investigated the potential of using a miRNA signature excreted from exosomes for radiosensitivity prediction. This chapter forms the basis of early stage experimental work for investigating radiosensitivity prediction using miRNA from exosomes from normal and radiosensitive cell lines but with implications for use in blood samples from cohorts of patients undergoing radiotherapy treatment

Work by Mitchell *et al* investigated if exosome quantification from urine of prostate cancer patients could predict radiotherapy treatment response. The work reported a 2-fold increase in exosome quantities in the urine of prostate cancer patients post androgen deprivation therapy. No pattern was observed in the radiotherapy treatment time and large



variation in exosome amount and quality was observed between individuals<sup>294</sup>. The work here aimed to go a step further and investigate if by profiling the miRNAs could be used for use on prostate cancer blood samples in future work. Only one of the 5 routinely used miRNAs was detected in exosomes secreted from AT2Bi (miR-451). miR-451 has been found to increase radiosensitivity of nasopharyngeal carcinoma cells through inhibiting Ras-related protein 14 (RAB14)<sup>378</sup>. Therefore, it was unfortunate that the exosome samples did not perform well for miRNA microarray analysis. This could be due to small numbers of exosomes detected in each of the exosome extract samples. For future work, a higher number of cells would be used and incubated for a longer period of time for harvesting of exosomes from culture media.

However, the let-7 family of miRNAs were of interest in this study. Let-7 miRNA's were the first discovered and are the most studied miRNA's and therefore have been reported to have diverse roles in embryogenesis, carcinogenesis and metabolism. It is interesting that a distinct set of let-7 miRNA's (hsa-let-7a/c/d/f/g/I and miR-98) were part of the top 88 miRNA's expressed and found to be downregulated in radiosensitive cells. Of further interest is that the same distinct set of let-7 miRNAs were reported to bind to and regulate Cyclin Dependent Kinase inhibitor 1a (CDKN1A or also known as p21) and proliferating cell nuclear antigen (PCNA) (expressed genes described in chapter 5). This is interesting as p21 is a crucial cell cycle inhibitor, which stops the progression of the cell cycle in response to irradiation. Therefore, the let-7 family of miRNAs could have crucial roles in cell cycle checkpoint response to cellular stress. More work is warranted in this area to investigate the functional effects of let-7 miRNAs on cell cycle response. PCNA acts as a clamp on DNA during replication. It has been found that DNA synthesis is also inhibited in response to cellular stress, which PCNA could have a role in<sup>335</sup>. Additionally, p21 inhibits PCNA during DNA synthesis if Cyclin/CDK complexes are absent<sup>332</sup>. It is

obvious why the roles of miRNAs are attractive targets for cancer therapies as they can be manipulated to control tumour suppressor genes or oncogenes for therapeutic gain.

Heat map analysis is a current method used which allows for immediate visualisation of gene expression data. In this work, the use of a heat map shows a clear distinction of normal vs radiosensitive samples based on their gene expression pattern. Although only four samples were used, this work has been done previously to identify radioresponsive biomarkers in cells vs whole blood. Kabacik *et al* conducted a study in 2011 and found clear subsets of genes activated in response to different doses<sup>331</sup>. This was also used in a study in 2015 by Ghandhi *et al* who identified p53 pathway and immune cell activation using heat map plots of gene expression profiling to clearly outline the different subsets of genes activated in response to different doses of irradiation and different dose rates<sup>380</sup>.

Of the top 5 expressed miRNA's in each cell line, no particular miRNA's of interest were observed except for miR-125b which has been shown to influence radiosensitivity. Shiiba *et al* demonstrated that inhibition of miR-125b was found in oral squamous cell carcinoma cell lines and when those cells were transfected with miR-125 a decreased proliferation rate in combination with increased x-ray radiosensitivity was discovered<sup>372</sup>. Although miRNA expression has been investigated for their potential use for maximising radiosensitivity for therapeutic gain, no study has yet confirmed the use of a miRNA signature for radiosensitivity prediction. The current study shows a distinct set of miRNA's found to be expressed in radiosensitive cells (AT) and not expressed in control cells.

## **6.5 Chapter Summary and conclusions**

Overall, good classification was observed between normal cell lines and radiosensitive cell lines using the top 50 differentially expressed miRNAs from micro-array analysis. The present work forms a basis for progression of work on prostate cancer patient blood

samples. The current data also provides a basis for future work into investigating the potential of a miRNA signature for radiosensitivity prediction. The hsa-let-7 family of miRNAs are involved in a number of processes such as cell cycle control and progression and oncogenesis. The current study is beneficial for future work which is needed to investigate the use of a gene signature for predicting late tissue toxicity following radiotherapy.

## **7. GENERAL THESIS DISCUSSION**

The ultimate goal of this work was 2 fold (1) to identify an efficient reliable predictive assay of radiosensitivity (2) to identify novel biomarker/s of radiosensitivity which can potentially be brought to the clinic to measure individual radiosensitivity in patients at their radiotherapy treatment planning stage and/or throughout the course of their radiotherapy to predict response. In order to obtain this ultimate goal, *in vitro* translational research studies incorporating healthy donor, prostate cancer patient samples and Ataxia-Telangiectasia radiosensitive cohorts were used to study varied radiosensitivity responses and their underlying molecular mechanisms of response. Cell cycle checkpoint control is well known to be central to the cellular DNA damage response (DDR) from ionising radiation exposure and this formed the basis of this thesis from a cellular to a molecular radiobiological level hence predictive assay to biomarker level respectively.

Individual variation in radiosensitivity was observed among all samples and cohorts and is well documented in the literature. There have been many attempts to find a predictive assay of radiation response *in vitro* to report individual radiosensitivity. The underlying molecular mechanisms of individual variation in radiosensitivity is attributed to the DNA damage response (DDR) sensors ( $\gamma$ H2AX, BRCA, 53BP1), major molecular signalling pathways involving Ataxia Telangiectasia Mutated (ATM) and P53, cell cycle checkpoints and inhibition of the cell cycle in response to ionising radiation such as CHK1 and CHK2, and the underlying miRNA's which bind to and regulate the activity of the different molecular players in the DDR cascade. Chapter 1 provides a detailed review of the literature about these key concepts directly relevant to this thesis.

Experimental Chapter 2 optimised and validated the well-known G2 chromosomal radiosensitivity assay with a healthy control cohort. This assay was chosen because it is a well-known to be a reliable *in vitro* predictive assay of radiosensitivity that can be

applied to blood samples directly from donors/patients and has potential clinical applications. Radiosensitivity cut off values and variation between donors was compared to other published studies for consistency. Within this work it was investigated if radiation sources and doses played a major role in biological variation between healthy donors. This was done because the blood samples from the HC cohort were irradiated using photons from a  $^{60}\text{Co}$  which was decommissioned and replaced with a linear accelerator (Linac). As expected the most radiosensitive dose was 0.5Gy delivered from a linac source. The different radiation sources did not alter the response.

In Experimental Chapter 3, PCa patients were recruited and the G2 chromosomal radiosensitivity assay applied at different time points during radiotherapy treatment (i.e. before and after hormone treatment, last day of radiotherapy and at the 2 and 8month follow up). This was done to determine if the G2 chromosomal radiosensitivity assay was not only a predictor of intrinsic radiosensitivity but also a method to monitor radiosensitivity response throughout a radiotherapy treatment regime. Chromosomal radiosensitivity and checkpoint response was a good indicator of bio dosimetry and good predictors of radiosensitivity with patterns based on time and dose.

Therefore, in Experimental Chapter 4, an array of DNA damage based assays including cellular viability was applied to Lymphoblastoid Cell Lines (LCL's) to two donors with confirmed Ataxia Telangiectasia (and compared to two healthy donors). Ataxia Telangiectasia cells were selected for this study as AT is a well-known radiosensitivity phenotype exhibiting extreme levels of cellular radiosensitivity. Further Cytogenetic techniques including G-Banding and FISH using cytogenetic markers were applied to these cells in a collaboration with Crumlin Genetics department. Interestingly, one of the healthy control cell lines was actually deemed to be radiosensitive with the cell based assays and was later confirmed to be a sufferer of Turners syndrome which has been

reported to display radiosensitivity. This cytogenetic study also confirmed the major role of the signalling protein ATM and the roles of the cell cycle checkpoint proteins in response to the DDR. Without ATM (as represented in the AT cells), aberrant cell growth, cell cycle checkpoint responses and reduced signalling of  $\gamma$ H2AX occurs as a result.

This allowed for the progression of gene expression studies in Experimental Chapter 5 which used genetic biomarkers obtained from bio dosimetry studies in Public Health England. The genes were cell cycle and DDR related genes (cyclin dependent kinase inhibitor 1a (CDKN1A also known as p21), proliferating cell nuclear antigen (PCNA), Sestrin 1 (SESN1) and ferredoxin reductase (FDXR)). Multiplex PCR was carried out as it was rapid and multiple patient's/donors samples could be done simultaneously. Although no significant changes were found in gene expression, different patterns of expression between HC, PCa and AT cells were found using the four genes in combination. These genes are of interest as they are active in the inhibition of the cell cycle in response to DNA damage, specifically p21 which is a cell cycle inhibitor, and is under control of p53 which in turn is controlled by ATM. P53 also interacts with SESN1 and p21 with PCNA so all of the genes studied except for FDXR interact with each other. FDXR was sensitive for bio dosimetry purposes from previous studies but is more involved in metabolism. This was promising, but longer time-points are needed to investigate this further. This study outlined the interesting changes in gene expression using Sestrin 1, which is modulated fully by p53 which could be an interesting family of genes to look at in future studies.

Finally, in Experimental Chapter 6 the AT and normal LCL's were used for the investigation of novel markers of radiosensitivity. 106 miRNA's showed excellent classification between normal and radiosensitive cells, and even classified the radiosensitive 'healthy' donor 2139 correctly as radiosensitive. This work was promising

for finding a potential novel biomarker of radiosensitivity. Additionally, the let 7 family of miRNA's were found to be upregulated and in the literature these miRNAs' are known to regulate cell cycle checkpoint proteins such as p21 and also interact with proliferating cell nuclear antigen (PCNA) which plays a crucial role in the replication fork machinery and inhibits the progression of DNA synthesis in response to irradiation stress.

Figure 7.1 summarises the progression of this research from predictive assays to biomarkers via cellular and cytogenetic to molecular research respectively. This also indicates that future molecular work would be required to find novel biomarkers of radiosensitivity.

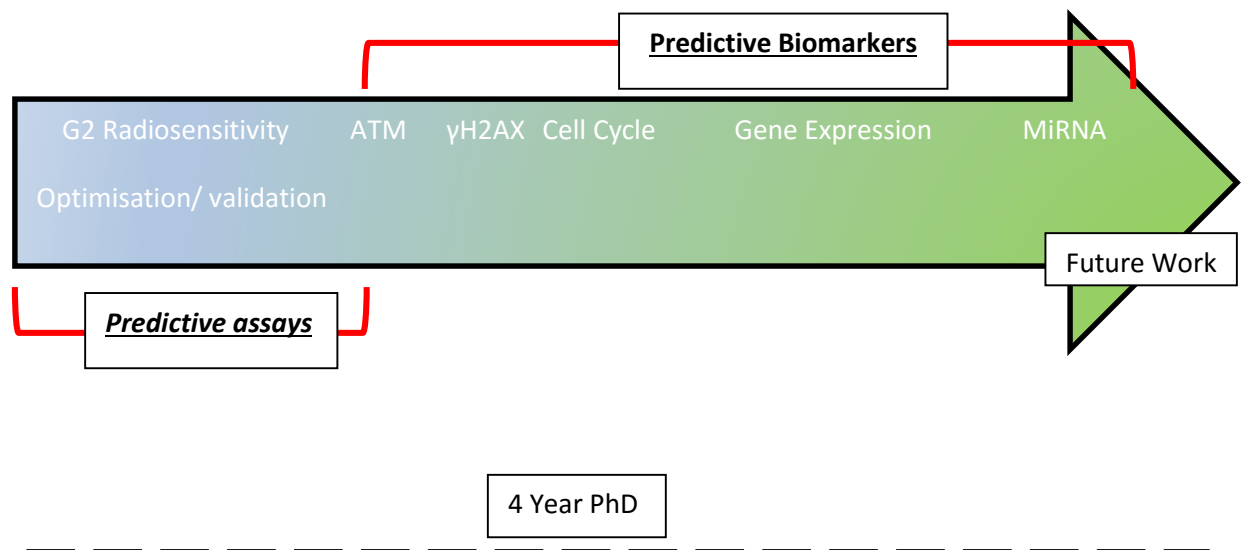


Figure 7.1 Progression of work and summary over 4 years of the PhD. G2 radiosensitivity studies were done firstly. Then more in depth, mechanistic work was done to investigate the role of the key molecular players involved in radiosensitivity including ATM, cell cycle checkpoint control, gene expression and finally progressing on to novel miRNA markers for radiosensitivity.

### Hypothesis of Intrinsic radiosensitivity

By investigating the underlying molecular mechanisms of radiosensitivity for novel biomarkers of radiosensitivity, specific DNA damage and repair genes emerged. Figure 8.2 below displays these genetic targets (in green) on a cellular level and nuclear level. In

figure 7.2 (right hand side) the DDR in the nucleus demonstrates the interconnections of the genes with the genes directly studied highlighted in green.

Additional extra-nuclear molecular targets also emerged as potential biomarkers of radiosensitivity and in figure 7.2 (left hand side). These included FDXR involved in metabolism, and miRNA's which are transported out of the nucleus and are encapsulated within exosomes for exporting out of the cell into the microenvironment (for example, the blood stream) where they can release miRNA's to regulate target genes. MiRNA's are depicted in boxes which regulate ATM, SESN1, P53 and P21. These were found to be downregulated in AT cells in chapter 6.



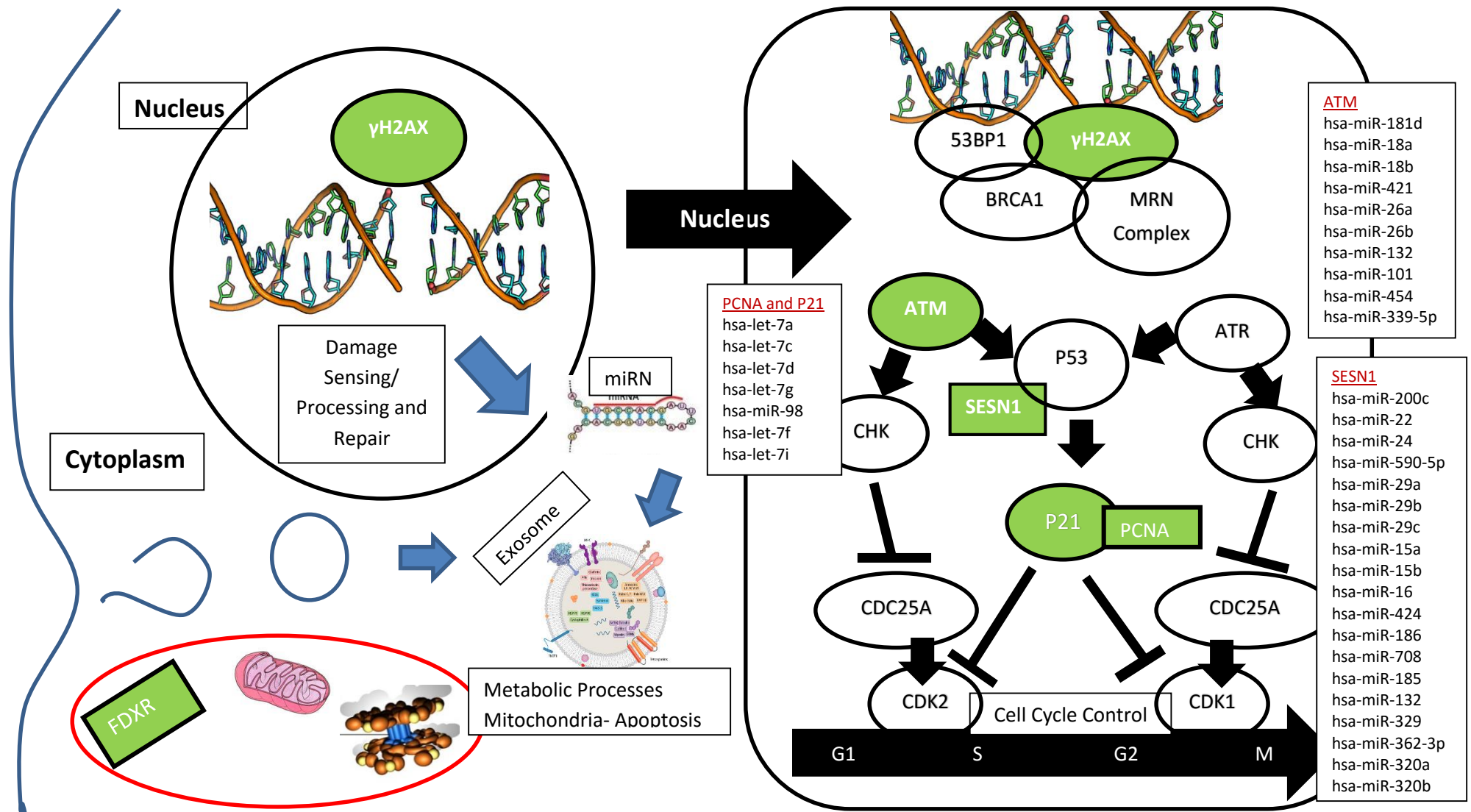


Figure 7.2 Summary of interplay between the molecular markers of radiosensitivity. Directly investigated in this work (Green). The cell nucleus and cytoplasm is shown in brief on the left depicting where DNA damage sensing and repair takes place, as well as the exocytosis of exosomes and their contents and metabolic processes involving FDXR and apoptosis. To the right, a more detailed summary of the nucleus and interplay of molecular markers in response to DNA damage is shown, MiRNA' which regulate PCNA, P21, SESN1 and ATM are shown in boxes.

## **8. LIMITATIONS AND FUTURE WORK**

Each chapter of work within this thesis yield information about the biological mechanisms of radiosensitivity for the development of a potential predictive biomarker or assay, but are not without limitations. For instance, in chapter 2 the main limitation outside the control of the research scientist is individual intrinsic variation. Although this falls within the ranges of previously published work, variation of radiosensitivity cannot be regulated but factors which affect it can be recorded. In chapter 2, these limitations are explored, finding more factors involved in variation of results.

As chapter 3 was a preliminary, pilot study for radiosensitivity analysis using prostate cancer donors, the main limitation was lack of donor samples at each treatment visit, for e.g. although more than 25 donors were analysed for visit 1, only 5 donor's samples had been obtained and analysed for this chapter. This work is currently ongoing.

Use of immortalised cell lines in chapter 4 was the major limitation of this work. It is known that immortalised cell lines lack key factors from the cellular microenvironment which may play a role in the stress response, which will ultimately influence assay results. In addition, the normal cell lines were not cooperative, i.e. the 2145 cell line had been cultured over time and had reached its hayflick limit, and the 2139 cell line could also have been cultured to a degree where it had incorporated genomic instability and therefore produced false positive results. The 2139 cell line was also a normal, control cell line which after cytogenetic characterisation was found to be abnormal. If the study was repeated, whole blood from healthy donors would be used and if immortalised cell lines were needed, these would be made from freshly obtained whole blood.

Again, the major limitations of chapter 5 were lack of donor samples and cell lines. This was primarily due to storage failure of some healthy control RNA extracted from whole blood which underwent defrosting in transit to England from Ireland. In addition, higher

dose points could be used to investigate gene expression profiles further, with particular attention on metabolomics pathways incorporating SESN1 and FDXR.

Finally, chapter 6 was a primary study using the same immortalised cell lines from chapter 4. Limitations associated with this batch of work involved the small number of exosomes secreted from each sample and failure of miRNA profiling using those exosome samples. If repeated in future work, a higher number of cells in a more concentrated volume of media would be used to improve exosomal yield. In addition, this method would benefit if whole blood lymphocytes were used instead of immortalised cell lines.

## 9. REFERENCES

1. Baskar, R., Ann-Lee, K., Yeo, R. & Yeoh, K.-W. Cancer and Radiation Therapy: Current Advances and Future Directions. *Int. J. Med. Sci.* **9**, 193–199 (2012).
2. Barnett, G. C. *et al.* Normal tissue reactions to radiotherapy: towards tailoring treatment dose by genotype. *Nat. Rev. Cancer* **9**, 134–42 (2009).
3. Center, M. M. *et al.* International Variation in Prostate Cancer Incidence and Mortality Rates. *Eur. Urol.* **61**, 1079–1092 (2012).
4. Morris, W. J. *et al.* Population-based 10-year oncologic outcomes after low-dose-rate brachytherapy for low-risk and intermediate-risk prostate cancer. *Cancer* **119**, 1537–46 (2013).
5. Mah, D. & Chen, C. C. Image guidance in radiation oncology treatment planning: the role of imaging technologies on the planning process. *Semin. Nucl. Med.* **38**, 114–8 (2008).
6. Röntgen, W. C. On a new kind of rays. *J. Franklin Inst.* **141**, 183–191 (1896).
7. Becquerel, J. & Crowther, J. Discovery of Radioactivity. *Nature* **161**, 609 (1948).
8. Curie, E. Marie and Pierre Curie and the discovery of radium. *Brit. J. Radiol.* **23**, 409–412 (1950).
9. Despeignes, V. Observation concernant un cas de cancer de l'estomac traité par les rayons Roentgen. *Lyon Med.* **82**, 428–430 (1896).
10. Baclesse, F. Comparative study of results obtained with conventional radiotherapy (200 KV) and cobalt therapy in the treatment of cancer of the larynx. *Clin. Radiol.* **18**, 292–300 (1967).
11. J., B. & L., T. Interpretation of some results of Radiotherapy and an Attempt at Determining a Logical Technique of Treatment. *Radiat. Res.* **11**, 587 – 588 (1959).
12. Coutard, H. Principles of X-ray therapy of malignant disease. *Lancet* **2**, 1–12 (1934).
13. Taylor, L. . History of the International Commission on Radiological Protection (ICRP). *Health Phys.* **1**, 97–104 (1958).
14. Green, D. T. & Errington, R. F. Design of a cobalt 60 beam therapy unit. *Brit. J. Radiol.* **25**, 319–323 (1952).
15. Fry, D. W. *et al.* A traveling wave linear accelerator for 4 MeV electrons. *Nature* **162**, (1948).
16. Tucker, S. L., Geara, F. B., Peters, L. J. & Brock, W. a. How much could the radiotherapy dose be altered for individual patients based on a predictive assay of normal-tissue radiosensitivity? *Radiother. Oncol.* **38**, 103–13 (1996).
17. Fernandez-Ots, A. & Crook, J. The role of intensity modulated radiotherapy in gynecological radiotherapy: Present and future. *Reports Pract. Oncol. Radiother.* (2013).

18. Holt, A., van Vliet-Vroegindeweij, C., Mans, A., Belderbos, J. S. & Damen, E. M. F. Volumetric-Modulated Arc Therapy for Stereotactic Body Radiotherapy of Lung Tumors: A Comparison With Intensity-Modulated Radiotherapy Techniques. *Int. J. Radiat. Oncol.* **81**, 1560–1567 (2011).
19. Wang, L. *et al.* Dosimetric comparison of stereotactic body radiotherapy using 4D CT and multiphase CT images for treatment planning of lung cancer: Evaluation of the impact on daily dose coverage. *Radiother. Oncol.* **91**, 314–324 (2009).
20. Thariat, J., Hannoun-Levi, J.-M., Sun Myint, A., Vuong, T. & Gérard, J.-P. Past, present, and future of radiotherapy for the benefit of patients. *Nat. Rev. Clin. Oncol.* **10**, 52–60 (2013).
21. Langendijk, J. A. *et al.* Selection of patients for radiotherapy with protons aiming at reduction of side effects: The model-based approach. *Radiother. Oncol.* **107**, 267–273 (2013).
22. Fujii, O. *et al.* A retrospective comparison of proton therapy and carbon ion therapy for stage I non-small cell lung cancer. *Radiother. Oncol.* (2013).
23. Sapkota, S., Kapoor, R. & Aggrawal, A. N. 60p A Randomized Trial Comparing Conventional Fractionation Versus Accelerated Hyperfractionation With Three Dimensional Conformal Radiotherapy (3d-Crt) And Concurrent Chemotherapy In Unresectable Non Small Cell Lung Cancer. *Lung Cancer* **80**, (2013).
24. Freund, L. *Grundriss der gesamten Radiotherapie fuer praktische Aerzte.* (Urban & Schwarzenberg, 1903).
25. Regaud, C. Sterilization rontgenienne totale et definitive, sans radiodermite, des testicules du Belier adulte: conditions de sa realisation. *Compt. Rend. Soc. de Biol* **70**, 202–3 (1911).
26. Urano, M., Ohara, K., Koike, S., Ando, K. & Nesumi, N. Repopulation in radiotherapy. (1976).
27. Ciervide, R. *et al.* Five year outcome of 145 patients with ductal carcinoma in situ (DCIS) after accelerated breast radiotherapy. *Int. J. Radiat. Oncol. Biol. Phys.* **83**, e159–64 (2012).
28. Vaupel, P. Tumor microenvironmental physiology and its implications for radiation oncology. *Semin. Radiat. Oncol.* **14**, 198–206 (2004).
29. Kallman, R. F. & Dorie, M. J. Tumor oxygenation and reoxygenation during radiation therapy: Their importance in predicting tumor response. *Int. J. Radiat. Oncol.* **12**, 681–685 (1986).
30. Bayer, C., Shi, K., Astner, S. T., Maftai, C.-A. & Vaupel, P. Acute versus chronic hypoxia: why a simplified classification is simply not enough. *Int. J. Radiat. Oncol. Biol. Phys.* **80**, 965–8 (2011).
31. Boder, E. Ataxia-telangiectasia: some historic, clinical and pathologic observations. *Birth Defects Orig. Artic. Ser.* **11**, 255–70 (1975).
32. McKinnon, P. J. ATM and ataxia telangiectasia. *EMBO Rep.* **5**, 772–6 (2004).
33. Savitsky, K. *et al.* A single ataxia telangiectasia gene with a product similar to PI-

- 3 kinase. *Science* **268**, 1749–53 (1995).
34. Gatti, R. A. *et al.* Localization of an ataxia-telangiectasia gene to chromosome 11q22-23. *Nature* **336**, 577–80 (1988).
  35. GeneCards. *Weizmann Institute of Science* 1 Available at: [www.genecards.org/cgi-bin/carddisp.pl?gene=ATM](http://www.genecards.org/cgi-bin/carddisp.pl?gene=ATM). (Accessed: 20th October 2015)
  36. Syllaba, L. & Henner, K. Contribution a l'indépendance de l'athetose double idiopathique et congenitale. *Rev. Neuro.* **1**, 541–62 (1926).
  37. SEDGWICK, R. P. & BODER, E. Progressive ataxia in childhood with particular reference to ataxia-telangiectasia. *Neurology* **10**, 705–15 (1960).
  38. Cox, R., Hosking, G. P. & Wilson, J. Ataxia telangiectasia. Evaluation of radiosensitivity in cultured skin fibroblasts as a diagnostic test. *Arch. Dis. Child.* **53**, 386–90 (1978).
  39. West, C. M., Elyan, S. a, Berry, P., Cowan, R. & Scott, D. A comparison of the radiosensitivity of lymphocytes from normal donors, cancer patients, individuals with ataxia-telangiectasia (A-T) and A-T heterozygotes. *Int. J. Radiat. Biol.* **68**, 197–203 (1995).
  40. Cesaretti, J. a *et al.* ATM sequence variants are predictive of adverse radiotherapy response among patients treated for prostate cancer. *Int. J. Radiat. Oncol. Biol. Phys.* **61**, 196–202 (2005).
  41. Taylor, A. M. R., Groom, A. & Byrd, P. J. Ataxia-telangiectasia-like disorder (ATLD)-its clinical presentation and molecular basis. *DNA Repair (Amst)*. **3**, 1219–25
  42. Matsumoto, Y. *et al.* Two unrelated patients with MRE11A mutations and Nijmegen breakage syndrome-like severe microcephaly. *DNA Repair (Amst)*. **10**, 314–321 (2011).
  43. Kim, Y. *et al.* Mutations of the SLX4 gene in Fanconi anemia. *Nat. Genet.* **43**, 142–6 (2011).
  44. Pinto, F. O. *et al.* Diagnosis of Fanconi anemia in patients with bone marrow failure. *Haematologica* **94**, 487–95 (2009).
  45. Zheng, Z. *et al.* Molecular defects identified by whole exome sequencing in a child with Fanconi anemia. *Gene* **530**, (2013).
  46. Gille, J., Floor, K., Kerkhoven, L. & Ameziane, N. Diagnosis of Fanconi Anemia: Mutation Analysis by Multiplex Ligation-Dependent Probe Amplification and PCR-Based Sanger Sequencing. *Anemia* (2012).
  47. Hebra, F. *On Diseases of the Skin, Including the Exanthemata, Volume 5.* (BiblioBazaar, 2009).
  48. Butt, F. M. A., Moshi, J. R., Owibingire, S. & Chindia, M. L. Xeroderma pigmentosum: a review and case series. *J. Cranio-Maxillofacial Surg.* **38**, 534–537 (2010).
  49. Svoboda, D. L., Briley, L. P. & Vos, J. M. Defective bypass replication of a leading

- strand cyclobutane thymine dimer in xeroderma pigmentosum variant cell extracts. *Cancer Res.* **58**, 2445–8 (1998).
50. Amor-Gu ret, M. Bloom syndrome, genomic instability and cancer: the SOS-like hypothesis. *Cancer Lett.* **236**, 1–12 (2006).
  51. Suhasini, A. N. *et al.* Interaction between the helicases genetically linked to Fanconi anemia group J and Bloom’s syndrome. *EMBO J.* **30**, 692–705 (2011).
  52. Dvorak, C. C. & Cowan, M. J. Radiosensitive severe combined immunodeficiency disease. *Immunol. Allergy Clin. North Am.* **30**, 125–42 (2010).
  53. Aloj, G. *et al.* Severe combined immunodeficiencies: new and old scenarios. *Int. Rev. Immunol.* **31**, 43–65 (2012).
  54. Kandath, C. *et al.* Mutational landscape and significance across 12 major cancer types. *Nature* **502**, 333–9 (2013).
  55. Doyle, B. *et al.* p53 mutation and loss have different effects on tumourigenesis in a novel mouse model of pleomorphic rhabdomyosarcoma. *J. Pathol.* **222**, 129–137 (2010).
  56. Ritter, M. A., Gilchrist, K. W., Voytovich, M., Chappell, R. J. & Verhoven, B. M. The role of p53 in radiation therapy outcomes for favorable-to-intermediate-risk prostate cancer. *Int. J. Radiat. Oncol.* **53**, 574–580 (2002).
  57. Bristow, R. G., Benchimol, S. & Hill, R. P. The p53 gene as a modifier of intrinsic radiosensitivity: implications for radiotherapy. *Radiother. Oncol.* **40**, 197–223 (1996).
  58. Sanford, K. K. *et al.* Factors affecting and significance of G 2 chromatin radiosensitivity in predisposition to cancer. *Int. J. Radiat. Biol.* **55**, 963–981 (1989).
  59. Sanford, K. K. *et al.* Factors Affecting and Significance of G 2 Chromatin Radiosensitivity in Predisposition to Cancer. *Int. J. Radiat. Biol.* **55**, 963–981 (1989).
  60. Bernstein, C., Prasad, A. R., Nfonsam, V. & Bernstein, H. DNA Damage , DNA Repair and Cancer. *New Res. Dir. DNA Repair* 413–466 (2013). doi:10.5772/53919
  61. Jena, N. R. DNA damage by reactive species: Mechanisms, mutation and repair. *J. Biosci.* **37**, 503–517 (2012).
  62. Gough, D. R. & Cotter, T. G. Hydrogen peroxide: a Jekyll and Hyde signalling molecule. *Cell Death Dis.* **2**, e213 (2011).
  63. Kondo, N., Takahashi, A., Ono, K. & Ohnishi, T. DNA Damage Induced by Alkylating Agents and Repair Pathways. *J. Nucleic Acids* **2010**, 1–7 (2010).
  64. Drabl s, F. *et al.* Alkylation damage in DNA and RNA—repair mechanisms and medical significance. *DNA Repair (Amst).* **3**, 1389–1407 (2004).
  65. Pfeifer, G. P. Formation and processing of UV photoproducts: effects of DNA sequence and chromatin environment. *Photochem. Photobiol.* **65**, 270–83 (1997).

66. Besaratinia, A. *et al.* DNA lesions induced by UV A1 and B radiation in human cells: comparative analyses in the overall genome and in the p53 tumor suppressor gene. *Proc. Natl. Acad. Sci. U. S. A.* **102**, 10058–10063 (2005).
67. Pfeifer, G. P. & Besaratinia, A. UV wavelength-dependant DNA damage and human non-melanoma and melanoma skin cancer. *Photochem. Photobiol.* **11**, 90–97 (2013).
68. van der Kogel, A. *Basic Clinical Radiobiology*. (Hodder Arnold, 2009).
69. Villegas, F., Tilly, N., Bäckström, G. & Ahnesjö, A. Cluster pattern analysis of energy deposition sites for the brachytherapy sources 103Pd, 125I, 192Ir, 137Cs, and 60Co. *Phys. Med. Biol.* **59**, 5531–43 (2014).
70. Warters, R. L. & Hofer, K. G. Cells Radionuclide Toxicity in Cultured Mammalian Cells. **358**, 348–358 (1977).
71. Montoro, A., Sebastià, N. & Rodrigo, R. Measuring the radiosensitivity of healthcare personnel in radiation-based medical diagnosis and treatment Industrial Hygiene. *mapfre.com*
72. Kadhim, M. a. *et al.* Non-targeted effects of ionising radiation-Implications for low dose risk. *Mutat. Res.* **752**, 84–98 (2013).
73. Alberg, A. J., Ford, J. G. & Samet, J. M. Epidemiology of lung cancer: ACCP evidence-based clinical practice guidelines (2nd edition). *Chest* **132**, 29S–55S (2007).
74. Liu, X., Zhu, M. & Xie, J. Mutagenicity of acrolein and acrolein-induced DNA adducts. *Toxicol. Mech. Methods* **20**, 36–44 (2010).
75. Chapman, J. R., Taylor, M. R. G. & Boulton, S. J. Playing the End Game: DNA Double-Strand Break Repair Pathway Choice. *Mol. Cell* **47**, 497–510 (2012).
76. Flynn, R. L. & Zou, L. ATR: a master conductor of cellular responses to DNA replication stress. *Trends Biochem. Sci.* **36**, 133–40 (2011).
77. Thompson, L. H. & Hinz, J. M. Cellular and molecular consequences of defective Fanconi anemia proteins in replication-coupled DNA repair: mechanistic insights. *Mutat. Res.* **668**, 54–72 (2009).
78. Lukas, J., Lukas, C. & Bartek, J. More than just a focus: The chromatin response to DNA damage and its role in genome integrity maintenance. *Nat. Cell Biol.* **13**, 1161–9 (2011).
79. Cieśla, J., Frączyk, T. & Rode, W. Phosphorylation of basic amino acid residues in proteins: important but easily missed. *Acta Biochim. Pol.* **58**, 137–48 (2011).
80. Rothbart, S. B. & Strahl, B. D. Interpreting the language of histone and DNA modifications. *Biochim. Biophys. Acta* **1839**, 627–43 (2014).
81. Thompson, L. H. Recognition, signaling, and repair of DNA double-strand breaks produced by ionizing radiation in mammalian cells: The molecular choreography. *Mutat. Res. Mutat. Res.* **751**, 158–246 (2012).
82. WEEMAES, C. M. R. *et al.* A New Chromosomal Instability Disorder: The



- Nijmegen Breakage Syndrome. *Acta Paediatr.* **70**, 557–564 (1981).
83. Harper, J. W. & Elledge, S. J. The DNA Damage Response: Ten Years After. *Molecular Cell* **28**, 739–745 (2007).
  84. Kozlov, S. V *et al.* Involvement of novel autophosphorylation sites in ATM activation. *EMBO J.* **25**, 3504–3514 (2006).
  85. Zhou, B. S. & Elledge, S. J. The DNA damage response: putting checkpoints in perspective. **408**, 433–439 (2000).
  86. Jeggo, P. A., Dobbs, T. A., Tainer, J. A. & Lees-Miller, S. P. A structural model for regulation of NHEJ by DNA-PKcs autophosphorylation. *DNA Repair (Amst)*. **9**, 1307–1314 (2010).
  87. Vignard, J., Mirey, G. & Salles, B. Ionizing-radiation induced DNA double-strand breaks: A direct and indirect lighting up. *Radiother. Oncol.* **108**, 362–369 (2013).
  88. Alberts, B. & Johnson, A. in *Molecular Biology of the Cell* 1053–1115 (Garland Science, 2008).
  89. Tonks, B. H. and N., Reinhardt, H. C. & Yaffe, M. B. Kinases that control the cell cycle in response to DNA damage: Chk1, Chk2, and MK2. *Curr. Opin. Cell Biol.* **21**, 245–255 (2009).
  90. Fernet, M., Mégnin-Chanet, F., Hall, J. & Favaudon, V. Control of the G2/M checkpoints after exposure to low doses of ionising radiation: implications for hyper-radiosensitivity. *DNA Repair (Amst)*. **9**, 48–57 (2010).
  91. Kruuv, J. & Sinclair, W. K. X-Ray Sensitivity of Synchronized Chinese Hamster Cells Irradiated during Hypoxia. (2010).
  92. Krueger, S. a, Wilson, G. D., Piasentin, E., Joiner, M. C. & Marples, B. The effects of G2-phase enrichment and checkpoint abrogation on low-dose hyper-radiosensitivity. *Int. J. Radiat. Oncol. Biol. Phys.* **77**, 1509–17 (2010).
  93. Lücke-Huhle, C., Blakely, E. a, Chang, P. Y. & Tobias, C. a. Drastic G2 arrest in mammalian cells after irradiation with heavy-ion beams. *Radiat. Res.* **79**, 97–112 (1979).
  94. Balliano, A. J. & Hayes, J. J. Base excision repair in chromatin: Insights from reconstituted systems. *DNA Repair (Amst)*. (2015). doi:10.1016/j.dnarep.2015.09.009
  95. Guillotin, D. & Martin, S. A. Exploiting DNA mismatch repair deficiency as a therapeutic strategy. *Exp. Cell Res.* **329**, 110–5 (2014).
  96. Spivak, G. Nucleotide excision repair in humans. *DNA Repair (Amst)*. (2015). doi:10.1016/j.dnarep.2015.09.003
  97. Goodhead, D. T. Initial events in the cellular effects of ionizing radiations: clustered damage in DNA. *Int. J. Radiat. Biol.* **65**, 7–17 (1994).
  98. Nikjoo, H., O’Neill, P., Goodhead, D. T. & Terrissol, M. Computational modelling of low-energy electron-induced DNA damage by early physical and chemical events. *Int. J. Radiat. Biol.* **71**, 467–83 (1997).

99. Axelle Renodon-Cornière, P. W. M. L. B. and F. F. *New Research Directions in DNA Repair*. (InTech, 2013). doi:10.5772/46014
100. Carr, A. M. & Lambert, S. Replication Stress-Induced Genome Instability: The Dark Side of Replication Maintenance by Homologous Recombination. *J. Mol. Biol.* (2013).
101. Auble, D. T., Ceballos, S. J. & Heyer, W.-D. Functions of the Snf2/Swi2 family Rad54 motor protein in homologous recombination. *Biochim. Biophys. Acta - Gene Regul. Mech.* **1809**, 509–523 (2011).
102. Jeggo, P. A. & Concannon, P. Immune diversity and genomic stability: opposite goals but similar paths. *J. Photochem. Photobiol. B Biol.* **65**, 88–96 (2001).
103. Downs, J. A. & Jackson, S. P. A means to a DNA end: the many roles of Ku. *Nat. Rev. Mol. Cell Biol.* **5**, 367–78 (2004).
104. Davis, A. J. & Chen, D. J. DNA double strand break repair via non-homologous end-joining. *Transl. Cancer Res.* **2**, 130–143 (2013).
105. Gottlieb, T. M. & Jackson, S. P. The DNA-dependent protein kinase: Requirement for DNA ends and association with Ku antigen. *Cell* **72**, 131–142 (1993).
106. Malivert, L. *et al.* Delineation of the Xrcc4-interacting region in the globular head domain of cernunnos/XLF. *J. Biol. Chem.* **285**, 26475–83 (2010).
107. Ma, Y., Pannicke, U., Schwarz, K. & Lieber, M. R. Hairpin Opening and Overhang Processing by an Artemis/DNA-Dependent Protein Kinase Complex in Nonhomologous End Joining and V(D)J Recombination. *Cell* **108**, 781–794 (2002).
108. Grawunder, U. *et al.* Activity of DNA ligase IV stimulated by complex formation with XRCC4 protein in mammalian cells. **388**, 492–495 (1997).
109. Vanden Berghe, T., Linkermann, A., Jouan-Lanhouet, S., Walczak, H. & Vandenabeele, P. Regulated necrosis: the expanding network of non-apoptotic cell death pathways. *Nat. Rev. Mol. Cell Biol.* **15**, 135–47 (2014).
110. Hayflick, L. & Moorhead, P. S. The serial cultivation of human diploid cell strains. *Exp. Cell Res.* **25**, 585–621 (1961).
111. Evan, G. I. & d’Adda di Fagagna, F. Cellular senescence: hot or what? *Curr. Opin. Genet. Dev.* **19**, 25–31 (2009).
112. Collado, M. & Serrano, M. Senescence in tumours: evidence from mice and humans. *Nat. Rev. Cancer* (2010).
113. d’Adda di Fagagna, F. Living on a break: cellular senescence as a DNA-damage response. *Nat. Rev. Cancer* **8**, 512–22 (2008).
114. Castedo, M. *et al.* Cell death by mitotic catastrophe: a molecular definition. *Oncogene* **23**, 2825–37 (2004).
115. Vitale, I., Galluzzi, L., Castedo, M. & Kroemer, G. Mitotic catastrophe: a mechanism for avoiding genomic instability. *Nat. Rev. Mol. Cell Biol.* **12**, 385–392 (2011).

116. Mukhtar, E., Adhami, V. M. & Mukhtar, H. Targeting microtubules by natural agents for cancer therapy. *Mol. Cancer Ther.* **13**, 275–84 (2014).
117. Lin, W. *et al.* Autophagy confers DNA damage repair pathways to protect the hematopoietic system from nuclear radiation injury. *Sci. Rep.* **5**, 12362 (2015).
118. Lopez, J. A., Brennan, A. J., Whisstock, J. C., Voskoboinik, I. & Trapani, J. A. Protecting a serial killer: pathways for perforin trafficking and self-defence ensure sequential target cell death. *Trends Immunol.* **33**, 406–12 (2012).
119. Ashkenazi, A., Holland, P. & Eckhardt, S. G. Ligand-based targeting of apoptosis in cancer: the potential of recombinant human apoptosis ligand 2/Tumor necrosis factor-related apoptosis-inducing ligand (rhApo2L/TRAIL). *J. Clin. Oncol.* **26**, 3621–30 (2008).
120. Roy, S. & Nicholson, D. Cross-talk in cell death signaling. *J. Exp. Med.* **192**, 21–6 (2000).
121. Elmore, S. Apoptosis: a review of programmed cell death. *Toxicol. Pathol.* **35**, 495–516 (2007).
122. Fulda, S. & Debatin, K.-M. Extrinsic versus intrinsic apoptosis pathways in anticancer chemotherapy. *Oncogene* **25**, 4798–811 (2006).
123. Fulda, S., Roos, W. P. & Kaina, B. DNA damage-induced cell death: From specific DNA lesions to the DNA damage response and apoptosis. *Cancer Lett.* **332**, 237–248 (2013).
124. Lee, A. S. The glucose-regulated proteins: stress induction and clinical applications. *Trends Biochem. Sci.* **26**, 504–10 (2001).
125. Marciniak, S. J. *et al.* CHOP induces death by promoting protein synthesis and oxidation in the stressed endoplasmic reticulum. *Genes Dev.* **18**, 3066–77 (2004).
126. Ouyang, L. *et al.* Programmed cell death pathways in cancer: a review of apoptosis, autophagy and programmed necrosis. *Cell Prolif.* **45**, 487–498 (2012).
127. *Protein Misfolding Disorders: A Trip Into the ER.* (Bentham Science Publishers, 2009).
128. Kadhim, M. a. *et al.* Non-targeted effects of ionising radiation-Implications for low dose risk. *Mutat. Res.* **752**, 84–98 (2013).
129. Hansemann, D. Ueber asymmetrische Zellteilung in Epithelkrebsen und deren biologische Bedeutung. *Arch. Pathol. Anat.* **119**, 299–326 (1890).
130. Winge, O. Zytologische untersuchungen uber die natur maligner tumoren. II. Teerkarzinome bei mausen. *Z. Zellforsch. Mikrosk. Anat.* **10**, 683–735 (1930).
131. Gagos, S. & Irminger-Finger, I. Chromosome instability in neoplasia: chaotic roots to continuous growth. *Int. J. Biochem. Cell Biol.* **37**, 1014–33 (2005).
132. Lee, A. J. X. *et al.* Chromosomal instability confers intrinsic multidrug resistance. *Cancer Res.* **71**, 1858–70 (2011).
133. Dworaczek, H. & Xiao, W. Xeroderma pigmentosum: a glimpse into nucleotide excision repair, genetic instability, and cancer. *Crit. Rev. Oncog.* **13**, 159–77

(2007).

134. Thibodeau, S. N., Bren, G. & Schaid, D. Microsatellite instability in cancer of the proximal colon. *Science* **260**, 816–9 (1993).
135. Buecher, B. *et al.* Role of microsatellite instability in the management of colorectal cancers. *Dig. Liver Dis.* **45**, 441–9 (2013).
136. Pikor, L., Thu, K., Vucic, E. & Lam, W. The detection and implication of genome instability in cancer. *Cancer Metastasis Rev.* **32**, 341–352 (2013).
137. Ben-David, U. Genomic instability, driver genes and cell selection: Projections from cancer to stem cells. *Biochim. Biophys. Acta* **1849**, 427–435 (2014).
138. West, C. M., Davidson, S. E., Roberts, S. a & Hunter, R. D. Intrinsic radiosensitivity and prediction of patient response to radiotherapy for carcinoma of the cervix. *Br. J. Cancer* **68**, 819–23 (1993).
139. West, C. M. L. L., Davidson, S. E., Burt, P. A. & Hunter, R. D. The intrinsic radiosensitivity of cervical carcinoma: correlations with clinical data. *Int. J. Radiat. Oncol.* **31**, 841–846 (1995).
140. West, C. M. . M. *et al.* Lymphocyte radiosensitivity is a significant prognostic factor for morbidity in carcinoma of the cervix. *Int. J. Radiat. Oncol. Biol. Phys.* **51**, 10–5 (2001).
141. Tam, K. F. *et al.* Potential application of the ATP cell viability assay in the measurement of intrinsic radiosensitivity in cervical cancer. *Gynecol. Oncol.* **96**, 765–770 (2005).
142. Heddle, J. A. *et al.* Micronuclei as an index of cytogenetic damage: Past, present, and future. *Environ. Mol. Mutagen.* **18**, 277–291 (1991).
143. Fenech, M. & Morley, A. A. Measurement of micronuclei in lymphocytes. *Mutat. Res. Mutagen. Relat. Subj.* **147**, 29–36 (1985).
144. Vral, A., Thierens, H., Baeyens, A. & Ridder, L. De. SHORT COMMUNICATION The Micronucleus and G 2 -Phase Assays for Human Blood Lymphocytes as Biomarkers of Individual Sensitivity to Ionizing Radiation: Limitations Imposed by Intraindividual Variability. *Radiat. Res.* **477**, 472–477 (2002).
145. Streffer, C. *et al.* Predictive assays for the therapy of rectum carcinoma. *Radiother. Oncol.* **5**, 303–310 (1986).
146. Encheva, E., Deleva, S., Hristova, R., Hadjidekova, V. & Hadjieva, T. Investigating micronucleus assay applicability for prediction of normal tissue intrinsic radiosensitivity in gynecological cancer patients. *Reports Pract. Oncol. Radiother.* **17**, 24–31 (2012).
147. Scott, D., Barber, J. B., Spreadborough, a R., Burrill, W. & Roberts, S. a. Increased chromosomal radiosensitivity in breast cancer patients: a comparison of two assays. *Int. J. Radiat. Biol.* **75**, 1–10 (1999).
148. Baria, K., Warren, C., Roberts, S. a, West, C. M. & Scott, D. Chromosomal radiosensitivity as a marker of predisposition to common cancers? *Br. J. Cancer*

- 84**, 892–6 (2001).
149. Shadley, J. D. & Wolff, S. Very low doses of X-rays can cause human lymphocytes to become less susceptible to ionizing radiation. *Mutagenesis* **2**, 95–6 (1987).
  150. Scott, D., Spreadborough, a. R. & Roberts, S. a. Less G2 arrest in irradiated cells of breast cancer patients than in female controls: a contribution to their enhanced chromosomal radiosensitivity? *Int. J. Radiat. Biol.* **79**, 405–411 (2003).
  151. Parshad, R., Sanford, K. K. & Jones, G. M. Chromatid damage after G2 phase x-irradiation of cells from cancer-prone individuals implicates deficiency in DNA repair. *Proc. Natl. Acad. Sci. U. S. A.* **80**, 5612–6 (1983).
  152. Scott, D., Spreadborough, a R. & Roberts, S. a. Radiation-induced G2 delay and spontaneous chromosome aberrations in ataxia-telangiectasia homozygotes and heterozygotes. *Int. J. Radiat. Biol.* **66**, S157–63 (1994).
  153. Narayan, a, Tuck-Muller, C., Weissbecker, K., Smeets, D. & Ehrlich, M. Hypersensitivity to radiation-induced non-apoptotic and apoptotic death in cell lines from patients with the ICF chromosome instability syndrome. *Mutat. Res.* **456**, 1–15 (2000).
  154. Wiegant, W. W. *et al.* A novel radiosensitive SCID patient with a pronounced G(2)/M sensitivity. *DNA Repair (Amst)*. **9**, 365–73 (2010).
  155. Papworth, R., Slevin, N., Roberts, S. a & Scott, D. Sensitivity to radiation-induced chromosome damage may be a marker of genetic predisposition in young head and neck cancer patients. *Br. J. Cancer* **84**, 776–82 (2001).
  156. Sanford, K. K., Parshad, R., Price, F. M., Tarone, R. E. & Benedict, W. F. Cytogenetic responses to G2 phase x-irradiation of cells from retinoblastoma patients. *Cancer Genet. Cytogenet.* **88**, 43–8 (1996).
  157. Andersson, H. C., Lewensohn, R. & Månsson-Brahme, E. Chromosomal sensitivity to X-ray irradiation during the G2 phase in lymphocytes of patients with hereditary cutaneous malignant melanoma as compared to healthy controls. *Mutat. Res.* **425**, 9–20 (1999).
  158. Howe, O. *et al.* Cell death mechanisms associated with G2 radiosensitivity in patients with prostate cancer and benign prostatic hyperplasia. *Radiat. Res.* **164**, 627–34 (2005).
  159. Parshad, R. *et al.* Deficient DNA repair capacity, a predisposing factor in breast cancer. *Br. J. Cancer* **74**, 1–5 (1996).
  160. Roberts, S. a *et al.* Heritability of cellular radiosensitivity: a marker of low-penetrance predisposition genes in breast cancer? *Am. J. Hum. Genet.* **65**, 784–94 (1999).
  161. Riches, A. . *et al.* Chromosomal radiosensitivity in G2-phase lymphocytes identifies breast cancer patients with distinctive tumour characteristics. *Br. J. Cancer* **85**, 1157–61 (2001).
  162. Baeyens, a *et al.* Chromosomal radiosensitivity in breast cancer patients with a known or putative genetic predisposition. *Br. J. Cancer* **87**, 1379–85 (2002).

163. Yoon, D.-S. *et al.* Variable levels of chromosomal instability and mitotic spindle checkpoint defects in breast cancer. *Am. J. Pathol.* **161**, 391–7 (2002).
164. Vral, A., Thierens, H., Baeyens, A. & De Ridder, L. Chromosomal aberrations and *in vitro* radiosensitivity: intra-individual versus inter-individual variability. *Toxicol. Lett.* **149**, 345–52 (2004).
165. Howe, O. *et al.* Elevated G2 Chromosomal Radiosensitivity in Irish Breast Cancer Patients: A comparison with other Studies. *Int. J. Radiat. Biol.* **81**, 373–378 (2005).
166. Hsieh, W.-T., Huang, K.-Y., Lin, H.-Y. & Chung, J.-G. *Physalis angulata* induced G2/M phase arrest in human breast cancer cells. *Food Chem. Toxicol.* **44**, 974–83 (2006).
167. Ernestos, B. *et al.* Increased chromosomal radiosensitivity in women carrying BRCA1/BRCA2 mutations assessed with the G2 assay. *Int. J. Radiat. Oncol. Biol. Phys.* **76**, 1199–205 (2010).
168. Baria, K. *et al.* Chromosomal radiosensitivity in young cancer patients : possible evidence of genetic predisposition. **78**, (2002).
169. Bryant, P. E. *et al.* The G2 chromosomal radiosensitivity assay: technical report. *Int. J. Radiat. Biol.* **78**, 863–866 (2002).
170. Smart, V. Chromosomal radiosensitivity: a study of the chromosomal G2 assay in human blood lymphocytes indicating significant inter-individual variability. *Mutat. Res. Mol. Mech. Mutagen.* **528**, 105–110 (2003).
171. Jäkel, O. The relative biological effectiveness of proton and ion beams. *Z. Med. Phys.* **18**, 276–285 (2008).
172. Georgakilas, A. G., Hada, M., Wu, H. & Cucinotta, F. A. mBAND analysis for high- and low-LET radiation-induced chromosome aberrations: A review. *Mutat. Res. Mol. Mech. Mutagen.* **711**, 187–192 (2011).
173. Ritter, S. *et al.* Chromosome aberrations in normal human fibroblasts analyzed in G0/G1 and G2/M phases after exposure in G0 to radiation with different linear energy transfer (LET). *Mutat. Res. Toxicol. Environ. Mutagen.* **756**, 101–107 (2013).
174. Lucas, J. N. *et al.* Rapid Translocation Frequency Analysis in Humans Decades after Exposure to Ionizing Radiation. *Int. J. Radiat. Biol.* **62**, 53–63 (2009).
175. Andrievski, A. & Wilkins, R. C. The response of gamma-H2AX in human lymphocytes and lymphocytes subsets measured in whole blood cultures. *Int. J. Radiat. Biol.* **85**, 369–76 (2009).
176. Celeste, A. *et al.* Genomic instability in mice lacking histone H2AX. *Science* **296**, 922–7 (2002).
177. Redon, C. E., Dickey, J. S., Bonner, W. M. & Sedelnikova, O. A.  $\gamma$ -H2AX as a biomarker of DNA damage induced by ionizing radiation in human peripheral blood lymphocytes and artificial skin. *Adv. Sp. Res.* **43**, 1171–1178 (2009).
178. Greenberg, R., Hendzel, M., Scully, R. & Xie, A. Double strand break repair functions of histone H2AX. *Mutat. Res. Mol. Mech. Mutagen.* **750**, 5–14 (2013).

179. Bourton, E. C., Plowman, P. N., Smith, D., Arlett, C. F. & Parris, C. N. Prolonged expression of the  $\gamma$ -H2AX DNA repair biomarker correlates with excess acute and chronic toxicity from radiotherapy treatment. *Int. J. cancer* **129**, 2928–34 (2011).
180. Ostling, O. & Johanson, K. J. Microelectrophoretic study of radiation-induced DNA damages in individual mammalian cells. *Biochem. Biophys. Res. Commun.* **123**, 291–8 (1984).
181. Singh, N. P., Stephens, R. E. & Schneider, E. L. Modifications of Alkaline Microgel Electrophoresis for Sensitive Detection of DNA Damage. *Int. J. Radiat. Biol.* **66**, 23–28 (2009).
182. Moneef, M. A. L. *et al.* Measurements using the alkaline comet assay predict bladder cancer cell radiosensitivity. *Br. J. Cancer* **89**, 2271–6 (2003).
183. Manning, G. *et al.* Assessing a new gene expression analysis technique for radiation biodosimetry applications. **46**, 1014–1018 (2011).
184. Nicolaj, C., Dikomey, E., Parliament, M., Mary, C. & West, L. Will SNPs be useful predictors of normal tissue radiosensitivity in the future? *Radiother. Oncol.* **105**, 283–288 (2012).
185. Mallal, S. *et al.* HLA-B\*5701 screening for hypersensitivity to abacavir. *N. Engl. J. Med.* **358**, 568–79 (2008).
186. Moore, J. *et al.* Radiotherapy for Prostate Cancer. **78**, 1292–1300 (2011).
187. Pernot, E. *et al.* Ionizing radiation biomarkers for potential use in epidemiological studies. *Mutat. Res.* **751**, 258–86 (2012).
188. Wan, G., Mathur, R., Hu, X., Zhang, X. & Lu, X. miRNA response to DNA damage. *Trends Biochem. Sci.* **36**, 478–484 (2011).
189. Sonenberg, N., Hay, N., Methetrairut, C. & Slack, F. J. MicroRNAs in the ionizing radiation response and in radiotherapy. *Curr. Opin. Genet. Dev.* **23**, 12–19 (2013).
190. Hu, H., Du, L., Nagabayashi, G., Seeger, R. C. & Gatti, R. A. ATM is down-regulated by N-Myc-regulated microRNA-421. *Proc. Natl. Acad. Sci. U. S. A.* **107**, 1506–11 (2010).
191. Hu, W. *et al.* Negative Regulation of Tumor Suppressor p53 by MicroRNA miR-504. *Mol. Cell* **38**, 689–699 (2010).
192. Winter, J., Jung, S., Keller, S., Gregory, R. I. & Diederichs, S. Many roads to maturity: microRNA biogenesis pathways and their regulation. *Nat. Cell Biol.* **11**, 228–234 (2009).
193. Emmert-Streib, F. *et al.* Collectives of diagnostic biomarkers identify high-risk subpopulations of hematuria patients: exploiting heterogeneity in large-scale biomarker data. *BMC Med.* **11**, 12 (2013).
194. Raman, C. V. The scattering of light in crystals. *J. Franklin Inst.* **232**, 203–211 (1941).
195. Nijssen, A. *et al.* Discriminating basal cell carcinoma from its surrounding tissue

- by Raman spectroscopy. *J. Invest. Dermatol.* **119**, 64–9 (2002).
196. de Jong, B. W. D. *et al.* Discrimination between nontumor bladder tissue and tumor by Raman spectroscopy. *Anal. Chem.* **78**, 7761–9 (2006).
  197. Tollefson, M. *et al.* Raman spectral imaging of prostate cancer: can Raman molecular imaging be used to augment standard histopathology? *BJU Int.* **106**, 484–8 (2010).
  198. Lyng, F. M. *et al.* Vibrational spectroscopy for cervical cancer pathology, from biochemical analysis to diagnostic tool. *Exp. Mol. Pathol.* **82**, 121–9 (2007).
  199. Meade, A. D., Byrne, H. J. & Lyng, F. M. Spectroscopic and chemometric approaches to radiobiological analyses. *Mutat. Res.* **704**, 108–14 (2010).
  200. Bonnier, F. *et al.* Analysis of human skin tissue by Raman microspectroscopy: Dealing with the background. *Vib. Spectrosc.* **61**, 124–132 (2012).
  201. Meade, A. D., Lyng, F. M., Knief, P. & Byrne, H. J. Growth substrate induced functional changes elucidated by FTIR and Raman spectroscopy in in-vitro cultured human keratinocytes. *Anal. Bioanal. Chem.* **387**, 1717–28 (2007).
  202. Puck, T. . & Marcus, P. . Action of X-rays on Mammalian Cells. *J. Exp. Med.* **103**, 653–666 (1956).
  203. Goodhead, D. T., Thacker, J. & Cox, R. Weiss Lecture. Effects of radiations of different qualities on cells: molecular mechanisms of damage and repair. *Int. J. Radiat. Biol.* **63**, 543–56 (1993).
  204. Goodhead, D. T. Mechanisms for the biological effectiveness of high-LET radiations. *J. Radiat. Res.* **40 Suppl**, 1–13 (1999).
  205. Anderson, R. M. *et al.* Complex chromosome aberrations in peripheral blood lymphocytes as a potential biomarker of exposure to high-LET alpha-particles. *Int. J. Radiat. Biol.* **76**, 31–42 (2000).
  206. Aypar, U., Morgan, W. F. & Baulch, J. E. Radiation-induced epigenetic alterations after low and high LET irradiations. *Mutat. Res. Mol. Mech. Mutagen.* **707**, 24–33 (2011).
  207. Barendsen, G. W. Responses Of Cultured Cells, Tumours, And Normal Tissues To Radiations Of Different Linear Energy Transfer. *pp 293-356 Curr. Top. Radiat. Res. Vol. IV. Ebert, Michael Howard, Alma (eds.). New York, John Wiley Sons, Inc., 1968.* (1968).
  208. Scholz, M. in *Microdosimetric Response of Physical and Biological Systems to Low - and High - LET Radiations* (ed. Horowitz, Y.) 12 – 13 (Elsevier, 2006).
  209. Franken, N. . *et al.* Comparison of RBE values of high-LET  $\alpha$ -particles for the induction of DNA-DSBs, chromosome aberrations and cell reproductive death. *Radiat. Oncol.* **6**, 64 (2011).
  210. Pujari, G., Sarma, A. & Chatterjee, A. The influence of reduced glutathione on chromosome damage induced by X-rays or heavy ion beams of different LETs and on the interaction of DNA lesions induced by radiations and bleomycin. *Mutat. Res. - Genet. Toxicol. Environ. Mutagen.* **696**, 154–159 (2010).



211. Bajjinskis, A., Olsson, G. & Harms-Ringdahl, M. The indirect effect of radiation reduces the repair fidelity of NHEJ as verified in repair deficient CHO cell lines exposed to different radiation qualities and potassium bromate. *Mutat. Res.* **731**, 125–32 (2012).
212. Wéra, A. ., Heuskin, A. ., Riquier, H., Michiels, C. & Lucas, S. Low-LET proton irradiation of A549 non-small cell lung adenocarcinoma cells: dose response and RBE determination. *Radiat. Res.* **179**, 273–81 (2013).
213. Themis, M., Garimberti, E., Hill, M. . & Anderson, R. . Reduced chromosome aberration complexity in normal human bronchial epithelial cells exposed to low-LET  $\gamma$ -rays and high-LET  $\alpha$ -particles. *Int. J. Radiat. Biol.* **89**, 934–43 (2013).
214. Hill, M. . The Variation in biological effectiveness of X-rays and gamma rays with energy. *Radiat. Prot. Dosimetry* **112**, 471–48 (2004).
215. Hunter, N. & Muirhead, C. . Review of relative biological effectiveness dependence on linear energy transfer for low-LET radiations. *J. Radiol. Prot.* **29**, 5–21 (2009).
216. Nikjoo, H. & Lindborg, L. Topical Review: RBE of low energy electrons and photons. *Phys. Med. Biol.* **55**, R65–R10 (2010).
217. Sax, K. Chromosome Aberrations Induced by X-Rays. *Genetics* **23**, 494–516 (1938).
218. Fowler, J. F. Nuclear particles in cancer treatment. (1981).
219. Lloyd, D. & Edwards, A. Chromosome aberrations in human lymphocytes effects of radiation quality dose and dose rate. *Radiation-Induced Chromosom. Damage Man* 23–49 (1983).
220. Edwards, A. A., Lloyd, D. C., Prosser, J. S., Finnon, P. & Moquet, J. E. Chromosome Aberrations Induced in Human Lymphocytes by 8.7 MeV Protons and 23.5 MeV Helium-3 Ions. *Int. J. Radiat. Biol.* **50**, 137–145 (1986).
221. Straume, T. High-Energy Gamma Rays in Hiroshima and Nagasaki: Implications for Risk and WR. *Health Phys.* **69**, 954–957 (1995).
222. Bauchinger, M. & Schmid, E. LET dependence of yield ratios of radiation-induced intra- and interchromosomal aberrations in human lymphocytes. *Int. J. Radiat. Biol.* **74**, 17–25 (1998).
223. Schmid, E., Regulla, D., Kramer, H.-M. & Harder, D. The effect of 29 kV X rays on the dose response of chromosome aberrations in human lymphocytes. *Radiat. Res.* **158**, 771–7 (2002).
224. ICRP: ICRP Publication 103. The 2007 Recommendations of the International Commission on Radiological Protection. *Ann. ICRP* **37**, (2007).
225. ICRU 29. Dose specification for reporting external beam therapy with photons and electrons. *J. ICRU* (1978).
226. Hsiao, Y. & Stewart, R. D. Monte Carlo simulation of DNA damage induction by x-rays and selected radioisotopes. *Phys. Med. Biol.* **53**, 233–44 (2008).

227. Taylor, a M. Chromosome instability syndromes. *Best Pract. Res. Clin. Haematol.* **14**, 631–44 (2001).
228. Thierens, H. *et al.* Chromosomal radiosensitivity study of temporary nuclear workers and the support of the adaptive response induced by occupational exposure. *Int. J. Radiat. Biol.* **78**, 1117–26 (2002).
229. De Ruyck, K. *et al.* Radiation-induced damage to normal tissues after radiotherapy in patients treated for gynecologic tumors: association with single nucleotide polymorphisms in XRCC1, XRCC3, and OGG1 genes and in vitro chromosomal radiosensitivity in lymphocytes. *Int. J. Radiat. Oncol. Biol. Phys.* **62**, 1140–9 (2005).
230. Howe, O. *et al.* Do radiation-induced bystander effects correlate to the intrinsic radiosensitivity of individuals and have clinical significance? *Radiat. Res.* **171**, 521–9 (2009).
231. De Ruyck, K. *et al.* Chromosomal radiosensitivity in head and neck cancer patients: evidence for genetic predisposition? *Br. J. Cancer* **98**, 1723–38 (2008).
232. Borgmann, K. *et al.* The potential role of G2- but not of G0-radiosensitivity for predisposition of prostate cancer. *Radiother. Oncol.* **96**, 19–24 (2010).
233. Brzozowska, K. *et al.* In vivo versus in vitro individual radiosensitivity analysed in healthy donors and in prostate cancer patients with and without severe side effects after radiotherapy. *Int. J. Radiat. Biol.* (2012). doi:10.3109/09553002.2012.666002
234. Borgmann, K. *et al.* Genetic determination of chromosomal radiosensitivities in G0- and G2-phase human lymphocytes. *Radiother. Oncol.* **83**, 196–202 (2007).
235. Borgmann, K. *et al.* Individual radiosensitivity measured with lymphocytes may predict the risk of acute reaction after radiotherapy. *Int. J. Radiat. Oncol. Biol. Phys.* **71**, 256–64 (2008).
236. Maguire, A. Assessment of individual radiosensitivity for applications in radiotherapeutic treatment planning: A Raman spectroscopic study. (2015).
237. Bruce Alberts, A. J. *Leukocyte also known as macrophages functions and percentage breakdown. Molecular Biology of the Cell* (Garland Science, 2002).
238. Fiandra, C. *et al.* Clinical use of EBT model Gafchromice film in radiotherapy. *Med. Phys.* **33**, 4314–9 (2006).
239. Lewis, D., Micke, A., Yu, X. & Chan, M. . An efficient protocol for radiochromic film dosimetry combining calibration and measurement in a single scan. *Med. Phys.* **39**, 6339 (2012).
240. Micke, A., Lewis, D. & Yu, X. Multichannel film dosimetry with nonuniformity correction. *Med. Phys.* **38**, 2523–34 (2011).
241. Software, G. GraphPad Prism 5. (2016).
242. Tsoulou, E., Baggio, L., Cherubini, R. & Kalfas, C. a. Low-dose hypersensitivity of V79 cells under exposure to gamma-rays and 4He ions of different energies: survival and chromosome aberrations. *Int. J. Radiat. Biol.* **77**, 1133–9 (2001).

243. Cuddihy, A. R. & O'Connell, M. J. Cell-cycle responses to DNA damage in G2. *Int. Rev. Cytol.* **222**, 99–140 (2003).
244. Marples, B. & Collis, S. J. Low-dose hyper-radiosensitivity: past, present, and future. *Int. J. Radiat. Oncol. Biol. Phys.* **70**, 1310–8 (2008).
245. Nam, H. *et al.* The ERK-RSK1 activation by growth factors at G2 phase delays cell cycle progression and reduces mitotic aberrations. *Cell. Signal.* **20**, 1349–58 (2008).
246. Pantelias, G. E. & Terzoudi, G. I. A standardized G2-assay for the prediction of individual radiosensitivity. *Radiother. Oncol.* **101**, 28–34 (2011).
247. Furlong, H., Mothersill, C., Lyng, F. M. & Howe, O. Apoptosis is signalled early by low doses of ionising radiation in a radiation-induced bystander effect. *Mutat. Res.* **741-742**, 35–43 (2013).
248. Jella, K. K., Garcia, A., McClean, B., Byrne, H. J. & Lyng, F. M. Cell death pathways in directly irradiated cells and cells exposed to medium from irradiated cells. *Int. J. Radiat. Biol.* **89**, 182–90 (2013).
249. Beels, L., Werbrouck, J. & Thierens, H. Dose response and repair kinetics of gamma-H2AX foci induced by in vitro irradiation of whole blood and T-lymphocytes with X- and gamma-radiation. *Int. J. Radiat. Biol.* **86**, 760–8 (2010).
250. Ramsey, M. J. *et al.* The effects of age and lifestyle factors on the accumulation of cytogenetic damage as measured by chromosome painting. *Mutat. Res.* **338**, 95–106 (1995).
251. Roberts, C. J., Morgan, G. R. & Danford, N. Effect of hormones on the variation of radiosensitivity in females as measured by induction of chromosomal aberrations. *Environ. Health Perspect.* **105 Suppl**, 1467–71 (1997).
252. National Cancer Registry Ireland | Essential information on cancer in Ireland. (2015). Available at: <http://www.ncri.ie/>. (Accessed: 8th December 2015)
253. Kryvenko, O. N., Balise, R., Prakash, N. S. & Epstein, J. I. African American Men with Gleason Score 3+3=6 Prostate Cancer Produce Less PSA Than Caucasian Men: A Potential Impact on Active Surveillance. *J. Urol.* (2015). doi:10.1016/j.juro.2015.08.089
254. Bratt, O. Hereditary prostate cancer: clinical aspects. *J. Urol.* **168**, 906–13 (2002).
255. Comprehensive Cancer Information - National Cancer Institute. Available at: <http://www.cancer.gov/>. (Accessed: 8th December 2015)
256. Leibovici, D. *et al.* Prostate cancer progression in the presence of undetectable or low serum prostate-specific antigen level. *Cancer* **109**, 198–204 (2007).
257. Lee, F. *et al.* Transrectal ultrasound in the diagnosis of prostate cancer: location, echogenicity, histopathology, and staging. *Prostate* **7**, 117–29 (1985).
258. Gleason, D. F. *The Veteran's Administration Cooperative Urologic Research Group: histologic grading and clinical staging of prostatic carcinoma. Urologic Pathology: The Prostate* (Lea and Febiger, 1977).

259. Humphrey, P. a. Gleason grading and prognostic factors in carcinoma of the prostate. *Mod. Pathol.* **17**, 292–306 (2004).
260. Edge, S. *et al.* *AJCC Cancer Staging Manual*. (Springer-Verlag New York, 2010).
261. Heidenreich, A. *et al.* Guidelines on Prostate Cancer. *Update* (2011).
262. Lu-Yao, G. L. & Yao, S. L. Population-based study of long-term survival in patients with clinically localised prostate cancer. *Lancet (London, England)* **349**, 906–10 (1997).
263. Adolfsson, J. Watchful waiting and active surveillance: the current position. *BJU Int.* **102**, 10–4 (2008).
264. Bianco, F. J., Scardino, P. T. & Eastham, J. A. Radical prostatectomy: long-term cancer control and recovery of sexual and urinary function ('trifecta'). *Urology* **66**, 83–94 (2005).
265. Young, H. The early diagnosis and radical cure of carcinoma of the prostate. *J. Urol.* **16**, 315–321 (1905).
266. Memmelaar, J. & Millin, T. Total prostatovesiculectomy; retropubic approach. *J. Urol.* **62**, 340–348 (1949).
267. Walsh, P. C. & Donker, P. J. Impotence following radical prostatectomy: insight into etiology and prevention. *J. Urol.* **128**, 492–7 (1982).
268. Badani, K. K., Kaul, S. & Menon, M. Evolution of robotic radical prostatectomy: assessment after 2766 procedures. *Cancer* **110**, 1951–8 (2007).
269. Briganti, A. *et al.* Validation of a nomogram predicting the probability of lymph node invasion based on the extent of pelvic lymphadenectomy in patients with clinically localized prostate cancer. *BJU Int.* **98**, 788–93 (2006).
270. Joslyn, S. A. & Konety, B. R. Impact of extent of lymphadenectomy on survival after radical prostatectomy for prostate cancer. *Urology* **68**, 121–5 (2006).
271. Murphy, G. P., Mettlin, C., Menck, H., Winchester, D. P. & Davidson, A. M. National patterns of prostate cancer treatment by radical prostatectomy: results of a survey by the American College of Surgeons Commission on Cancer. *J. Urol.* **152**, 1817–9 (1994).
272. Boda-Heggemann, J. *et al.* Accuracy of ultrasound-based image guidance for daily positioning of the upper abdomen: an online comparison with cone beam CT. *Int. J. Radiat. Oncol. Biol. Phys.* **74**, 892–7 (2009).
273. Zelefsky, M. J. *et al.* Long-term outcome of high dose intensity modulated radiation therapy for patients with clinically localized prostate cancer. *J. Urol.* **176**, 1415–9 (2006).
274. Kupelian, P. *et al.* Improved biochemical relapse-free survival with increased external radiation doses in patients with localized prostate cancer: the combined experience of nine institutions in patients treated in 1994 and 1995. *Int. J. Radiat. Oncol. Biol. Phys.* **61**, 415–9 (2005).
275. Beckendorf, V. *et al.* The GETUG 70 Gy vs. 80 Gy randomized trial for localized

- prostate cancer: feasibility and acute toxicity. *Int. J. Radiat. Oncol. Biol. Phys.* **60**, 1056–65 (2004).
276. D'Amico, A. V, Chen, M.-H., Renshaw, A. A., Loffredo, M. & Kantoff, P. W. Androgen suppression and radiation vs radiation alone for prostate cancer: a randomized trial. *JAMA* **299**, 289–95 (2008).
  277. Peeters, S. T. H. *et al.* Dose-response in radiotherapy for localized prostate cancer: results of the Dutch multicenter randomized phase III trial comparing 68 Gy of radiotherapy with 78 Gy. *J. Clin. Oncol.* **24**, 1990–6 (2006).
  278. Zelefsky, M. J. *et al.* Incidence of late rectal and urinary toxicities after three-dimensional conformal radiotherapy and intensity-modulated radiotherapy for localized prostate cancer. *Int. J. Radiat. Oncol. Biol. Phys.* **70**, 1124–9 (2008).
  279. Cahlon, O. *et al.* Ultra-high dose (86.4 Gy) IMRT for localized prostate cancer: toxicity and biochemical outcomes. *Int. J. Radiat. Oncol. Biol. Phys.* **71**, 330–7 (2008).
  280. Salembier, C. *et al.* Tumour and target volumes in permanent prostate brachytherapy: a supplement to the ESTRO/EAU/EORTC recommendations on prostate brachytherapy. *Radiother. Oncol.* **83**, 3–10 (2007).
  281. Lee, L. N., Stock, R. G. & Stone, N. N. Role of hormonal therapy in the management of intermediate- to high-risk prostate cancer treated with permanent radioactive seed implantation. *Int. J. Radiat. Oncol. Biol. Phys.* **52**, 444–52 (2002).
  282. Hoskin, P. J., Motohashi, K., Bownes, P., Bryant, L. & Ostler, P. High dose rate brachytherapy in combination with external beam radiotherapy in the radical treatment of prostate cancer: initial results of a randomised phase three trial. *Radiother. Oncol.* **84**, 114–120 (2007).
  283. Stephenson, A. J. *et al.* Predicting the outcome of salvage radiation therapy for recurrent prostate cancer after radical prostatectomy. *J. Clin. Oncol.* **25**, 2035–41 (2007).
  284. Wiegel, T. *et al.* Achieving an undetectable PSA after radiotherapy for biochemical progression after radical prostatectomy is an independent predictor of biochemical outcome—results of a retrospective study. *Int. J. Radiat. Oncol. Biol. Phys.* **73**, 1009–16 (2009).
  285. Bagshaw, M. A., Cox, R. S. & Ray, G. R. Status of radiation treatment of prostate cancer at Stanford University. *NCI Monogr.* 47–60 (1988).
  286. Leibel, S. A., Fuks, Z., Zelefsky, M. J. & Whitmore, W. F. The effects of local and regional treatment on the metastatic outcome in prostatic carcinoma with pelvic lymph node involvement. *Int. J. Radiat. Oncol. Biol. Phys.* **28**, 7–16 (1994).
  287. Huggins, C. & Hodges, C. V. Studies on prostatic cancer: I. The effect of castration, of estrogen and of androgen injection on serum phosphatases in metastatic carcinoma of the prostate. 1941. *J. Urol.* **168**, 9–12 (2002).
  288. Roach, M. *et al.* Short-term neoadjuvant androgen deprivation therapy and external-beam radiotherapy for locally advanced prostate cancer: long-term results of RTOG 8610. *J. Clin. Oncol.* **26**, 585–91 (2008).

289. Bolla, M. *et al.* Long-term results with immediate androgen suppression and external irradiation in patients with locally advanced prostate cancer (an EORTC study): a phase III randomised trial. *Lancet (London, England)* **360**, 103–6 (2002).
290. Pilepich, M. V *et al.* Androgen suppression adjuvant to definitive radiotherapy in prostate carcinoma--long-term results of phase III RTOG 85-31. *Int. J. Radiat. Oncol. Biol. Phys.* **61**, 1285–90 (2005).
291. Horwitz, E. M. *et al.* Ten-year follow-up of radiation therapy oncology group protocol 92-02: a phase III trial of the duration of elective androgen deprivation in locally advanced prostate cancer. *J. Clin. Oncol.* **26**, 2497–504 (2008).
292. Bolla, M. *et al.* Duration of Androgen Suppression in the Treatment of Prostate Cancer. *N. Engl. J. Med.* **360**, 2516–2527 (2009).
293. Radiotherapy | Irish Cancer Society. (2015). Available at: <http://www.cancer.ie/cancer-information/treatments/radiotherapy#sthash.2U1WbM1P.dpbs>. (Accessed: 10th January 2016)
294. Mitchell, P. J. *et al.* Can urinary exosomes act as treatment response markers in prostate cancer? *J. Transl. Med.* **7**, 4 (2009).
295. Schnarr, K., Boreham, D., Sathya, J., Julian, J. & Dayes, I. S. Radiation-induced lymphocyte apoptosis to predict radiation therapy late toxicity in prostate cancer patients. *Int. J. Radiat. Oncol. Biol. Phys.* **74**, 1424–30 (2009).
296. Yao, B. *et al.* Estimation of the biological dose received by five victims of a radiation accident using three different cytogenetic tools. *Mutat. Res.* **751**, 66–72 (2013).
297. Samiee, S. *et al.* Dicentric Chromosome Assay: A Potential In Vitro Biomarker for Radiosensitivity. *Int. J. Radiat. Oncol.* **84**, S676–S677 (2012).
298. Hille, A. *et al.* Spontaneous and radiation-induced chromosomal instability and persistence of chromosome aberrations after radiotherapy in lymphocytes from prostate cancer patients. *Radiat. Environ. Biophys.* **49**, 27–37 (2010).
299. Martin, L. M., Marples, B., Lynch, T. H., Hollywood, D. & Marignol, L. Exposure to low dose ionising radiation: Molecular and clinical consequences. *Cancer Lett.* **349**, 98–106 (2014).
300. Resnick, M. J. *et al.* Long-term functional outcomes after treatment for localized prostate cancer. *N. Engl. J. Med.* **368**, 436–45 (2013).
301. Louis-Bar, D. Sur un syndrome progressif comprenant des télangiectasies capillaires cutanées et conjonctivales symétriques, à disposition naevoïde et des troubles cérébelleux. *Confin. Neurol.* **4**, 32–42 (1941).
302. Crawford, T. O., Skolasky, R. L., Fernandez, R., Rosquist, K. J. & Lederman, H. M. Survival probability in ataxia telangiectasia. *Arch. Dis. Child.* **91**, 610–1 (2006).
303. Oxford, J. M., Harnden, D. G., Parrington, J. M. & Delhanty, J. D. Specific chromosome aberrations in ataxia telangiectasia. *J. Med. Genet.* **12**, 251–62 (1975).

304. Waldmann, T. & Mcintire, K. R. Serum-Alpha-Fetoprotein Levels In Patients With Ataxia-Telangiectasia. *Lancet* **300**, 1112–1115 (1972).
305. Koksai, Y. *et al.* *Dysgerminoma In A Child With Ataxia–Telangiectasia. Pediatric Hematology and Oncology* (Taylor & Francis, 2009).
306. McGrath-Morrow, S. A., Collaco, J. M., Detrick, B. & Lederman, H. M. Serum Interleukin-6 Levels and Pulmonary Function in Ataxia-Telangiectasia. *J. Pediatr.* (2016). doi:10.1016/j.jpeds.2016.01.002
307. Squadrone, S. *et al.* Blood metal levels and related antioxidant enzyme activities in patients with ataxia telangiectasia. *Neurobiol. Dis.* **81**, 162–167 (2015).
308. Higurashi, M. & Conen, P. E. In vitro chromosomal radiosensitivity in ‘chromosomal breakage syndromes’. *Cancer* **32**, 380–383 (1973).
309. Scott, D., Jones, L. A., Elyan, S. A. G Spreadborough, A., Cowan, R. & Ribiero, G. Identification of AT heterozygotes. In *Ataxia-Telangiectasia. Springer Berlin Heidelberg*. 101–116 (1993).
310. Taylor, A. M. R. *et al.* Ataxia telangiectasia: a human mutation with abnormal radiation sensitivity. *Nature* **258**, 427–429 (1975).
311. Taylor, A. M. R., Metcalfe, J. A., Oxford, J. M. & Harnden, D. G. Is chromatid-type damage in ataxia telangiectasia after irradiation at G0 a consequence of defective repair? *Nature* **260**, 441–443 (1976).
312. Bender, M. A., Rary, J. M. & Kale, R. P. G2 chromosomal radiosensitivity in ataxia telangiectasia lymphocytes. *Mutat. Res. Mol. Mech. Mutagen.* **152**, 39–47 (1985).
313. Teive, H. A. G. *et al.* Ataxia-telangiectasia — A historical review and a proposal for a new designation: ATM syndrome. *J. Neurol. Sci.* **355**, 3–6 (2015).
314. Verhagen, M. M. M. *et al.* Presence of ATM protein and residual kinase activity correlates with the phenotype in ataxia-telangiectasia: a genotype-phenotype study. *Hum. Mutat.* **33**, 561–71 (2012).
315. Concannon, P. ATM homepage - LOVD - Leiden Open Variation Database - Leiden Open Variation Database. (2016). Available at: [http://chromium.lovd.nl/LOVD2/home.php?select\\_db=ATM&used\\_old\\_url](http://chromium.lovd.nl/LOVD2/home.php?select_db=ATM&used_old_url). (Accessed: 16th February 2016)
316. Shiloh, Y. ATM and related protein kinases: safeguarding genome integrity. *Nat. Rev. Cancer* **3**, 155–168 (2003).
317. Fernet, M., Moullan, N., Lauge, a, Stoppa-Lyonnet, D. & Hall, J. Cellular responses to ionising radiation of AT heterozygotes: differences between missense and truncating mutation carriers. *Br. J. Cancer* **90**, 866–73 (2004).
318. Coriell. Coriell Biorepository. (2016).
319. Cellosaurus. ExPASy Bioinformatics Resource Portal. (2016). Available at: [http://web.expasy.org/cellosaurus/CVCL\\_V545](http://web.expasy.org/cellosaurus/CVCL_V545). (Accessed: 10th February 2016)
320. Heng, H. H. Q. *et al.* Why it is crucial to analyze non clonal chromosome aberrations or NCCAs? *Mol. Cytogenet.* **9**, 15 (2016).

321. Porcedda, P. *et al.* Two-tier analysis of histone H2AX phosphorylation allows the identification of Ataxia Telangiectasia heterozygotes. *Radiother. Oncol.* **92**, 133–7 (2009).
322. Kuppuswamy, C. S. & Kannan, H. C. Localized Chromosomal Radiosensitivity as a Biomarker in Amenorrhea with Normal Karyotypes. *Int. J. Heal. Rehabil. Sci.* **1**, (2012).
323. Ierardi-Curto, L. Chromosomal Breakage Syndromes: Background, Pathophysiology, Ataxia Telangiectasia. *Medscape News and Perspectives* (2015). Available at: <http://emedicine.medscape.com/article/951148-overview>. (Accessed: 25th January 2016)
324. Bourguignon, M. H. *et al.* Genetic and epigenetic features in radiation sensitivity Part I: cell signalling in radiation response. *Eur. J. Nucl. Med. Mol. Imaging* **32**, 229–46 (2005).
325. Bentzen, S. M., Christensen, J. J., Overgaard, J. & Overgaard, M. Some methodological problems in estimating radiobiological parameters from clinical data. Alpha/beta ratios and electron RBE for cutaneous reactions in patients treated with postmastectomy radiotherapy. *Acta Oncol.* **27**, 105–16 (1988).
326. Burrill, W., Barber, J. B., Roberts, S. A., Bulman, B. & Scott, D. Heritability of chromosomal radiosensitivity in breast cancer patients: a pilot study with the lymphocyte micronucleus assay. *Int. J. Radiat. Biol.* **76**, 1617–9 (2000).
327. Andreassen, C. N., Alsner, J. & Overgaard, J. Does variability in normal tissue reactions after radiotherapy have a genetic basis – where and how to look for it? *Radiother. Oncol.* **64**, 131–140 (2002).
328. Andreassen, C. Prediction of normal tissue radiosensitivity from polymorphisms in candidate genes. *Radiother. Oncol.* **69**, 127–135 (2003).
329. Fernet, M. & Hall, J. Genetic biomarkers of therapeutic radiation sensitivity. *DNA Repair (Amst)*. **3**, 1237–43 (2004).
330. Ho, A. Y. *et al.* Genetic Predictors of Adverse Radiotherapy Effects: The Gene-PARE project. *Int. J. Radiat. Oncol. Biol. Phys.* **65**, 646–655 (2006).
331. Kabacik, S. *et al.* Gene expression following ionising radiation: identification of biomarkers for dose estimation and prediction of individual response. *Int. J. Radiat. Biol.* **87**, 115–129 (2011).
332. Waga, S., Hannon, G. J., Beach, D. & Stillman, B. The p21 inhibitor of cyclin-dependent kinases controls DNA replication by interaction with PCNA. *Nature* **369**, 574–8 (1994).
333. Cazzalini, O. *et al.* CBP and p300 acetylate PCNA to link its degradation with nucleotide excision repair synthesis. *Nucleic Acids Res.* **42**, 8433–48 (2014).
334. Wang, C. *et al.* Up-regulation of p21WAF1/CIP1 by miRNAs and its implications in bladder cancer cells. *FEBS Lett.* **588**, 4654–4664 (2014).
335. Mailand, N., Gibbs-Seymour, I. & Bekker-Jensen, S. Regulation of PCNA–protein interactions for genome stability. *Nat. Rev. Mol. Cell Biol.* **14**, 269–282 (2013).



336. Cayrol, C., Knibiehler, M. & Ducommun, B. p21 binding to PCNA causes G1 and G2 cell cycle arrest in p53-deficient cells. *Oncogene* **16**, 311–20 (1998).
337. Budanov, A. V, Sablina, A. A., Feinstein, E., Koonin, E. V & Chumakov, P. M. Regeneration of peroxiredoxins by p53-regulated sestrins, homologs of bacterial AhpD. *Science* **304**, 596–600 (2004).
338. Budanov, A. V & Karin, M. p53 target genes sestrin1 and sestrin2 connect genotoxic stress and mTOR signaling. *Cell* **134**, 451–60 (2008).
339. Correa, C. R. & Cheung, V. G. Genetic variation in radiation-induced expression phenotypes. *Am. J. Hum. Genet.* **75**, 885–90 (2004).
340. Kopnin, P. B., Agapova, L. S., Kopnin, B. P. & Chumakov, P. M. Repression of sestrin family genes contributes to oncogenic Ras-induced reactive oxygen species up-regulation and genetic instability. *Cancer Res.* **67**, 4671–8 (2007).
341. Hwang, P. M. *et al.* Ferredoxin reductase affects p53-dependent, 5-fluorouracil-induced apoptosis in colorectal cancer cells. *Nat. Med.* **7**, 1111–7 (2001).
342. Stoimenov, I. & Helleday, T. PCNA on the crossroad of cancer. *Biochem. Soc. Trans.* **37**, 605–13 (2009).
343. Braunstein, S., Badura, M. L., Xi, Q., Formenti, S. C. & Schneider, R. J. Regulation of protein synthesis by ionizing radiation. *Mol. Cell. Biol.* **29**, 5645–56 (2009).
344. El-Saghire, H. *et al.* Gene set enrichment analysis highlights different gene expression profiles in whole blood samples X-irradiated with low and high doses. *Int. J. Radiat. Biol.* **89**, 628–38 (2013).
345. Whitney, A. R. *et al.* Individuality and variation in gene expression patterns in human blood. *Proc. Natl. Acad. Sci. U. S. A.* **100**, 1896–901 (2003).
346. Finnon, P. *et al.* Correlation of in vitro lymphocyte radiosensitivity and gene expression with late normal tissue reactions following curative radiotherapy for breast cancer. *Radiother. Oncol.* **105**, 329–36 (2012).
347. Zhou, T. *et al.* Ataxia telangiectasia-mutated dependent DNA damage checkpoint functions regulate gene expression in human fibroblasts. *Mol. Cancer Res.* **5**, 813–22 (2007).
348. György, B. *et al.* Membrane vesicles, current state-of-the-art: Emerging role of extracellular vesicles. *Cell. Mol. Life Sci.* **68**, 2667–2688 (2011).
349. TRAMS, E., LAUTER, C., NORMANSALEM, J. & HEINE, U. Exfoliation of membrane ecto-enzymes in the form of micro-vesicles. *Biochim. Biophys. Acta - Biomembr.* **645**, 63–70 (1981).
350. Harding, C., Heuser, J. & Stahl, P. Endocytosis and intracellular processing of transferrin and colloidal gold-transferrin in rat reticulocytes: demonstration of a pathway for receptor shedding. *Eur. J. Cell Biol.* **35**, 256–63 (1984).
351. Kowal, J., Tkach, M. & Théry, C. Biogenesis and secretion of exosomes. *Curr. Opin. Cell Biol.* **29**, 116–125 (2014).
352. Danesh, A. *et al.* Exosomes from red blood cell units bind to monocytes and induce

- proinflammatory cytokines, boosting T-cell responses in vitro. *Blood* **123**, 687–96 (2014).
353. Aatonen, M. T. *et al.* Isolation and characterization of platelet-derived extracellular vesicles. *J. Extracell. vesicles* **3**, (2014).
354. Ju, R. *et al.* Angiopoietin-2 secretion by endothelial cell exosomes: regulation by the phosphatidylinositol 3-kinase (PI3K)/Akt/endothelial nitric oxide synthase (eNOS) and syndecan-4/syntenin pathways. *J. Biol. Chem.* **289**, 510–9 (2014).
355. Montecalvo, A. *et al.* Mechanism of transfer of functional microRNAs between mouse dendritic cells via exosomes. *Blood* **119**, 756–66 (2012).
356. Kozomara, A. & Griffiths-Jones, S. miRBase. Available at: <http://www.mirbase.org/>. (Accessed: 17th February 2016)
357. BARTEL, D. MicroRNAs Genomics, Biogenesis, Mechanism, and Function. *Cell* **116**, 281–297 (2004).
358. Wang, C. *et al.* A Five-miRNA Panel Identified From a Multicentric Case–control Study Serves as a Novel Diagnostic Tool for Ethnically Diverse Non-small-cell Lung Cancer Patients. *EBioMedicine* 1–9 (2015). doi:10.1016/j.ebiom.2015.07.034
359. Mishra, S., Srivastava, A. K., Suman, S., Kumar, V. & Shukla, Y. Circulating miRNAs revealed as surrogate molecular signatures for the early detection of breast cancer. *Cancer Lett.* (2015). doi:10.1016/j.canlet.2015.07.045
360. Kara, M. *et al.* Differential expressions of cancer-associated genes and their regulatory miRNAs in colorectal carcinoma. *Gene* **567**, 81–86 (2015).
361. Hu, S. *et al.* Infiltrating T cells promote prostate cancer metastasis via modulation of FGF11→miRNA-541→androgen receptor (AR)→MMP9 signaling. *Mol. Oncol.* **9**, 44–57 (2015).
362. Tang, M. & Xie, Y.-J. The Role of miRNAs in Prostate Cancer. *J. Gastrointest. Dig. Syst.* **03**, 3–5 (2013).
363. Cheng, G. Circulating miRNAs : Roles in cancer diagnosis , prognosis and therapy. *Adv. Drug Deliv. Rev.* **81**, 75–93 (2015).
364. Jella, K. K. *et al.* Exosomes are involved in mediating radiation induced bystander signaling in human keratinocyte cells. *Radiat. Res.* **181**, 138–45 (2014).
365. Al-Mayah, A. H. J., Irons, S. L., Pink, R. C., Carter, D. R. F. & Kadhim, M. a. Possible Role of Exosomes Containing RNA in Mediating Nontargeted Effect of Ionizing Radiation. *Radiat. Res.* **177**, 539–545 (2012).
366. Ye, C. *et al.* MicroRNA-145 contributes to enhancing radiosensitivity of cervical cancer cells. *FEBS Lett.* **589**, 702–9 (2015).
367. He, Z., Liu, Y., Xiao, B. & Qian, X. miR-25 modulates NSCLC cell radiosensitivity through directly inhibiting BTG2 expression. *Biochem. Biophys. Res. Commun.* **457**, 235–41 (2015).
368. Lee, K. M., Choi, E. J. & Kim, I. A. microRNA-7 increases radiosensitivity of

- human cancer cells with activated EGFR-associated signaling. *Radiother. Oncol.* **101**, 171–6 (2011).
369. Guo, P. *et al.* MiR-26a enhances the radiosensitivity of glioblastoma multiforme cells through targeting of ataxia-telangiectasia mutated. *Exp. Cell Res.* **320**, 200–8 (2014).
370. Liang, L. *et al.* MicroRNA-223 enhances radiation sensitivity of U87MG cells in vitro and in vivo by targeting ataxia telangiectasia mutated. *Int. J. Radiat. Oncol. Biol. Phys.* **88**, 955–60 (2014).
371. O'Brien, K. *et al.* Exosomes from triple-negative breast cancer cells can transfer phenotypic traits representing their cells of origin to secondary cells. *Eur. J. Cancer* **49**, 1845–59 (2013).
372. Shiiba, M. *et al.* MicroRNA-125b regulates proliferation and radioresistance of oral squamous cell carcinoma. *Br. J. Cancer* **108**, 1817–21 (2013).
373. Roush, S. & Slack, F. J. The let-7 family of microRNAs. *Trends Cell Biol.* **18**, 505–516 (2008).
374. Papagiannakopoulos, T., Shapiro, A. & Kosik, K. S. MicroRNA-21 targets a network of key tumor-suppressive pathways in glioblastoma cells. *Cancer Res.* **68**, 8164–72 (2008).
375. Thum, T. *et al.* MicroRNA-21 contributes to myocardial disease by stimulating MAP kinase signalling in fibroblasts. *Nature* **456**, 980–4 (2008).
376. Kulshreshtha, R. *et al.* A microRNA signature of hypoxia. *Mol. Cell. Biol.* **27**, 1859–67 (2007).
377. Gao, J. & Liu, Q.-G. The role of miR-26 in tumors and normal tissues (Review). *Oncol. Lett.* **2**, 1019–1023 (2011).
378. Zhang, T. *et al.* MiR-451 increases radiosensitivity of nasopharyngeal carcinoma cells by targeting ras-related protein 14 (RAB14). *Tumour Biol.* **35**, 12593–9 (2014).
379. Gu, X., Li, J.-Y., Guo, J., Li, P.-S. & Zhang, W.-H. Influence of MiR-451 on Drug Resistances of Paclitaxel-Resistant Breast Cancer Cell Line. *Med. Sci. Monit.* **21**, 3291–7 (2015).
380. Ghandhi, S. A. *et al.* Radiation dose-rate effects on gene expression for human biodosimetry. *BMC Med. Genomics* **8**, 22 (2015).
381. Asashima, M. *et al.* Checkpoint mechanisms in the cell cycle | Introduction to Life Science | University of Tokyo. *A comprehensive approach to life science* (2011). Available at: [http://cslls-text3.c.u-tokyo.ac.jp/active/13\\_03.html](http://cslls-text3.c.u-tokyo.ac.jp/active/13_03.html). (Accessed: 15th October 2015)
382. Favalaro, B., Allocati, N., Graziano, V., Di Ilio, C. & De Laurenzi, V. Role of apoptosis in disease. *Aging (Albany. NY)*. **4**, 330–349 (2012).
383. Lucia Comet Assay. 1 (2016). Available at: <http://www.lucia.cz/en/front-page/lucia-comet-assay>. (Accessed: 23rd May 2016)

384. Radiation Biology Centre. Chromatid Type Aberrations. 1 (2009). Available at: <http://www.rbc.kyoto-u.ac.jp/db/MSSFiles/Criteria2.html>. (Accessed: 25th November 2015)

## **10. APPENDICES**

### **10.1 Inclusion/Exclusion Criteria for Prostate Cancer Donor Recruitment**

#### **Inclusion Criteria:**

1. Patients undergoing a radical course of RT for high-risk disease (defined according to the National Comprehensive Cancer Network Practice Guidelines in Oncology v.1 as one or more of the NCCN high risk criteria > or equal to T3, > or equal to Gleason 8, PSA > 20ng/ml)
2. Only patients requiring neo-adjuvant / adjuvant hormonal therapy will be included in this study
3. Absence of distant metastases as demonstrated by history and physical examination, FBC, screening profile including liver function tests, PSA and bone scan
4. All patients must have an MRI/CT of the prostate and pelvis to investigate the nodal status and precise T-stage. This MRI/CT scan must be performed prior to commencement of hormonal therapy. Suspicious nodes need to be histologically proven to be benign before the patient can be included in the study). M0 on staging.
5. No previous surgery for urinary conditions except TURP or TRUS
6. KPS > or equal to 60
7. Age >18 years
8. Provision of written informed consent in line with ICH-GCP guidelines

#### **Exclusion Criteria:**

1. Previous RT to the pelvic region

2. The patient has nodal involvement or it is decided to electively treat pelvic lymph nodes
3. The patient has had a bilateral orchiectomy
4. The patient has previously received a full course of hormonal treatment for his prostate cancer
5. The patient has or has had other malignancies within the last 5 years (non-melanoma skin cancer is permitted)
6. Evidence of any other significant clinical disorder or laboratory finding that makes it undesirable for the patient to participate in the trial or if it is felt by the research/ medical team that the patient may not be able to comply with the protocol
7. Patients who have had a prostatectomy
8. The presence of hip prostheses

## 10.2 Reagents, Suppliers and Catalogue numbers

<u>Product</u>	<u>Company</u>	<u>Catalogue Number</u>
<b><u>Blood, Lymphocyte extraction and Cell Culture</u></b>		
Vacutainers	Sarstedt	04.1921.100
RPMI	Sigma	R8758 LOT# RNBC7450
MEM-F12	Sigma	M2279
PHA	PAA Laboratories	J01-006 LOT# J00612-0914
Dulbecco's PBS	Sigma	D8537 LOT#RNBC28878
Histopaque - 1077	Sigma	10771
L-Glutamine	ThermoFisher Scientific	25030081
Penicillen-Streptomycin	Gibco	15070063
<b><u>G2 Chromosomal Radiosensitivity Assay</u></b>		
Colcemid	Gibco	J01-003 LOT# J00312-0259
Potassium Chloride	Sigma	P3911-500g 077K0024
Methanol	Sigma	32213-2.5L LOT# 5ZBC1035V
Acetic Acid	Merck Millipore	K42840763141
Gurr's pH 6.8 buffer	VWR	331932D 111952
Giemsa	Sigma	WG16-500ml 71M4343
DPX	VWR	360294H Batch#HX135994
<b><u><math>\gamma</math>H2AX Assay</u></b>		
Paraformaldehyde	Sigma	F8775-500ML
Triton - X	Sigma	T8787-50ML
Anti-Phospho Histone H2AX	Millipore	Clone JBW301 CAT#05- 636
Alexa Fluor 488	Invitrogen	A11017
Propidium Iodide	Sigma	P4864
<b><u>RNA/ DNA Extraction, Quantification and Qualitation</u></b>		
Rnase Away	Fisher Scientific	7002
Tri Reagent BD	Sigma	T3809-200mls LOT#SLBC3837V
Chloroform	Sigma	B9673-200mls LOT#MKBP2795V
Isopropanol	Sigma	19516 - 500mls LOT#SHBB6114V
Ethanol	Merck Millipore	K38656983 817
Qiagen Blood and Tissue Kit	Qiagen	69504 133218099
Agarose	Sigma	A9539 - 50g 071M0551V
Bionic Buffer	Sigma	B6185 - 1L 035k6143

Gel Red	Biotium	41003
1kb plus RNA Ladder	Invitrogen	10787-018
0.5 - 10kb RNA Ladder	Invitrogen	15623-200
6 x DNA	Invitrogen	10787-017
<b><u>CDNA Synthesis, RT-PCR and MORTPCR</u></b>		
PerfeCTa ® MultiPlex qPCR SuperMix	Quanta Biosciences	Cat# 95063-200
3'6-Carboxyfluorescein (FAM)	Eurogentec Ltd	MD-FL001-03100
6-Hexachlorofluorescein (HEX)	Eurogentec Ltd	MD-FL010-05100
Texas Red	Eurogentec Ltd	AS-81130
CY5	Eurogentec Ltd	Cat#81255
<b><u>FISH</u></b>		
DAPI Stain	Fisher Scientific	10374168
IGH, Breakapart Probe	Abbott	05J73-001
ATM/TP53 Dual Colour Probe	Abbott	08L53-020
CEP X Probe	Abbott	06N29-020
<b><u>Protein Extraction, Western Blotting</u></b>		
RIPA Buffer	Sigma	R0278
BioRad DC Protein Estimation Kit	Biorad	Cat#5000111
SDS	Sigma	L3771-100G
Acrylamide	Biorad	1610180
Tris Base	Sigma	11814273001
Ammonium Persulfate	Sigma	A3678-100G
Temed	Sigma	T9281-25ML
Prestained Protein Ladder	ThermoFisher Scientific	10748010
1% Low Fat Powdered Milk	Marvel	N/a
Nitrocellulose Membrane	Biorad	162-0115
TSG101	Abcam	AB83
HRP	BioLegend	Cat#405306
ECL	Pierce	Cat#32106
<b><u>Other</u></b>		
ApoTox Kit	Promega	Cat#G6320



## 10.3 Protocols used in this thesis

### Tissue Culture

#### 1.1. G2 Blood Culture

- a) 3x 2ml cultures are set up for different doses.
- b) Put 2mls of whole blood into each T25 flask.
- c) Add 18mls of prewarmed media.
- d) Add 200 $\mu$ l of PHA
- e) Wrap in tinfoil and incubate standing upright in incubator for 3 days.

#### 1.2. Separation of monocytes from lymphocytes by plastic adhesion for Raman

- a) Count cell/PBS suspension
- b) Plate at approx.  $5 \times 10^6$  cells in 8 cm<sup>2</sup> tissue culture dishes (Nunc)
- c) Incubate 2 h at 37°C, 5% CO<sub>2</sub>.
- d) Non-adherent cells (lymphocytes) can be pelleted and resuspended in full media and further cultured.
- e) Wash adherent cells (monocytes) with pre-warmed PBS and further cultured in fresh full media.
- f) Set up 4 x 2ml cell cultures, (monocytes and lymphocytes) add 18mls of media, and 200 $\mu$ l of PHA. and Culture for 3 days.

#### 1.3. Histopaque Isolation of LCL's for Raman Spectroscopy

- a) To a 15ml conical centrifuge tube, add 3ml of Histopaque – 1077 and bring to room temperature.
- b) Carefully layer 3ml of whole blood on to histopaque.

- c) Centrifuge at 400g for exactly 30mins at room temperature. Centrifugation at lower temperatures results in cell clumping.
- d) After centrifugation, carefully aspirate the upper layer with a Pasteur pipette to within 0.5cm of the opaque interface containing mononuclear cells. Discard upper layer.
- e) Carefully transfer the opaque interface with a Pasteur pipette into a clean conical centrifuge tube.
- f) Wash the cells by adding 10mls of isotonic PBS or appropriate cell culture medium, and mix by gently drawing in and out of Pasteur pipette.
- g) Centrifuge at 250g for 10mins.
- h) Aspirate the supernatant and discard.
- i) Resuspend the cell pellet with 5ml of isotonic PBS or appropriate cell culture medium and mix.
- j) Centrifuge at 250g for 10mins
- k) Repeat steps for washing, discard supernatant and resuspend cell pellet in 0.5mls of PBS.

#### 1.4. Lymphoblastoid Cell Line Culture

- A. LCL's were maintained in standard RPMI medium (Sigma) supplemented with 10% Foetal bovine serum (FBS), L-Glutamine and incubated at 37°C with 5% CO<sub>2</sub>.
- B. 2139, AT2Bi and AT3Bi were sub cultured 3 times weekly
- C. 2145 was sub cultured weekly

## 2. Irradiation Procedures

- A. All Irradiations carried out in St. Luke's Hospital, Rathgar, Dublin
- B.  $^{60}\text{Co}$  irradiations conducted using Teletherapy unit (Theratron 780 E, MDS Canada)
- C. Linac Irradiations conducted using 6 MV photon beam and a 12 MeV electron beam on an Elekta Precise Linac.
- D. Doses of 0.05Gy, 0.5Gy, 2Gy and 5Gy were delivered to cells (explained throughout chapters)

### 3. Cytogenetics

#### 3.1. G2 Chromosomal Radiosensitivity Assay

- A. Add 0.2ml colcemid (10 $\mu\text{g/ml}$ ) 30mins post irradiation and leave for 60mins.
- B. Split the contents of each flask between 2 x 12.5ml plastic centrifuge tubes and plunge the tubes into a bucket of ice: agitate to cool rapidly.
- C. Spin at 1000rpm for 5 mins (Refrigerated centrifuge)
- D. Remove supernatant, add 5ml pre cooled 0.075M KCL and leave in the ice bucket for 20mins.
- E. Spin at 1000rpm for 5mins
- F. Remove supernatant to about 1ml above cell pellet, mix cells, add freshly made fixative (3:1 Methanol: Glacial acetic acid) and mix.
- G. Spin immediately at 1000rpm for 5mins, change fixative and leave in fridge overnight. (Can be left longer if necessary).
- H. Allow the cells to come to room temperature, wash in fresh fixative twice and make slides.
- I. Stain in 2% Giemsa (GURRS) in PH 6.8 buffer for 5mins. Rinse in tap water, clear in xylene and mount in DPX.

### Scoring

- J. All aberrations are scored. These will be mainly chromatid gaps and breaks with a few isochromatid breaks and exchanges. When calculating aberration yields we exclude exchanges because there is evidence that repair involving exchanges is different from that involving repair of breaks.
- K. Gaps are only counted if they are wider than the diameter of the chromatid. Inclusion of smaller gaps gives greater variability of results.
- L. Subtract spontaneous yields from yields observed in irradiated cells to obtain the yield of radiation-induced aberrations.

### 3.2. G-Banding

- a) Age the slides for 1 minute in the UV box.
- b) Place the slide on the slide rack and cover with 30% hydrogen peroxide solution for one minute
- c) Using a plastic transfer pipette, rinse the slide with 0.9% NaCl solution
- d) Place the slide in the trypsin solution for the selected time. This time will vary depending on the conditions in the lab
- e) Start the timer
- f) Using 1ml plastic transfer pipettes, make up the stain solution (banding strength) in plastic Universal container; one part Leishmann stain and two parts Gurr buffer
- g) Stop the timer

- h) Remove the slide from the trypsin solution and rinse with 0.9% NaCl solution
  
- i) Using a plastic transfer pipette, rinse with Gurr buffer and place the slide on the slide rack
  
- j) Flood the slide with the stain solution and set the timer for 1 minute
  
- k) After 1 minute, using a plastic transfer pipette, rinse the slide with Gurr buffer and immediately with distilled water
  
- l) Carefully drain the excess water from the slide on to tissue. Dry the back of the slide and the frosted part of the slide using tissue taking care not touch the front of the slide
  
- m) Put the slide on to the slide dryer and allow the surface to dry completely
  
- n) Place the slide on some tissue and drop a small amount of DPX mountant on the surface of the slide
  
- o) Put a coverslip on the centre of the slide taking care to avoid all air bubbles
  
- p) Put the slide on to the slide dryer, which is located within a fume hood, until the DPX mountant is completely dry
  
- Evaluate the slide under the microscope set up for bright-field use, noting conditions of under or over banding or staining

Fix spacing here. No need for so much spacing

- Adjust the amount of time in trypsin and hydrogen peroxide as necessary (see troubleshooting notes) until a test slide produces acceptable banding results.
- Run the remaining slide required for analysis through the banding protocol using the times determined by the test run(s)

### 3.3. Fluorescent *In Situ* Hybridisation

#### Harvesting Protocol

#### PROCEDURE

This method follows on from DOC249 *Set-Up of Cultures from Postnatal Solid Tissue*.

- Ensure the laminar flow hood is running efficiently DOC321 and wipe the working area with 1% Virkon
- Flasks are assessed for growth. On the day of harvest, remove the samples from the incubator and place in the sample rack within the laminar flow hood
- Using a sterile 1ml pipette add 100ul of colcemid (CT) and return to the CO<sub>2</sub> incubator for 1hrs. Write 'C' on the flask with a water resistant felt tip pen indicating that colcemid has been added
- Following 1hr incubation, the flasks are returned to the hood. Label sterile 15ml centrifuge tubes with pre-printed patient laboratory labels, the corresponding unique letter and date and place in the hood
- The culture medium is removed and placed in the corresponding pre-labelled tube.
- Using a 1ml pipette, transfer the media containing the suspended cells with colcemid from the flask into the appropriately labelled 15ml tube.
- Centrifuge tubes for 10 minutes at 1000 rpm
- Pour off supernatant into 1% Virkon, and resuspend the pellet by gently flicking the base of each tube
- Add excess (8-10ml) pre-warmed 0.075M KCl (**KCl**) to each tube. Invert each tube to ensure proper mixing and return to the incubator for 20 minutes
- After 20 minutes place the tubes in the centrifuge. Add any appropriate balances, seal buckets and spin for 10 minutes at 1000 rpm

- k. Following centrifugation, return the tubes to the hood, remove the supernatant and resuspend the pellet by gently flicking the base of each tube. At this point, remove tubes from the long term tissue culture laboratory. The remainder of the procedure is carried out in cytogenetic laboratory 2
- l. Using a sterile 1ml pipette, add ~1ml of fresh 3:1 fixative to each tube in a drop-wise manner. Mix continuously by gently flicking the base of each tube
- m. Top up the flask to 10ml using the fresh 3:1 fixative
- n. Place the tubes in the centrifuge. Add any appropriate balances, seal buckets and spin for 10 minutes at 1000rpm
- o. Following centrifugation, remove the supernatant leaving approximately 0.5ml in each tube. Resuspend the pellet by gently flicking the base of each tube
- p. Top up the flask to 10ml using the fresh 3:1 fixative
- q. Repeat steps q) & r) for a total of 3 times
- r. Following centrifugation, remove the supernatant leaving approximately 0.5-1ml in each tube depending on the size of the pellet
- s. Samples are now ready for slide making

### Slide Making Protocol

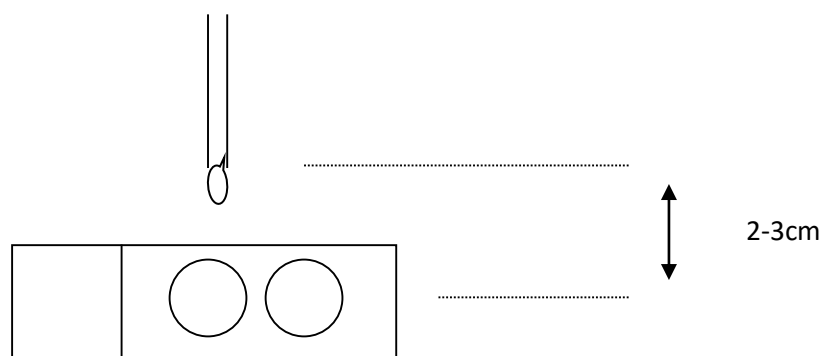
#### PROCEDURE

##### **Notes**

- Only one sample should be open at any one time
  - Label slides in pencil by copying the patient name, lab number, your initials, and culture ID to the slide immediately after dropping the suspension
  - While slides are drying they should be placed to avoid any splashes etc. arising when slides from subsequent cultures are prepared
  - A maximum of 4 slides will be made on each culture unless otherwise specified
  - Any changes to the slide making protocol must be discussed with a senior staff member and documented prior to the change
- A. Place the tubes containing the cell suspensions in the centrifuge and spin at 1500rpm for 5 minutes (last stage of harvest, see appropriate procedure for specimen type)

- B. Place a single sheet of clean tissue paper on the hotplate B set at 7.1 on the dial in the Down flow slide making hood
- C. Place 1-2 clean sheet(s) of tissue paper in front of you in the Down flow slide making hood for blotting slides
- D. Uncap one tube and remove the supernatant using a pipette and discard into a waste container taking care not to disturb the pellet
- E. If required, use a 3ml plastic pipette to add fresh Carnoy 3:1 fixative drop-wise until the suspension is slightly cloudy and discard pipette into waste container
- F. Using the forceps remove one slide from the beaker containing slides in fresh cold distilled water. When taking the slide out of the beaker the water should be retained on the slide.
- G. Keeping the slide horizontal, holding a fresh 3ml pipette at approximately 2-3cm away from the slide add two drops of cell suspension towards the middle of the slide (see Fig 1)
- H. Place the slide on clean tissue paper
- I. Using the pencil, clearly copy the lab number, patient initial and surname; culture type, slide number and your initials to the frosted part of the slide
- J. Return the remaining supernatant to the open culture tube
- K. Discard the pipette into waste container

**Fig 1: Slide making technique**



- A. Place the slide on the tissue on the hotplate to dry
- B. Once the slide has dried, assess its suitability under phase contrast microscope, see below



- C. If the metaphases look unsuitable for analysis and the slide-making may need modification
- D. Troubleshoot and repeat points g) to m)
- E. If the slide is suitable make the remaining 3 slides in the same way f)-j)
- F. Recap the tube
- G. Place slides from each patient on an individual slide tray, cover the tray and move it away from slide making area
- H. Repeat process for each sample
- I. Initial the set-up/harvest list and file in constitutional set-up/harvest list folder

#### 4. Molecular Extractions

##### 4.1. Protein Extraction

Procedure for lysis of suspension cultured cells as per RIPA protocol (Sigma)

- A. Pellet the cells by centrifugation at 450 x g for 5 minutes.
- B. Carefully remove the medium from the cell pellet by decantation or aspiration.
- C. Wash the cells to remove residual medium. Add a volume of a physiological wash solution, such as DPBS, equal to the original medium volume. Mix or vortex briefly to resuspend the cells completely.
- D. Centrifuge for 5 minutes at 450 x g to pellet the cells and carefully remove wash solution supernatant. Repeat the wash once in order to remove any other minor contaminants. More washing steps can be done, but two is usually sufficient to remove nearly all of the contaminants.
- E. After removal of the final wash solution from the cells, add an appropriate volume of RIPA Buffer (1 ml per 0.5 to 5 x 10<sup>7</sup> cells) to the cell pellet, and mix or vortex briefly to resuspend the cells completely. Incubate on ice or in a refrigerator (2–8 °C) for five minutes. Vortex briefly to resuspend and lyse residual cells.
- F. The lysate can either be used immediately or quick frozen in liquid nitrogen and stored at –70 °C for future use.

- G. Clarify the lysate by centrifugation at 8,000 x g for 10 minutes at 4 °C to pellet the cell debris.
- H. Note: If a mucoid aggregate of denatured nucleic acids is present, carefully remove it with a micropipette before centrifugation.
- I. Carefully transfer the supernatant containing the soluble protein to a tube on ice for immunoprecipitation or other analysis.

Protein estimation using the Bio Rad DC protein estimation kit

### **Method**

- A. Mix 500ul of solution A to 10ul of reagent S into a fresh Eppendorf and label it Mix/Reagent A.
- B. Pipette 2.5ul of each standard in descending order in the labelled wells in a micro-titre 96 well plate.
- C. Pipette 2.5ul of each sample in triplicate in three wells
- D. Pipette 25ul of the mix/reagent A solution to all of the wells used in the plate
- E. Pipette 200ul of Reagent B to all of the used wells also
- F. Mix gently
- G. Read on spec at 705nm

Note: **The standards are BSA made up in the protein lysis buffer at concentrations of 2mg/ml to 10mg/ml**

### 4.2. RNA Extraction

#### Cell Lysis

- A. Add 200µl of blood to 1ml of Tri Reagent. Store in -80 At This Stage
- B. Shake well or vortex

#### Phase Separation

- C. Store for 5mins @ RT

- D. Add 200µl of chloroform
- E. Cover and shake for 15 seconds
- F. Store @ RT for 2-5mins
- G. Centrifuge @ 12000g for 15mins @4°C
- H. Transfer aqueous (colourless) layer to new tube (RNA)

#### RNA Precipitation

- I. Add 500µl of Isopropanol
- J. Store @ RT for 5-10mins
- K. Centrifuge @ 12000g for 10mins @4-25°C
- L. Gel or white pellet forms

#### RNA Wash

- M. Remove supernatant
- N. Mix RNA pellet in 1ml of 75% ethanol & vortex
- O. Centrifuge @12000g for 5mins @4 - 25°C

#### RNA Solubilisation

- P. Remove ethanol wash
- Q. Air dry RNA pellet for 5mins (do not let dry completely)
  - Dissolve RNA in 50µl of DEPC treated water or 0.5% SDS

#### 4.3. DNA Extraction (DNeasy Blood and Tissue DNA extraction Kit)

##### **Before Starting:**

- A. Buffer AL may form precipitate in storage. If necessary, warm to 56°C until fully dissolved
- B. For step 2, Buffer AL *without* added ethanol is needed

- C. Buffer AW1 and AW2 are concentrates. Ensure appropriate amount of ethanol (96%-100%) has been added to make a working solution
- D. Preheat a thermomixer/shaking water bath/rocking platform to 56°C for use in step 2

### **Protocol**

- A. Non nucleated blood – Pipette 20µl of proteinase k into a 1.5ml or 2ml micro centrifuge tube. Add 50-100µl of anti-coagulated blood. Adjust volume to 220µl with PBS.
- B. Add 200µl of Buffer AL without Ethanol. Mix by vortexing and incubate at 56°C for 10mins
- C. Add 200µl of ethanol (96%-100%) to sample, mix by vortexing
- D. Pipette mix into DNeasy mini spin column placed in a 2ml collection tube (provided). Centrifuge at >6000xg for 1min. Discard flow through and collection tube
- E. Place DNeasy mini spin column in a new 2ml collection tube, add 500µl of Buffer AW1 and centrifuge for 1min at >6000xg. Discard flow through and collection tube.
- F. Place DNeasy mini spin column in a new 2ml tube, add 500µl of Buffer AW2 and centrifuge for 3mins at 20,000xg to dry the DNeasy membrane. Discard flow through and collection tube
- G. Place DNeasy mini spin column in a clean 1.5ml/2ml micro centrifuge tube (not provided) and pipette 200µl of buffer AE directly on to DNeasy membrane. Incubate at RT for 1min, then centrifuge for 1min at >6000xg to elute
- H. Repeat step 7 for maximum DNA yield

Estimate: Protocol steps = 25mins, Preparation time = 15mins, Between steps = 15mins

Total Estimated Time = 55mins → 1hr

## 5. Assays for Radiobiological Studies

### 5.1. Cell survival

- E. 1hr before irradiation, subculture cells (LCL's) in concentrations of  $1 \times 10^5$ /ml (5mls total)
- F. Irradiate flasks at 0.05Gy, 0.5Gy, 2Gy and sham irradiate 0Gy control
- G. Incubate in incubator at 37°C in 5% Co<sub>2</sub> for 72hrs
- H. Using coulter counter, do cell counts in triplicate on all cell lines and doses
- I. Repeat experiment x3 times

### 5.2. $\gamma$ H2AX flow and confocal

#### 5.2.1. $\gamma$ H2AX Foci Induction by Confocal Microscopy

- A. Centrifuge samples 400g 5mins
- B. Resuspend in 500ul Triton X solution
- C. Incubate 5mins RT
- D. Spin 400g 5mins
- E. Resuspend in 200ul blocking solution
- F. Incubate 30mins RT
- G. Centrifuge 400g 5mins
- H. Resuspend in 150ul Primary AB solution
- I. Incubate 2hrs at RT (or overnight in fridge)

- J. PBS Wash x 3 (500ul 400g 5mins)
- K. Resuspend in 150ul Secondary AB solution
- L. Incubate in dark 1hr
- M. PBS Wash x 3 (500ul 400g 5mins)
- N. Resuspend in 100ul PI Solution
- O. Incubate 10mins RT
- P. PBS Wash x 3 (500ul 400g 5mins)
- Q. Resuspend in 100ul of PBS
- R. Make cytopins – 800rpm 5mins
- S. Mount with vectashield and secure with nail varnish
- T. Store in fridge until use

#### 5.2.2. Confocal Microscope Parameters

- A. Machine is switched on and let to set up for 10-15 mins (noises are normal)
- B. Open LSM and click ‘Scan New Image’ and ‘Start Expert Mode’
- C. To set up go to ‘File’ and ‘Acquire only’
- D. Acquire laser 2 → Argon (Standby first) then on
- E. Acquire laser → Hene1 (on)
- F. Go to micro – objective – change to low power for starting
- G. Transmitted light – configure – fitc/rhodamine → apply
- H. Made new database – filename is ‘Lisa’ under gammaH2AX
- I. If coming back, just load the file by ‘open database’ and click ‘Re-use’
- J. Lasers are always first thing to configure. Check back and they should be ready, with Argon at 50%
- K. When beginning to scan slides, click micro and scan control. Multiple windows will remain open on the monitor for use back and fourth

- L. Use objective x10 or x20 to begin and setting PH1 on the microscope
- M. Load slide face down and focus using 'Vis' on computer and make sure the transmission light is on
- N. Find cluster of cells and focus
- O. Take slide off, chose oil objective and change to setting PH3 on microscope
- P. Drop of oil on the slide and place face down on lens of microscope
- Q. Focus cells then click 'LSM'
- R. Click fast xy and split xy so channels can be observed and focused on the monitor
- S. Adjust palette by clicking 'range detector.' Here you can adjust gain, but record the numbers to use the same settings for one experiment throughout
- T. Adjust background by clicking 'Amplifier offset'
- U. Minimum of 100 cells per slide are recorded
- V. Turn lasers off (Argon goes on standby first until ready to switch off)
- W. Close all other windows
- X. Clean lens with Zeiss solution and clean slide
- Y. Wait for fan of the laser control to switch off before switching computer and machine off

### 5.3. Flow cytometry parameters

- A. Samples up to step 14, part 5.2.1 were resuspended in 1ml of PI/ PBS solution per sample
- B. Measure total, median and mean fluorescence intensity of H2AX using a CyFlow (Partec) flow cytometer.
- C. Record a minimum of 10,000 events per sample
- D. On the monitor, exclude cell aggregates and debris by forward and side scatter discriminative characteristics

### 5.4. Cell Viability/Cytotoxicity/Caspase Activation

These were measured using ApoTox kit (Promega)

- A. Thaw each assay component as follows:
- B. Assay Buffer: 37°C water bath
- A. GF-AFC Substrate: 37°C water bath
- B. bis-AAF-R110 Substrate: 37°C water bath
- C. Caspase-Glo® 3/7 Buffer: Room temperature
- D. Caspase-Glo® 3/7 Substrate: Room temperature
- E. Transfer the contents of the GF-AFC Substrate and bis-AAF-R110 Substrate into 2.0 or 2.5ml of Assay Buffer, depending on the plate format used.
- F. For 96-well plates, transfer 10µl of each substrate into 2ml of Assay Buffer.
- G. Mix the Assay Buffer containing substrates by vortexing the contents until the substrates are thoroughly dissolved. This mixture will be referred to as the Viability/Cytotoxicity Reagent.
- H. Transfer the contents of the Caspase-Glo® 3/7 Buffer bottle into the amber bottle containing Caspase-Glo® 3/7 Substrate.
- I. Mix by swirling or inverting the contents until the substrate is thoroughly dissolved to form the Caspase-Glo® 3/7 Reagent (~20 seconds).
- J. Set up 96-well assay plates containing cells in medium at the selected density
- K. Add test compounds and vehicle controls to appropriate wells for a final volume of 100µl per well.
- L. Culture cells for the desired test exposure period. Note: When characterizing new compounds, it is important to use in multiple exposure periods to assess the full effect on cellular health
- M. Add 20µl of Viability/Cytotoxicity Reagent containing both GF-AFC Substrate and bis-AAF-R110 Substrate to all wells, and briefly mix by orbital shaking (300–500rpm for ~30 seconds)



- N. Incubate for 30 minutes at 37°C
- O. Measure fluorescence at the following two wavelength sets: 400Ex/505Em (Viability)  
485Ex/520Em (Cytotoxicity)
- P. Add 100µl of Caspase-Glo® 3/7 Reagent to all wells, and briefly mix by orbital shaking (300–500rpm for ~30 seconds) Note: Incubation times longer than 30 minutes may improve assay sensitivity and dynamic range
- Q. Incubate for 30 minutes at room temperature
- R. Measure luminescence (caspase activation, a hallmark of apoptosis)

## 6. Exosome Isolation and Characterisation

### 6.1. Isolation Procedure

- A. Culture cells for 3 days in Medium replaced with DMEM containing 10% exosome-depleted-FBS
- B. Centrifuge samples at 2000 g for 10 min at 4°C
- C. Filter to eliminate cells and dead cells using 0.45 µm pore filters
- D. Ultracentrifuge at 110,000 g for 75 min at 4°C
- E. Wash Exosome pellets phosphate buffered solution (PBS)
- F. Repeat ultracentrifugation and resuspend in PBS

### 6.2. SDS-PAGE, Western Blotting and Antigen Binding

- A. Set up Bio-rad rig as directed (by Orla) the evening before the gels will be done. Fill the rig up with deionised water or alcohol to ensure that there are no leaks.
- B. Set up the separating Gel first (% separating gel depends on size of desired protein). The general rule is the smaller the protein the larger the % separating Gel. In this case, 10% will be done. Check the SDS-PAGE concs.

- C. Add all of the solutions together accordingly. **Always remember to add the 10% APS (aliquoted in the freezer) and Temed last as they solidify the gel solution.**
- D. Quickly mix and pipette approx. 4mls (2/3 the size of the whole area) into the gel rig. Carefully add a layer of isopropanol over the gel to create a defined edge on the gel. Allow to set for approx. 10 mins.
- E. Carefully pour off the isopropanol using tissue at the edge of the rig to clear off the excess.
- F. Add all of the solutions for the 4% stacking gel together (again remember APS and Temed last)
- G. Pipette carefully into the rig on top of the separating gel and carefully add in the comb (from sideways). Allow to set for approx. 10 mins.
- H. Meanwhile prepare the lysed protein samples for SDS-PAGE by aliquoting the desired amount in  $\mu\text{l}$  into separate Eppendorf tubes. Add the SDS-gel loading dye (approx.  $10\mu\text{l}$ ) and boil in a heating block (use PCR machine) for 3 mins at  $100^{\circ}\text{C}$ . This is to linearize the proteins for the gel.
- I. Dry load or wet load the wells of the prepared Gel with the protein samples. **Do not forget the protein ladder.**
- J. Fill the inside of the rig to the top with running buffer and place the lid on top. Set the electrophoresis power unit to 20mA per gel and run for approximately 1-1.5hrs until the samples/blue dye front reaches the bottom of the gel.

### **Step 3: Western Blotting**

- K. Undo the Gel rig as instructed (by Orla) and carefully take the spacers out from between the glass plates. The plates usually separate and the gel remains on one plate. Cut off the stacking layer of the gel.

- L. The membrane is immersed with transfer buffer and placed on top of the gel. Two pieces of blotting paper (pre-cut to size) are also immersed in transfer buffer and placed over the membrane and the gel. Two pieces of blotting paper are immersed in transfer buffer and placed on the other side of the gel. Tease out all air bubbles by gently rolling a long pipette over the sandwich.
- M. The sandwich is placed in the Bio-Rad transfer cassette with the membrane to the black side. The clamp is closed and placed into the transfer rig. **The general rule is the membrane to the positive side (red) and the gel to the negative side (black).** Thus, black side of cassette to the red side of the transfer rig. Fill with cool transfer buffer (always keep 1X transfer buffer in the fridge).
- N. Set the power unit to 100 volts for 1 hr. Check the current also while it has started to run to ensure that it is running OK. This is done by switching to Amps.

#### **Step 4: Antibody-Antigen binding**

- O. Carefully remove the membrane from the cassette and peeling off the other layers. Place the membrane into a large Petri dish or trough and add 20mls of 5% (1g in 20mls tris buffer) milk solution for 1 hour at RT on the shaker. This is to block the membrane.
- P. Make up the primary antibody in 3% protein solution (0.3g in 10mls tris buffer).
- Q. Add the primary antibody to the membrane overnight and leave on the shaker.
- R. Wash off the solution from the membrane by doing 3 x 10 minute washes in Tris-T.
- S. Add the secondary antibody (also made up in 3% protein solution) to the membrane for 1 hour on the shaker.
- T. Wash off the solution from the membrane by doing 3 x 10 minute washes in Tris-T.

## **Step 5: Visualisation of desired protein**

### **Chemilluminescence**

- U. Using the homemade ECL chemiluminescent kit (solution A and B) place over the membrane for 1 minute.
- V. Carefully place the membrane into the exposure cassette.
- W. In a dark room, carefully open the X-ray film and place over the membrane and expose for 1 min and 5 mins. Develop X-ray film and dry. If there is not enough exposure, re-do the chemilluminescence step and expose for longer.

### **Staining**

- X. DAB can be used to stain the membrane for the specific protein. Make up 10mls of DAB and add hydrogen peroxide to activate the chromogen. Add to membrane and the protein of interest can be visualised.

### 6.3. Exosome identification by TEM

- A. To further eliminate contaminating proteins, resuspend the exosome enriched pellet in PBS and ultracentrifuge at 120 000 x g for 70 minutes at 4 °C to re-pellet the exosomes.
- B. Take a small aliquot of the sample for protein isolation and total protein measurement. Make sure that only a small part of the sample is lysed and used for the protein measurement and keep the intact exosomes, solved in PBS, separate on ice or at -80 °C for further experiments.
- C. Place a drop, approximately 10 µg of exosomal protein of the intact exosomes resuspended in PBS, on a Parafilm. Then, with forceps, gently position a formvar

coated 1 grid on top of each drop for 30-60 minutes. Assure that the grid is positioned with the coating side facing the drop containing exosomes.

- D. Place three drops, each 30  $\mu$ l, of PBS on the Parafilm and wash the grid by sequentially positioning the grid on top of the droplets of PBS, and use an absorbing paper in between. Use the absorbing paper gently just by holding it closely to the side of the grid, without making contact with the coated area.
- E. Fix the sample by deposit a drop of 2% paraformaldehyde on the Parafilm and place the grid on top of the drop for 10 minutes.
- F. Repeat the washing step in point 4, substituting ddH<sub>2</sub>O for PBS.
- G. Contrast the sample by adding a drop of 2% uranyl acetate to the Parafilm and incubate the grid on top of the drop for 15 minutes. Wick away the stain and allow to dry

**10.4 Raw Data**  
**Chapter 2 Raw Data**

<u>Code</u>	<u>Irradiated</u>	<u>Plasma</u>	<u>G2/mitotic</u>	<u>H2AX</u>	<u>AGE</u>	<u>SMOKER</u>	<u>SEX</u>
HC1	0	1	0	0			M
HC2	1	1	1	1	37		M
HC3	1	1	1	1	23		M
HC4	0	1	0	0			M
HC5	1	1	1	1	26		M
HC6	0	1	0	0			F
HC7	1	1	1	0	23		M
HC8	1	1	1	1	23		F
HC9	1	1	1	1	22		F
HC10	1	1	1	1	29		F
HC11	1	1	1	1	26		F
HC12	1	1	1	1	21		F
HC13	1	1	1	1	30		F
HC14	1	1	1	1	37	YES	M
HC15	1	1	1	1	40		F
HC16	1	1	1	1	54		F
HC17	1	1	1	1	56		M
HC18	1	1	1	1	35		M
HC19	1	1	1	1	48		F
HC20	1	1	1	1	32	YES	M
HC21	1	1	1	1	31		M
HC22	1	1	1	1	23		F
HC23	1	1	1	1	24		F
HC24	1	1	1	1	31	YES	F
HC25	1	1	1	1	33	YES	M
HC26	1	1	1	1	23	YES	M
HC27	1	1	1	1	31		F
HC28	1	1	1	1	38		F
HC29	1	1	1	1	38		M
HC30	1	1	1	0	41		M
HC31	1	1	1	0	33		F
HC32	1	1	1	0	43		F
HC33	1	1	1	0	42		F
HC34	1	1	1	0	31		M
HC35	1	1	1	0	24		M
HC36	1	1	1	0	30		M
HC37	1	1	1	0	29		F
HC38	1	1	1	0	23	YES	F
HC39	1	1	1	0	23	YES	M
HC40	1	1	1	0	25		F
HC41	1	1	1	0	29	YES	M
HC42	1	1	1	0	28		F
HC43	1	1	1	0	22		F

HC44	1	1	1	1	25		F
HC45	1	1	1	1	29		M

Patient ID	Date	Mitotic Index			MIn		G2 Score			I. Induced G2 Score	
		0 Gy	0.05 Gy	0.5 Gy	0.05 Gy	0.5 Gy	0 Gy	0.05 Gy	0.5 Gy	0.05 Gy	0.5 Gy
HC3 Whole Blood	06/07/2012	1.6	1.7	0.7	-0.1	0.9	4	40	116	36	112
HC3 Lymphocytes	06/07/2012	1.6	2.1	0.8	-0.5	0.8	4	40	96	36	92
HC7 Whole Blood	29/03/2012	1.5	1.2	0.5	0.3	1	0	68	156	68	156
HC7 Lymphocytes	29/03/2012	1.1	0.6	0.7	0.5	0.4	4	36	83	32	79
HC25 Whole Blood	06/07/2012	0.8	0.7	0.5	0.1	0.3	0	28	172	28	172
HC25 Lymphocytes	06/07/2012	2.5	1	1	1.5	1.5	4	32	132	28	128

Donor	Mitotic Index			MIn		G2 Score			I. Induced G2 Score	
	0Gy	0.5Gy	2Gy	0.5Gy	2Gy	0Gy	0.5Gy	2Gy	0.5Gy	2Gy
<b>HC3</b>	3.4	2	1.1	1.4	2.3	4	123	420	119	416
<b>HC5</b>	3.6	1.2	1.3	2.4	2.3	0	148	424	148	424
<b>HC27</b>	1	1.8	1.4	-0.8	-0.4	8	184	664	176	656

Patient ID	Date	Mitotic Index			MIn		G2 Score			I. Induced G2 Score		
		0Gy	0.05 Gy	0.5 Gy	0.05 Gy	0.5 Gy	0Gy	0.05 Gy	0.5Gy	0.05Gy	0.5Gy	
HC3 1	20/04/2012	2.5	2	1.3	0.5	1.2	4	60	156	56	152	
HC3 2	06/07/2012	1.6	1.7	0.7	-0.1	0.9	4	40	116	36	112	
HC3 3	13/07/2012	2.7	1.9	0.4	0.8	2.3	4	32	132	28	128	
HC3 4	20/07/2012	2	1.1	1.1	0.9	0.9	4	32	134	28	130	
HC3 5	27/07/2012	3.6	2.7	1.6	0.9	2	0	32	126	32	126	
HC3 6	16/01/2014	3.6	2	0.7	1.6	2.9	4	36	124	32	120	
										Mean	35.33333	128
										St.DE V	10.55778	13.44619
										Coeff. %	29.8805	10.50484



Patient ID	Date	Mitotic Index			MIn		G2 Score			I. Induced G2 Score	
		0G y	0.05 Gy	0.5 Gy	0.05 Gy	0.5 Gy	0G y	0.05 Gy	0.5Gy	0.5Gy	0.5Gy
HC8 1	27/07/2012	2.2	1.5	0.6	0.7	1.2	8	64	116	56	108
HC8 2	16/01/2014	2.1	2.2	0.9	0.7	1.1	0	44	170	44	170
HC8 3	10/03/2014	1.6	2.5	0.8	0.7	1.8	12	28	138	16	126
HC8 4	10/04/2014	2.8	2.1	1	1.2	1.2	8	56	188	48	180
HC8 5	30/05/2014	1.5	1.4	0.7	0.1	0.8	8	44	156	36	148
									Mean	40	146.4
									St.DE V	15.231	29.913
										55	21
									Coeff. %	38.078	20.432
										87	52

Patient ID	Date	Mitotic Index			MIn		G2 Score			I. Induced G2 Score	
		0G y	0.05 Gy	0.5 Gy	0.05 Gy	0.5 Gy	0G y	0.05 Gy	0.5Gy	0.5Gy	0.5Gy
HC38 1	16/01/2014	2.5	0.4	1.4	2.1	1.1	4	36	116	32	114
HC38 2	10/03/2014	3.6	1.7	0.6	1.9	3	4	32	122	28	118
HC38 3	30/05/2014	1.7	1.5	0.8	0.2	0.9	16	44	208	28	192
HC38 5	08/12/2014	4	4.4	2.2	-0.4	1.5	4	48	160	44	156
HC38 6	14/04/2015	3.9	2.9	4.2	1	-0.3	4	28	128	24	124
									Mean	31.2	140.8
									St.DE V	7.6941	33.063
										54	58
									Coeff. %	24.660	23.482
										75	65

Donor	Mitotic Index			Mitotic Inhibition	
	0Gy	0.05Gy	0.5Gy	0.05Gy	0.5Gy
HC2	1.9	3.4	1.5	-1.5	0.4
HC3	2.5	2	1.3	0.5	1.2
HC5	3.9	3.1	1.3	0.8	2.6
HC7	1.5	1.2	0.5	0.3	1
HC8	2.1	1.4	0.9	0.7	1.2
HC9	1.2	1.1	0.5	0.1	0.7
HC10	3.6	2.6	1.1	1	2.5
HC11	2.6	2.1	1.3	0.5	1.3
HC12	3.5	2.8	1.2	0.7	2.3
HC13	1.6	1.5	1	0.1	0.6
HC14	2.2	1.9	0.9	0.3	1.3
HC15	2.5	1.5	0.8	1	1.7
HC16	1.8	1.6	1.1	0.2	0.7
HC17	1.1	1.4	0.8	-0.3	0.3
HC18	2.5	1.8	1.4	0.7	1.1
HC19	2.8	1.4	0.6	1.4	2.2
HC20	3.4	1.7	0.8	1.7	2.6
HC21	3.2	1.4	0.7	1.8	2.5
HC22	3.2	2	0.4	1.2	2.8
HC23	1.7	0.8	1.1	0.9	0.6
HC24	1.4	1.5	0.6	-0.1	0.8
HC25	0.8	0.7	0.5	0.1	0.3
HC26	3	1.3	0.4	1.7	2.6
HC27	1.2	2.4	0.4	-1.2	0.8
HC28	1.1	0.8	0.3	0.3	0.8
HC29	1.4	1.1	0.9	0.3	0.5
HC30	2.6	1.9	0.8	0.7	1.8
HC31	0.9	0.5	0.7	0.4	0.2
HC32	1.4	1.5	0.7	-0.1	0.7
HC33	1.6	1.8	0.5	-0.2	1.1
HC34	2.5	1.2	1.1	1.3	1.4
HC35	3.3	2	2.2	1.3	1.1
HC36	3.3	1.9	1.9	1.4	1.4
HC37	1.5	0.6	0.1	0.9	1.4
HC38	2.5	0.4	1.4	2.1	1.1
HC39	2.8	1.6	1.8	1.2	1
HC40	2.5	1.3	0.5	1.2	2
HC41	3.4	4.4	1.5	-1	1.9
HC42	4.4	2.4	2.9	2	1.5
HC43	2.9	1.9	0.9	1	2
HC44	3.1	3.3	1.6	-0.2	1.5
HC45	4.3	2.8	1.3	1.5	3
Mean	2.39762	1.7619	1.00476	0.63571	1.39286
ST.DEV	0.95214	0.83226	0.55302	0.81923	0.76872

Coefficient of Variation (%)	39.7121	47.2365	55.0398	128.867	55.1898
------------------------------	---------	---------	---------	---------	---------

Donor	Lisa G2 Scores			I. Induced G2 Score	
	0Gy	0.05Gy	0.5Gy	0.05Gy	0.5Gy
HC 2	8	60	128	52	120
HC 3	4	60	156	56	152
HC 5	20	40	160	20	140
HC 7	0	68	156	68	156
HC 8	8	64	116	56	108
HC 9	4	68	152	64	148
HC 10	4	40	92	36	88
HC 11	8	56	106	48	98
HC 12	8	44	90	36	82
HC 13	4	40	184	36	180
HC 14	8	32	94	24	86
HC 15	8	32	110	24	102
HC 16	8	24	126	16	118
HC 17	4	40	100	36	96
HC 18	8	48	218	40	210
HC 19	8	24	124	16	116
HC 20	0	32	92	32	92
HC 21	8	32	142	24	134
HC 22	0	44	94	44	94
HC 23	4	48	150	44	146
HC 24	4	28	134	24	130
HC 25	0	28	172	28	172
HC 26	4	32	100	28	96
HC 27	0	32	152	32	152
HC 28	4	28	148	24	144
HC 29	0	36	132	36	132
HC 30	4	28	126	24	122
HC 31	0	40	124	40	124
HC 32	4	32	104	28	100
HC 33	16	36	112	20	96
HC 34	4	44	116	40	112
HC 35	8	36	142	28	134
HC 36	4	32	138	28	134
HC 37	4	36	106	32	102
HC 38	4	36	116	32	112
HC 39	12	56	158	44	146
HC 40	4	36	146	32	142
HC 41	0	36	108	36	108
HC 42	4	44	148	40	144
HC 43	8	36	106	28	98

HC 44	4	40	134	36	130
HC 45	20	64	132	44	112
Mean	5.61905	40.7619	129.619	35.1429	124
ST.DEV	4.76242	12.024	27.6326	12.0336	27.7304
Coefficient of Variation (%)	84.7549	29.4981	21.3183	34.242	22.3632

<u>Donor</u>	<u>0Gy</u>	<u>0.05Gy</u>	<u>0.5Gy</u>
HC2	0	12 dicent + 4endo	0
HC3	0	8 dicent	10 dicent + 4 cring
HC5	0	8 cring	4 acentric
HC7	0	16 dicent	0
HC8	0	4 acentric + 4 dicent	0
HC9	0	8 acentric	2 cring
HC10	0	4 endo + 8 Dicent	6 dicent
HC11	0	0	4 dicent
HC12	0	0	0
HC13	0	8 dicent	0
HC14	4 dicent	8 dicent	0
HC15	0	0	2 cring
HC16	0	0	0
HC17	0	0	4 dicent
HC18	4 endo	4 cring	4 dicent
HC19	4 dicent	8 dicent	0
HC20	0	4 endo	0
HC21	4 dicent	8 dicent	6 dicent
HC22	0	0	0
HC23	0	8 dicent	0
HC24	0	12 dicent	0
HC25	0	4 tetra	6 dicent
HC26	0	0	0
HC27	0	0	6 tetra
HC28	0	0	0
HC29	0	0	2 cring
HC30	0	0	2 dicent
HC31	0	0	0
HC32	0	0	0
HC33	0	0	0
HC34	0	4 dicent	0
HC35	0	4 dicent	2 tetra
HC36	0	0	2 tetra
HC37	0	0	2 tetra
HC38	0	0	0
HC39	0	8 dicent	0
HC40	0	0	2 endo

HC41	0	4 tetra	2 dicent
HC42	0	0	2 dicent + 2 Tetra
HC43	0	4 tetra	0
HC44	0	0	14 dicent
HC45	4 dicent	20 dicent + 4 endo	6 dicent + 2 endo

<b>Mitotic Index</b>									
	<sup>60</sup> Co Irradiation			Linac Photon Irradiation			Linac Electron Irradiation		
<u>Donor</u>	0 Gy	0.05Gy	0.5Gy	0 Gy	0.05Gy	0.5Gy	0 Gy	0.05Gy	0.5Gy
1 <u>HC2</u>	2.9	1.5	1.2	2.9	0.6	0.5	2.9	2.4	1.4
2 <u>HC3</u>	3.6	1.2	1.4	3.6	1.8	1.3	3.6	2.7	1.9
3 <u>HC7</u>	2.4	2.3	1.7	2.4	1.3	1.8	2.4	1.5	2.5
4 <u>HC8</u>	1.2	0.5	0.1	1.2	0.6	0.8	1.2	1.7	1.1
5 <u>HC21</u>	2.1	1.4	2	3	2.6	2.4	N/A	N/A	N/A
6 <u>HC23</u>	2.7	1.4	2	2.7	1.4	1.1	2.7	1.5	1.9
7 <u>HC30</u>	2.6	1.9	0.8	2.6	1.9	1.1	2.6	1.7	1
8 <u>HC31</u>	0.9	0.5	0.7	0.9	0.6	0.9	0.9	1.2	0.7
9 <u>HC32</u>	1.4	1.5	0.7	1.4	0.8	1	1.4	1.7	1
10 <u>HC33</u>	1.6	1.8	0.5	1.6	0.9	1.6	1.6	0.6	0.4
11 <u>HC34</u>	2.5	1.2	1.1	2.5	1.5	0.8	2.5	1.7	1.7
12 <u>HC35</u>	3.3	2	2.2	3.3	3.2	1.6	3.3	1.9	1.6
13 <u>HC36</u>	3.3	1.9	1.9	3.3	1.5	1.8	3.3	2	2
14 <u>HC37</u>	1.5	0.6	0.1	1.5	0.4	0.1	1.5	0.8	0.7
15 <u>HC38</u>	2.5	0.4	1.4	2.5	0.9	0.5	2.5	2	1.1
16 <u>HC39</u>	2.8	1.6	1.8	2.8	2.2	1.5	2.8	2.2	1
17 <u>HC40</u>	2.5	1.3	0.5	2.5	1.4	0.7	2.5	2.2	0.6
18 <u>HC41</u>	3.4	4.4	1.5	3.4	2.1	1.3	NONE	NONE	NON E
19 <u>HC42</u>	4.4	2.4	2.9	4.4	2.3	1.3	NONE	NONE	NON E
20 <u>HC43</u>	2.9	1.9	0.9	2.9	1.3	1.2	NONE	NONE	NON E

<b>MIn</b>										
	<sup>60</sup> Co Irradiation			Linac Photon Irradiation			Linac Electron Irradiation			
<b>Donor</b>	0	0.05Gy	0.5Gy	0	0.05Gy	0.5Gy	0	0.05Gy	0.5Gy	
1	<u>HC2</u>		1.4	1.7		2.3	2.4		0.5	1.5
2	<u>HC3</u>		2.4	2.2		1.8	2.3		0.9	1.7
3	<u>HC7</u>		0.1	0.7		1.1	0.6		0.9	-0.1
4	<u>HC8</u>		0.7	1.1		0.6	0.4		-0.5	0.1
5	<u>HC21</u>		0.7	0.1		0.4	0.6		NONE	NONE
6	<u>HC23</u>		1.3	0.7		1.3	1.6		1.2	0.8
7	<u>HC30</u>		0.7	1.8		0.7	1.5		0.9	1.6
8	<u>HC31</u>		0.4	0.2		0.3	0		-0.3	0.2
9	<u>HC32</u>		-0.1	0.7		0.6	0.4		-0.3	0.4
10	<u>HC33</u>		-0.2	1.1		0.7	0		1	1.2
11	<u>HC34</u>		1.3	1.4		1	1.7		0.8	0.8
12	<u>HC35</u>		1.3	1.1		0.1	1.7		1.4	1.7
13	<u>HC36</u>		1.4	1.4		1.8	1.5		1.3	1.3
14	<u>HC37</u>		0.9	1.4		1.1	1.4		0.7	0.8
15	<u>HC38</u>		2.1	1.1		1.6	2		0.5	1.4
16	<u>HC39</u>		1.2	1		0.6	1.3		0.6	1.8
17	<u>HC40</u>		1.2	2		1.1	1.8		0.3	1.9
18	<u>HC41</u>		-1	1.9		1.3	2.1	NONE	NONE	NONE
19	<u>HC42</u>		2	1.5		2.1	3.1	NONE	NONE	NONE
20	<u>HC43</u>		1	2		1.6	1.7	NONE	NONE	NONE

<b>G2 Score</b>										
	<sup>60</sup> Co Irradiation			Linac Photon Irradiation			Linac Electron Irradiation			
<b>Donor</b>	0	0.05Gy	0.5Gy	0	0.05Gy	0.5Gy	0	0.05Gy	0.5Gy	
1	<u>HC2</u>	12	48	142	12	32	100	12	32	102
2	<u>HC3</u>	4	32	162	4	48	124	4	48	130
3	<u>HC7</u>	8	40	154	8	36	116	8	48	126
4	<u>HC8</u>	0	44	170	0	40	96	0	40	168
5	<u>HC21</u>	12	44	100	4	48	120	N/a	N/a	N/a
6	<u>HC23</u>	8	36	134	8	32	156	8	40	114
7	<u>HC30</u>	4	28	126	4	40	128	4	32	88
8	<u>HC31</u>	0	40	124	0	40	106	0	44	106
9	<u>HC32</u>	4	32	104	4	36	98	4	36	90
10	<u>HC33</u>	16	36	112	16	36	104	16	40	130
11	<u>HC34</u>	4	44	116	4	36	102	4	44	154
12	<u>HC35</u>	8	36	142	8	36	136	8	32	112
13	<u>HC36</u>	4	32	138	4	28	118	4	44	104
14	<u>HC37</u>	4	36	106	4	32	106	4	36	142
15	<u>HC38</u>	4	36	116	4	36	110	4	40	122

16	<u>HC39</u>	12	56	158	12	48	132	12	48	142
17	<u>HC40</u>	4	36	146	4	48	156	4	44	128
18	<u>HC41</u>	0	36	108	0	36	130	N/a	N/a	N/a
19	<u>HC42</u>	4	44	148	4	40	114	N/a	N/a	N/a
20	<u>HC43</u>	8	36	106	8	40	126	N/a	N/a	N/a

<b>Radiation induced G2 Score</b>										
		<sup>60</sup> Co Irradiation			Linac Photon Irradiation			Linac Electron Irradiation		
<u>Donor</u>		0	0.05Gy	0.5Gy	0	0.05Gy	0.5Gy	0	0.05Gy	0.5Gy
1	<u>HC2</u>		36	130		20	88		20	90
2	<u>HC3</u>		28	158		44	120		44	126
3	<u>HC7</u>		32	146		28	108		40	118
4	<u>HC8</u>		44	170		40	96		40	168
5	<u>HC21</u>		32	88		44	116		N/a	n/A
6	<u>HC23</u>		28	126		24	148		32	106
7	<u>HC30</u>		24	122		36	124		28	84
8	<u>HC31</u>		40	124		40	106		44	106
9	<u>HC32</u>		28	100		32	94		32	86
10	<u>HC33</u>		20	96		20	88		24	114
11	<u>HC34</u>		40	112		32	98		40	150
12	<u>HC35</u>		28	134		28	128		24	104
13	<u>HC36</u>		28	134		24	114		40	100
14	<u>HC37</u>		32	102		28	102		32	138
15	<u>HC38</u>		32	112		32	106		36	118
16	<u>HC39</u>		44	146		36	120		36	130
17	<u>HC40</u>		32	142		44	152		40	124
18	<u>HC41</u>		36	108		36	130	N/a	N/a	N/a
19	<u>HC42</u>		40	144		36	110	N/a	N/a	N/a
20	<u>HC43</u>		28	98		32	118	N/a	N/a	N/a

		Dose in mGy	0	5	50	500	5000
200 kV	Media		100	106.5	102.8	86.9	16.9
	std dev		11.3	10.2	16.3	19.1	0.7
6 MV	Media		100	93.4	88.7	84.6	15
	std dev		2.7	3.1	2.1	2.8	3.4
10 MV	Media		100	98	99.1	82.5	21.2
	std dev						

	std dev	13.7	10.5	16.7	6.9	5.3
15 MV	Media	100	93.5	88.7	84.6	15
	std dev	2.7	3.1	2.1	2.8	3.4

### Chapter 3 Raw Data

Donor	Date of Exp.	AGE	MITOTIC INDEX			Mitotic Inhibition		G2 RADIOSENSITIVITY SCORE			Radiation Induced G2 Score	
			0G Y	0.05 GY	0.5 GY	0.05 Gy	0.5 Gy	0G Y	0.05 GY	0.5 GY	0.05 Gy	0.5 Gy
PC001 V1	06/05/2 014	66	3. 6	1.8	0.9	1.8	2.7	12	32	210	20	198
PC002 V1	30/06/2 014	72	2. 4	1	1.1	1.4	1.3	4	64	184	60	180
PC003 V1	05/08/2 014	66	0. 4	0.2	0.6	0.2	-0.2	0	44	192	44	192
PC004 V1	22/09/2 014	85	4. 8	2.9	1.7	1.9	3.1	8	80	218	72	210
PC005 V1	20/10/2 014	60	2. 5	1	1	1.5	1.5	12	44	190	32	178
PC007 V1	16/12/2 014	58	1. 3	0.6	1.3	0.7	0	52	48	170	-4	118
PC009 V1	12/01/2 015		1. 2	1.6	0.6	-0.4	0.6	20	52	186	32	166
PC010 V1	19/01/2 015		3. 4	1.5	1.3	1.9	2.1	12	52	200	40	188
PC011 V1	20/01/2 015	67	2	1	0.4	1	1.6	24	52	138	28	114
PC013 V1	09/02/2 015		0. 3	0.7	0.2	-0.4	0.1	8	40	134	32	126
PC014 V1	11/02/2 015		2. 6	1.6	1.7	1	0.9	24	64	234	40	210
PC015 V1	16/02/2 015	76	0. 5	0.1	0.5	0.4	0	16	40	154	24	138
PC016 V1	16/02/2 015	60	0. 9	0.6	0.8	0.3	0.1	8	36	134	28	126
PC017 V1	03/03/2 015		2. 3	1.9	0.6	0.4	1.7	12	32	96	20	84
PC018 V1	23/03/2 015	69	1. 3	0.8	0.9	0.5	0.4	24	44	134	20	110
PC019 V1	26/03/2 015	76	2	1.3	1.1	0.7	0.9	16	32	174	16	158
PC020 V1	07/04/2 015	68	2. 1	1.5	1.2	0.6	0.9	20	40	184	20	164
PC021 V1	13/04/2 015	68	2. 3	2.3	2.3	0	0	16	40	216	24	200



PC022 V1	19/05/2 015	62	3. 8	3.4	1.5	0.4	2.3	12	40	144	28	132
PC023 V1	19/05/2 015	77	1. 8	1.4	1	0.4	0.8	12	40	140	28	128
PC024 V1	25/05/2 015	72	1. 2	0	0.1	1.2	1.1	12	43	150	31	138
PC025 V1	25/05/2 015		0. 9	0.1	0.3	0.8	0.6	4	40	130	36	126

Donor	Date of Exp.	AG E	MITOTIC INDEX			Mitotic Inhibition		G2 RADIOSENSITIVITY SCORE			Radiation Induced G2 Score	
			0G Y	0.05 GY	0.5 GY	0.05 Gy	0.5 Gy	0G Y	0.05 GY	0.5 GY	0.05 Gy	0.5 Gy
PC001 V2	30/09/20 14	66	0. 7	1	0.5	-0.3	0.2	0	44	202	44	202
PC002 V2	07/08/20 14	72	2	2.5	0.9	-0.5	1.1	8	44	138	36	130
PC003 V2	17/11/20 14	66	1. 4	0.8	0.4	0.6	1	36	52	140	16	104
PC004 V2	02/10/20 14	85	0	2.5	2.4	-2.5	-2.4	8	52	154	44	146
PC005 V2	09/12/20 14	60	1. 2	0.4	0.6	0.8	0.6	32	36	195	4	163
PC006 V2	12/11/20 14	67	2. 2	0.9	1.6	1.3	0.6	24	44	202	20	178
PC008 V2	23/04/20 15		0. 4	0.4	0.2	0	0.2	13	55	160	42	147
PC009 V2	25/05/20 15		1. 8	0	0.3	1.8	1.5	5	71	148	66	143
PC010 V2	24/06/20 015		2. 7	2.6	1.3	0.1	1.4	12	72	260	60	248
PC011 V2	29/07/20 15	67	2	0.4	0.2	1.6	1.8	12	44	205	32	193
PC012 V2	13/05/20 15	-	2. 4	0.9	0.9	1.5	1.5	8	45	140	37	132
PC013 V2	25/06/20 15		4. 1	1.2	0.4	2.9	3.7	0	44	132	44	132
PC014 V2	22/04/20 15		1	0	0	1	1	20	60	158	40	138
PC015 V2	25/06/20 15	76	1. 3	1.4	0.1	-0.1	1.2	16	60	220	44	204
PC018 V2	22/04/20 15	69	3. 7	1.4	1.6	2.3	2.1	12	48	160	36	148

Donor	Date of Exp.	AGE	MITOTIC INDEX			Mitotic Inhibition		G2 RADIOSENSITIVITY SCORE			Radiation Induced G2 Score	
			OG Y	0.05 GY	0.5 GY	0.05 Gy	0.5 Gy	OG Y	0.05 GY	0.5 GY	0.05 Gy	0.5 Gy
PC001 V3	01/12/2014	66	3.3	2.8	1.7	0.5	1.6	48	76	270	28	222
PC002 V3	06/10/2014	72	2.5	1.4	1.4	1.1	1.1	44	64	212	20	168
PC003 V3	19/01/2015	66	0.1	1.4	0	-1.3	0.1	12	92	190	80	178
PC004 V3	09/12/2014	85	0.6	0.6	0.4	0	0.2	24	40	188	16	164
PC005 V3	09/02/2015	60	0.6	0.5	0.7	0.1	-0.1	28	60	204	32	176
PC006 V3	19/01/2015	67	0.9	1	0.2	-0.1	0.7	20	56	268	36	248
PC009 V3	28/07/2015		1.9	1.4	0.5	0.5	1.4	8	72	160	64	152
PC012 V3	15/07/2015	-	7.3	6.3	3.9	1	3.4	0	40	140	40	140
PC014 V3	25/06/2015		0.4	0.1	0.1	0.3	0.3	12	50	100	38	88
PC018 V3	25/06/2015	69	0.9	0.5	0	0.4	0.9	8	64	140	56	132

Donor	Date of Exp.	AGE	MITOTIC INDEX			Mitotic Inhibition		G2 RADIOSENSITIVITY SCORE			Radiation Induced G2 Score	
			OG Y	0.05 GY	0.5 GY	0.05 Gy	0.5 Gy	OG Y	0.05 GY	0.5 GY	0.05 Gy	0.5 Gy
PC001 V4	16/02/2015	66	1	0.7	0.7	0.3	0.3	16	72	172	56	156
PC002 V4	08/12/2014	72	2.1	2.5	2	-0.4	0.1	60	76	202	16	142
PC003 V4	24/03/2015	66	1.4	1.3	0.7	0.1	0.7	12	72	206	60	194
PC004 V4	24/02/2014	85	0.5	0.3	0.1	0.2	0.4	50	50	170	0	120
PC005 V4	13/04/2015	60	0.9	0.9	0.3	0	0.6	12	56	104	44	92
PC006 V4	24/03/2015	67	1	0.6	0.2	0.4	0.8	16	44	170	28	154
PC014 V4			0.8	0.4	0.6	0.4	0.2	20	52	176	32	156

Donor	Date of Exp.	AGE	MITOTIC INDEX			Mitotic Inhibition		G2 RADIOSENSITIVITY SCORE			Radiation Induced G2 Score	
			OG Y	0.05 GY	0.5 GY	0.05 Gy	0.5 Gy	OG Y	0.05 GY	0.5 GY	0.05 Gy	0.5 Gy

<b>Donor</b>	<b>Date of Exp.</b>	<b>AG E</b>	<b>OG Y</b>	<b>0.05 GY</b>	<b>0.5 GY</b>	<b>0.05 Gy</b>	<b>0.5 Gy</b>	<b>OG Y</b>	<b>0.05 GY</b>	<b>0.5 GY</b>	<b>0.05 Gy</b>	<b>0.5 Gy</b>
PC001 V5	15/06/2015	66	1.3	0.9	1.2	0.4	0.1	8	48	196	40	188
PC002 V5		72	4.7	2	1.8	2.7	2.9	16	64	212	48	196
PC004 V5		85	2	1.6	0.9	0.4	1.1	16	36	200	20	184

Dicentrics

<b>Donor</b>	<b>OGY</b>	<b>0.05GY</b>	<b>0.5GY</b>
PC001 V1	0	4	6
PC002 V1	0	8	10
PC003 V1	0	0	0
PC004 V1	0	12	16
PC005 V1	4	8	12
PC007 V1	8	16	12
PC009 V1	4	4	8
PC010 V1	4	12	0
PC011 V1	4	0	0
PC013 V1	0	0	16
PC014 V1	4	4	6
PC015 V1	4	0	8
PC016 V1	0	4	6
PC017 V1	0	4	10
PC018 V1	8	4	6
PC019V1	4	0	4
PC020V1	0	4	8
PC021V1	4	4	8
PC022V1	4	4	8
PC023V1	4	0	12
PC024V1	4	0	30
PC025V1	0	5	5

<b>Donor</b>	<b>OGY</b>	<b>0.05GY</b>	<b>0.5GY</b>
PC001 V2	0	0	2
PC002 V2	0	8	8
PC003 V2	12	0	0
PC004 V2	0	12	28
PC005 V2	4	0	6
PC006 V2	8	4	20
PC008 V2	0	8	0
PC009 V2	4	14	4
PC010 V2	0	12	0
PC011 V2	0	0	4

PC012 V2	0	12	21
PC013 V2	0	0	8
PC014 V2	8	0	14
PC015 V2	4	4	0
PC018 V2	0	0	12

<u>Donor</u>	<u>0GY</u>	<u>0.05GY</u>	<u>0.5GY</u>
PC001 V3	12	20	10
PC002 V3	16	16	16
PC003 V3	4	12	10
PC004 V3	8	12	20
PC005 V3	12	4	16
PC006 V3	4	4	8
PC009 V3	8	0	4
PC012 V3	0	12	4
PC014 V3	0	0	0
PC018 V3	8	12	0

<u>Donor</u>	<u>0GY</u>	<u>0.05GY</u>	<u>0.5GY</u>
PC001 V4	8	4	0
PC002 V4	20	28	24
PC003 V4	0	16	12
PC004 V4	0	0	0
PC005 V4	8	16	4
PC006 V4	4	4	10
PC014 V4	12	0	0

<u>Donor</u>	<u>0GY</u>	<u>0.05GY</u>	<u>0.5GY</u>
PC001 V5	0	0	12
PC002 V5	4	4	4
PC004 V5	0	0	4

<u>Donor</u>	<u>0GY</u>	<u>0.05GY</u>	<u>0.5GY</u>
SPC001	8	20	14
SPC003	4	4	8
SPC004	4	4	8

Chapter 4 Raw Data

0Gy		1hr		72hr	
21		48		97	
39	0	77	0	88	5
21	14	20	51	88	
45	24	27	06	31	6
A		60		86	
T2		16		60	
Bi	0	4	0	1	
A	10	73	24	44	
T3	76	68	39	66	
Bi	20	7	6	5	

0.05Gy		1hr		72hr	
21	20				
39	87				0
	7	0	0		
21	10	46	41		
45	56	13	48		0
	88	9	8		
A		44		22	
T2		63		86	
Bi		8	0	5	
A		70	75	94	
T3		03	34	57	
Bi	0	0	8	7	

0.5Gy		1hr		72hr	
21	10	72			
39	01	91		58	
	29	9	0	55	
21	92	78		11	
45	08	49		31	
	9	3	0	66	
A		99			
T2		77			
Bi		5	0	0	
A	58	64			
T3	46	54			
Bi	0	7	0	0	

2Gy		1hr		72hr	
21	13	13			
39	61	22			
	39	26	0	0	
21		16		15	
45	0	59		89	
		06	0	03	
A	11	58			
T2	25	10			
Bi	82	0	0	0	
A		16		15	
T3		59		89	
Bi	0	06	0	03	

0Gy	1hr		72hr	
213	1	1		
9	0	7		
	5	8	0	0
214	1	1	1	4
5	1	7	6	2
	0	0	7	0
AT2	1	1		
Bi	6	1		
	4	3	0	0
AT3	1			
Bi	7			
	1	6	0	0

0.05 Gy	1hr		72hr	
213		1	2	
9		8	4	9
	0	2	9	6
214	1			
5	5	5		
	6	1	0	0
AT2		1		
Bi		7		
		3	0	0
AT3		1	4	
Bi	5	3	3	
	0	2	6	0

0.5 Gy	1hr		72hr	
213		2		9
9		6	5	8
	0	9	7	4
214		4		
5	8	3		
	6	7	7	0
AT2		1		
Bi		9	9	
		5	7	0
AT3	1		2	
Bi	0		2	
	7	0	2	0

2Gy	1hr		72hr	
213	1	2	5	3
9	6	7	6	9
	8	6	5	9
214		1		1
5	5	3		4
	3	9	0	8
AT2			1	
Bi	5		4	
	6	8	6	0
AT3		5		4
Bi	0	7	2	4
		3	6	2

0Gy	1hr		72hr	
213	0.	5.	1.	3.
9	5	1	8	6
214	3.	4.	12	9.
5	8	8	.8	3
AT2	2.		4.	
Bi	1	5	5	4
AT3	3.	1.	3.	2.
Bi	9	3	1	2

0.05 Gy	1hr		72hr	
213	2.	5.	2.	2.
9	4	5	7	6
214	6.	4.	6.	
5	3	4	7	0
AT2		3.	1.	1.
Bi		4	1	4
AT3		4.	12	
Bi	2	7	.3	4

0.5 Gy	1hr		72hr	
213	0.	7.	5.	5.
9	6	7	6	2
214		9.	6.	
5	4	1	4	6
AT2		5.	5.	0.
Bi		2	9	4
AT3	4.	1.	2.	
Bi	5	1	4	0

2Gy	1hr		72hr	
213	5.	9.	11	3.
9	4	5	.1	3
214	1.	3.	7.	10
5	9	2	9	.3
AT2	3.	2.	7.	1.
Bi	6	2	4	5
AT3	1.	10	2.	6.
Bi	3	.4	5	8

yH2AX Foci 72hr Data

	2139			2145			AT2Bi			AT3Bi		
<b>0Gy</b>	0.25	0.43	0.46	0.94	0.78	0.68	0.53	0.30	0.30	0.78	0.36	0.60
<b>0.05Gy</b>	0.21	0.22	0.24	0.57	0.59	0.65	0.58	0.50	0.47	0.62	0.79	0.63
<b>0.5Gy</b>	0.49	0.48	0.46	0.68	0.83	0.90	1.15	1.13	1.18	1.20	1.13	1.09
<b>2Gy</b>	0.89	0.71	0.79	0.84	0.68	0.76	0.57	1.05	0.96	1.40	1.18	1.19

ApoTox Viability % of Control

	JHP		2139		2145		AT2Bi		AT3Bi	
<b>0 Gy 1h</b>	100.0 0	100.0 0	100.0 0	100.0 0	100.0 0	100.0 0	100.0 0	100.0 0	100.0 0	100.0 0
<b>0.05 Gy 1h</b>	89.90	96.61	110.9 4	112.7 9	96.15	82.89	97.61	91.23	89.07	97.99
<b>0.5 Gy 1h</b>	95.20	91.49	104.9 3	106.6 8	103.8 8	91.54	110.9 8	79.74	98.86	95.22
<b>2 Gy 1h</b>	100.0 7	94.45	123.1 2	112.6 1	102.0 4	92.21	112.6 7	86.31	112.5 3	110.1 1
<b>0Gy 24h</b>	100.0 0	100.0 0	100.0 0	100.0 0	100.0 0	100.0 0	100.0 0	100.0 0	100.0 0	100.0 0
<b>0.05 Gy 24h</b>	95.82	89.55	86.67	94.31	84.26	93.73	231.3 4	88.95	50.16	93.91
<b>0.5 Gy 24h</b>	95.76	87.53	86.67	100.4 1	102.6 8	92.70	227.8 9	76.04	47.06	88.80
<b>2 Gy 24h</b>	100.1 2	90.30	80.00	95.05	92.56	87.19	220.4 9	81.80	51.00	86.10

Apotox Viability 1- 24hrs

	JHP		2139		2145		AT2Bi		AT3Bi	
<b>0Gy</b>	2.137 48	1.399 927	2.728 215	2.271 17	2.334 138	1.472 293	1.043 216	1.706 539	4.815 922	1.596 269
<b>0.05 Gy</b>	2.278 27	1.297 65	2.131 217	1.899 106	2.045 422	1.664 845	2.472 36	1.663 899	2.711 961	1.529 798
<b>0.5Gy</b>	2.150 024	1.339 393	2.253 306	2.137 668	2.306 967	1.490 846	2.142 143	1.627 26	2.292 654	1.488 669
<b>2Gy</b>	2.138 636	1.338 539	1.772 735	1.917 125	2.117 241	1.392 173	2.041 501	1.617 481	2.182 676	1.248 202

Apotox Cytotoxicity % of Control

	JHP		2139		2145		AT2Bi		AT3Bi	
<b>0 Gy 1h</b>	100.0 0	100.0 0	100.0 0	100.0 0	100.0 0	100.0 0	100.0 0	100.0 0	100.0 0	100.0 0
<b>0.05 Gy 1h</b>	87.97	42.03	101.7 2	99.95	102.4 1	96.32	90.95	96.45	311.6 7	100.2 1
<b>0.5 Gy 1h</b>	92.40	39.02	148.2 8	100.1 1	135.2 7	99.06	116.6 3	88.74	271.0 1	94.48
<b>2 Gy 1h</b>	93.28	41.35	111.2 3	105.8 3	124.4 6	104.7 9	109.0 9	93.20	264.7 7	105.8 7
<b>0Gy 24h</b>	100.0 0	100.0 0	100.0 0	100.0 0	100.0 0	100.0 0	100.0 0	100.0 0	100.0 0	100.0 0
<b>0.05 Gy 24h</b>	84.07	87.38	92.31	88.62	106.1 9	82.51	422.2 0	86.43	46.10	84.48

<b>0.5 Gy 24h</b>	84.85	84.58	107.6 9	97.13	82.91	88.32	416.0 8	79.93	66.04	82.85
<b>2 Gy 24h</b>	92.37	88.00	100.0 0	195.2 6	94.26	87.79	441.0 9	97.23	58.64	83.71

Apotox Cytotoxicity 1- 24hrs

	<b>JHP</b>		<b>2139</b>		<b>2145</b>		<b>AT2Bi</b>		<b>AT3Bi</b>	
<b>0Gy</b>	2.16	0.55	2.25	1.71	1.79	1.46	0.40	1.67	6.96	1.39
<b>0.05Gy</b>	2.07	1.14	2.04	1.51	1.86	1.25	1.84	1.49	1.03	1.17
<b>0.5Gy</b>	1.99	1.18	1.64	1.66	1.10	1.30	1.42	1.50	1.70	1.22
<b>2Gy</b>	2.14	1.16	2.02	3.15	1.36	1.22	1.60	1.74	1.54	1.10

Apotox Caspase Activity % of Control

	<b>JHP</b>		<b>2139</b>		<b>2145</b>		<b>AT2Bi</b>		<b>AT3Bi</b>	
<b>0 Gy 1h</b>	100.0 0	100.0 0	100.0 0	100.0 0	100.0 0	100.0 0	100.0 0	100.0 0	100.0 0	100.0 0
<b>0.05 Gy 1h</b>	61.05	32.25	98.76	35.73	114.2 1	41.80	102.3 0	109.4 3	101.7 2	126.8 3
<b>0.5 Gy 1h</b>	48.07	78.45	101.3 9	102.8 8	102.4 9	111.2 5	115.1 0	99.58	96.77	116.9 3
<b>2 Gy 1h</b>	61.21	74.31	85.85	87.20	104.0 0	123.4 9	104.2 8	106.3 5	99.02	106.1 9
<b>0Gy 24h</b>	100.0 0	100.0 0	100.0 0	100.0 0	100.0 0	100.0 0	100.0 0	100.0 0	100.0 0	100.0 0
<b>0.05 Gy 24h</b>	86.40	113.6 4	92.20	106.1 4	93.78	103.6 9	0.00	88.32	48.32	108.7 5
<b>0.5 Gy 24h</b>	115.7 6	177.2 7	101.6 9	120.9 6	104.7 1	90.08	0.00	98.65	56.76	95.78
<b>2 Gy 24h</b>	101.4 5	126.8 2	118.5 7	94.59	107.2 3	90.74	0.00	93.74	72.64	100.4 7

ApoTox Caspase Activity 1-24hrs

	<b>JHP</b>		<b>2139</b>		<b>2145</b>		<b>AT2Bi</b>		<b>AT3Bi</b>	
<b>0Gy</b>	0.93	0.36	1.48	1.31	1.77	1.34	0.00	1.47	4.91	1.24
<b>0.05Gy</b>	1.32	1.28	1.38	3.89	1.45	3.34	1.82	1.19	2.33	1.07
<b>0.5Gy</b>	2.24	0.82	1.49	1.54	1.81	1.09	1.62	1.46	2.88	1.02
<b>2Gy</b>	1.54	0.62	2.05	1.42	1.83	0.99	2.05	1.30	3.60	1.18

Cell Counts 72hrs post irradiation

	<b>0Gy</b>			<b>0.05Gy</b>			<b>0.5Gy</b>			<b>2Gy</b>		
<b>214 5</b>	236 46	2826 6	3771 6	2683 8	3175 2	2780 4	242 76	264 60	371 70	283 50	274 26	295 26
<b>213 9</b>	800 94	1037 84	1002 12	8719 2	9370 2	9823 8	861 00	866 04	774 90	617 82	575 82	490 98
<b>AT2 Bi</b>	395 22	1008 42	1579 20	1177 26	8933 4	1173 90	860 58	795 48	844 62	777 42	696 78	541 80

<b>AT3</b>	795	1189	1025	1100	1015	8353	740	470	649	434	360	378
<b>Bi</b>	90	86	64	82	56	8	04	40	32	28	36	84

Mitotic Index (MI) and Mitotic Inhibition (MI<sub>n</sub>)

<b>MI</b>	<b>2139</b>			<b>2145</b>			<b>AT2Bi</b>			<b>AT3Bi</b>		
<b>0Gy</b>	2.3	1.5	0	2.1	1.4	1.4	2.3	1	1.1	1.9	0.8	0.2
<b>0.05Gy</b>	1.7	1.5	0	1	1.1	1.1	1.8	2.1	0.8	2.7	0.6	0.4
<b>0.5Gy</b>	1.1	0.6	0	0.3	0.3	0.3	2.6	1.3	0.2	1.2	1.2	0.2
<b>2Gy</b>	0.4	0.8	0.2	0.5	0.4	0.4	1	1.2	0.2	1	0.7	0.6

<b>MI<sub>n</sub></b>	<b>2139</b>			<b>2145</b>			<b>AT2Bi</b>			<b>AT3Bi</b>		
<b>0.05Gy</b>	0.6	0	0	1.1	0.3	0.3	0.5	-1.1	0.3	-0.8	0.2	-0.2
<b>0.5Gy</b>	1.2	0.9	0	1.8	1.1	1.1	-0.3	-0.3	0.9	0.7	-0.4	0
<b>2Gy</b>	1.9	0.7	-0.2	1.6	1	1	1.3	-0.2	0.9	0.9	0.1	-0.4

G2 Scoring and Radiation Induced G2 Scores (RIG2)

<b>G2 Score</b>	<b>2139</b>			<b>2145</b>			<b>AT2Bi</b>			<b>AT3Bi</b>		
<b>0Gy</b>	16	4	20	8	20	8	28	28	35	52	20	30
<b>0.05Gy</b>	32	36	30	32	64	32	56	36	65	60	62	50
<b>0.5Gy</b>	160	228	260	112	148	112	124	220	150	252	208	190
<b>2Gy</b>	428	616	380	348	388	348	352	732	140	372	708	310

<b>RIG2</b>	<b>2139</b>			<b>2145</b>			<b>AT2Bi</b>			<b>AT3Bi</b>		
<b>0.05Gy</b>	16	32	10	24	44	24	28	8	30	8	42	20
<b>0.5Gy</b>	144	224	240	104	128	104	96	192	115	200	188	160
<b>2Gy</b>	412	612	360	340	368	340	324	704	105	320	688	280

### Chapter 5 Raw Data

MQRT –PCR - Normalised Data (Fold Change)

<b>Sample</b>	<b>PCNA</b>	<b>FDXR</b>	<b>P21</b>	<b>SESN1</b>
AT2Bi 0.05Gy 1hr	0.919177	1.110493	1.032746	1.11577
AT2Bi 0.5Gy 1hr	0.754587	1.270328	1.016582	0.880653
AT2Bi 2Gy 1hr	0.745508	1.287842	1.029392	0.967804
AT3Bi 0.05Gy 1hr	0.902605	0.911643	1.030412	1.122742
AT3Bi 0.5Gy 1hr	0.888705	0.781666	0.895406	1.008241
AT3Bi 2Gy 1hr	0.949094	0.89301	0.980568	1.324691
AT2Bi 0.05Gy 24hr	0.868377	0.86088	0.934733	1.086126
AT2Bi 0.5Gy 24hr	0.918508	1.245308	1.174283	1.624216
AT2Bi 2Gy 24hr	1.241255	1.830222	1.672011	2.189475
AT3Bi 0.05Gy 24hr	0.784252	0.349404	0.804571	0.702519
AT3Bi 0.5Gy 24hr	0.841185	0.780811	1.131008	1.132107



AT3Bi 2Gy 24hr	0.842179	0.815155	1.549165	1.209027
----------------	----------	----------	----------	----------

**Healthy Controls - Normalised Data (fold change)**

Sample	PCNA	FDXR	P21	SESN1
HC2 0.05Gy	1.110126	0.877863	1.281174	1.322508
HC2 0.5Gy	1.119646	1.578781	2.058172	3.278546
HC3 0.05Gy	1.397979	0.662263	1.948526	1.177761
HC3 0.5Gy	1.521833	2.164034	3.280928	4.46511
HC5 0.05Gy	0.860438	1.624883	0.847281	1.076097
HC5 0.5Gy	0.890608	1.559131	1.974453	1.911292
HC8 0.05Gy	0.952913	1.07103	0.499578	0.738732
HC8 0.5Gy	1.786761	1.518046	0.944732	1.940352
HC9 0.05Gy	0.991377	1.318096	0.826383	0.832364
HC9 0.5Gy	1.302731	2.523767	1.779014	3.627248
HC14 0.05Gy	0.962132	1.025735	1.230263	0.734703
HC14 0.5Gy	1.355342	0.877589	1.665457	1.247238
HC16 0.05Gy	1.322959	2.391783	0.816146	3.545202
HC19 0.05Gy	0.988173	1.404782	1.755273	1.287977
HC19 0.5Gy	0.879663	2.31001	1.983739	1.715043
HC20 0.05Gy	0.868947	0.953691	2.597556	1.192586
HC21 0.05Gy	1.052153	0.841791	0.954154	1.049787
HC22 0.05Gy	0.879997	0.817977	0.790888	1.1716
HC22 0.5Gy	0.912996	2.612916	2.064115	2.844642
HC26 0.05Gy	1.255739	1.208948	0.879326	0.639961
HC27 0.05Gy	0.861952	0.922499	0.84357	1.054141
HC27 0.5Gy	1.265653	0.945579	1.07601	2.26491
HC44 0.05Gy	1.069835	1.016579	1.114588	1.307459
HC44 0.5Gy	1.040415	1.215458	0.624157	1.340188
HC45 0.05Gy	0.909927	0.774047	0.989748	0.689184
HC45 0.5Gy	0.917717	1.082442	1.261589	1.190184
HC46 0.05Gy	0.834676	1.66211	0.729044	0.623268
HC46 0.5Gy	0.963741	1.53199	0.909161	0.825911
HC47 0.05Gy	0.961919	1.760766	1.414731	1.465533
HC47 0.5Gy	1.04936	1.274469	1.790858	1.75134
HC48 0.05Gy	1.033921	1.003336	1.010927	0.915691
HC48 0.5Gy	1.041853	0.950855	1.076004	1.194177
HC50 0.05Gy	1.080487	1.250464	2.05233	1.345692
HC50 0.5Gy	1.119204	1.010686	1.545948	0.826563

**Healthy Controls Just 0.05Gy**

Sample	PCNA	FDXR	P21	SESN1
HC2 0.05Gy	1.110126	0.877863	1.281174	1.322508
HC3 0.05Gy	1.397979	0.662263	1.948526	1.177761
HC5 0.05Gy	0.860438	1.624883	0.847281	1.076097
HC8 0.05Gy	0.952913	1.07103	0.499578	0.738732

HC9 0.05Gy	0.991377	1.318096	0.826383	0.832364
HC14 0.05Gy	0.962132	1.025735	1.230263	0.734703
HC16 0.05Gy	1.322959	2.391783	0.816146	3.545202
HC19 0.05Gy	0.988173	1.404782	1.755273	1.287977
HC20 0.05Gy	0.868947	0.953691	2.597556	1.192586
HC21 0.05Gy	1.052153	0.841791	0.954154	1.049787
HC22 0.05Gy	0.879997	0.817977	0.790888	1.1716
HC26 0.05Gy	1.255739	1.208948	0.879326	0.639961
HC27 0.05Gy	0.861952	0.922499	0.84357	1.054141
HC44 0.05Gy	1.069835	1.016579	1.114588	1.307459
HC45 0.05Gy	0.909927	0.774047	0.989748	0.689184
HC46 0.05Gy	0.834676	1.66211	0.729044	0.623268
HC47 0.05Gy	0.961919	1.760766	1.414731	1.465533
HC48 0.05Gy	1.033921	1.003336	1.010927	0.915691
HC50 0.05Gy	1.080487	1.250464	2.05233	1.345692
Mean	1.020824	1.188876	1.188499	1.166855
St.DEV	0.159527	0.427568	0.540988	0.633251

<b>Healthy Controls Just 0.5Gy</b>				
<b>Sample</b>	<b>PCNA</b>	<b>FDXR</b>	<b>P21</b>	<b>SESN1</b>
HC2 0.5Gy	1.119646	1.578781	2.058172	3.278546
HC3 0.5Gy	1.521833	2.164034	3.280928	4.46511
HC5 0.5Gy	0.890608	1.559131	1.974453	1.911292
HC8 0.5Gy	1.786761	1.518046	0.944732	1.940352
HC9 0.5Gy	1.302731	2.523767	1.779014	3.627248
HC14 0.5Gy	1.355342	0.877589	1.665457	1.247238
HC19 0.5Gy	0.879663	2.31001	1.983739	1.715043
HC22 0.5Gy	0.912996	2.612916	2.064115	2.844642
HC27 0.5Gy	1.265653	0.945579	1.07601	2.26491
HC44 0.5Gy	1.040415	1.215458	0.624157	1.340188
HC45 0.5Gy	0.917717	1.082442	1.261589	1.190184
HC46 0.5Gy	0.963741	1.53199	0.909161	0.825911
HC47 0.5Gy	1.04936	1.274469	1.790858	1.75134
HC48 0.5Gy	1.041853	0.950855	1.076004	1.194177
HC50 0.5Gy	1.119204	1.010686	1.545948	0.826563
Mean	1.144502	1.543717	1.602289	2.028183
St.DEV	0.259536	0.592095	0.662057	1.080612

**Prostate Cancer - Normalised Data (Fold Change)**

<b>Sample</b>	<b>PCNA</b>	<b>FDXR</b>	<b>P21</b>	<b>SESN1</b>
PC001 V1 0.05Gy	1.063391	1.03777	1.402611	0.967529
PC001 V1 0.5Gy	0.893782	1.381058	1.90267	1.86981
PC002 V4 0.05Gy	0.994958	0.882049	1.304527	0.9542
PC002 V4 0.5Gy	1.111059	0.841627	1.947614	1.709929
PC003 V1 0.05Gy	1.033709	0.728164	0.734806	0.613978
PC003 V1 0.5Gy	1.039751	0.493734	0.380631	0.365461
PC005 V1 0.05Gy	0.946253	1.077003	1.867887	1.290449
PC005 V1 0.5Gy	0.815879	2.475847	2.14395	1.740451
PC005 V2 0.05Gy	1.334633	0.952007	0.298479	0.523459
PC005 V2 0.5Gy	1.505957	0.625373	0.443468	0.487382
PC007 V2 0.05Gy	1.035384	0.720189	0.830568	0.981592
PC007 V2 0.5Gy	1.041125	0.975453	1.425653	2.061837
PC009 V1 0.05Gy	0.817622	1.697529	1.09141	1.627669
PC009 V1 0.5Gy	1.021685	0.990841	0.795585	1.925674
PC012 V2 0.05Gy	0.876305	0.786333	1.211596	0.930966
PC012 V2 0.5Gy	0.81104	0.601146	0.957512	0.747135
PC017 V1 0.05Gy	1.068953	1.072219	1.014133	1.034365
PC017 V1 0.5Gy	1.044253	1.448709	1.335709	1.584734
PC018 V1 0.05Gy	0.934593	1.272675	0.704984	0.897611
PC018 V1 0.5Gy	0.848493	0.979243	0.565337	1.314584
PC018 V2 0.05Gy	1.081918	0.975362	1.766153	1.361897
PC018 V2 0.5Gy	0.999578	1.178319	1.358757	1.62562

**Prostate Cancer Just 0.05Gy**

<b>Sample</b>	<b>PCNA</b>	<b>FDXR</b>	<b>P21</b>	<b>SESN1</b>
PC001 V1 0.05Gy	1.063391	1.03777	1.402611	0.967529
PC002 V4 0.05Gy	0.994958	0.882049	1.304527	0.9542
PC003 V1 0.05Gy	1.033709	0.728164	0.734806	0.613978
PC005 V1 0.05Gy	0.946253	1.077003	1.867887	1.290449
PC005 V2 0.05Gy	1.334633	0.952007	0.298479	0.523459
PC007 V2 0.05Gy	1.035384	0.720189	0.830568	0.981592
PC009 V1 0.05Gy	0.817622	1.697529	1.09141	1.627669
PC012 V2 0.05Gy	0.876305	0.786333	1.211596	0.930966
PC017 V1 0.05Gy	1.068953	1.072219	1.014133	1.034365
PC018 V1 0.05Gy	0.934593	1.272675	0.704984	0.897611
PC018 V2 0.05Gy	1.081918	0.975362	1.766153	1.361897

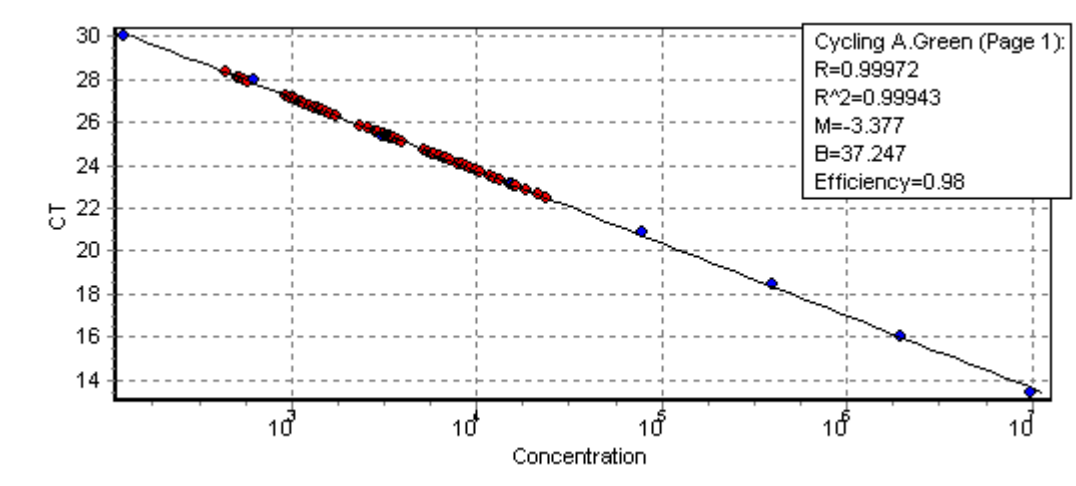
**Prostate Cancer Just 0.5Gy**

<b>Sample</b>	<b>PCNA</b>	<b>FDXR</b>	<b>P21</b>	<b>SESN1</b>
---------------	-------------	-------------	------------	--------------

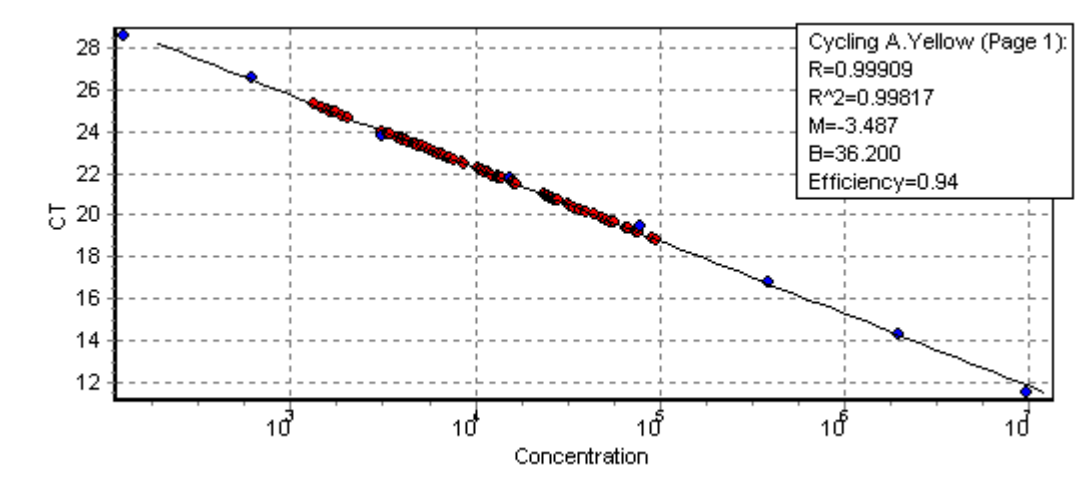
PC001 V1 0.5Gy	0.893782	1.381058	1.90267	1.86981
PC002 V4 0.5Gy	1.111059	0.841627	1.947614	1.709929
PC003 V1 0.5Gy	1.039751	0.493734	0.380631	0.365461
PC005 V1 0.5Gy	0.815879	2.475847	2.14395	1.740451
PC005 V2 0.5Gy	1.505957	0.625373	0.443468	0.487382
PC007 V2 0.5Gy	1.041125	0.975453	1.425653	2.061837
PC009 V1 0.5Gy	1.021685	0.990841	0.795585	1.925674
PC012 V2 0.5Gy	0.811104	0.601146	0.957512	0.747135
PC017 V1 0.5Gy	1.044253	1.448709	1.335709	1.584734
PC018 V1 0.5Gy	0.848493	0.979243	0.565337	1.314584
PC018 V2 0.5Gy	0.999578	1.178319	1.358757	1.62562

## MQRT-PCR Efficiency Graphs

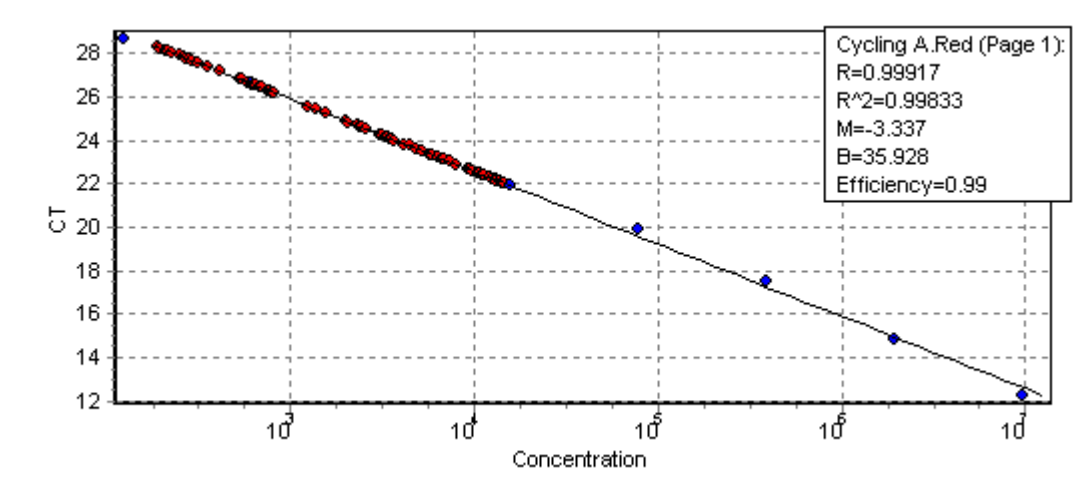
PC 100 WELL ROTOR PLATE 1



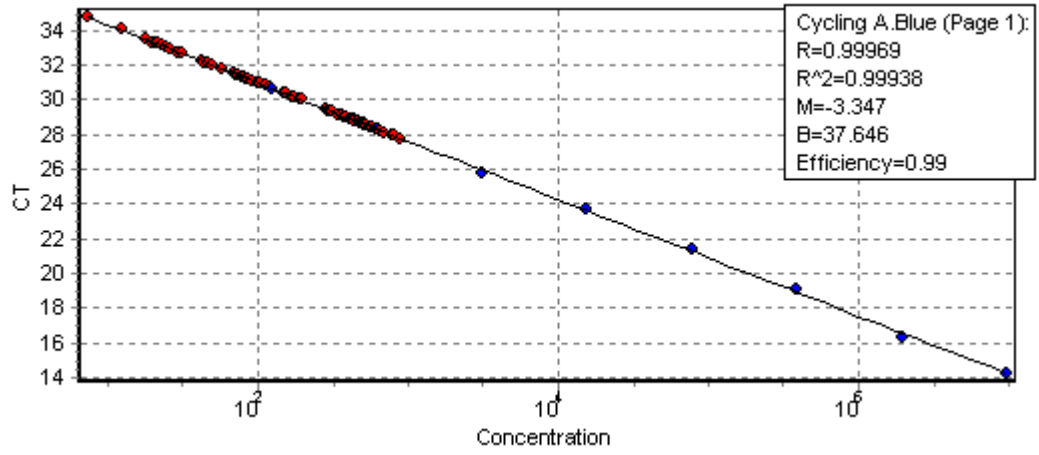
HPRT 0.01908 (9)



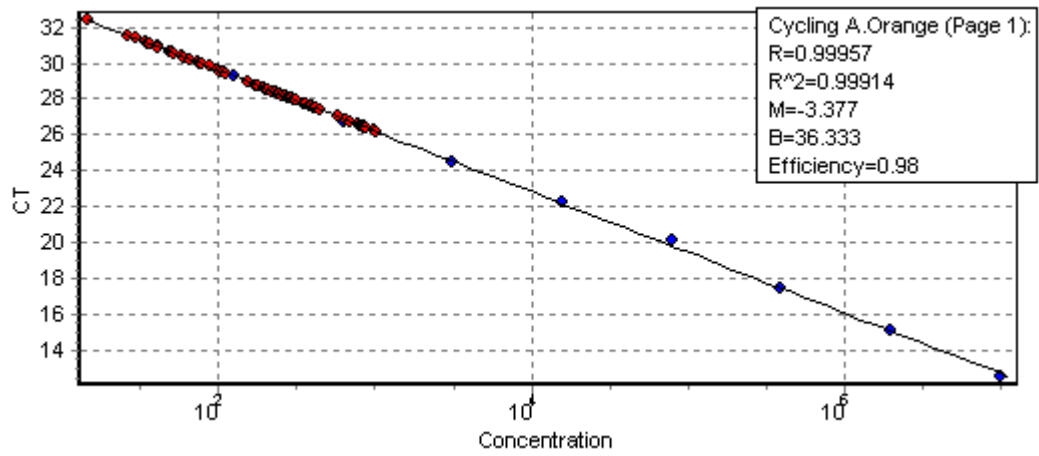
PCNA 0.01908 (9)



P21 0.03962 (9)

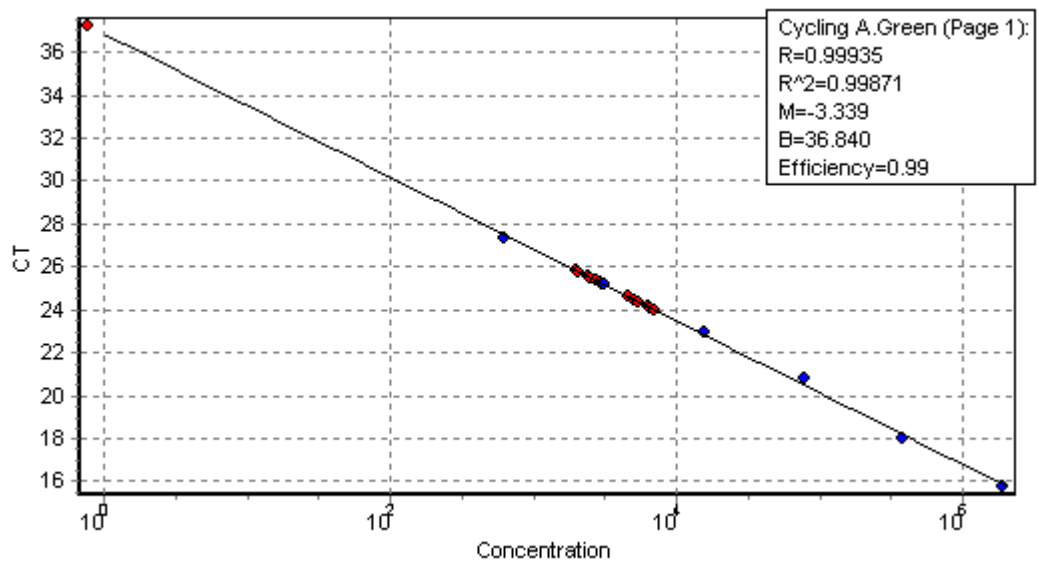


SESN1 0.0223 (9)

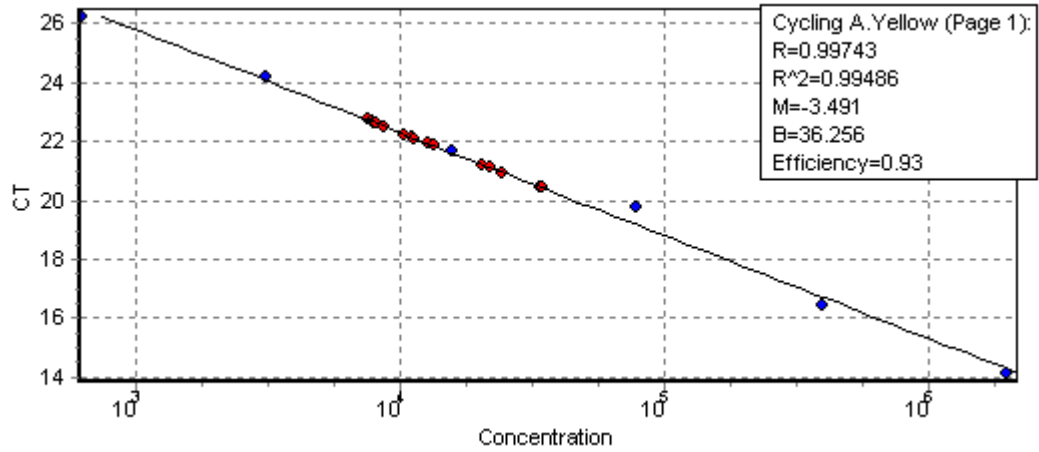


FDXR 0.16541 (9)

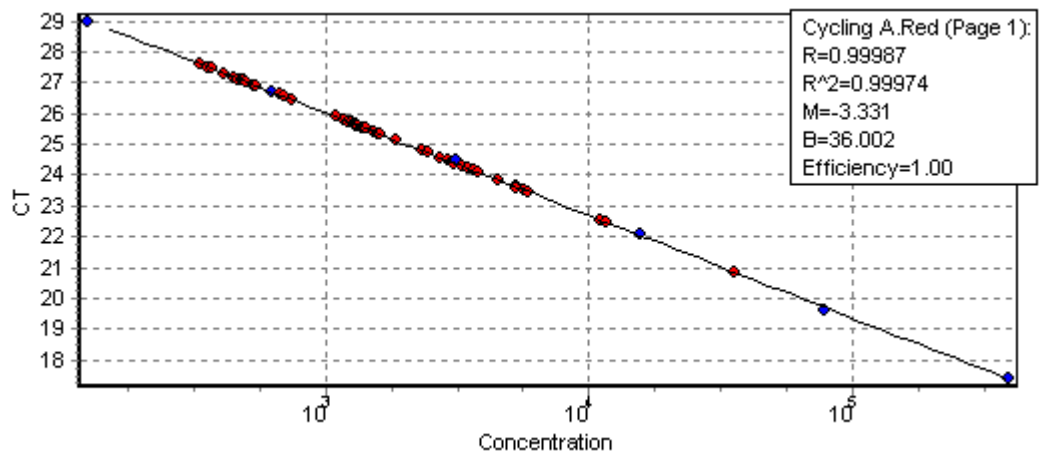
PC Plate 2 (72 well ROTOR)



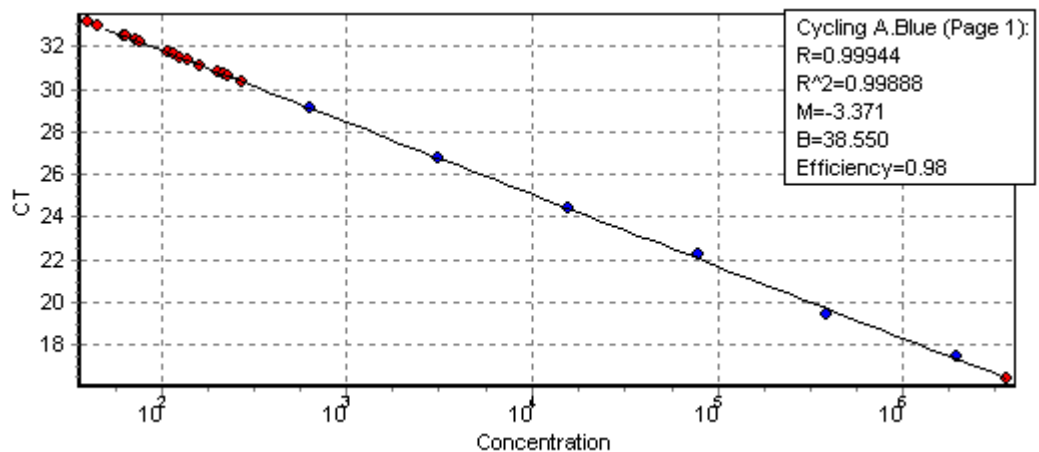
HPRT 0.02655 (1,8,9)



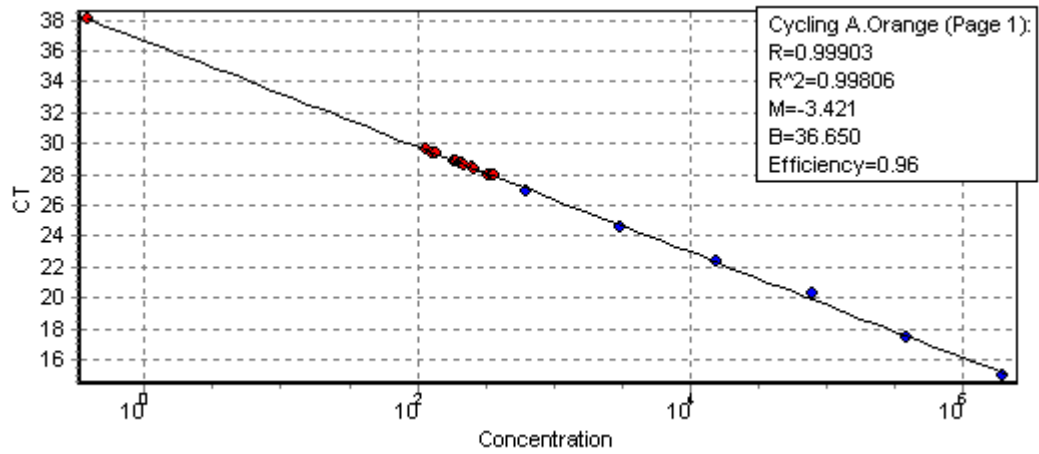
PCNA 0.01908 (1,8,9)



P21 0.03962 (1,8,9)

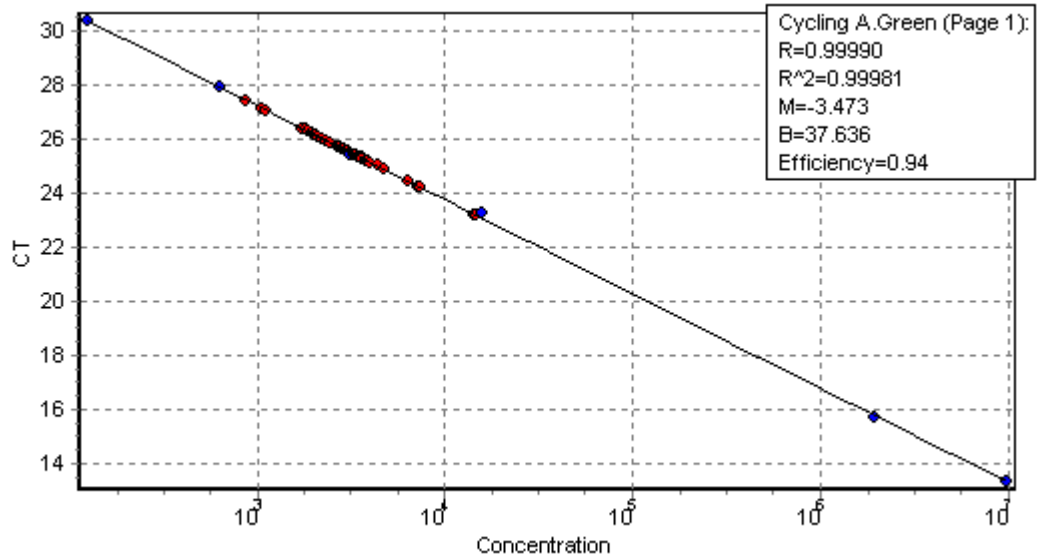


SES1 0.0223 (1,8,9)

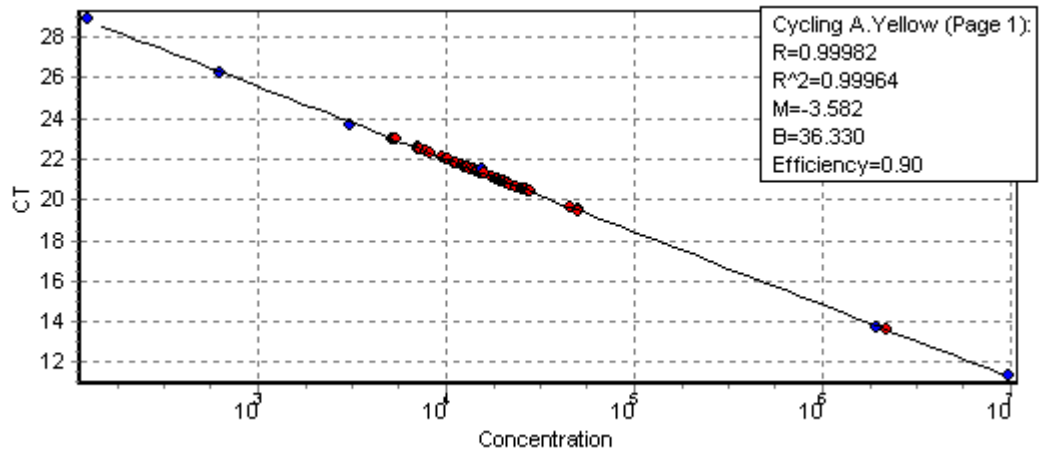


FDXR 0.01908 (1,8,9)

HC PLATE 1

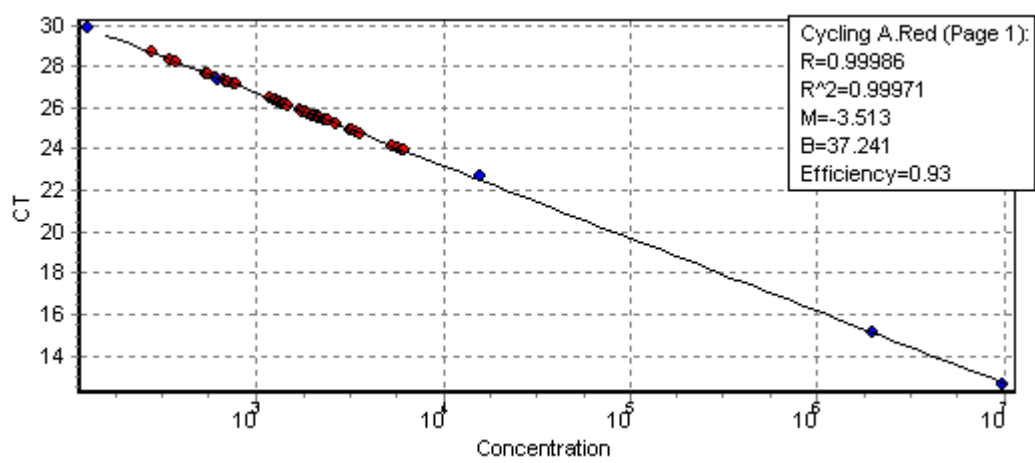


HPRT 0.02655 (3,4,9)

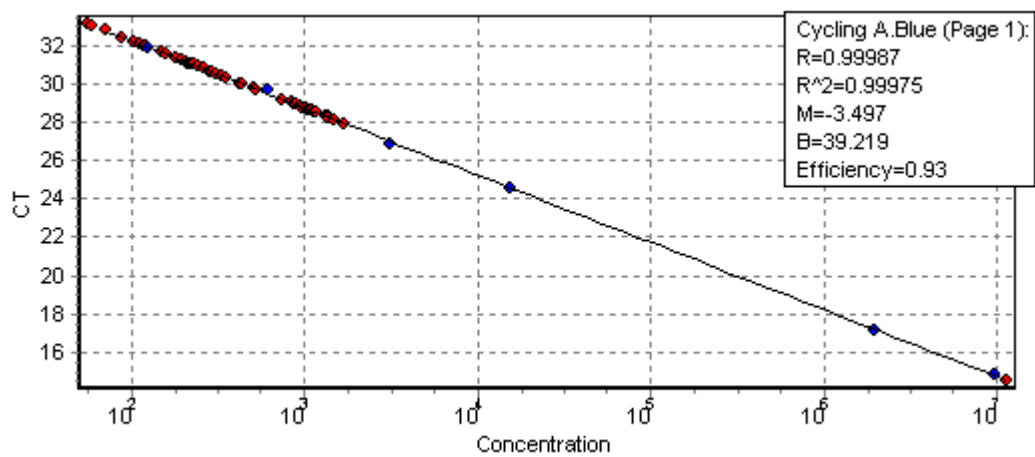


PCNA 0.01908 (3,4,9)

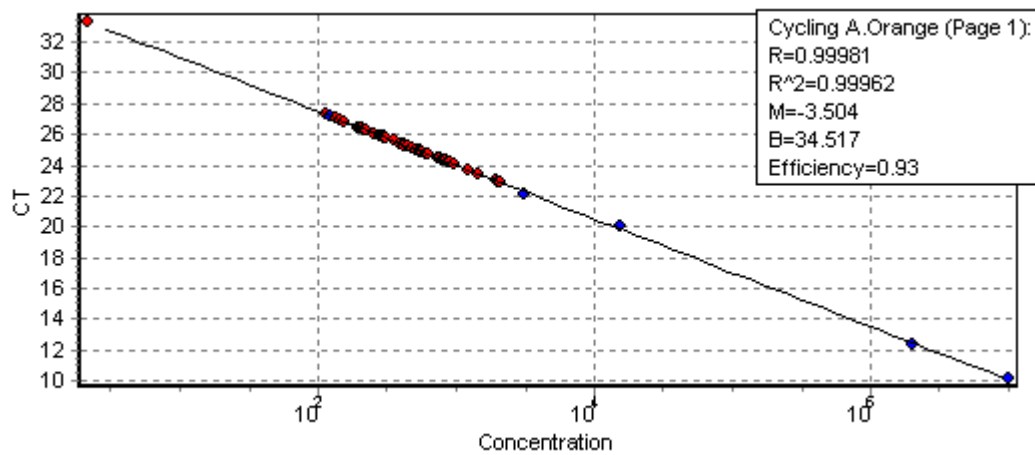




P21 0.03962 (3,4,9)

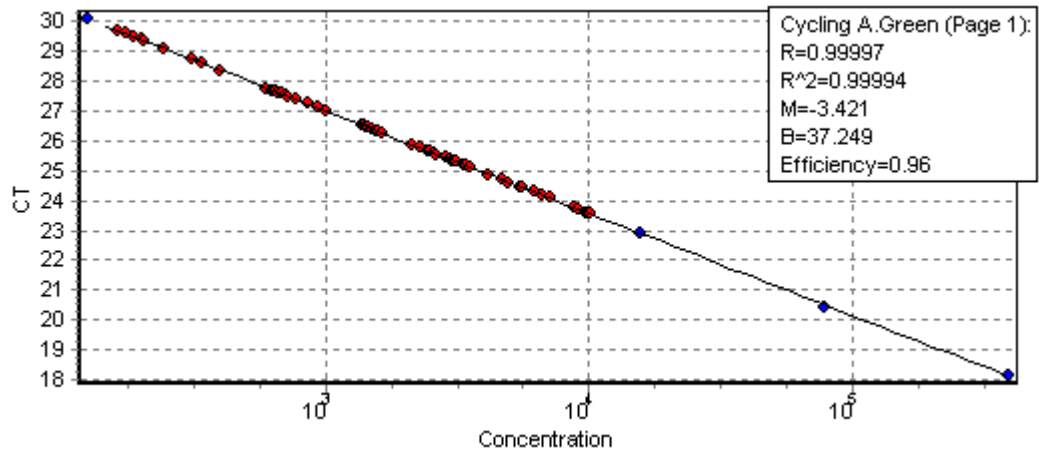


SESN1 0.0223 (3,4,9)

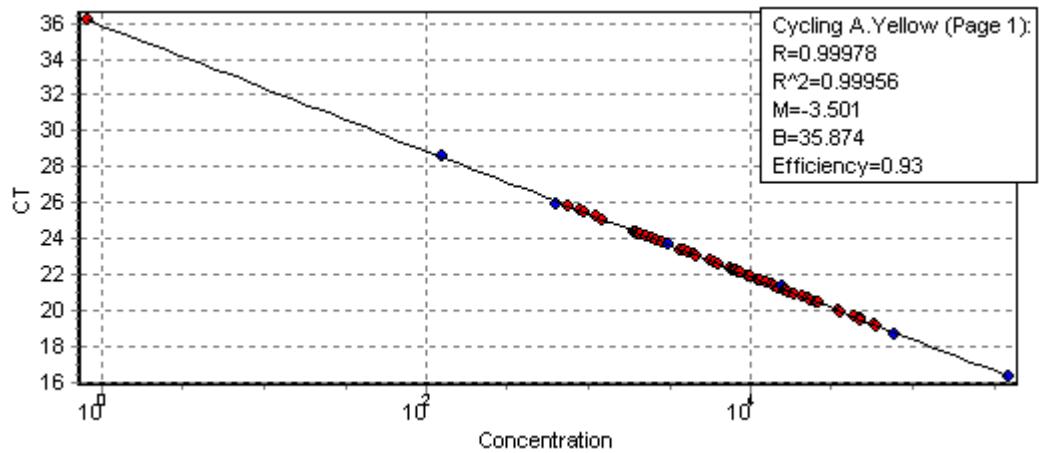


FDXR 0.16541 (3,4,9)

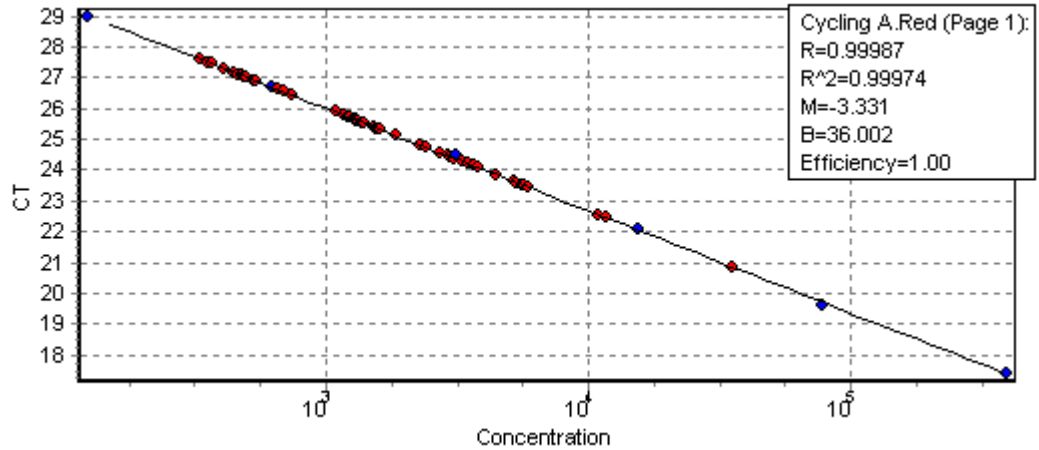
HC PLATE 2



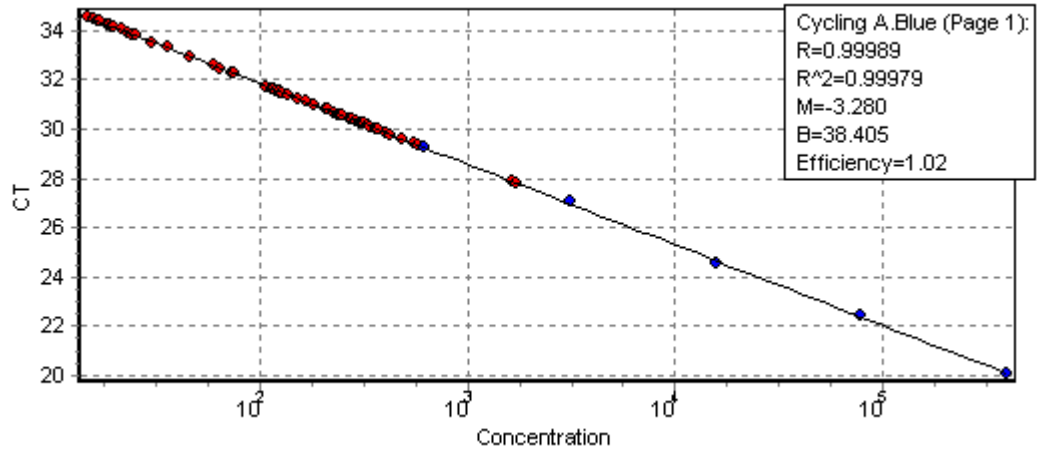
HPRT 0.02655 (1,2,9)



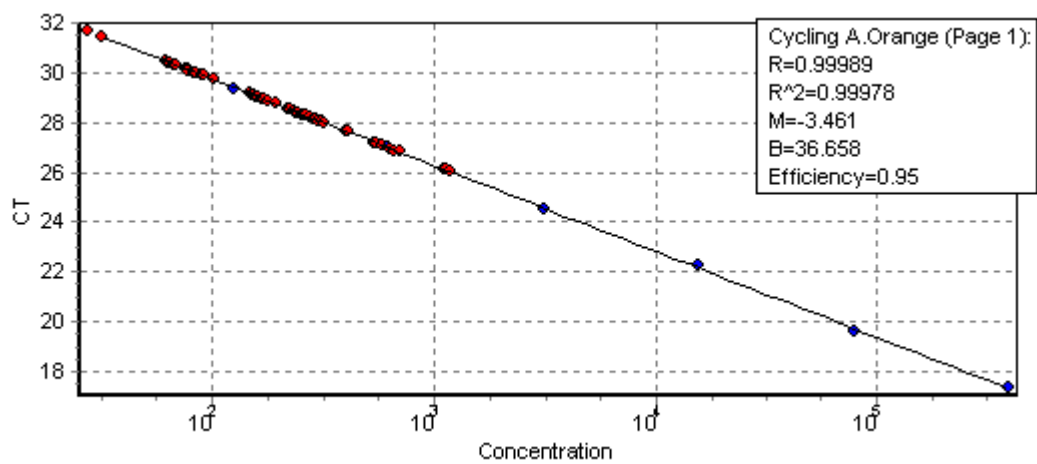
PCNA 0.01908 (1,2,9)



P21 0.03962 (1,2,9)

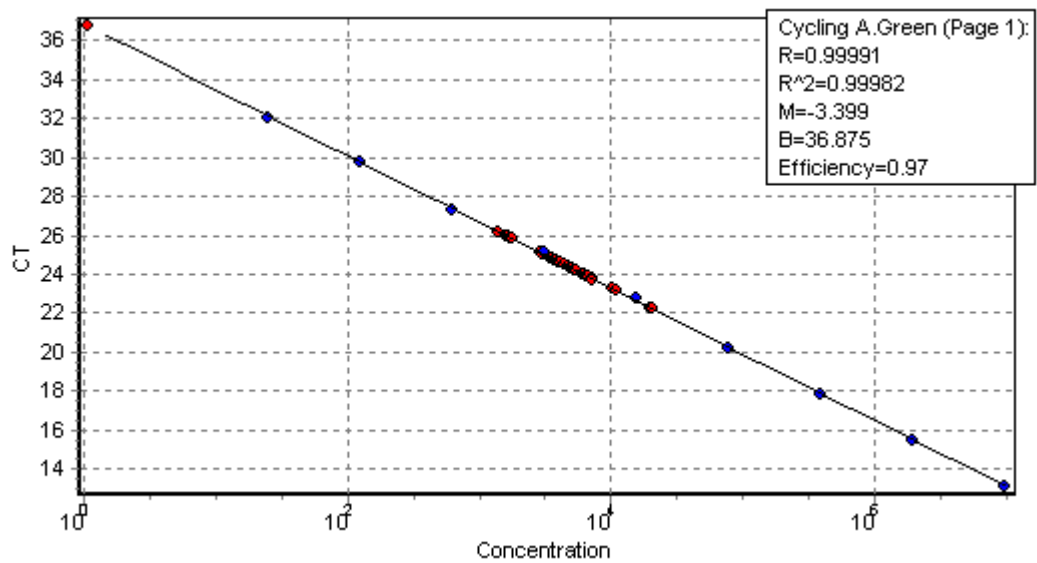


SESN1 0.0223 (1,2,9)

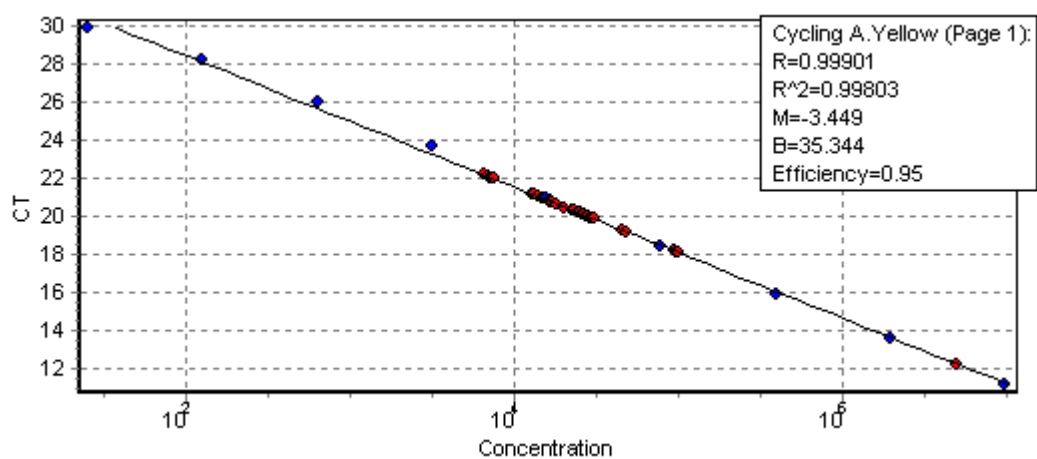


FDXR 0.16541 (1,2,9)

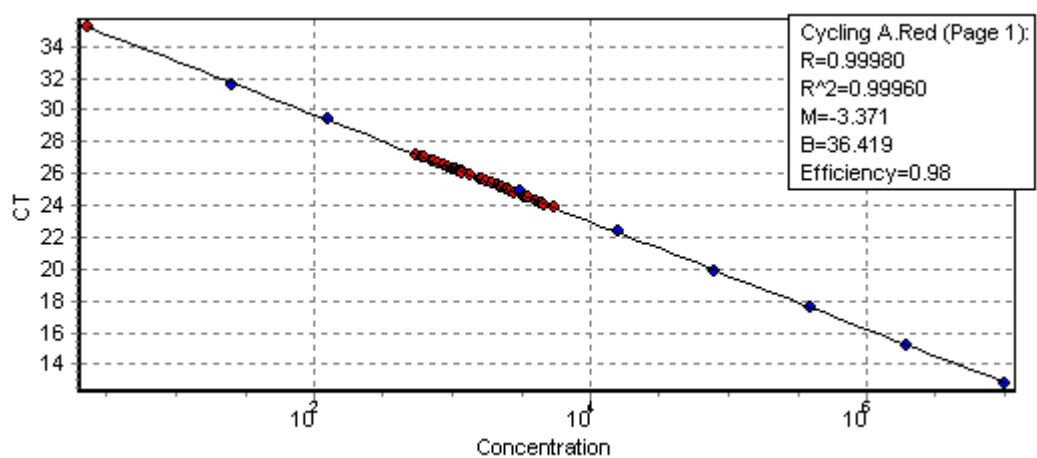
HC PLATE 3



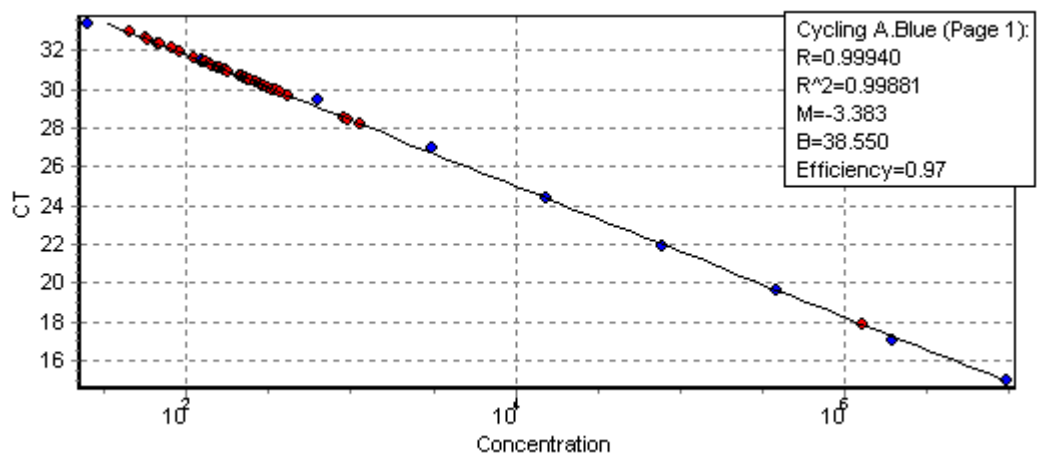
HPRT 0.02655



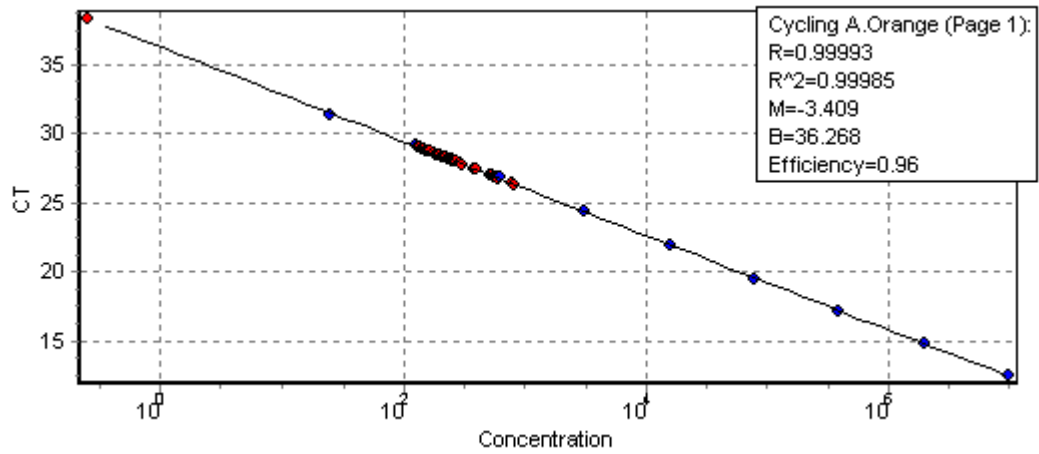
PCNA 0.01908



P21 0.03962

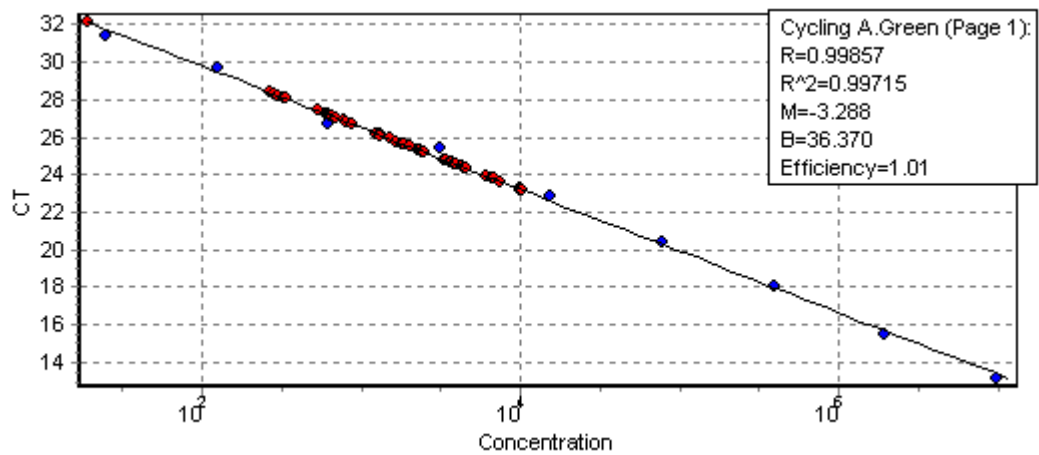


SES1 0.0223

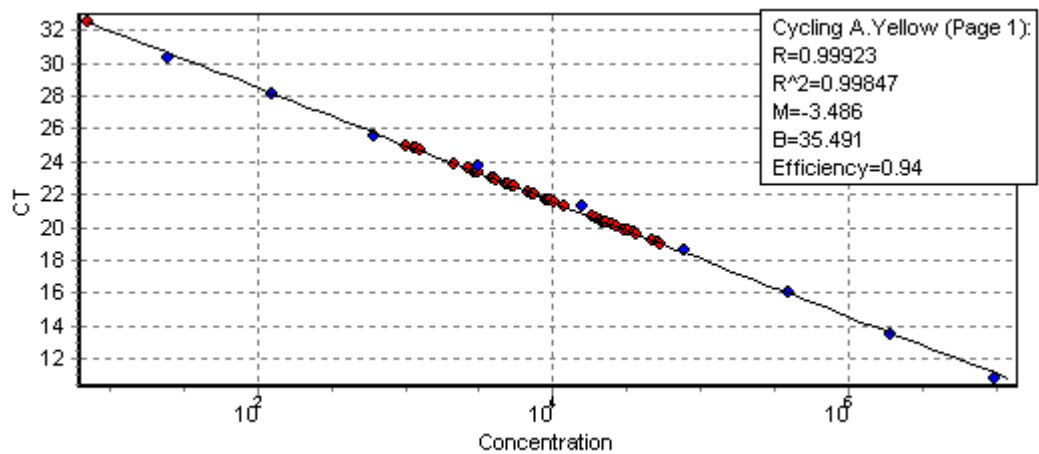


FDXR 0.16541

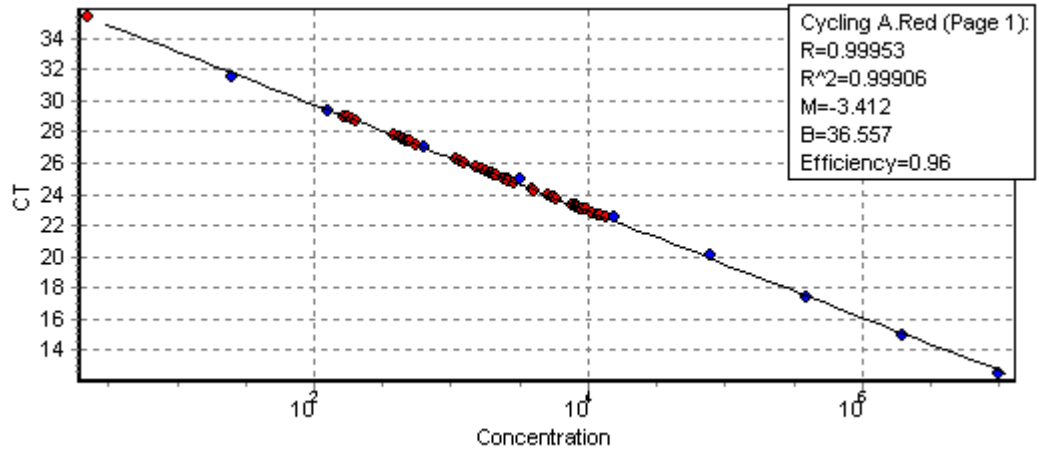
PC 72 WELL ROTOR PLATE 1



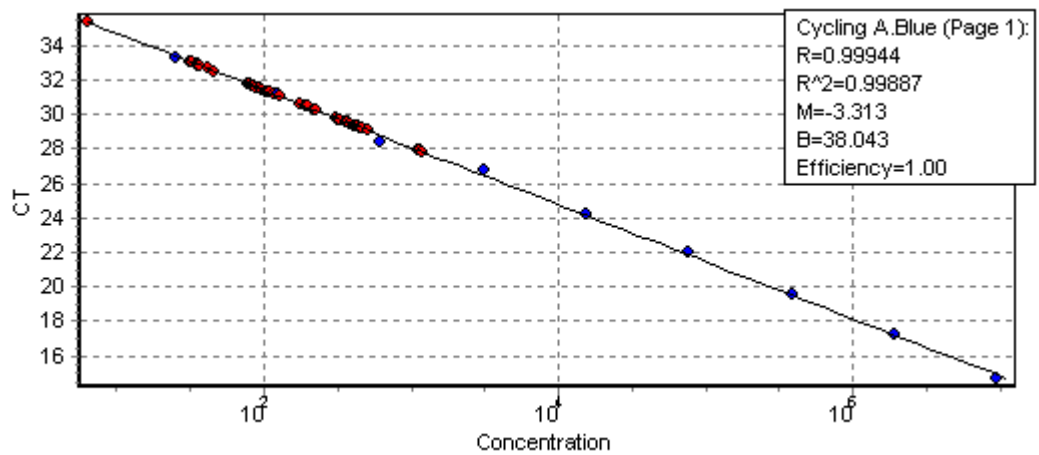
HPRT 0.02655



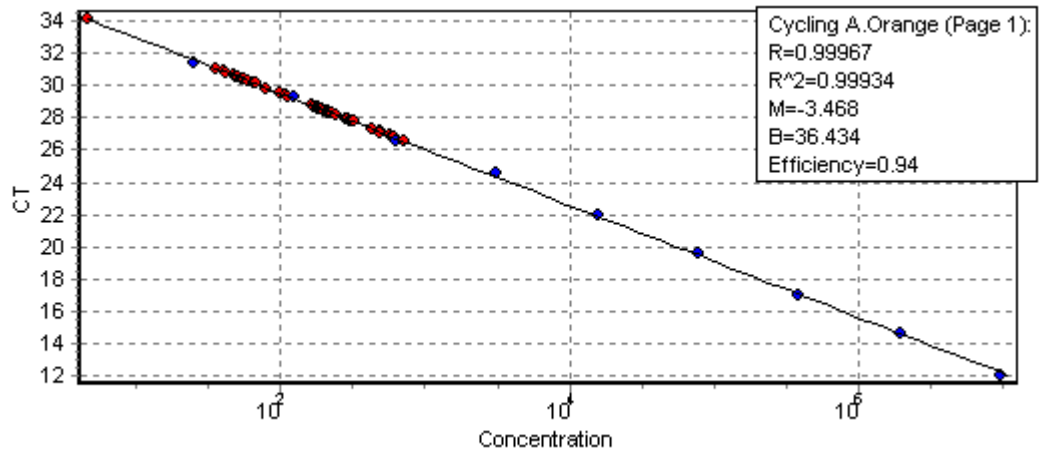
PCNA 0.01908



P21 0.03962



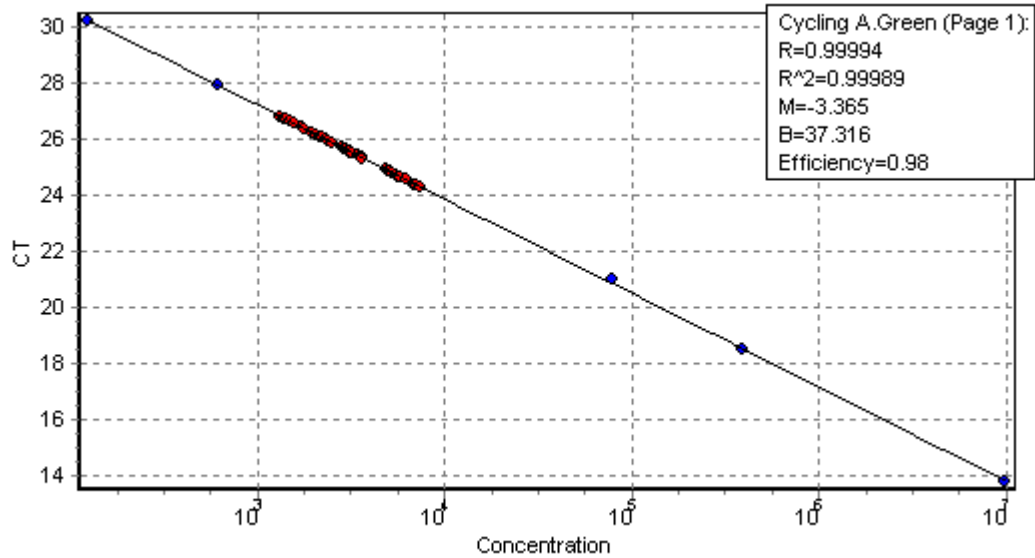
SESN1 0.0223



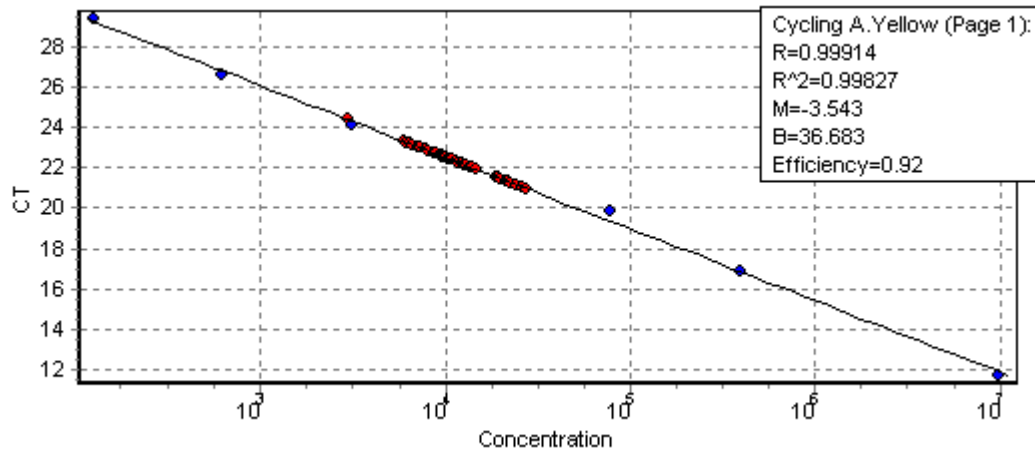
FDXR 0.16541

PC 72 WELL ROTOR PLATE 2

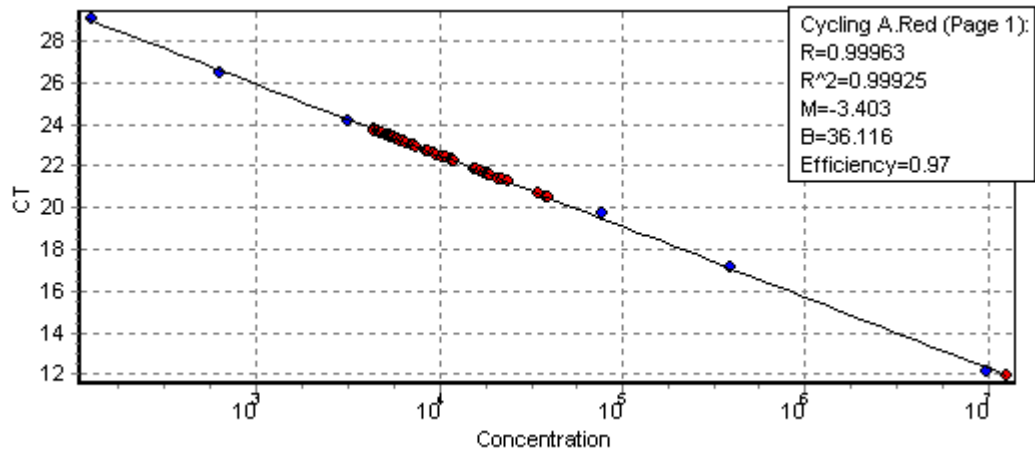
CELL LINE PLATE 1



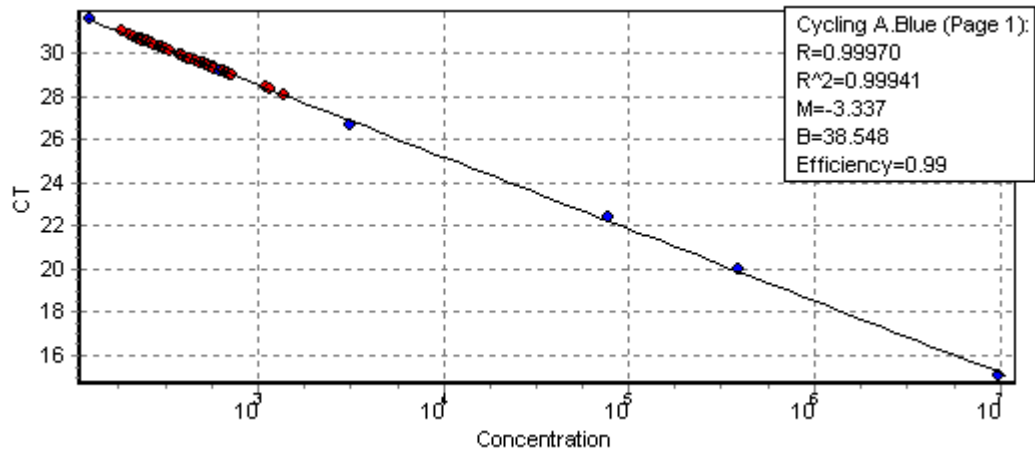
HPRT 0.02655 (2,5,9)



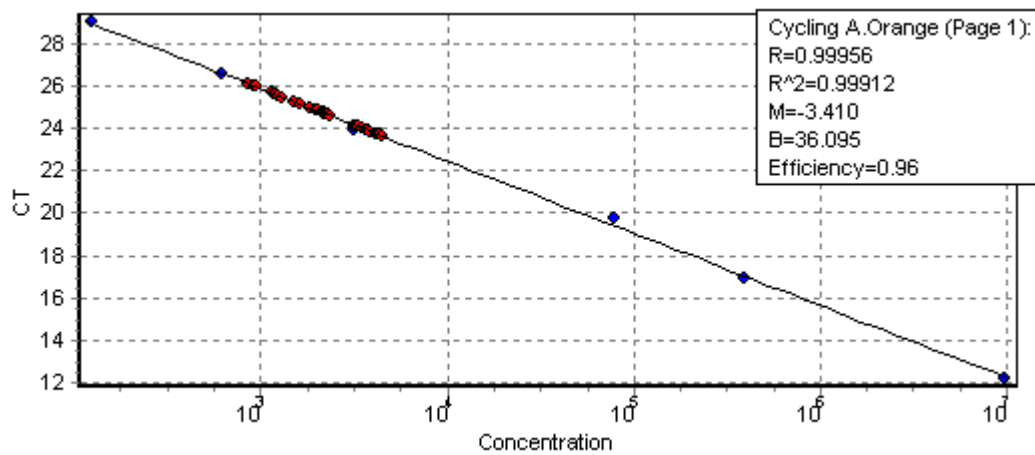
PCNA 0.01908 (2,5,9)



P21 0.03962 (2,5,9)



SESN1 0.0223 (2,5,9)



FDXR 0.16541 (2,5,9)

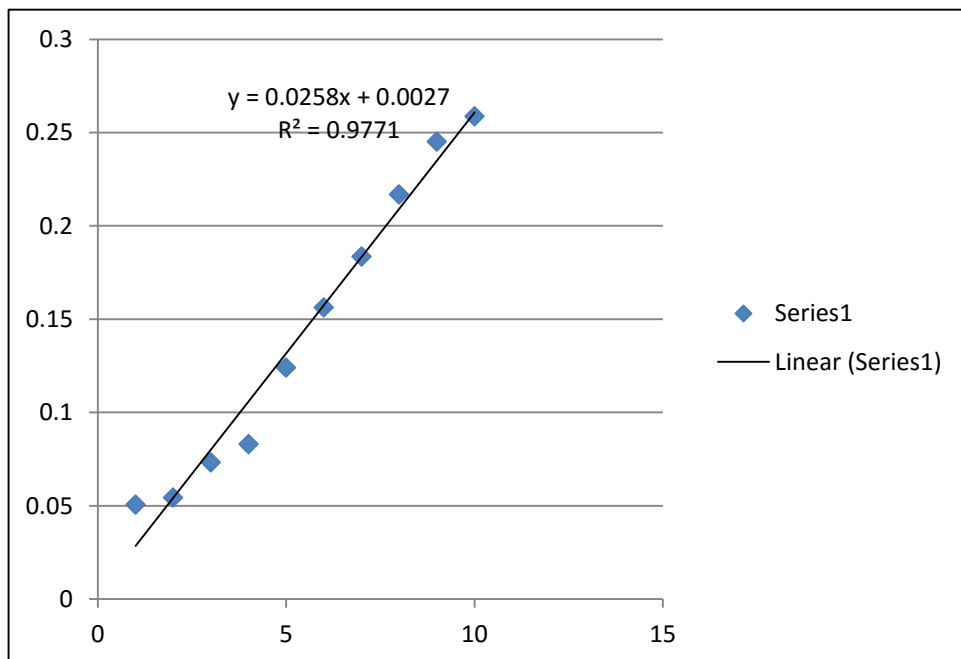
## Chapter 6 Raw Data

### Protein Loading from Cells

1.4	0.2204	0.2561	0.2999	0.2588	0.050667	
1.2	0.2133	0.2845	0.238	0.245266667	0.054467	
1	0.1712	0.1904	0.1893	0.183633333	0.073367	
0.8	0.2179	0.2194	0.2133	0.216866667	0.083067	
0.6	0.1759	0.1421	0.151	0.156333333	0.124133	
0.4	0.1291	0.1136	0.1297	0.124133333	0.156333	
0.2	0.0856	0.0841	0.0795	0.083066667	0.183633	
0.1	0.0732	0.0719	0.075	0.073366667	0.216867	
0.5	0.0553	0.0543	0.0538	0.054466667	0.245267	
0.01	0.0511	0.051	0.0499	0.050666667	0.2588	

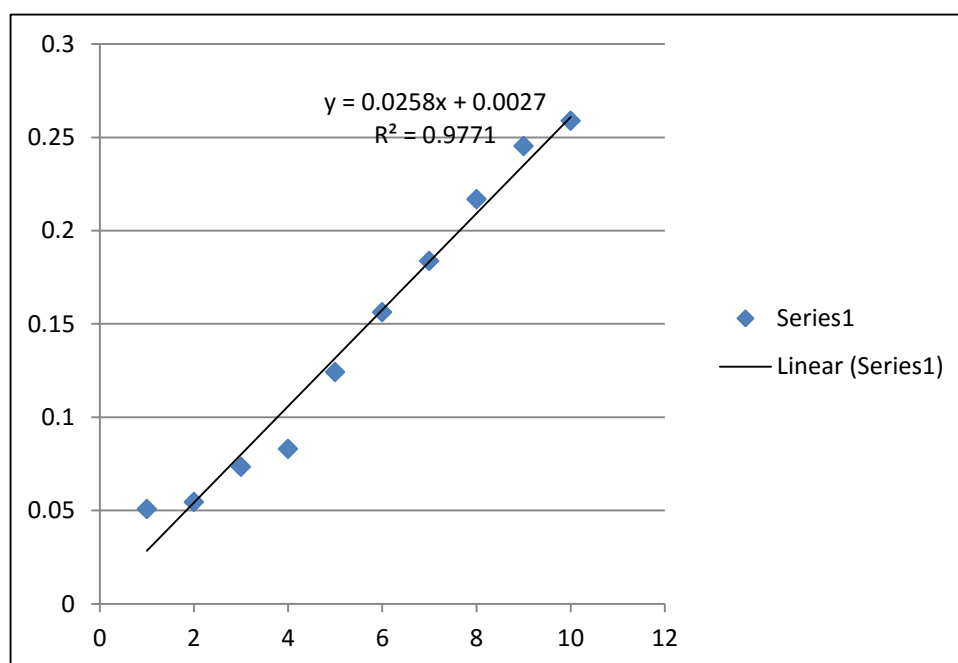


2139				Average	µg/µl	µl needed for 50µg
0Gy	0.1938	0.1909	0.2247	0.203133333	7.768734	6.436055214
0.05Gy	0.2466	0.2098	0.2596	0.238666667	9.145995	5.466873852
0.5Gy	0.1852	0.2245	0.2135	0.207733333	7.947028	6.291659893
2Gy	0.2113	0.1603	0.2442	0.205266667	7.851421	6.368273819
2145						
0Gy	0.1758	0.2308	0.204	0.203533333	7.784238	6.423236515
0.05Gy	0.1916	0.1729	0.1768	0.180433333	6.888889	7.258064516
0.5Gy	0.2131	0.1751	0.1674	0.1852	7.073643	7.068493151
2Gy	0.2288	0.2207	0.1735	0.207666667	7.944444	6.293706294
AT2Bi						
0Gy	0.2107	0.2189	0.2302	0.219933333	8.419897	5.938315176
0.05Gy	0.2184	0.2451	0.2303	0.231266667	8.859173	5.643867581
0.5Gy	0.2195	0.2019	0.2034	0.208266667	7.9677	6.275336468
2Gy	0.3004	0.3065	0.3402	0.3157	12.13178	4.121405751
AT3Bi						
0Gy	0.2196	0.2518	0.2429	0.2381	9.124031	5.480033985
0.05Gy	0.2695	0.2414	0.2137	0.241533333	9.257106	5.401256106
0.5Gy	0.2262	0.1919	0.1889	0.202333333	7.737726	6.461846719
2Gy	0.2096	0.1809	0.1864	0.1923	7.348837	6.803797468



## Protein Loading from Exosomes

<u>2139</u>				Average	µg/µl	µl needed for 50µg
<u>0Gy</u>	0.0792	0.0793	0.0821	0.0802	3.003876	16.64516129
<u>0.05Gy</u>	0.0958	0.0924	0.0741	0.087433	3.284238	15.22423289
<u>0.5Gy</u>	0.0791	0.0724	0.0693	0.0736	2.748062	18.19464034
<u>2Gy</u>	0.0874	0.0803	0.0715	0.079733	2.985788	16.7459974
-						
<u>2145</u>						
<u>0Gy</u>	0.0752	0.0836	0.0641	0.0743	2.775194	18.01675978
<u>0.05Gy</u>	0.0743	0.0777	0.0662	0.072733	2.71447	18.4198001
<u>0.5Gy</u>	0.1049	0.0642	0.0691	0.0794	2.972868	16.81877445
<u>2Gy</u>	0.0724	0.0717	0.0632	0.0691	2.573643	19.42771084
-						
<u>AT2Bi</u>						
<u>0Gy</u>	0.0763	0.073	0.0754	0.0749	2.79845	17.86703601
<u>0.05Gy</u>	0.0726	0.0805	0.0709	0.074667	2.789406	17.92496526
<u>0.5Gy</u>	0.0855	0.0874	0.0798	0.084233	3.160207	15.8217498
<u>2Gy</u>	0.0845	0.0741	0.0778	0.0788	2.949612	16.95137976
-						
<u>AT3Bi</u>						
<u>0Gy</u>	0.0966	0.093	0.0864	0.092	3.46124	14.44568869
<u>0.05Gy</u>	0.0789	0.1427	0.1019	0.107833	4.074935	12.27013316
<u>0.5Gy</u>	0.1209	0.1033	0.1434	0.122533	4.644703	10.76495132
<u>2Gy</u>	0.1018	0.0853	0.0848	0.090633	3.408269	14.6702047



Sample ID	UniSp6	miR-142		miR-451	miR-23a	miR-30c	miR-103a
2145 Exo	17.7	0		0	0	0	0
AT3Bi Exo	17.8	0		0	0	0	0
AT2Bi Exo	17.9	0		36.8	0	0	0
2139 Exo	17.8	0		0	0	0	0
AT3Bi Cell	17.8	23.2		37.8	27	27.5	25.9
2139 Cell	17.8	23.3		36.8	26.7	27.2	25.6
AT2Bi Cell	17.9	22.2		0	27.7	27.6	25.8
2145 Cell	17.8	29.6		37.9	32.5	32.8	30.7
Blank	17.8	0		0	0	0	0
design_target_name	42070.0	42071.0	42072.0	42073.0		Count	St. dev
	0	0	0	0			
	AT3Bi Cell	2139 Cell	AT2Bi Cell	2145 Cell			
hsa-miR-138-5p	28.13	26.79	29.66	36.08		4.00	4.11
hsa-miR-210-3p	28.03	28.69	27.58	35.34		4.00	3.65
hsa-miR-142-5p	27.94	27.98	26.71	34.71		4.00	3.63
hsa-miR-29b-3p	28.88	28.90	27.79	35.53		4.00	3.54
hsa-miR-320b	29.02	29.29	29.42	36.15		4.00	3.46
hsa-miR-155-3p	30.52	30.06	29.17	36.68		4.00	3.43
hsa-miR-142-3p	23.86	23.89	22.55	30.10		4.00	3.39
hsa-miR-29c-3p	27.95	28.18	27.88	34.62		4.00	3.31
hsa-miR-106b-5p	28.13	27.90	27.71	34.48		4.00	3.29
hsa-miR-15b-5p	29.27	29.85	29.22	35.79		4.00	3.18
hsa-miR-19a-3p	26.85	26.15	25.53	32.43		4.00	3.17
hsa-miR-18b-5p	29.46	28.59	28.63	35.15		4.00	3.15
hsa-miR-30e-5p	29.81	29.21	29.11	35.62		4.00	3.14
hsa-let-7f-5p	27.75	27.30	27.04	33.48		4.00	3.07
hsa-miR-9-5p	29.75	32.05	31.45	36.90		4.00	3.07
hsa-miR-19b-3p	25.16	24.80	24.22	30.80		4.00	3.06
hsa-miR-185-5p	30.02	29.83	29.94	36.05		4.00	3.06
hsa-miR-16-2-3p	30.97	30.71	30.51	36.83		4.00	3.06
hsa-miR-29a-3p	26.46	27.53	26.16	32.67		4.00	3.04
hsa-miR-30b-5p	29.55	29.63	27.95	34.85		4.00	3.01
hsa-miR-874-3p	30.54	30.72	30.91	36.62		4.00	2.95
hsa-let-7c-5p	29.47	30.29	29.37	35.52		4.00	2.94
hsa-miR-21-5p	23.91	24.05	23.36	29.60		4.00	2.93
hsa-miR-20a-5p	25.60	25.04	24.81	30.94		4.00	2.91
hsa-miR-32-5p	31.52	29.84	29.66	35.91		4.00	2.91
hsa-miR-26a-5p	29.70	30.50	30.59	35.96		4.00	2.88
hsa-miR-30d-5p	30.89	30.55	29.51	35.95		4.00	2.87
hsa-let-7d-5p	28.28	28.24	28.20	33.98		4.00	2.87
hsa-let-7a-5p	26.07	26.78	26.13	31.94		4.00	2.83
hsa-miR-15a-5p	27.89	27.63	26.95	33.05		4.00	2.81

hsa-miR-484	31.52	31.49	30.72	36.70		4.00	2.76
hsa-miR-103a-3p	26.57	25.97	26.34	31.78		4.00	2.76
hsa-miR-101-3p	30.51	29.77	29.26	35.25		4.00	2.75
hsa-miR-16-5p	24.16	24.28	23.90	29.56		4.00	2.73
hsa-miR-22-3p	30.20	30.09	29.98	35.54		4.00	2.73
hsa-let-7g-5p	26.59	26.45	26.22	31.86		4.00	2.73
hsa-miR-155-5p	22.55	22.79	22.08	27.89		4.00	2.72
hsa-miR-151a-5p	30.46	31.65	31.90	36.62		4.00	2.72
hsa-let-7i-5p	27.87	27.99	27.72	33.27		4.00	2.71
hsa-miR-423-3p	28.02	27.80	27.95	33.32		4.00	2.70
hsa-miR-331-3p	29.66	29.75	29.79	35.12		4.00	2.70
hsa-miR-24-3p	27.49	27.04	27.82	32.75		4.00	2.67
hsa-miR-107	27.95	27.98	27.93	33.28		4.00	2.66
hsa-miR-27b-3p	30.85	31.07	30.20	35.95		4.00	2.65
hsa-miR-27a-3p	30.33	30.50	30.57	35.75		4.00	2.64
hsa-miR-146a-5p	25.53	24.91	25.31	30.50		4.00	2.64
hsa-miR-320a	27.54	27.82	27.63	32.93		4.00	2.64
hsa-miR-17-3p	29.51	29.72	29.65	34.86		4.00	2.62
hsa-miR-342-3p	27.73	27.65	29.66	33.22		4.00	2.61
hsa-miR-454-3p	31.59	31.03	31.10	36.42		4.00	2.60
hsa-miR-106a-5p	26.01	25.54	25.58	30.89		4.00	2.60
hsa-miR-18a-5p	29.21	28.36	28.29	33.71		4.00	2.58
hsa-miR-140-3p	29.69	29.76	29.07	34.58		4.00	2.55
hsa-miR-34a-5p	26.89	26.54	26.72	31.80		4.00	2.55
hsa-miR-148a-3p	27.68	28.97	27.90	33.11		4.00	2.53
hsa-miR-1260a	26.78	26.81	26.47	31.68		4.00	2.50
hsa-miR-92a-3p	25.50	25.98	25.55	30.62		4.00	2.48
hsa-miR-361-3p	30.77	31.65	30.91	35.96		4.00	2.46
hsa-miR-365a-3p	27.70	27.30	27.70	32.45		4.00	2.45
hsa-miR-148b-3p	29.89	29.97	29.93	34.81		4.00	2.44
hsa-miR-339-5p	28.48	28.50	28.05	33.20		4.00	2.44
hsa-miR-30c-5p	27.49	27.51	27.36	32.29		4.00	2.42
hsa-miR-320c	31.09	30.86	31.03	35.79		4.00	2.40
hsa-miR-26b-5p	31.30	31.48	31.17	36.10		4.00	2.39
hsa-miR-132-3p	29.82	29.45	31.16	34.68		4.00	2.38
hsa-miR-193b-3p	26.05	25.56	26.13	30.65		4.00	2.38
hsa-miR-7-5p	32.32	31.54	31.43	36.45		4.00	2.38
hsa-miR-98-5p	31.79	30.65	31.06	35.83		4.00	2.38
hsa-miR-23a-3p	27.48	27.11	27.80	32.11		4.00	2.34
hsa-let-7i-3p	32.15	32.68	32.15	36.91		4.00	2.30
hsa-miR-23b-3p	29.53	29.47	29.62	34.14		4.00	2.30
hsa-miR-181b-5p	29.78	28.38	28.79	33.37		4.00	2.27
hsa-miR-191-5p	28.11	27.96	28.66	32.66		4.00	2.23
hsa-miR-222-3p	28.78	27.92	27.60	32.41		4.00	2.21
hsa-miR-181a-5p	27.07	26.06	26.44	30.87		4.00	2.21
hsa-miR-339-3p	31.83	31.27	31.20	35.80		4.00	2.21

mmu-miR-378a-3p	28.37	27.01	27.69	31.90		4.00	2.18
hsa-miR-93-5p	27.86	27.56	27.79	32.00		4.00	2.14
hsa-miR-146b-5p	31.08	31.03	31.15	35.34		4.00	2.13
hsa-miR-425-5p	28.67	29.07	29.01	33.15		4.00	2.13
hsa-miR-423-5p	29.49	29.54	29.64	33.77		4.00	2.11
hsa-miR-940	30.84	32.32	32.10	35.66		4.00	2.06
hsa-miR-197-3p	31.60	31.31	31.19	35.46		4.00	2.05
hsa-miR-25-3p	28.75	28.22	28.21	32.45		4.00	2.05
hsa-miR-660-5p	32.47	31.67	31.35	35.80		4.00	2.04
hsa-miR-128-3p	31.82	30.96	30.86	35.17		4.00	2.02
hsa-miR-362-3p	33.11	31.84	31.93	36.05		4.00	1.97
hsa-miR-150-5p	33.30	33.88	32.06	36.53		4.00	1.89
hsa-miR-152-3p	32.90	34.36	31.87	36.17		4.00	1.87
hsa-miR-551b-3p	30.35	31.02	28.72	33.20		4.00	1.86
hsa-miR-532-3p	32.17	31.65	32.67	35.62		4.00	1.78
hsa-miR-664a-3p	32.61	32.98	32.22	36.09		4.00	1.77
hsa-miR-590-5p	33.05	31.79	31.52	35.37		4.00	1.75
hsa-miR-192-5p	33.91	33.23	31.95	36.08		4.00	1.73
hsa-miR-221-3p	31.35	30.12	30.23	33.44		4.00	1.54
hsa-miR-181a-2-3p	33.27	32.73	32.38	35.68		4.00	1.49
hsa-miR-301b	33.72	34.15	34.12	36.89		4.00	1.46
hsa-miR-93-3p	32.75	31.53	31.38	34.49		4.00	1.44
hsa-miR-200c-3p	32.57	31.65	32.30	34.94		4.00	1.43
hsa-miR-15b-3p	32.74	31.96	32.30	35.08		4.00	1.41
hsa-miR-26b-3p	34.61	34.61	33.58	36.72		4.00	1.32
hsa-miR-181d-5p	35.49	33.78	36.31	36.65		4.00	1.28
hsa-miR-186-5p	33.49	32.92	33.06	35.49		4.00	1.19
hsa-miR-188-5p	36.65	35.93	34.74	36.82		4.00	0.95
hsa-miR-421	36.42	35.80	36.04	36.46		4.00	0.31
hsa-miR-329-3p	35.05	35.48	35.35	35.48		4.00	0.20
hsa-miR-335-3p	BF	32.05	36.52	36.63		3.00	2.61
hsa-miR-455-3p	34.97	36.01	31.48	ND		3.00	2.37
hsa-miR-138-1-3p	32.33	31.66	35.51	ND		3.00	2.06
hsa-let-7d-3p	32.71	32.76	35.82	ND		3.00	1.78
hsa-miR-501-3p	36.81	33.50	35.68	ND		3.00	1.69
hsa-miR-143-3p	31.51	31.36	34.34	ND		3.00	1.68
hsa-miR-19a-5p	35.84	36.98	33.71	ND		3.00	1.66
hsa-miR-582-5p	32.64	30.65	33.80	ND		3.00	1.59
hsa-miR-125b-5p	31.54	34.59	33.46	ND		3.00	1.55
hsa-miR-497-5p	36.29	33.99	36.76	ND		3.00	1.48
hsa-miR-135a-5p	34.21	36.51	33.87	ND		3.00	1.43
hsa-miR-223-3p	30.64	33.48	31.81	ND		3.00	1.43
hsa-miR-651-5p	36.99	34.89	34.30	ND		3.00	1.41
hsa-miR-205-5p	31.88	ND	31.94	34.24		3.00	1.35
hsa-let-7e-5p	33.90	36.59	35.20	BF		3.00	1.34

hsa-miR-513a-3p	34.39	35.63	36.98	ND		3.00	1.30
hsa-miR-99a-5p	31.73	34.25	32.78	ND		3.00	1.27
hsa-miR-424-3p	34.52	ND	32.98	35.44		3.00	1.24
hsa-miR-501-5p	34.12	35.29	36.50	ND		3.00	1.19
hsa-miR-34b-5p	34.23	34.11	36.18	ND		3.00	1.16
hsa-miR-629-5p	35.30	34.67	33.11	ND		3.00	1.13
hsa-miR-328-3p	33.02	35.13	34.00	ND		3.00	1.06
hsa-miR-146a-3p	33.84	33.45	31.84	ND		3.00	1.06
hsa-miR-330-3p	33.54	35.62	34.49	BF		3.00	1.04
hsa-miR-24-2-5p	34.11	34.96	36.16	ND		3.00	1.03
hsa-miR-29c-5p	33.14	33.32	34.99	ND		3.00	1.02
hsa-miR-146b-3p	34.08	36.11	35.09	ND		3.00	1.01
hsa-miR-769-5p	33.75	33.27	35.16	ND		3.00	0.98
hsa-miR-92a-1-5p	31.36	33.00	31.33	ND		3.00	0.96
hsa-miR-215-5p	33.51	34.69	32.82	ND		3.00	0.94
hsa-miR-195-5p	35.53	33.65	34.77	ND		3.00	0.94
hsa-miR-16-1-3p	34.45	34.73	32.97	ND		3.00	0.94
hsa-miR-141-3p	33.95	32.10	33.29	ND		3.00	0.94
hsa-miR-9-3p	32.90	34.20	34.71	ND		3.00	0.93
hsa-miR-324-5p	32.05	30.95	32.74	ND		3.00	0.90
hsa-miR-194-5p	34.09	34.69	32.93	ND		3.00	0.90
hsa-miR-19b-1-5p	34.15	32.79	32.47	ND		3.00	0.89
hsa-miR-191-3p	34.14	35.60	35.69	ND		3.00	0.87
hsa-miR-671-3p	34.33	34.12	32.73	ND		3.00	0.87
hsa-miR-342-5p	33.47	33.69	35.02	ND		3.00	0.84
hsa-miR-181a-3p	34.36	33.28	32.93	ND		3.00	0.74
hsa-miR-33a-5p	32.48	32.56	31.24	BF		3.00	0.74
hsa-miR-28-5p	35.28	35.56	ND	36.68		3.00	0.74
hsa-miR-378a-5p	32.55	31.17	32.26	BF		3.00	0.73
hsa-let-7f-1-3p	34.45	34.55	35.71	ND		3.00	0.70
hsa-miR-576-5p	35.81	34.97	34.47	BF		3.00	0.68
hsa-miR-301a-3p	32.58	31.57	31.34	ND		3.00	0.66
hsa-miR-671-5p	36.30	35.04	35.32	ND		3.00	0.66
hsa-miR-219a-5p	35.54	35.01	34.24	ND		3.00	0.65
hsa-miR-135b-5p	35.37	36.59	35.61	ND		3.00	0.65
hsa-miR-132-5p	33.03	34.23	33.94	BF		3.00	0.63
hsa-miR-106b-3p	33.27	32.98	32.10	ND		3.00	0.61
hsa-miR-589-3p	35.27	36.08	36.43	ND		3.00	0.60
hsa-miR-30e-3p	32.48	32.03	31.30	BF		3.00	0.60
hsa-miR-574-3p	32.47	33.39	33.57	ND		3.00	0.59
hsa-miR-21-3p	32.78	32.17	31.62	BF		3.00	0.58
hsa-miR-25-5p	33.60	34.72	33.98	ND		3.00	0.57
hsa-miR-22-5p	31.77	32.66	32.76	ND		3.00	0.54
hsa-miR-642a-5p	34.15	35.03	34.06	ND		3.00	0.54
hsa-miR-942-5p	34.49	33.63	34.61	ND		3.00	0.54
hsa-miR-361-5p	31.16	30.50	30.18	BF		3.00	0.50

hsa-miR-486-5p	33.65	33.17	32.66	BF		3.00	0.50
hsa-miR-590-3p	35.71	35.44	34.78	ND		3.00	0.48
hsa-miR-505-3p	33.80	33.06	33.94	ND		3.00	0.47
hsa-miR-532-5p	33.17	32.34	32.37	ND		3.00	0.47
hsa-miR-28-3p	34.18	35.06	34.91	ND		3.00	0.47
hsa-miR-941	33.35	34.28	33.84	ND		3.00	0.47
hsa-miR-181c-5p	33.77	33.63	34.50	ND		3.00	0.46
hsa-miR-877-5p	33.15	33.14	33.92	BF		3.00	0.45
hsa-miR-17-5p	32.32	32.19	31.49	ND		3.00	0.45
hsa-miR-545-3p	BF	36.65	35.81	36.01		3.00	0.44
hsa-miR-502-3p	32.87	33.73	33.28	ND		3.00	0.43
hsa-miR-29a-5p	31.79	31.22	30.96	ND		3.00	0.43
hsa-miR-625-3p	32.81	33.58	33.52	ND		3.00	0.43
hsa-miR-188-3p	35.43	34.61	34.95	ND		3.00	0.42
hsa-miR-130a-3p	33.65	34.32	33.58	BF		3.00	0.41
hsa-let-7f-2-3p	34.64	34.72	35.36	ND		3.00	0.40
hsa-miR-130b-5p	33.19	33.66	32.88	ND		3.00	0.39
hsa-miR-500a-5p	34.56	35.26	35.18	ND		3.00	0.38
hsa-miR-425-3p	31.88	32.59	32.07	ND		3.00	0.37
hsa-miR-374b-5p	31.34	30.86	31.54	BF		3.00	0.35
hsa-miR-148b-5p	36.21	36.27	36.83	ND		3.00	0.34
hsa-miR-140-5p	31.62	30.97	31.13	ND		3.00	0.34
hsa-miR-20a-3p	31.53	30.97	30.93	ND		3.00	0.34
hsa-miR-362-5p	36.28	35.70	36.27	BF		3.00	0.33
hsa-miR-491-5p	32.32	32.29	32.86	BF		3.00	0.32
hsa-miR-27b-5p	36.13	36.65	36.12	ND		3.00	0.31
hsa-miR-296-5p	31.36	31.20	31.78	ND		3.00	0.30
hsa-miR-652-3p	31.66	31.25	31.09	BF		3.00	0.29
hsa-miR-29b-2-5p	33.00	32.76	33.31	ND		3.00	0.27
hsa-miR-7-1-3p	31.62	32.04	31.52	ND		3.00	0.27
hsa-miR-374a-5p	32.91	32.48	32.96	BF		3.00	0.27
hsa-miR-330-5p	34.23	34.02	34.54	ND		3.00	0.26
hsa-miR-151a-3p	33.97	34.40	34.37	ND		3.00	0.24
hsa-miR-1248	35.26	34.80	35.14	ND		3.00	0.24
hsa-miR-624-5p	36.12	36.07	36.48	ND		3.00	0.23
hsa-miR-766-3p	31.28	31.21	31.61	BF		3.00	0.21
hsa-miR-193b-5p	31.62	31.98	31.64	ND		3.00	0.20
hsa-let-7g-3p	32.53	32.79	32.87	ND		3.00	0.18
hsa-miR-130b-3p	32.58	32.44	32.35	BF		3.00	0.11
hsa-miR-18a-3p	31.90	31.85	31.80	BF		3.00	0.05
hsa-let-7b-5p	30.64	34.47	ND	ND		2.00	2.71
hsa-miR-335-5p	36.72	33.08	ND	ND		2.00	2.58
hsa-miR-663a	33.29	ND	ND	36.74		2.00	2.44
hsa-miR-450a-5p	35.01	ND	32.82	ND		2.00	1.55
hsa-miR-181c-3p	35.31	33.31	BF	ND		2.00	1.42
hsa-miR-99b-5p	33.79	ND	35.77	ND		2.00	1.40

hsa-miR-33b-5p	35.14	BF	36.73	ND		2.00	1.13
hsa-miR-363-3p	31.67	ND	30.30	ND		2.00	0.97
hsa-miR-374b-3p	ND	34.91	36.26	ND		2.00	0.95
hsa-miR-33a-3p	BF	35.42	36.74	ND		2.00	0.93
hsa-miR-505-5p	35.52	36.78	BF	ND		2.00	0.89
hsa-miR-629-3p	34.88	36.08	ND	ND		2.00	0.84
hsa-miR-33b-3p	34.83	36.01	ND	ND		2.00	0.83
hsa-miR-513c-5p	33.90	ND	35.08	ND		2.00	0.83
hsa-miR-199a-3p	ND	35.55	36.72	ND		2.00	0.83
hsa-miR-542-5p	34.64	ND	35.64	BF		2.00	0.71
hsa-miR-708-5p	35.61	ND	34.74	ND		2.00	0.62
hsa-miR-20b-5p	34.90	ND	34.04	ND		2.00	0.61
hsa-miR-92b-3p	BF	36.68	35.83	ND		2.00	0.60
hsa-miR-618	34.76	BF	33.94	BF		2.00	0.58
hsa-miR-744-3p	BF	34.86	35.62	ND		2.00	0.54
hsa-miR-15a-3p	BF	34.89	35.61	ND		2.00	0.50
hsa-miR-1271-5p	ND	35.66	34.96	ND		2.00	0.49
hsa-miR-744-5p	35.02	34.47	ND	ND		2.00	0.39
hsa-miR-320d	32.02	ND	32.50	BF		2.00	0.34
hsa-miR-30d-3p	ND	35.50	35.02	ND		2.00	0.34
hsa-miR-10a-5p	36.02	ND	35.61	ND		2.00	0.29
hsa-miR-200b-3p	35.57	35.97	BF	ND		2.00	0.29
hsa-miR-212-3p	33.29	33.60	ND	ND		2.00	0.22
hsa-miR-34b-3p	35.99	36.26	ND	ND		2.00	0.19
hsa-miR-145-5p	32.70	32.49	ND	ND		2.00	0.15
hsa-miR-34c-5p	36.64	36.46	ND	ND		2.00	0.13
hsa-miR-324-3p	30.66	30.49	BF	BF		2.00	0.12
hsa-miR-24-1-5p	36.63	36.46	ND	ND		2.00	0.12
hsa-miR-221-5p	BF	34.64	34.77	ND		2.00	0.09
hsa-miR-503-5p	33.60	ND	33.71	ND		2.00	0.08
hsa-miR-424-5p	31.94	BF	32.03	BF		2.00	0.06
hsa-miR-96-5p	35.07	ND	35.15	ND		2.00	0.06
hsa-miR-346	35.64	35.72	ND	ND		2.00	0.05
hsa-miR-550a-3p	34.92	ND	34.99	ND		2.00	0.05
hsa-miR-331-5p	35.63	35.65	ND	ND		2.00	0.01
hsa-miR-99b-3p	ND	36.58	ND	ND		1.00	ND
hsa-miR-99a-3p	ND	ND	35.89	ND		1.00	ND
hsa-miR-92a-2-5p	ND	BF	35.81	ND		1.00	ND
hsa-miR-877-3p	ND	ND	36.21	ND		1.00	ND
hsa-miR-769-3p	ND	ND	36.70	ND		1.00	ND
hsa-miR-7-2-3p	ND	ND	36.80	ND		1.00	ND
hsa-miR-649	ND	ND	36.18	ND		1.00	ND
hsa-miR-628-3p	ND	ND	36.89	ND		1.00	ND
hsa-miR-627-5p	36.90	BF	BF	ND		1.00	ND
hsa-miR-616-5p	ND	36.00	ND	ND		1.00	ND
hsa-miR-604	BF	ND	36.75	ND		1.00	ND



hsa-miR-584-5p	ND	36.89	ND	ND		1.00	ND
hsa-miR-579-3p	BF	36.25	ND	ND		1.00	ND
hsa-miR-571	ND	ND	34.88	ND		1.00	ND
hsa-miR-566	ND	ND	36.94	ND		1.00	ND
hsa-miR-562	ND	ND	36.95	ND		1.00	ND
hsa-miR-543	36.93	ND	ND	ND		1.00	ND
hsa-miR-455-5p	ND	ND	34.78	ND		1.00	ND
hsa-miR-454-5p	35.75	BF	ND	ND		1.00	ND
hsa-miR-411-5p	ND	ND	ND	36.02		1.00	ND
hsa-miR-345-5p	31.50	BF	BF	BF		1.00	ND
hsa-miR-340-5p	ND	35.76	ND	ND		1.00	ND
hsa-miR-340-3p	ND	36.48	ND	ND		1.00	ND
hsa-miR-32-3p	BF	36.16	ND	ND		1.00	ND
hsa-miR-30c-1-3p	ND	BF	36.71	ND		1.00	ND
hsa-miR-30b-3p	36.67	ND	BF	ND		1.00	ND
hsa-miR-300	BF	BF	34.50	ND		1.00	ND
hsa-miR-23b-5p	35.24	ND	ND	ND		1.00	ND
hsa-miR-23a-5p	ND	BF	34.70	ND		1.00	ND
hsa-miR-218-5p	ND	ND	35.61	ND		1.00	ND
hsa-miR-200a-3p	ND	ND	36.63	ND		1.00	ND
hsa-miR-199b-5p	36.59	ND	BF	ND		1.00	ND
hsa-miR-1972	BF	33.13	BF	BF		1.00	ND
hsa-miR-196a-5p	36.82	ND	ND	ND		1.00	ND
hsa-miR-192-3p	ND	36.19	ND	ND		1.00	ND
hsa-miR-190a-5p	BF	36.15	ND	ND		1.00	ND
hsa-miR-1908-5p	35.69	ND	ND	ND		1.00	ND
hsa-miR-18b-3p	BF	ND	35.89	ND		1.00	ND
hsa-miR-182-5p	35.08	ND	ND	ND		1.00	ND
hsa-miR-147b	ND	ND	36.58	ND		1.00	ND
hsa-miR-143-5p	36.65	ND	ND	ND		1.00	ND
hsa-miR-139-5p	36.52	ND	ND	ND		1.00	ND
hsa-miR-134-5p	ND	ND	36.44	ND		1.00	ND
hsa-miR-133b	ND	ND	35.97	ND		1.00	ND
hsa-miR-1296-5p	ND	35.60	ND	ND		1.00	ND
hsa-miR-1272	36.14	BF	ND	ND		1.00	ND
hsa-miR-1270	ND	BF	36.57	ND		1.00	ND
hsa-miR-125b-2-3p	ND	BF	36.85	ND		1.00	ND
hsa-miR-1256	ND	36.11	ND	ND		1.00	ND
hsa-miR-1255b-5p	ND	36.57	ND	ND		1.00	ND
hsa-miR-1244	ND	ND	36.61	ND		1.00	ND
hsa-miR-1224-3p	35.53	BF	ND	ND		1.00	ND
hsa-miR-10b-3p	ND	36.79	ND	BF		1.00	ND
hsa-let-7b-3p	36.50	ND	ND	ND		1.00	ND
hsa-miR-95-3p	BF	ND	BF	ND		0.00	ND
hsa-miR-944	ND	ND	BF	ND		0.00	ND

hsa-miR-937-3p	ND	ND	BF	BF		0.00	ND
hsa-miR-922	BF	ND	ND	ND		0.00	ND
hsa-miR-887-3p	BF	ND	BF	ND		0.00	ND
hsa-miR-885-3p	BF	ND	BF	ND		0.00	ND
hsa-miR-875-3p	ND	ND	ND	BF		0.00	ND
hsa-miR-765	ND	ND	BF	ND		0.00	ND
hsa-miR-760	BF	ND	BF	ND		0.00	ND
hsa-miR-708-3p	ND	BF	BF	ND		0.00	ND
hsa-miR-663b	BF	BF	BF	BF		0.00	ND
hsa-miR-654-5p	ND	ND	ND	BF		0.00	ND
hsa-miR-645	ND	ND	ND	BF		0.00	ND
hsa-miR-632	ND	ND	BF	ND		0.00	ND
hsa-miR-628-5p	ND	ND	BF	ND		0.00	ND
hsa-miR-615-3p	BF	ND	ND	ND		0.00	ND
hsa-miR-603	ND	ND	ND	BF		0.00	ND
hsa-miR-598-3p	BF	BF	BF	BF		0.00	ND
hsa-miR-595	BF	ND	ND	ND		0.00	ND
hsa-miR-589-5p	ND	ND	BF	ND		0.00	ND
hsa-miR-580-3p	ND	ND	BF	ND		0.00	ND
hsa-miR-577	BF	ND	ND	ND		0.00	ND
hsa-miR-576-3p	ND	BF	BF	ND		0.00	ND
hsa-miR-570-3p	ND	ND	BF	ND		0.00	ND
hsa-miR-564	ND	ND	BF	ND		0.00	ND
hsa-miR-551b-5p	BF	ND	ND	ND		0.00	ND
hsa-miR-548i	BF	ND	ND	ND		0.00	ND
hsa-miR-548d-5p	ND	BF	BF	ND		0.00	ND
hsa-miR-548c-5p	BF	BF	BF	BF		0.00	ND
hsa-miR-548a-5p	BF	ND	ND	ND		0.00	ND
hsa-miR-548a-3p	BF	BF	BF	ND		0.00	ND
hsa-miR-524-5p	ND	ND	ND	ND		0.00	ND
hsa-miR-520h	ND	ND	ND	ND		0.00	ND
hsa-miR-518f-5p	BF	ND	ND	ND		0.00	ND
hsa-miR-518d-5p	ND	ND	ND	ND		0.00	ND
hsa-miR-513b-5p	BF	ND	BF	ND		0.00	ND
hsa-miR-507	BF	ND	ND	ND		0.00	ND
hsa-miR-499a-5p	ND	BF	ND	ND		0.00	ND
hsa-miR-496	ND	BF	ND	ND		0.00	ND
hsa-miR-491-3p	BF	ND	BF	ND		0.00	ND
hsa-miR-485-3p	BF	ND	ND	ND		0.00	ND
hsa-miR-483-5p	ND	BF	ND	BF		0.00	ND
hsa-miR-451a	ND	BF	ND	ND		0.00	ND
hsa-miR-410-3p	BF	ND	ND	ND		0.00	ND
hsa-miR-382-3p	ND	BF	BF	ND		0.00	ND
hsa-miR-380-5p	ND	ND	ND	ND		0.00	ND
hsa-miR-379-5p	ND	ND	ND	ND		0.00	ND
hsa-miR-376c-3p	BF	ND	BF	BF		0.00	ND

hsa-miR-373-3p	ND	ND	ND	ND		0.00	ND
hsa-miR-34a-3p	BF	BF	BF	BF		0.00	ND
hsa-miR-326	ND	BF	BF	BF		0.00	ND
hsa-miR-30a-3p	ND	BF	BF	ND		0.00	ND
hsa-miR-27a-5p	ND	ND	ND	BF		0.00	ND
hsa-miR-222-5p	ND	ND	BF	ND		0.00	ND
hsa-miR-219a-1-3p	ND	BF	ND	ND		0.00	ND
hsa-miR-216a-5p	ND	BF	ND	ND		0.00	ND
hsa-miR-212-5p	BF	ND	ND	ND		0.00	ND
hsa-miR-211-5p	BF	ND	ND	ND		0.00	ND
hsa-miR-2110	BF	BF	BF	BF		0.00	ND
hsa-miR-20b-3p	ND	ND	BF	ND		0.00	ND
hsa-miR-208a-3p	ND	ND	BF	ND		0.00	ND
hsa-miR-206	ND	ND	ND	ND		0.00	ND
hsa-miR-199a-5p	ND	BF	BF	ND		0.00	ND
hsa-miR-1913	ND	ND	ND	ND		0.00	ND
hsa-miR-187-5p	BF	ND	ND	ND		0.00	ND
hsa-miR-183-5p	ND	ND	BF	ND		0.00	ND
hsa-miR-1539	ND	ND	BF	BF		0.00	ND
hsa-miR-1471	ND	ND	BF	ND		0.00	ND
hsa-miR-139-3p	ND	BF	ND	ND		0.00	ND
hsa-miR-138-2-3p	ND	BF	BF	ND		0.00	ND
hsa-miR-137	BF	ND	BF	ND		0.00	ND
hsa-miR-127-3p	ND	ND	BF	ND		0.00	ND
hsa-miR-125a-5p	BF	BF	BF	BF		0.00	ND
hsa-miR-125a-3p	BF	ND	ND	ND		0.00	ND
hsa-miR-1249	ND	BF	ND	ND		0.00	ND
hsa-miR-1205	ND	BF	ND	ND		0.00	ND
hsa-miR-1203	ND	BF	ND	ND		0.00	ND
hsa-miR-1184	ND	BF	ND	ND		0.00	ND
hsa-miR-1183	BF	ND	ND	ND		0.00	ND
hsa-miR-10b-5p	ND	ND	BF	ND		0.00	ND
hsa-miR-101-5p	BF	ND	ND	ND		0.00	ND
hsa-let-7a-3p	BF	ND	ND	ND		0.00	ND
Count	252.00	244.00	254.00	113.00			
Global mean	29.64	29.47	29.29	34.27			

<b>Patient code:</b>										
<b>Slide code:</b>		MI normal	MI low	Metaphases clear	Metaphases unclear	Abbs clear	Abbs unclear			<b>G2 Score: /25</b>
<b>Date:</b>										<b>Total:</b>

**Slide Comments:**

No of Interphase cells in field	No of mitosis in field	Ct gap	Ct break	Ct fragment	Ct Minute	Terminal deletion	Inter-arm exchange	Other Abb type	Total no of Abbs	Vernier reading
1										
2										
3										
4										
5										
6										
7										
8										
9										
10										
11										
12										
13										
14										
15										
16										
17										
18										
19										
20										
21										
22										
23										
24										
25										

<b>Vernier readings of Endoreduplication events:</b>		<b>Vernier readings of Tetraploidy events:</b>	
--	--	--	--

Patient code:		Mitotic Index:	
Slide code:		Mitotic Index:	
Date:			
Slide Comments:			
No of Interphase cells in field	No of mitosis in field	No of Interphase cells in field	No of mitosis in field
1		41	
2		42	
3		43	
4		44	
5		45	
6		46	
7		47	
8		48	
9		49	
10		50	
11		51	
12		52	
13		53	
14		54	
15		55	
16		56	
17		57	
18		58	
19		59	
20		60	
21		61	
22		62	
23		63	
24		64	
25		65	
26		66	
27		67	
28		68	
29		69	
30		70	
31		71	
32		72	
33		73	
34		74	
35		75	
36		76	
37		77	
38		78	
39		79	
40		80	
TOTAL:		TOTAL:	